



NATIONAL TECHNICAL UNIVERSITY OF ATHENS
SCHOOL OF MECHANICAL ENGINEERING
SECTION OF MECHANICAL DESIGN & AUTOMATIC CONTROL



Motion planning and control of cooperating robotic systems in orbit

PhD THESIS

A Dissertation submitted to the Department of
Mechanical Engineering of the National
Technical University of Athens, in partial
fulfillment of the
Degree of Doctor of Philosophy

GEORGIOS REKLEITIS

Supervisor: Prof. E. G. Papadopoulos

ATHENS 2015



NATIONAL TECHNICAL UNIVERSITY OF ATHENS
SCHOOL OF MECHANICAL ENGINEERING
SECTION OF MECHANICAL DESIGN & AUTOMATIC CONTROL
Control Systems Laboratory

PhD Thesis

**Motion planning and control of cooperating robotic
systems in orbit**

Georgios Rekleitis

Supervisor: Prof. E. G. Papadopoulos

ATHENS 2015

Cover image source: NASA.

This work is dedicated to Maria and Marina

Abstract

Both interplanetary traveling crafts and stationary systems will be in need of servicing, such as assembly, maintenance, replacement of broken/expendable modules, refueling, inspection and repair. To relieve astronauts from dangerous extra-vehicular activities, enhance performance and extend the feasible tasks range, the international research community has been focusing on the realization of autonomous robotic servicing. While important tasks, such as orbital assembly and debris handling, require passive object handling capabilities, the actual handling of a secured passive object by a number of free-flying robotic servicers, has not been studied adequately, with several issues still open.

On-orbit object handling has similarities to cooperative manipulation of passive objects on earth, with the additional complexities that in space no fixed ground to support the manipulators exists, thus letting momentum changes to play a key role in body motion. One more issue arises from the fact that orbital system thrusters are of on-off control nature. In order to protect the thruster valves from the extreme space conditions, proportional or pulse-width-modulation (PWM) thrusters are not used in space, at least not as PWM is used on terrestrial systems, thus reducing system positioning capabilities, when only thrusters are used.

The introduction of a number of manipulator-equipped free-flying servicers, where both on-off thruster propulsion and manipulator continuous forces/ torques are used for passive object handling, both for the case of firm grasp and in the more general case of point contact, between the servicer manipulator end-effectors and the passive object, is presented in this thesis.

The design of a controller for the free-flying servicer manipulators that enables the stable handling of the passive object by the servicers, in trajectory tracking scenarios, as well as the design of a controller for the free-flying servicer bases that enables them to move within the workspace of their manipulators, under the influence of the reaction generalized forces from their manipulator bases, is also presented. An initial comparison between the choice of three small free-flying robotic servicers and a single, larger one is also conducted.

A spatial system of robotic servicers handling a passive object is highly non-linear. Unfortunately, there is not much generally applied theory on the field of non-linear system

robustness. One method is to use linearization, under certain assumptions, in order to be able to use linear systems robustness tools. The sensitivity of the controller for the 3D motion of the handled passive object in space in terms of parameter estimation is also studied in this work.

Finally, the design of a two-layer optimization process that allows for i) optimal selection of contact points between the manipulator end-effectors and the passive object, for both contact cases and ii) force distribution so that the required control generalized force for the passive object motion, is applied by the manipulator end-effectors, is also presented.

Acknowledgments

First and foremost I would like to thank my advisor, Prof. Evangelos Papadopoulos, for the supervision and support, during the research and writing of this work. His scientific rigor and enthusiasm for his work are both motivating and inspiring.

I would also like to thank my other two advisors, Prof. Konstantinos (Kostas) J. Kyriakopoulos and Prof. Nikolaos Krikelis for their valuable help and comments during the writing of this thesis.

Moreover, I would like to thank all the members of the Control Systems Lab (past and present) of their continuous support and help. They have all contributed immensely to my personal and professional time at the National Technical University of Athens, being a great source of friendship as well as good advice and collaboration.

Finally, I would like to thank my parents, my brother and my wife Maria. Their help, love and support throughout the years was a great inspiration to hard work.

Table of Contents

Abstract	5
Acknowledgments	7
Table of Figures	10
Table of Tables	15
1 Introduction	16
1.1 Motivation	16
1.2 Literature Review	21
1.2.1 On-Orbit Servicing	21
1.2.2 Handling of a Passive Object in Space	30
1.3 Contribution	33
1.4 Thesis Summary	34
2 Servicing Concepts	36
2.1 On-orbit Servicing	36
2.2 Orbital Debris Disposer	39
2.2.1 Simplified Model Analysis	39
2.2.2 Control Law and Constraints	40
2.2.3 Simulation Results	44
2.3 Concept On-Orbit Manipulation of a Passive Object by Cooperating Free-Flying Robots	47
2.3.1 Object Control with Direct Thrusting	50
2.3.2 Object Control with Manipulator-Equipped Servicers	51
2.3.3 Control Design	56
2.3.4 Simulation Results	64
2.4 Conclusion	73
3 On-Orbit Passive Object Handling by Cooperating Space Robotic Servicers	75
3.1 Spatial System Dynamics	78
3.2 One Large vs. a Number of Small Servicers	81

3.3	Control Design	84
3.3.1	Passive object motion without use of thrusters.....	84
3.3.2	Controller derivation and generalized forces constraints: firm grasp case.....	90
3.3.3	Controller derivation and generalized forces constraints: point contact case..	95
3.3.4	Manipulator force distribution.....	95
3.3.5	Free-flying servicer control	98
3.4	Stability and Robustness	104
3.4.1	Stability of the Passive Object Motion	104
3.4.2	Robustness of the Passive Object Motion	105
4	Simulation Results	113
4.1	Spatial Control of a Passive Object	115
4.1.1	Point contact case	116
4.1.2	Firm grasp case.....	123
4.2	Robustness of the Passive Object Motion Demonstration	125
4.3	One vs. Three Servicers.....	134
4.3.1	Simulation (a).....	135
4.3.2	Simulation (b).....	138
5	Conclusions and Future Work	141
5.1	Conclusions.....	141
5.2	Future Work	143
	References	145
	Appendix A	155
	Appendix B	156
	Appendix C	162
	Appendix D	169

Table of Figures

Figure 1-1. Actual and expected satellite launches (source: EUROCONSULT).	16
Figure 1-2. Discovery astronaut Steve Bowen works outside the International Space Station during the STS-133 mission's second spacewalk, March 2, 2011. (source: NASA).	17
Figure 1-3. On the left, Canadarm2 moves toward the new P5 truss section for a hand-off from Space Shuttle Discovery's Canadarm, on December 11, 2006. On the right, the Italian-built Permanent Multipurpose Module is transferred by Canadarm2, from Space Shuttle Discovery's payload bay to be permanently attached to the ISS, on March 1, 2013. (source: NASA).	19
Figure 1-4. Astronaut Steven Smith working at the end of Discovery's Canadarm as he did maintenance work on the Hubble Space Telescope, on February 15, 1997 (left). Astronauts F. Story Musgrave, anchored on the end of the shuttle's robotic arm, and Jeffrey A. Hoffman inside the orbiter's payload bay, conduct the fifth and final spacewalk to fix Hubble during the shuttle Endeavour's 1993 servicing mission to the orbiting observatory (right) (source: NASA).	22
Figure 1-5. Experimental test-beds for OOS scenarios emulations. On the left is the robotic docking emulator of CSA (source: CSA). On the right, the EPOS system of DLR is simulating the relative motion between a target and a chases satellite (source: DLR).	23
Figure 1-6. OOS successful tests. On the left, an artist's representation of the ETS-VII experiment (source: JAXA). On the right, the Orbital Express experiment docking phase, as photographed by a camera at the end-effector of its own manipulator. (source: DARPA).	24
Figure 1-7. Dextre, as photographed by an Expedition 27 crew member (top left), JEMRMS on the exterior of the Kibo laboratory of the ISS and the station's Canadarm2 (top right), (source: NASA) and ERA undergoing tests at ESA's facilities (source: ESA).	25
Figure 1-8. Dextre robot moves the RRM Multifunction Tool towards the RRM module (left) and the Dextre robot performing a new set of satellite-servicing tasks on the RRM module, during the second part of the Gas Fittings Removal task (right), (source: NASA).	25

Figure 1-9. Robotic systems tested inside the ISS. On the left, Expedition 18 crewmember Michael Fincke as he works with SPHERES in the US Laboratory of the ISS. On the right, Robonaut 2 humanoid robot holds an instrument to measure air velocity during another system check out in the Destiny laboratory of the ISS. (source: NASA).....	26
Figure 1-10. Artist's representations of: XSS-11 satellite (left), (source: US Air Force Research Laboratory/MDA) and the PRISMA mission (right), (source: SSC).	27
Figure 1-11. Artist's representation of the TECSAS system (left), (source: CSA) and the DEOS system (right), (source: Space Tech GmbH).....	28
Figure 1-12. Artist's representations of ConeXpress-OLEV (left), (source: Orbital Recovery Corp.) and SMART-OLEV (right), (source: NordicSpace).....	28
Figure 1-13. The FRENDA under full-scale rendezvous and autonomous robotics grapple testing (top), (source: Naval Research Laboratory) and an artist's representation of the PHOENIX OOS program (bottom), (source: DARPA).	29
Figure 1-14. Artist impressions of: a servicing satellite refueling another satellite in Earth orbit (left), (source: MacDonald Dettwiler Associates Corporation) and of ATK satellite (the base for the MEV project), as it approaches a satellite to be serviced (right) (source: ATK).....	30
Figure 1-15. Handling of a rigid passive body by a number of cooperating free-flyers equipped with manipulators, in space structure assembly operations.	31
Figure 2-1. OOS concepts. (a) – (c) capturing and (d) – (3) handling tasks.	37
Figure 2-2. Graphic representation of the Orbital Debris Disposer.....	39
Figure 2-3. A 1D model of the orbital debris disposer.	40
Figure 2-4. (a) Relative positions response and (b) velocities for control gains $K_1 = 80$ kg/s and $K_2 = 400$ kg/s, that do not satisfy any constraints for successful capture.	44
Figure 2-5. (a) Relative positions response and (b) velocities for control gains $K_1 = 250$ kg/s and $K_2 = 30$ kg/s, that satisfy the constraints for successful capture.	45
Figure 2-6. Motion snapshots of the orbital debris disposer during capture. (a) $t = 0.0$ s, first contact, (b) $t = 0.32$ s, net's maximum deformation, (c) $t = 7.8$ s, all bodies move together.	45
Figure 2-7. (a) Relative positions response and (b) velocities for control gains $K_1 = 250$ kg/s and $K_2 = 30$ kg/s that satisfy the constraints of Eqs. (8), (9), (14) and (16) for successful capture, but with inaccurate estimation of the debris mass, thus resulting in non-zero steady-state relative speed $x_3 - x_2 \neq 0$, as opposed to Figure 2-5.	46

Figure 2-8. (a) Handling of a passive object by firmly attached thruster pack (pure on-off control) (b) Servicer equipped with thrusters, reaction wheels and a manipulator for the handling of a passive object.....	48
Figure 2-9. Model of a passive object / servicers system controlled by thrusters.	50
Figure 2-10. Typical response of On-Off PD control, with limit cycle.....	51
Figure 2-11. A passive (center) object handled by servicers with manipulators.	52
Figure 2-12. Handling of the passive object by use of manipulator forces only. Initial (a) and final (b) position of the system.....	53
Figure 2-13. Flowchart of the control algorithm for the simplified one-dimensional model of two free-flying robotic servicers, handling a passive object.	64
Figure 2-14. Response of the system with manipulators, for a trapezoidal profile desired velocity.....	66
Figure 2-15. Required forces of the system with manipulators, for trapezoid profile on desired velocity.	66
Figure 2-16. Response of the system with manipulators, for sinusoidal position.	67
Figure 2-17. Required forces of the system with manipulators, for sinusoidal desired position.....	68
Figure 2-18. System with manipulators response, for Simulation 3.....	69
Figure 2-19. Required forces of the system with manipulators, for Simulation 3.....	69
Figure 2-20. Position error as a function of time and corresponding consumed energy (a), (c) without manipulators, and (b), (d) with.....	71
Figure 2-21. Response of the system with manipulators, for a trapezoidal profile desired velocity (second controller).	72
Figure 2-22. Comparison between the two proposed controllers. Passive object position error for (a) the controller of Eqs. (69) and (72) and (b) the controller of Eqs. (65) and (67) . Energy consumption for (c) the controller of Eqs. (69) and (72) and (d) the controller of Eqs. (65) and (67).	73
Figure 3-1. In the point contact case, two single-manipulator robots cannot exert a moment around the line defined by the two contact points A and B.....	77
Figure 3-2. Passive object (0) and the i^{th} free-flyer with a single manipulator.....	80
Figure 3-3. Pushing the servicer away from the passive object, in the case of one, large servicer.....	82
Figure 3-4. Spatial handling of the passive object by use of manipulator forces only.	85

Figure 3-5. Spatial handling of the passive object by use of manipulator forces only, in simple motion.....	87
Figure 3-6. Switching strategy for a single thruster, for the servicer position control.	101
Figure 3-7. Servicer attitude control, with switching strategy when the reaction wheels (continuous moment) reach their limits.....	102
Figure 3-8. Flowchart of the servicers control algorithm.....	104
Figure 4-1. Concept of a passive object in space, handled by three single-manipulator robotic servicers.....	113
Figure 4-2. Passive object inertial x-axis desired trajectory.....	116
Figure 4-3. Top view of the passive object and three single manipulator robotic servicers at their desired relative position and relative orientation. For Servicer 1, the maximum manipulator reach position is also shown.....	117
Figure 4-4. Actual trajectories of the passive object coordinates.....	118
Figure 4-5. Point contact case: Tracking errors in (a) object position and (b) attitude, (c) servicer base displacement, and (d) attitude.....	118
Figure 4-6. (a) Tracking errors in servicer base displacement, (b) typical manipulator applied forces, (c) thruster forces and (d) torques by reaction wheels and thrusters for one of the servicers.....	119
Figure 4-7. Typical manipulator joint-angles (a) and joint-torques (b).....	120
Figure 4-8 Typical manipulator joint-angles and fuel consumption, for the initial servicer control gains (a and c) and for increased gains (b and d).....	121
Figure 4-9. Tracking error and corresponding fuel consumption as a function of time. (a), (d) with manipulators, (b), (e) without manipulators (PWPF thrusters), and (c), (f) without manipulators (pure on-off thrusters).....	123
Figure 4-10. Firm grasp case: Tracking errors in (a) object position and (b) attitude, (c) servicer base displacement, and (d) attitude.....	124
Figure 4-11. Tracking error history and corresponding consumed energy for servicers with manipulators. (a), (c) point contact case, (b), (d) firm grasp case.....	124
Figure 4-12. Point contact case with inaccuracies: Tracking errors in (a) object position and (b) attitude, (c) servicer base displacement, and (d) attitude.....	126
Figure 4-13. Tracking errors e_0 for the passive object motion, for the system without (a) and the system with (b) uncertainty.....	129

Figure 4-14. Upper six values of vector \mathbf{A}_d , corresponding to the position/orientation steady-state errors for the passive object (a) and actual passive object position/orientation errors (b).....	130
Figure 4-15. Comparison between position/orientation tracking errors (b, d, f) and the corresponding expected values (a, c, e), for zero to 25 s (a, b), 38 s to 48 s (c, d) and 103 s to 126 s (e, f).	131
Figure 4-16. Eigenvalues of matrices \mathbf{F}_{dD} and \mathbf{F}_{dP} for the case with uncertainty parameters of Eq. (207) ((a) and (b)) and for the case with uncertainty parameters of Eq. ((c) and (d)).	132
Figure 4-17. Comparison between position/orientation tracking errors (b, d) and the corresponding expected values (a, c), for zero to 23 s (a, b) and 110 s to 130 s (c, d), for uncertainty parameters as in Eq. (208).	133
Figure 4-18. Passive object tracking errors \mathbf{e}_0 (a), and comparison between position/orientation tracking errors (c and e) and the corresponding expected values (b and d), for the system with uncertainty.	134
Figure 4-19. Passive object tracking errors (a, b) and fuel consumption (c, d), for the case of three servicers (a, c) and single-servicer (b, c).	137
Figure 4-20. Manipulator reach for (a) the three-servicers case, as well as (b) the single-servicer case.	137
Figure 4-21. Thruster firing (a, b) and reaction wheel and thruster torque (c, d), for the three-servicers case (a, c), as well as the single-servicer case (b, d).	138
Figure 4-22. Passive object tracking errors (a, b) and fuel consumption (c, d), for the case of three servicers (a, c) and single-servicer (b, c), for the second simulation.	140

Table of Tables

Table 1-1. Debris removal methods.....	20
Table 2-1. Advantages and disadvantages for the proposed OOS concepts depicted in Figure 2-1.	38
Table 3-1. Comparison between the single, large servicer and the several smaller servicers cases.....	84
Table 4-1. Passive object and servicer characteristics.....	114
Table 4-2. Passive object desired motion parameters (Trajectory 1).....	115
Table 4-3. Control gains for the point contact case.	117
Table 4-4. Introduced inaccuracies	125
Table 4-5. Passive object desired motion parameters (Trajectory 2).....	133
Table 4-6. Control gains for the single-servicer case.	136
Table 4-7. Control gains for the three-servicers case.	136
Table 4-8. Step commands.....	138
Table 4-9. Control gains for the three-servicers case.	139
Table 4-10. Control gains for the single servicer case.....	139

1 Introduction

1.1 Motivation

The commercialization of space has led to the growth of the number of structures on orbit over the decades, especially of satellites. This trend is going to continue, as can be seen in Figure 1-1, [53].

Two decades of the satellite market by client

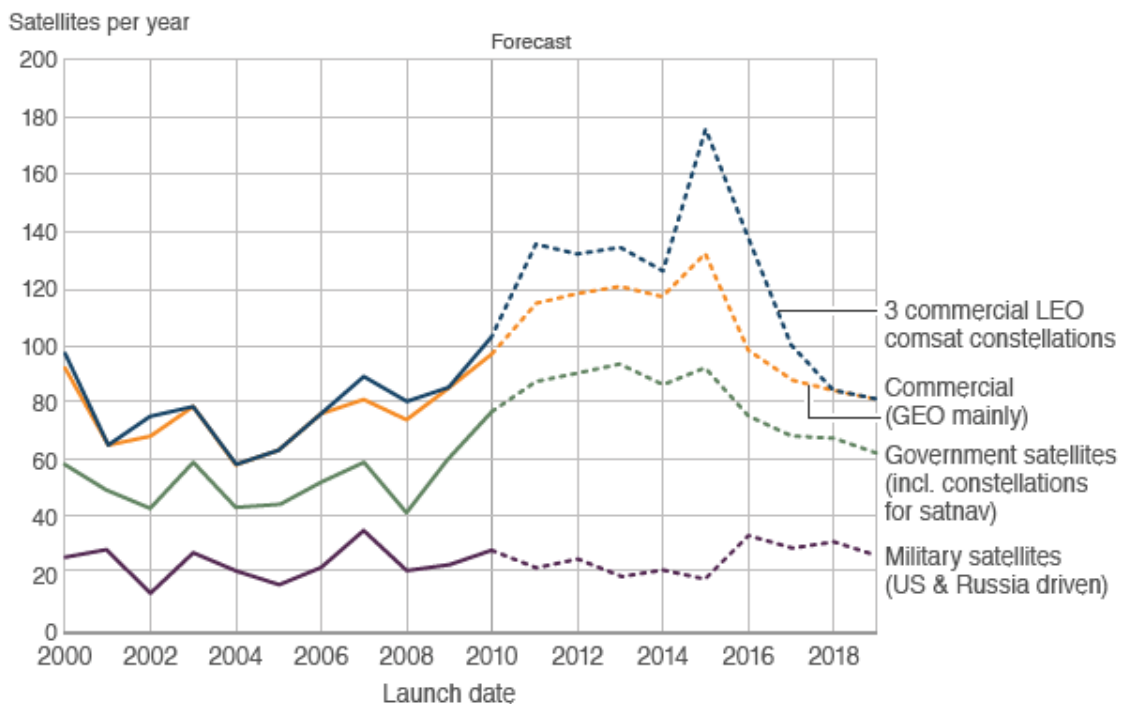


Figure 1-1. Actual and expected satellite launches (source: EUROCONSULT).

Moreover, as countries with no major role so far in the deployment of satellites, realize their importance in communications, defense, etc. [62], [63], [64], satellite launching may be even more augmented. It should be noted that peaks on the satellites-per-year launches as the one predicted for the middle of the coming decade, are periodic, since most commercial satellite constellations need maintenance-replacement every 10 to 15 years [21]. This commercialization of space and the growing number of orbital structures, has led to the need for tasks such as construction, docking and inspection, astronaut assistance, maintenance and repair to prevent lasting damages and orbital debris handling and disposal. Both interplanetary traveling crafts and stationary systems (both commercial and scientific), will be in need of servicing, such as assembly, maintenance,

replacement of broken or expendable modules such as batteries, refueling, internal and external inspection and repair. Current space servicing level is limited to orbital systems, thus being called On Orbit Servicing (OOS). Numerous construction and repair missions on the International Space Station (ISS) [45], [46] as well as the repair missions on the Hubble Space Telescope [59] point out the importance of such tasks. Space servicing such as fuel refill, damage repair and expendable modular unit replacement, can vastly extend the life of multi-million space devices. Astronauts currently accomplish such tasks by Extra-Vehicular Activities (EVAs), see Figure 1-2, but these are dangerous and subject to limitations such as the force/ torque an astronaut can apply, the motions that can be performed or even the EVA temporal constraints.



Figure 1-2. Discovery astronaut Steve Bowen works outside the International Space Station during the STS-133 mission's second spacewalk, March 2, 2011. (source: NASA).

To relieve astronauts from EVA, enhance performance and extend the range of feasible tasks, teleoperated or fully automated robotic OOS must be developed. Robotic space servicing can be safer and cheaper than any other alternative, if every servicing task becomes validated as a robust standard procedure, as opposed to the multi-month preparation phase of the current level of (orbital) servicing. Space servicing enabling human/robot interaction or even pure robotic space servicing can be both safer and less expensive than pure astronaut servicing, since there is no life support cost. To that end,

each robotics augmented space servicing task must be a robust standard procedure, as opposed to the multi-month planning and testing phases of current OOS.

Space systems servicing should not be limited to orbital systems. The further away from Earth humans venture, the more critical is the ability to maintain and repair their equipment. This is more true for systems such as structures stationed far from Earth's easy reach, such as the proposed space telescopes at the Lagrangian Point [56], [57] (although this project is abandoned now, others will almost certainly follow) and spacecrafts en route to other planets. For both cases, teleoperated or fully automated robotic servicing systems must be developed.

One of the most important tasks in space servicing is the handling of a secured passive object, with several servicing missions in need of it, the most important being handling of orbital-construction parts, debris handling and deorbiting, and handling of fuel-less satellites (as part of refueling missions).

As human presence evolves in space, the need for more orbital structures is increasing. More are likely to be needed around the Earth, and even around other large celestial bodies such as the Moon and Mars. The construction of such systems will require handling of passive assembly parts. Moreover, this task will be in demand in the assembly of large space telescopes and possibly of other scientific platforms in space.

The need for robotic augmentation of space assembly tasks was recognized from the early stages of orbital construction. During the construction of the ISS, robotic servicing was employed in the form of the Remote Manipulator System (Canadarm), mounted on the Space Shuttle, and later on, in the form of the Mobile Servicing System (Canadarm2), mounted on the ISS. Since Canadarm2 was installed on the ISS, the two arms have been used repeatedly to hand over segments of the station for assembly from the Canadarm to the Canadarm2, as seen in Figure 1-3.

In the above cases though, the manipulator base is so large compared to the handled object that the base can be considered quasi-fixed. Similarly, the maximum allowed payload for the space Shuttle with Canadarm2 mounted on it, was one third of its total mass. To handle larger payloads, additional servicers would be required. Moreover, systems like the above are designed for limited on orbit mobility and cannot be available on demand at various locations on orbit. They also move payloads with respect to their base, and not with respect to a Cartesian frame or to another object. In the former motion,

attitude disturbances may not be important, while in the later they must be compensated. To address all these challenges, the introduction of multiple cooperating robotic servicers handling a payload of size comparable or larger than their own will be required.

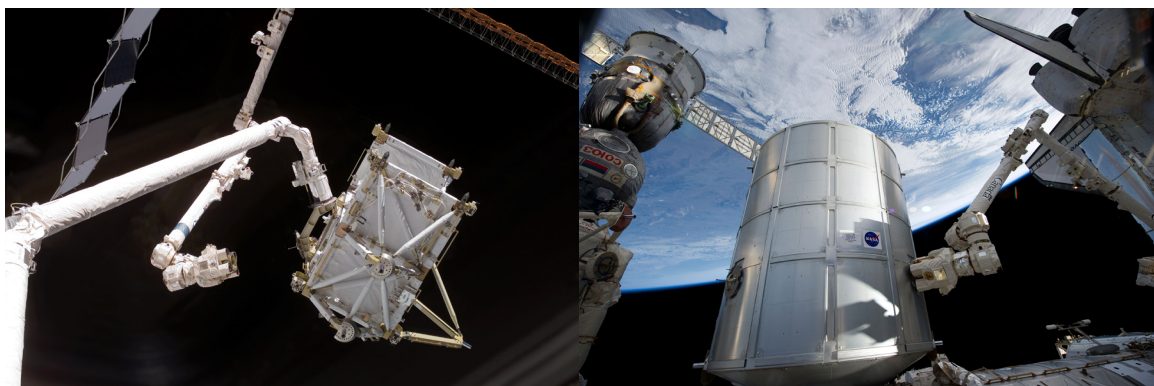


Figure 1-3. On the left, Canadarm2 moves toward the new P5 truss section for a hand-off from Space Shuttle Discovery's Canadarm, on December 11, 2006. On the right, the Italian-built Permanent Multipurpose Module is transferred by Canadarm2, from Space Shuttle Discovery's payload bay to be permanently attached to the ISS, on March 1, 2013. (source: NASA).

Space debris, also called orbital or artificial debris, is defined as the collection of man-made objects orbiting Earth that are no longer functional. The principle sources of space debris are satellite launches, spontaneous explosions due to the erosion of the fuel tanks and collisions in space [85]. It is estimated that on orbit there are more than 20.000 pieces larger than 10 cm, 600.000 pieces larger than 1cm, and in total more than 300 million larger than 1 mm. It is clear from these statistics that space debris represents a significant percentage of the man-made orbital objects.

Space debris is an ongoing and increasing hazard for space operations; it is uncontrollable, and the orbits of these debris fragments often overlap the trajectories of spacecrafts. Space debris pose a significant collision risk that could cause severe damage to satellites, resulting in major problems in navigation, communication, meteorology and other applications where satellites are essential. Additionally, the congestion of debris in Low Earth Orbit (LEO) and mostly in Geostationary Earth Orbit (GEO), results in fewer usable slots for satellite operators. The orbiting space debris are also a cause of major concern for human spaceflight, since even a small collision with a space shuttle or with ISS could prove catastrophic, as was also illustrated in the movie Gravity [43]. Debris larger than 10 cm are classified as big and can result in complete destruction and catastrophic fragmentation.

From the above discussion, the need for space debris mitigation is clear. Unless active removal of existing orbital debris actually happens, the amount of debris larger than 10 cm will continue to increase due to collisions between existing satellites and fragments, even if no new missions are launched, [87] and [88]. It is expected that the number of total space debris is set to increase by at least 5% per year. As the number of artificial satellites and debris orbiting Earth increases, the probability of collisions between satellites also increases. These collisions produce orbiting fragments, each of which would increase the probability of further collisions, eventually leading to chains of successive collisions, leading to the growth of a belt of debris around the Earth, a situation that is called the Kessler Syndrome.

Several methods for debris removal have been proposed, which are presented in Table 1-1, for debris larger than 10 cm [19]:

Table 1-1. Debris removal methods.

<i>Method</i>	<i>Orbit / Target Size</i>	<i>Comments</i>
Solar and Magnetic Sail	LEO, MEO, GEO / >1m	Drag augmentation, limited to larger debris. Attachment of sail and sail technology complex, unproven.
Momentum and Electrodynamic Tethers	LEO / >10cm	Attractive in principle, cost. Numerous engineering challenges, unproven concept
Capture Vehicle	LEO, MEO, GEO / >10cm	Manoeuvrable spacecraft that captures targets, functions in different orbits. Technical and operational requirements.
Attachable De-orbiting Module	LEO, MEO, GEO / >1m	Functions in different orbits, technology in development.

Most of these methods lack the needed technical and scientific maturity to become viable solutions for the near and mid-term future and rely on unproven technology. In the case of tethers and solar sails, there has yet to been a proof of concept let alone an actual debris demonstration and it is unlikely that they will be technologically mature by 2020-2025. Additionally, the uncontrolled re-entry of debris poses additional risks.

Besides orbital debris mitigation tasks, another important area where handling of a secured passive object in space is required is satellite refueling. Fuel is a very scarce and important commodity in space. Since currently there are no refueling capabilities, for the majority of the existing satellites, operational life is terminated when they run out of fuel, while their other subsystems are still operational [21]. This practice leads to a tremendous waste of resources and money spent for the construction and installation of the satellites in the orbital environment, not to mention the billions of dollars that have been paid out in insurance claims. This also leads to the derelict satellites being left as orbital debris, not only increasing their number, but also the probability of them colliding with each other, thus leading to a further increase of the number of orbital debris, which is a very serious issue as already discussed. The existence of refueling options for the orbiting satellites would greatly extend the life of satellites, while lowering the increase of the orbital debris.

Recently, the importance of orbital refueling has been acknowledged and several servicing-refueling (test) missions have been proposed. A proposed architecture involves the existence of orbital propellant depots. In this scenario, satellites in need for refueling will be towed to a fuel depot for servicing. The handling of the passive fuel-less satellite must be performed by a number of orbital servicers, in order to move it with respect to the depot, in Cartesian space.

From the abovementioned cases it is clear that robotic OOS will soon be in high demand, with handling of a passive object being one of the most important tasks, with several critical applications.

1.2 Literature Review

1.2.1 On-Orbit Servicing

Since the dangerous repairs due to the loss of Skylab's sun shield in 1973, tools, techniques, robotics and spacesuits have been improved immensely. The increasing need for OOS was demonstrated by servicing missions as early as the 80s, such as the 1984

retrieval missions (the Solar Max retrieval, repair and reposition by astronauts in the Space Shuttle Challenger [79], and the retrieval of two more satellites using Manned Maneuvering Units, and their return to Earth for repair [47]) and the 1984 Orbital Refueling System (ORS), in which components of the ORS were connected in an EVA demonstrating that it is possible to refuel satellites in orbit [86]. The Hubble repair missions that came later [59] were so successful that questions arose regarding whether we might try repairing and refueling satellites that weren't designed to be serviced, even more so since the Hubble repair missions also demonstrated how much servicing missions can be augmented by the use of robotic mechanisms, as can be also seen in Figure 1-4.

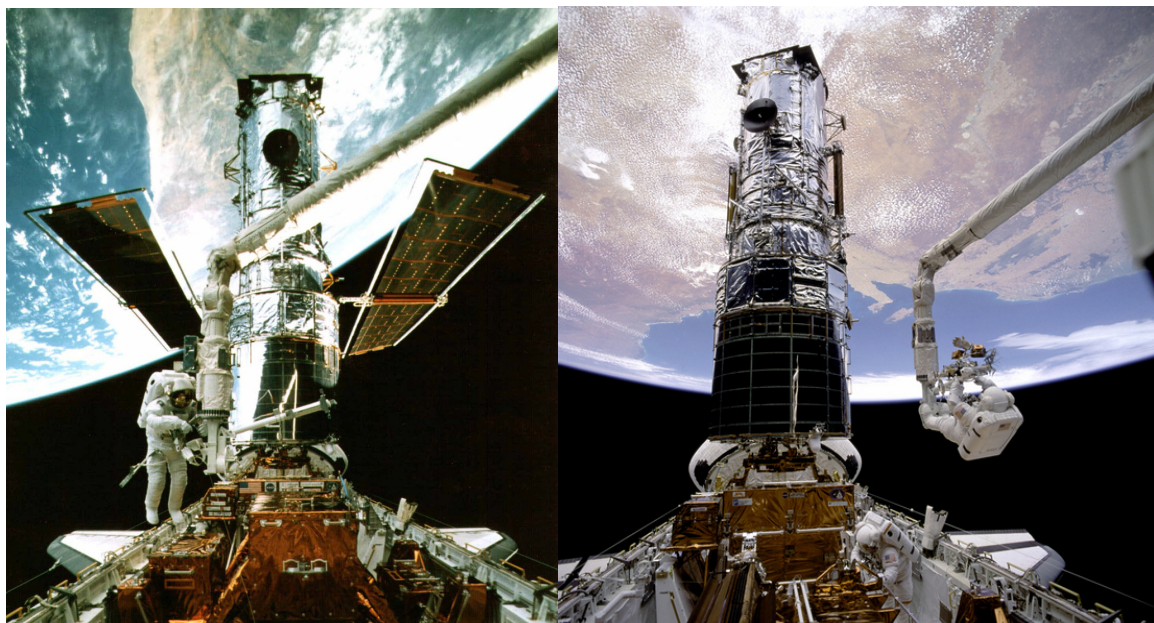


Figure 1-4. Astronaut Steven Smith working at the end of Discovery's Canadarm as he did maintenance work on the Hubble Space Telescope, on February 15, 1997 (left). Astronauts F. Story Musgrave, anchored on the end of the shuttle's robotic arm, and Jeffrey A. Hoffman inside the orbiter's payload bay, conduct the fifth and final spacewalk to fix Hubble during the shuttle Endeavour's 1993 servicing mission to the orbiting observatory (right) (source: NASA).

During the last two decades, robotic OOS has been discussed and a number of architectures have been proposed [30], [35], [75], [76], [113]. To relieve astronauts from EVA, enhance performance and extend the range of feasible tasks, besides the numerous instances where a robotic manipulator aided astronauts in these tasks [45], [59], the international research community has been focusing on the realization of autonomous robotic OOS, having produced theoretical approaches and test-beds [102], [16], see also Figure 1-5, as well as some very promising experimental platforms, already tested in space, such as the ROCVISS system on ISS [14], [93].

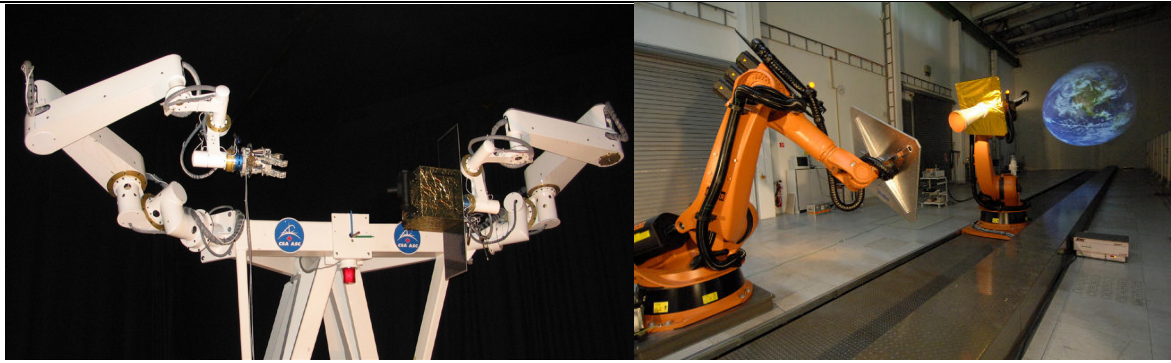


Figure 1-5. Experimental test-beds for OOS scenarios emulations. On the left is the robotic docking emulator of CSA (source: CSA). On the right, the EPOS system of DLR is simulating the relative motion between a target and a chases satellite (source: DLR).

The first robotics demonstration mission in space, was DLR's Robot Technology Experiment (ROTEX). Although ROTEX was teleoperated, it was the first successful attempt to study and experimentally demonstrate robotics technologies in space, performing a variety of different applications, aiming among others at assembly and external servicing demonstration tasks, such as assembling of mechanical truss structure, connection/disconnection of electrical plug and grasping of floating object [94]. The first notable case of autonomous OOS demonstration flight was JAXA's Experimental Test Satellite VII (ETS-VII), see also Figure 1-6, with the objective to verify robotic technologies for autonomous orbital operations such as ORU exchange, deployment of a space structure and capture and berthing with a target satellite [117].

The goal of the 2005 Demonstration for Autonomous Rendezvous Technology (DART) program was to demonstrate completely autonomous on-orbit rendezvous between DART and the Multiple paths Beyond-Line-of-sight COMMunications (MUBLCOM) satellite [90]. While DART did not proceed as planned, the lessons learned from the mishap helped enable the future development of autonomous OOS, such as the highly successful Orbital Express, which is the most known effort in autonomous rendezvous, docking and refueling (among other OOS tasks), seen also in Figure 1-6. The OOS tasks successfully demonstrated by the Orbital Express mission consisted of six rendezvous exercises and several refueling and Orbital Replaceable Unit (ORU) replacement tasks. The rendezvous exercises included station-keeping, elliptical and circular fly-around inspections, corridor approaches to fixed and rotating target satellite, day and night captures, both direct and robotic-arm ones, demonstrating the first fully autonomous rendezvous and direct capture and autonomous and ground-commanded

aborts. The refueling tasks consisted of fifteen propellant (hydrazine) transfers at varying levels of autonomy both pressure-fed and pump-fed and both from servicer to target satellite and from target satellite to servicer, while eight ORU transfers also took place, consisting of both supplemental battery and backup flight computer units at varying levels of autonomy both from servicer to target satellite and from target satellite to servicer [54].

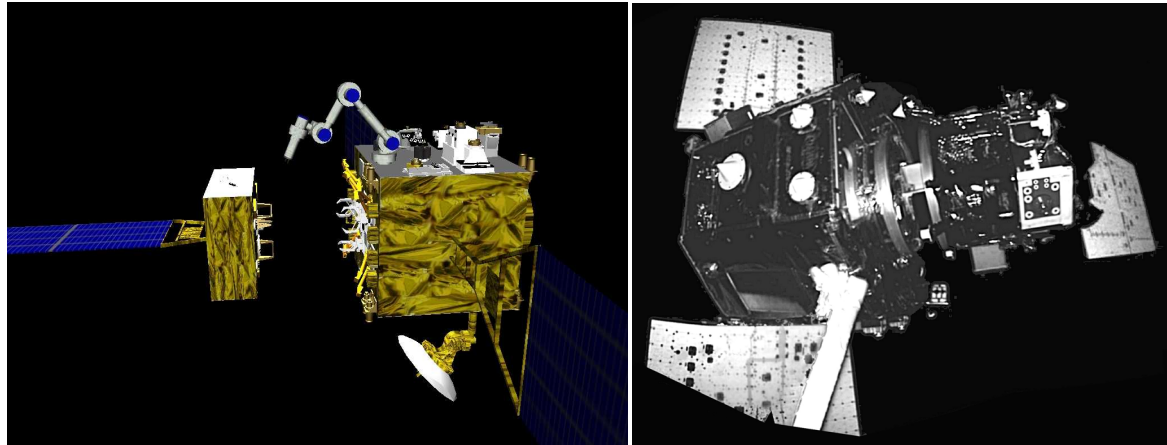


Figure 1-6. OOS successful tests. On the left, an artist's representation of the ETS-VII experiment (source: JAXA). On the right, the Orbital Express experiment docking phase, as photographed by a camera at the end-effector of its own manipulator. (source: DARPA).

Besides these missions that have been completed in the past, there are also on-going robotic missions and test-beds in space, both autonomous and teleoperated, such as the ISS robotic arms. These are CSA's Shuttle Remote Manipulator System (SRMS), also known as Canadarm [50], Mobile Servicing System (MSS), also known as Canadarm2 [51] and the Special Purpose Dexterous Manipulator (SPDM) also known as Dextre [52] and JAXA's Japanese Experiment Module Remote Manipulator System (JEMRMS) [44]. ESA's European robotic Arm (ERA), is going to be added the ISS manipulators in the near future [55]. Most of these manipulators are seen in Figure 1-7.

Another notable ongoing robotic project, currently on board the ISS, is NASA's human-like (torso, head and arms) robot Robonaut 2, also seen in Figure 1-9, which is designed in order to use tools designed for humans and its primary objective is to test human-like robotic operation in zero gravity and the feasibility of a human-like robot to work "shoulder-to-shoulder" with astronauts [27].

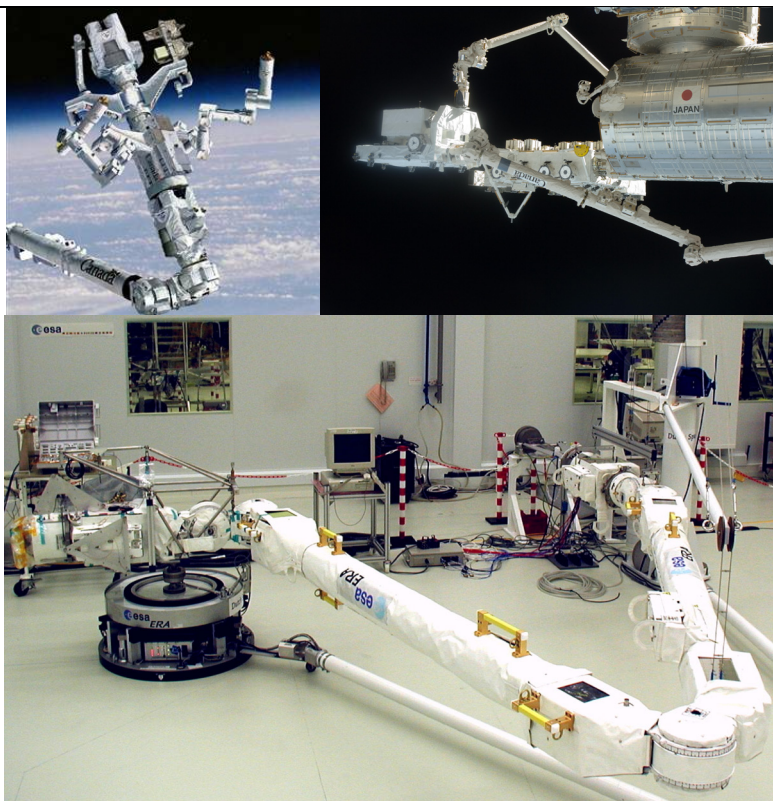


Figure 1-7. Dextre, as photographed by an Expedition 27 crew member (top left), JEMRMS on the exterior of the Kibo laboratory of the ISS and the station's Canadarm2 (top right), (source: NASA) and ERA undergoing tests at ESA's facilities (source: ESA).

Recently, NASA proceeded with another complex scenario: refueling and servicing satellite systems not designed for such tasks, namely the Robotic Refueling Mission (RRM), seen in Figure 1-8. For the purposes of this project, NASA has developed mock-up systems, which resembled a target satellite (RRM module) and dedicated tools to be operated by Dextre.



Figure 1-8. Dextre robot moves the RRM Multifunction Tool towards the RRM module (left) and the Dextre robot performing a new set of satellite-servicing tasks on the RRM module, during the second part of the Gas Fittings Removal task (right), (source: NASA).

The RRM performed the phase 1 of its demonstration mission, which consisted of using the tools to remove the fittings that many spacecraft have for the filling of special coolant gases, snipping lock wires and removing caps, accessing a fuel valve similar to those commonly used on satellites today and transferring liquid ethanol through a sophisticated robotic fueling hose. Moreover, it also performed tasks such as removing the coaxial radio frequency (RF) connector, robotically unscrewing of satellite bolts (fasteners) and finally slicing off thermal blanket tape and folding back a thermal blanket to access the contents underneath. After successfully completing the first phase of its mission, the RRM waited for the delivery of the second tool pack, required for the phase 2 of the mission, which includes among others, cryogen replenishment tasks and close-range and midrange inspection [48].

The first and maybe the least complex task of OOS, is inspection, for which two main approaches have been proposed and already tested in space. The oldest and most reliable approach is to mount the visual sensor on a robotic manipulator and guide the manipulator so as to inspect space structures [40], [72]. This method, though, poses several restrictions due to manipulator finite work envelope and the need for teleoperation for safety reasons. To overcome these restrictions free flying camera systems have been developed [7], [36], [104] while some have been already tested in space [36], [104], see also Figure 1-9. Moreover, some other concepts are currently in the phase of development [80], [111].



Figure 1-9. Robotic systems tested inside the ISS. On the left, Expedition 18 crewmember Michael Fincke as he works with SPHERES in the US Laboratory of the ISS. On the right, Robonaut 2 humanoid robot holds an instrument to measure air velocity during another system check out in the Destiny laboratory of the ISS. (source: NASA).

Another very important task is formation flying. Two missions that have successfully demonstrated the feasibility of autonomous formation flying in space are the Experimental Satellite System 11 (XSS-11) mission, which demonstrated accurate detection, tracking and pose estimation of on-orbit targets [35] and the Prototype Research Instruments and Space Mission technology Advancement (PRISMA) mission, main goals of which were to perform Autonomous formation flying, homing and rendezvous, proximity operations or rendezvous tests, including final approach and recede operations, as well as sensor technology experiments [42]. Artist's representations of both missions are shown in Figure 1-10.



Figure 1-10. Artist's representations of: XSS-11 satellite (left), (source: US Air Force Research Laboratory/MDA) and the PRISMA mission (right), (source: SSC).

Important robotic tasks, such as orbital assembly and debris handling, require passive object handling capabilities. The first step in the handling procedure is to securely grasp the passive object. This procedure includes tasks such as motion identification and matching, the actual docking and even de-tumbling of the passive object, whenever this is necessary. Studies in this field have provided several theoretical approaches and experimental facilities [3], [4], [5], [6], [16], [65], [78], [89], [102], [105], [115], [116], [118], [119], [120]. Besides the already mentioned past missions of ROTEX, ETS-VII, DART and Orbital Express, several architectures and autonomous docking missions are currently at various stages of development. Note that most of these missions also include a form of OOS, such as ORU replacement, refueling or handling of a firmly grasped passive object. TECSAS (TECHnology SATellite for demonstration and verification of Space systems) was a project consisting of a servicer satellite equipped with a robotic arm and a target microsatellite to be captured and serviced in orbit [108]. While the multi-nation effort of TECSAS was discontinued in 2006 due to the priority shift of some participating agencies, Germany nevertheless continued their development work under the Deutsche

Orbital Servicing Mission (DEOS) mission. This project is an in-flight technology demonstration mission focusing on the robotics approach to both service and dispose of malfunctioned satellites in LEO [49], [95]. Artist representations of both missions are shown in Figure 1-11.



Figure 1-11. Artist's representation of the TECSAS system (left), (source: CSA) and the DEOS system (right), (source: Space Tech GmbH).

Also in Europe, the project ConeXpress-OLEV was conducted under ESA's ARTES 4 public-private-partnership initiative. This type of service was tailored to client satellites whose payload still works properly but who ran out of fuel, using the OLEV as a post-docking extension of the serviced satellite that provides the required propulsion and navigation capabilities (Figure 1-12). Rendezvous and docking is divided into three separate phases: final transfer, rendezvous and docking [21]. At some point, the main contractor of the ConeXpress-OLEV project pulled out and the remaining partners formed in 2007 a new venture, offering the SMART-OLEV project (Figure 1-12).

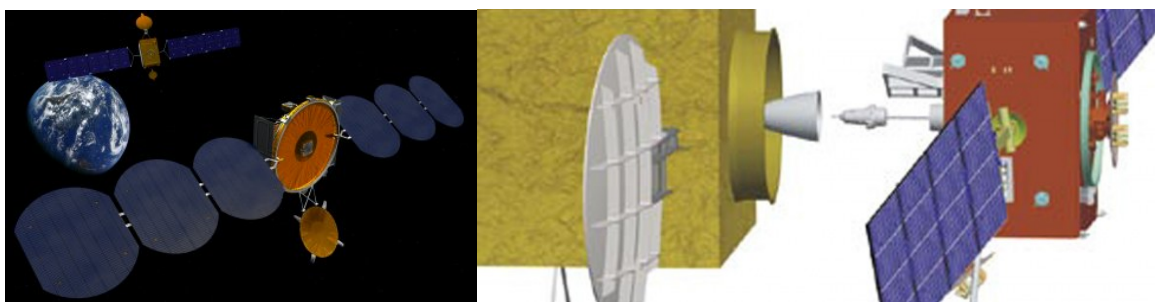


Figure 1-12. Artist's representations of ConeXpress-OLEV (left), (source: Orbital Recovery Corp.) and SMART-OLEV (right), (source: NordicSpace).

A typical SMART-OLEV servicing scenario would consist of orbit transfer in order to match the serviced satellite orbit, rendezvous and docking phase and on station operations. The latter include navigation and guidance to keep the client satellite in its

proper orbital slot while also removing inclination from it. At end-of-life the client will be transferred to a disposal orbit and an undocking process will be performed [66].

The Spacecraft for the Universal Modification of Orbits (SUMO) sponsored by DARPA, was going to demonstrate machine vision, robotics, and autonomous control on board the satellite to accomplish an automatic rendezvous [76]. The SUMO program was renamed to Front-end Robotics Enabling Near-term Demonstration (FREND) with the objective of performing autonomous rendezvous and docking with satellites that have not been built to enable robotic servicing [68], see also Figure 1-13. The FREND robotic arm is being currently utilized in a new DARPA OSS program, called PHOENIX, which is aimed at removal and reuse of some existing parts of decommissioned satellites in GEO orbit and its first keystone mission in 2015 plans to demonstrate harvesting an existing, cooperative, retired satellite aperture, by physically separating it from the host non-working satellite using on-orbit grapple tools controlled remotely from the earth [110] (Figure 1-13).



Figure 1-13. The FREND under full-scale rendezvous and autonomous robotics grapple testing (top), (source: Naval Research Laboratory) and an artist's representation of the PHOENIX OOS program (bottom), (source: DARPA).

Space Infrastructure Servicing (SIS) is a spacecraft being developed by Canadian aerospace firm MacDonald, Dettwiler and Associates (MDA) to operate as a small-scale in-space refueling and servicing depot for communication satellites in geosynchronous

orbit. The SIS servicer would rendezvous and dock with the target satellite, attaching itself to the ring around the satellite's apogee-boost motor (Figure 1-14). Controlled from a ground station, the SIS robotic arm would then reach through the nozzle of the apogee motor to find and unscrew the satellite's fuel cap. Finally, the SIS vehicle would reclose the fuel cap after delivering the agreed amount of propellant [61].

In the United States, ViviSat and ATK (Alliant Techsystems Inc.) have been developing a tug technology to provide supplemental attitude and propulsive capabilities. Named the Mission Extension Vehicle (MEV) it provides life extension and other services. MEV will connect to the target satellite in the same way as MDA's SIS, but will not transfer fuel (Figure 1-14). It will rather use its own thrusters to supply attitude control for the target, in a concept very similar to the European OLEV [60].

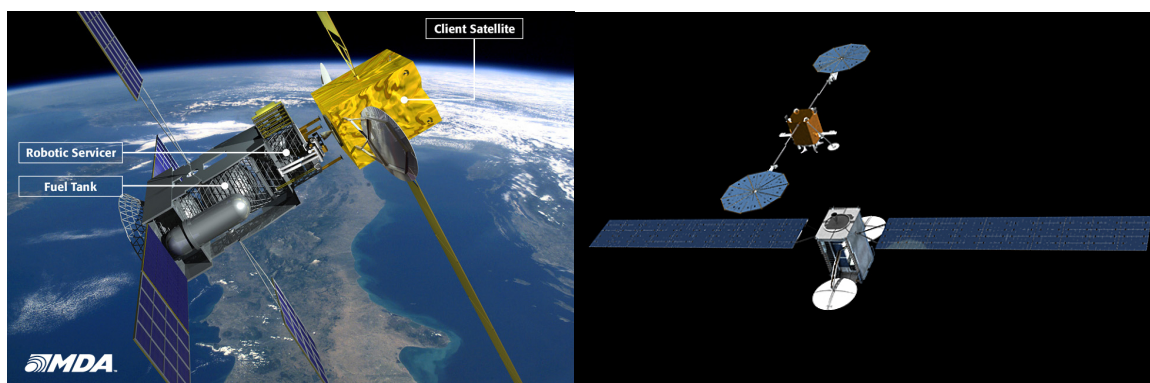


Figure 1-14. Artist impressions of: a servicing satellite refueling another satellite in Earth orbit (left), (source: MacDonald Dettwiler Associates Corporation) and of ATK satellite (the base for the MEV project), as it approaches a satellite to be serviced (right) (source: ATK)

1.2.2 Handling of a Passive Object in Space

Actual handling of a secured passive object has not been studied adequately and issues such as large object handling remain open. On-orbit object handling has similarities to cooperative manipulation of passive objects on earth [17], [20], [22], [31], [33], [34], [39], [67], [70], [77], [81], [82], [103], [112], with the additional complexities that in space no fixed ground to support the manipulators exists, thus letting momentum changes to play a key role in body motion. In addition, the development of control forces is of an on-off nature, thus reducing system positioning capabilities.

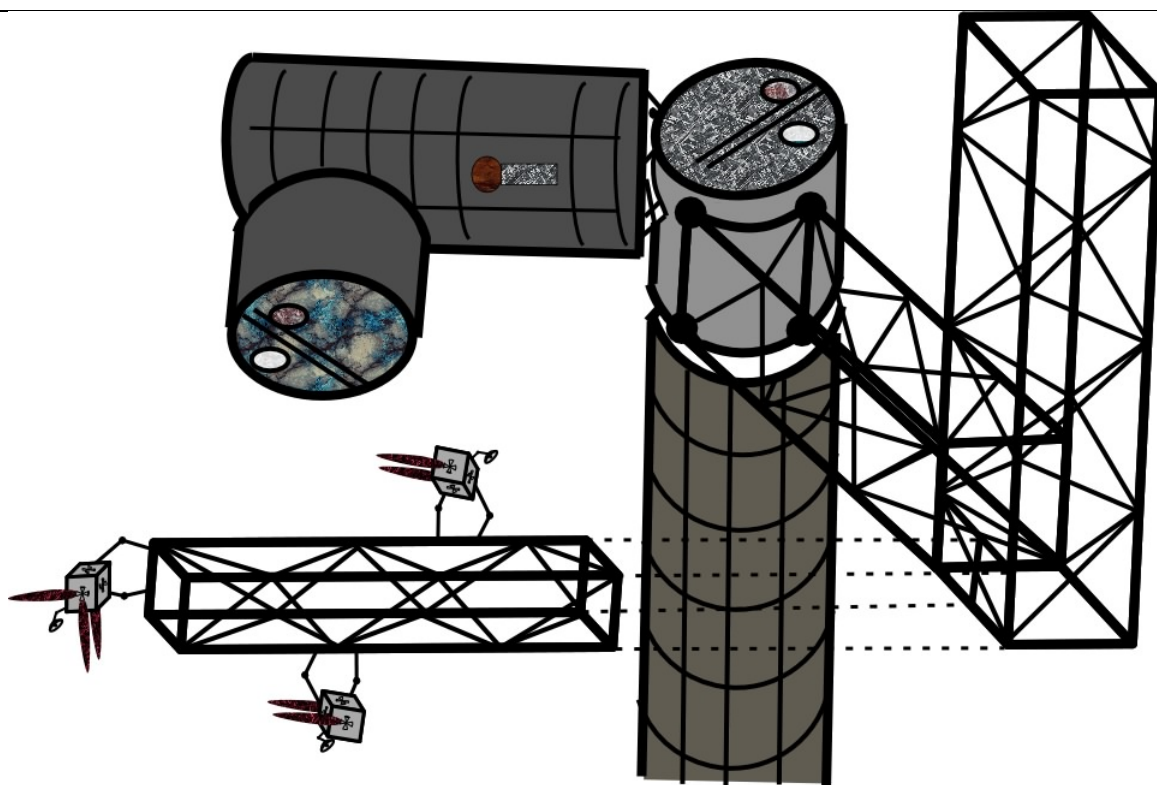


Figure 1-15. Handling of a rigid passive body by a number of cooperating free-flyers equipped with manipulators, in space structure assembly operations.

Another issue that frequently is a key aspect of a passive object handling process is the force distribution. Whenever a desired generalized force must be applied on a passive object through a number of servicers, a procedure must be found to distribute this force to the servicer end-effectors. Several methods for force distribution, developed for terrestrial systems, exist in the literature, depending on the problem solved, i.e. number of contacts, type of contacts, type of motion expected, etc. [74], [24], [15], [23], [25]. In the case of systems in space, no fixed base exists, and a servicer's base is "flying" consuming thruster fuel.

Although several prototype robotic servicers have been proposed and studied since the 1990's [54], [78], [113], [117], [119], only a few studies exist concerning the dynamics and control of an already secured object. Dubowsky et al. proposed a control method for handling large flexible objects, aiming at reducing flexibility-induced vibrations. Robotic servicers use their thrusters as a low frequency control of rigid body motion, and their manipulators, as a high frequency control, cancelling out vibrations this motion causes on the flexible modes [29]. Moreover, Yoshida and Abiko proposed an adaptive controller in order to cancel out vibrations caused by flexibilities in the manipulator structure itself [1]. Fitz-Coy and Hiramatsu presented a post-docking control approach based on game theory,

minimizing interaction forces, and thus helping avoid the loss of firm grasp [41]. Moosavian et al. presented a passive object manipulation method by a single servicer with multiple manipulators, aiming at an object prescribed impedance behavior, in case of contact with the environment [84]. In a simplified 2D example, Toglia *et al.* presented a multiple servicer manipulation method of a passive object, focusing on the modularity of the system, and taking advantage of actuation and sensor redundancy, [114]. Everist et al. proposed a free-flying servicer concept for handling and assembling space construction rods, using proportional thrusters under PD control [32].

Orbital system thrusters, though, are of on-off control nature. To protect thruster valves from the extreme space conditions, proportional or Pulse-Width-Modulation (PWM) thrusters are not used in space, at least not as PWM is used on terrestrial systems. This is because, in order to generate low control inputs (e.g. when the tracking errors need to be kept low), a typical PWM controller would have the thrusters switching rapidly (several thousand times per second – motor PWM reaches a frequency of 30 KHz), aiming at precise approximation of proportional control forces. Unfortunately, electromechanical thruster valves are not able to follow the rapid PWM commands of the controller, thus deteriorating the response of the controller and generally its overall performance. Rapid on-off switching of a thruster may result in valve closing before it has fully opened, or opening before it has closed fully. This leads to the formation of ice in the nozzle, which leads to deterioration of the performance of the thruster and eventual damages. For this reason, space systems thrusters have a *minimum on* and *off* time. For example, the performance of ASTRIUM thrusters deteriorates to levels below 80%, if the duration of thrust pulses is less than 300 ms, even for 1N thrusters [11]. On the other hand, in order for 10N thrusters to perform at 100% of their capability, a minimum thrust pulse duration of 500 ms is required [12].

Simple on-off thruster operation is not subject to these limitations and is preferred in space applications. However, on-off thrusting results either in chattering, which wears the thrusters and increases fuel consumption, or in deadband-induced limit cycles, that reduce fuel consumption but also positioning accuracy [18], [71], compared to non on-off control. A form of PWM, called Pulse-Width-Pulse-Frequency (PWPF) modulator, can take into account minimum on and off times, and therefore can be (and is) employed in space systems, along with simple on-off thruster operation [10]. However, such modulators are

used in attitude control where thruster firing is sparse, and not in trajectory tracking of an object, where the controller must update thrust values several times per second.

A spatial system of robotic servicers handling a passive object, is highly non-linear. However, a general non-linear system robustness theory is not developed yet [69]. Rather, most works focus on the special characteristics of the system under discussion, taking them into account to prove stability under uncertainties, as, for example, in [13], [2]. A possibility is to use linearization, under certain assumptions, in order to be able to use linear systems robustness tools [28].

1.3 Contribution

The main contributions of the present work are:

1. The introduction of a number of manipulator-equipped free-flying servicers for the cooperative manipulation of passive objects on orbit, where both on-off thruster propulsion and manipulator continuous forces/ torques are used for passive object handling. It is shown that, since the relative motion between the servicers and the passive object only needs to be bounded, the servicers can be free to move in some envelope with respect to the passive object under scarce thruster firing, while their manipulators can apply continuous forces on the passive object, filtering the on-off thruster force effects on it.
2. The introduction of a system (manipulator-equipped free-flying servicers) that can handle a passive object in space, both for the case of firm grasp and for the more general case of point contact, between the servicer manipulator end-effectors and the passive object. The latter was deemed necessary, even though it is a far more restrictive case, since appropriate appendages that can be used as firm grasp handles, are not always available (e.g. in the case of orbital debris handling).
3. The design of a controller for the *free-flying servicer manipulators* that enables the stable handling of the passive object by the servicers, in trajectory tracking scenarios.
4. The design of a controller for the *free-flying servicer bases* that enables them to move within the workspace of their manipulators, under the influence of the reaction generalized forces from their manipulator bases.
5. The development of a two-layer optimization process that allows for (i) optimal selection of contact points between the manipulator end-effectors and the passive object, for both contact cases and for (ii) force distribution so that the required control generalized force for the passive object motion, is applied by the manipulator end-effectors.

6. The sensitivity of the controller for the 3D motion of the handled passive object in space in terms of parameter estimation was also studied in this work.

7. An initial study of the limits of the motion of the passive object, when the servicers are utilizing only their manipulators (thrusters being turned off), was also conducted.

8. An initial comparison between the choice of three small free-flying robotic servicers and a single, larger one was also conducted.

1.4 Thesis Summary

This thesis consists of five chapters. The **first chapter** is an introductory one, which includes the motivation and the contribution of this work, as well as the literature review. The **second chapter** presents two servicing concepts and analyses them through simplified one-dimensional models. In the first concept, to capture orbital debris, a net held by a ring is controlled by a number of free-flying robotic servicers equipped with manipulators. In the second concept, a passive object is handled by a number of free-flying robotic servicers equipped with manipulators, in order to perform a trajectory tracking motion, while at the same time mitigating the limit-cycle effects. Two one-dimensional simplified models are presented (one for each concept) and basic insight is obtained to evaluate the concept feasibility. This leads to the adoption of the second concept as the more promising and the one that is to be further analyzed in the subsequent chapters.

In the **third chapter** the main issues of a spatial system of a number of manipulator equipped robotic free-flying servicers handling a passive object are presented. The dynamics of such a system are developed, with the free-flying servicers using both on-off thrusters and manipulator continuous forces/ torques applied on an object, in order to remove the effect of limit cycles on the object, and improve its handling both in terms of accuracy and of fuel consumed. Both the case of object firm grasp by manipulator end-effectors, and the more restrictive case of point contacts are presented and studied. The main differences in the passive object motion between the cases of a single, large servicer versus a number of smaller servicers are also discussed. An initial study of the limits of the motion of the passive object, when the servicers are utilizing only their manipulators (thrusters being turned off), is conducted for the case of object firm grasp by manipulator end-effectors. Then, the controller of the passive object trajectory tracking motion is derived, based on insight gained by the one-dimensional model study, for both contact cases. The main issues for such a controller are discussed, such as force distribution and

generalized forces constraints, and a two-layer optimization process is proposed as a solution. The top-level optimization is running off-line and providing the optimal contact points for the manipulator end-effectors, while the low-level is running on-line and acts as a force constrained distribution method. Then, the controller for the robotic servicer bases motion is developed. Since the relative motion between the servicers and the passive object only needs to be bounded, the servicers are allowed to freely move in some envelope with respect to the passive object under scarce thruster firing, while their manipulators can apply continuous forces on the passive object, filtering the on-off thruster force effects on it, thus aiming at lower fuel consumption and tracking errors. Finally, the stability and parametric uncertainty robustness of the passive object motion is also presented at this section.

In the **fourth chapter**, the validity of the developed theory for the spatial system is demonstrated via simulations. First, the simulation environment is briefly presented. Then, a number of simulation results are presented in order to verify whether or not it is better, in terms of fuel consumption, for the same passive object tracking errors to have pure on-off control (i.e. servicers firmly attached on the passive object) or manipulator equipped servicers, for both manipulator end-effector grasping modes, when the goal is trajectory tracking control of a passive object. Finally, simulation results on the comparison between the case of a single, large servicer versus the case of a number of small servicers, for the handling of a passive object, are also presented.

In the **fifth chapter**, the main conclusions of this research are briefly presented, as well as the suggested future work.

The thesis is accompanied by a CD in which the full text of the thesis is included, as well as the files needed to reproduce the simulation results.

The main parts of this thesis have been published in refereed international conferences and a journal [98], [101], [100], [96], [97], [99].

2 Servicing Concepts

In this section, a number of concepts of OOS tasks are presented and briefly discussed. Concepts for the two most promising OOS tasks are presented in more detail. The first task is the capture of tumbling orbital debris, by a net deployed by a number of manipulator-equipped, free-flying robotic servicers. A simplified model is presented and a controller is derived, in order to gain basic insight on the concept. The performance of the system is then briefly discussed. The second task is the handling of a passive object in space, by a number of manipulator-equipped, free-flying robotic servicers. A one-dimensional simplified model is presented and a controller is developed, in order to gain basic insight on the concept. The performance on the system is briefly discussed and based on the performance of the simplified models, a choice is made regarding to which one shows more promise, in terms of feasibility and performance.

2.1 On-orbit Servicing

There are several tasks in the field of OOS that are quite important in terms of addressing real orbital servicing problems, while at the same time posing significant research questions. At the early stages of this work, two OOS areas with particular merit were discussed, namely the one of capturing/de-tumbling an uncontrollable passive object and the one of handling an already captured uncontrollable passive object.

To tackle these challenging tasks, a number of novel ideas were created, as can be seen in Figure 2-1. In Figure 2-1a, the capturing of a tumbling passive object by means of a net controlled by a number of free-flying servicers, is depicted. The servicers control the position of a ring, on which the net is secured. The net has some degree of elasticity, allowing a bouncing motion that keeps the passive object in contact with the net. In Figure 2-1b, another scenario for the capturing of a tumbling passive object is depicted. In this case, a somewhat flexible appendage with an actuated hook-like end-effector gripper is used to hook on an appropriate appendage of the passive object and then firmly grasp it. The flexibility of the servicer appendage would provide enough time to the end-effector gripper to firmly grasp the passive object appendage. This approach would lead the servicer to a tumbling motion along with the passive object, a motion that can be mitigated and eventually brought to a halt, by the servicers' thrusters. In Figure 2-1c the scenario of capturing a tumbling passive object by hitting it by a harpoon-like object, fired from the

servicer and connected to it by a tether, is depicted. Again, the servicer may be forced to a tumbling motion, which can be alleviated by its thrusters. Note that this method can be used only on passive objects that are characterized as non-reparable orbital debris, since it may very well be catastrophic for the passive object.

In Figure 2-1d and e, the task of handling an already captured passive object, by a number of manipulator equipped servicers, is depicted. In Figure 2-1d the manipulator end-effectors can firmly grasp the passive object by an appropriate appendage, while in Figure 2-1e there is only point-contact between the end-effectors and the passive object.

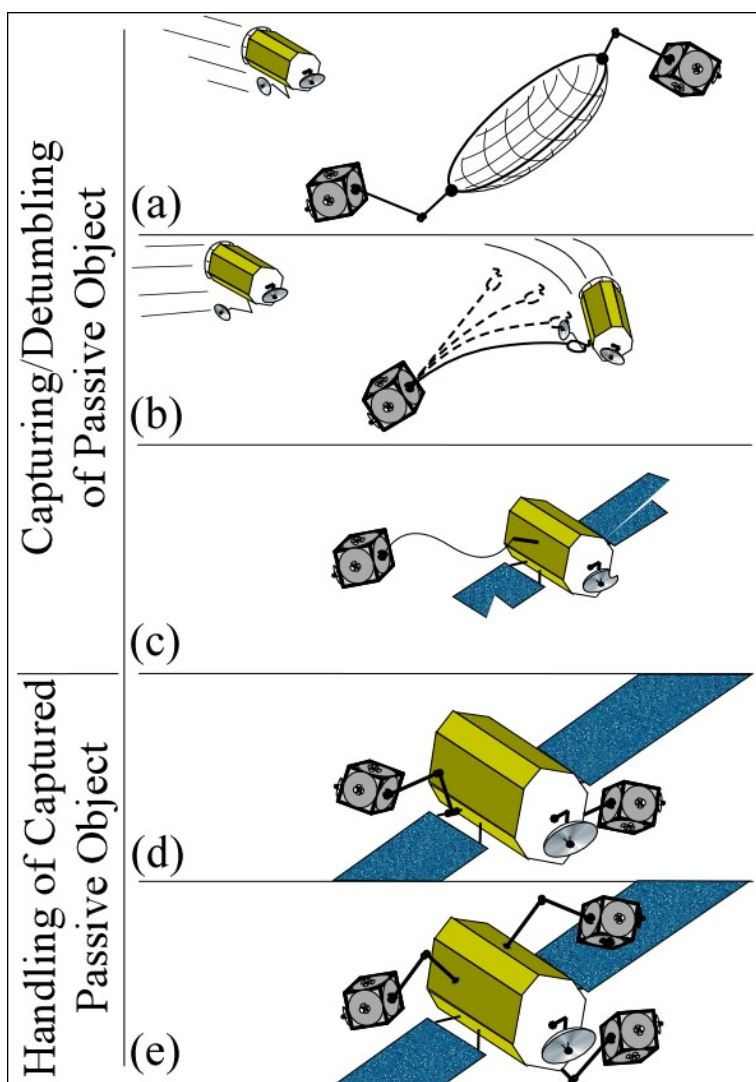


Figure 2-1. OOS concepts. (a) – (c) capturing and (d) – (e) handling tasks.

In Table 2-1, the advantages and disadvantages of each scenario are presented. Case (c) is rejected, not only because it can be used only where the integrity of the passive object to be captured is of no concern (debris), but mainly because of the risk of producing additional small orbital debris, during the impact. Even though case (b) displays lower risk

of harming the captured object, the higher complexity in the motion matching and the higher risk of losing the object led to the choice of case (a) to be studied. Moreover, because of the risk of harming the passive object during the impact with the net, this case will be studied as an Orbital Debris Disposer, even though this is somewhat restrictive. Finally, both cases (d) and (e) are going to be studied as two alternative (but very similar nevertheless) scenarios of the handling of an already captured passive object task.

Table 2-1. Advantages and disadvantages for the proposed OOS concepts depicted in Figure 2-1.

	Advantages	Disadvantages
(a)	<ul style="list-style-type: none"> * No need for motion alignment * Can capture both debris and satellites 	<ul style="list-style-type: none"> * May harm an operable satellite
(b)	<ul style="list-style-type: none"> * Can capture both debris and satellites, with lower risk of harming a satellite 	<ul style="list-style-type: none"> * Need for hook position matching with the object appendage motion path * Higher risk of losing the object
(c)	<ul style="list-style-type: none"> * No need for any motion alignment * No need for motion control during capturing 	<ul style="list-style-type: none"> * Harmful and invasive. Only valid for debris retrieval. * Impact may result in additional small debris creation
(d)	<ul style="list-style-type: none"> * More secure * Proportional manipulator forces provide more flexibility than pure on-off control 	<ul style="list-style-type: none"> * Need for an appropriate appendage on the passive object
(e)	<ul style="list-style-type: none"> * No need for appropriate appendage on the passive object (more general case) * Proportional manipulator forces provide more flexibility than pure on-off control, in terms of accuracy and higher manipulation capabilities 	<ul style="list-style-type: none"> * Less secure

The two chosen scenarios, namely the capturing of a passive object by means of a net controlled by free-flying servicers (for capture) and the handling of a passive object by a number of cooperating, manipulator-equipped free-flying servicers (for handling) are studied in detail both for the firm grasp and point contact case, through simplified one-dimensional models.

2.2 Orbital Debris Disposer

A main problem in capturing orbital debris is that there is no predetermined way of grabbing them, since they include no attachment points. Moreover, their motion can be complex, as they may be tumbling in orbit, making it even more difficult to track and capture, even if their motion itself is predictable. This work studies a method of capturing orbital debris, employing a coordinated swarm of free-flying robots. Using their manipulators, these free-flyers move a rigid ring with a net, and fly before the debris with a relative velocity such that the debris is slowly approaching the net, see Figure 2-2. As the debris is approaching, for safety and fuel economy reasons, the robots turn to free-floating mode, i.e. their satellite base is uncontrolled [92], and wait for the collision. The collision must be such that the robot system and the debris will continue moving together, with the debris in the net, thus making it much easier to remove it from the orbit. To do this, the robot system initial configuration and velocities, as well as the gains of the manipulator joint control algorithms must be chosen appropriately. In the present work, the study of a one-dimensional model of the interaction is presented as a proof of concept, but also aiming at a better understanding of the behavior of such systems.

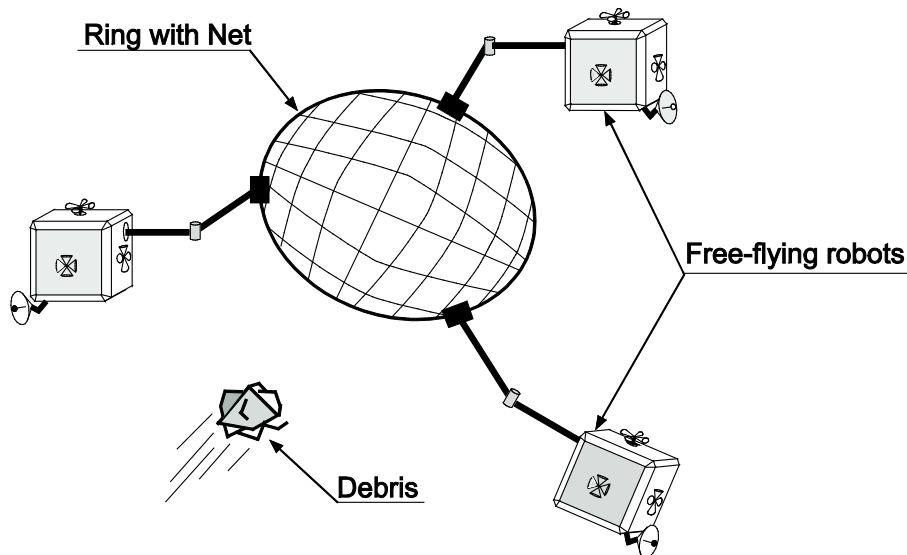


Figure 2-2. Graphic representation of the Orbital Debris Disposer.

2.2.1 Simplified Model Analysis

The system in Figure 2-2 is modeled as a uni-dimensional three-body system, see Figure 2-3. Body m_1 represents the debris, body m_2 with the spring k and the damper b represent

the net, and body m_3 , the free-flying satellites. The manipulators apply forces u . The natural spring length is x_0 .

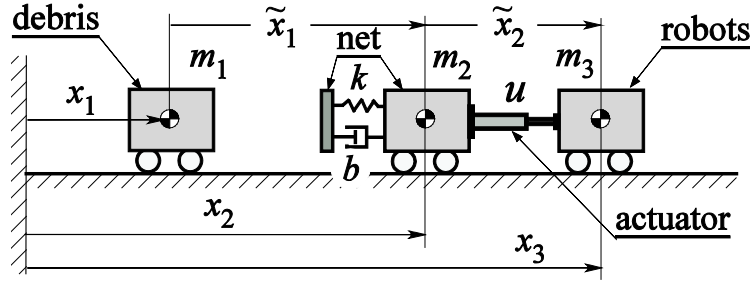


Figure 2-3. A 1D model of the orbital debris disposer.

The system equations of motion, describing the system, are:

$$\begin{aligned}
 & \left. \begin{aligned} m_1 \ddot{x}_1 &= 0 \\ m_2 \ddot{x}_2 &= -u \\ m_3 \ddot{x}_3 &= u \end{aligned} \right\} \text{if } \tilde{x}_1 = x_2 - x_1 > x_{net0} \\
 & \left. \begin{aligned} m_1 \ddot{x}_1 + b(\dot{x}_1 - \dot{x}_2) + k(x_0 - (x_2 - x_1)) &= 0 \\ m_2 \ddot{x}_2 - b(\dot{x}_1 - \dot{x}_2) - k(x_0 - (x_2 - x_1)) &= -u \\ m_3 \ddot{x}_3 &= u \end{aligned} \right\} \text{if } \tilde{x}_1 = x_2 - x_1 \leq x_{net0}
 \end{aligned} \quad (1)$$

where x_{net0} is the unloaded spring length of the mass-spring-dumper subsystem that describes the net. The upper part of Eq. (1) describes the system before the debris / net contact, while the lower part describes the system following the debris / net contact.

The above system has no external forces acting on it, therefore its linear momentum is conserved. Thus, by adding all three of them and integrating the result once to obtain,

$$m_1 \dot{x}_1 + m_2 \dot{x}_2 + m_3 \dot{x}_3 = L \quad (2)$$

where L is the system linear momentum. Note that if two of the velocities are driven to their desired values, the third will be given by Eq. (2). This allows us to study the first two equations of motion, in which x_3 is missing. Without loss of generality, we assume that the free spring length is zero ($x_0 = 0$), and obtain,

$$\begin{aligned}
 m_1 \ddot{x}_1 + b(\dot{x}_1 - \dot{x}_2) + k(x_1 - x_2) &= 0 \\
 m_2 \ddot{x}_2 - b(\dot{x}_1 - \dot{x}_2) - k(x_1 - x_2) &= -u
 \end{aligned} \quad (3)$$

2.2.2 Control Law and Constraints

The problem addressed next is how to actuate the manipulators so that after the collision transient, all bodies move with the *same* velocity. This is important, because

otherwise, in the absence of mechanical handles or special latching mechanisms, after the impact, the debris will separate from the net and be lost before it is captured.

From an analytical point of view, this means that two relative speeds (i.e. of the debris m_1 and of the free-flyer m_3) must be set with a single control force u (under-actuation). To achieve this, the control force u must be such that the net (mass-spring-damper) returns to its equilibrium point without overshooting, while at the same time the net and the debris acquire the desired speed. Should the mass-spring-damper system overshoot the equilibrium, the debris will acquire a velocity resulting in its loss from the net, as will be shown later on the chapter by simulation.

The analysis starts by observing that if all body steady state velocities $\dot{x}_{i,ss}$ are equal, then they must be equal to the system center of mass (CM) velocity given by:

$$\dot{x}_{1,ss} = \dot{x}_{2,ss} = \dot{x}_{3,ss} = L / M \quad (4)$$

where M is the total system mass. This observation directs us to controller force choice as:

$$u(\dot{x}_1, \dot{x}_2, L) = K_1 (\dot{x}_2(t) - \dot{x}_1(t)) + K_2 (\dot{x}_2(t) - L / M) \quad (5)$$

where K_1 and K_2 are unknown control gains. In Eq. (5), the first term attempts to make the relative velocity of the debris and the net zero, while the second one to make the absolute velocity of the net equal to the CM velocity. If two of the three bodies' velocities attain the velocity given by Eq. (4), then, Eq. (2) guarantees that the third will also be the same. Therefore, in principle this controller can achieve the goal of equal velocities.

If the input u for the system described by Eq. (3) is as shown in Eq. (5), then the general form for the response for $x_1(t)$ and $x_2(t)$, is given by:

$$x_1(t) = c_{11}t + c_{12} + c_{13}e^{\lambda_1 t} + c_{14}e^{\lambda_2 t} + c_{15}e^{\lambda_3 t} \quad (6)$$

$$x_2(t) = c_{21}t + c_{22} + c_{23}e^{\lambda_1 t} + c_{24}e^{\lambda_2 t} + c_{25}e^{\lambda_3 t} \quad (7)$$

where the c_{ij} ($i = 1, 2, j = 1, \dots, 5$) coefficients depend on system parameters and initial conditions, while the λ_i eigenvalues depend on system parameters, only. The fact that the system has an initial non-zero velocity and thus momentum (see Eq. (2)), results in the appearance of the terms $c_{11}t$ and $c_{21}t$ in Eqs. (6) and (7) respectively. This means, in steady-state, the position x_1 of the debris and the position x_2 of the net are linear functions of time and that these objects move with constant steady-state velocities, equal to c_{11} and c_{21} respectively. Note that both λ_i and c_{ij} are, in general, complex numbers.

Next, the constraints under which the system will yield the desired response are studied. These constraints are classified as (a) “stability” constraints (SC), so that the velocities of the debris, the net and the robots will converge to certain real values, (b) “contact” constraints (CC), so that the debris will not separate from the net after the impact and, (c) “assumption” constraints (AC), so that the development of the SC and the CC hold true. Starting from Eqs. (6) and (7), certain ACs are made in order to separate the different types of responses. For example, in Eqs. (6) and (7) real λ_i 's may be assumed, in order to avoid oscillations in the response, and this would be an initial AC type of constraint. Then, we examine under which SCs and CCs, each type of response yields the same steady-state velocity for all three objects, i.e. debris, net and servicer. Note that, during this process, additional ACs may have to be made. Different ACs result in different groups of constraints to be satisfied. The SC, CC, and AC combinations are grouped together and used to compute feasible solutions. In more detail, using a set of initial conditions, namely the observed relative velocities, and the system parameters, such as the body masses and the spring-damper coefficients, the various groups of constraints result in some feasible control pairs K_1 and K_2 . To this end, for a set of system parameters and initial conditions, plots of a group of constraints are drawn in the gain space (\mathbb{R}^2 , denoting all possible combinations of control gains K_1 and K_2), for identifying the feasible subspaces in which the acceptable sets of control gains lie. If at least one such set exists, it will ensure the desired response of the system. If such a subspace does not exist, a different set of constraints is tried, until a feasible set of gains results. Otherwise, since the debris velocity cannot be changed, the capturing system approach velocity may have to be adjusted by thruster firing. For brevity, here we present the analysis of only one such constraint group.

First the initial AC of real λ_i 's is made. Real λ_i 's are more likely to yield a feasible solution, since complex λ_i 's mean that the response shown on Eqs. (6) and (7) would include oscillations. Nevertheless, the cases of λ_i 's being complex or some of them being complex and some real can be treated the same way as the one that follows. With the AC of real λ_i 's and by differentiating Eqs. (6) and (7), it can be shown that all steady state velocities can be made equal to the constant c_{i1} , defined in Eqs. (6), (7), with $i = 1, 2$, if,

$$\lambda_1, \lambda_2, \lambda_3 < 0 \quad (8)$$

Equation (8) yields the only set of SC constraints, which must be satisfied to attain the desired goal. Moreover, taking into account Eq. (4), it can be shown that the following condition must hold,

$$c_{11} = c_{21} = L / M \quad (9)$$

Equation (9) is the first CC that must be satisfied, in order for Eq. (4) to hold true. Next, the remaining CCs are derived. These result from the fact that, after the first time at which the net starts deforming, the debris must be in contact with the net. Using Eq. (9), Eqs. (6) and (7) yield the initial form of the single CC:

$$\tilde{x}_1 = x_2(t) - x_1(t) = (c_{22} - c_{12}) + \sum_{i=1}^3 ((c_{2i+2} - c_{1i+2})e^{\lambda_i - 2t}) \leq x_0 = 0 \quad (10)$$

Next, Eq. (10) is analyzed aiming at obtaining conditions that are independent of instance. To this aim, additional conditions are derived from Eq. (10).

The steady state of Eqs. (6) and (7) is reached at infinite time. Then, the following must hold,

$$\lim_{t \rightarrow \infty} (x_2(t) - x_1(t)) = x_0 = 0 \Rightarrow c_{22} - c_{12} = 0 \quad (11)$$

Thus, the CC given by Eq. (10) becomes:

$$(c_{23} - c_{13})e^{\lambda_1 t} + (c_{24} - c_{14})e^{\lambda_2 t} + (c_{25} - c_{15})e^{\lambda_3 t} \leq 0 \quad (12)$$

At $t = 0$ (first contact) we have $x_2(0) - x_1(0) = x_0 = 0$, thus, from Eqs. (6), (7), (9) and (11), we have:

$$(c_{23} - c_{13}) + (c_{24} - c_{14}) + (c_{25} - c_{15}) = 0 \quad (13)$$

It is clear that the three terms in Eq. (13) cannot have the same sign. Two possibilities exist here, i.e. we may have one or two negative terms. For brevity, we will present only case (b). Without loss of generality, we assume:

$$c_{23} - c_{13} < 0, \quad c_{24} - c_{14}, \quad c_{25} - c_{15} \geq 0 \quad (14)$$

Inequalities in Eq. (14) yield another set of AC, which must hold in order for the following development of the CC given by Eq. (12) to hold. Different assumptions will lead to a different development of the contact constraint and, thus, to a different group of constraints. Dividing Eq. (12) by $c_{23} - c_{13}$, the CC yields:

$$\frac{c_{24} - c_{14}}{c_{23} - c_{13}} e^{(\lambda_2 - \lambda_1)t} + \frac{c_{25} - c_{15}}{c_{23} - c_{13}} e^{(\lambda_3 - \lambda_1)t} \geq -1 \quad (15)$$

From Eq. (13), we see that constraint (15) holds as equality for $t = 0$. Thus, Eq. (15) holds true if and only if:

$$\lambda_2 - \lambda_1 < 0 \quad \text{and} \quad \lambda_3 - \lambda_1 < 0 \quad (16)$$

Inequalities (16) are another CC for this case. SC (8), AC (14) and CCs (9) and (16) along with the AC that λ_i are real, make the first group of constraints that, if satisfied, the system will have the desired response. For different assumptions, such as Eqs. (14), different groups of constraints have been derived. As mentioned above, to each such group, a range of control gains may correspond and yield the desired response.

2.2.3 Simulation Results

In order to display the performance of the proposed system described by Eq. (1), several simulations were run. In those, a debris of mass m_1 is assumed to approach and finally hit the moving net(m_2)-robot(m_3) system, as seen in Figure 2-3. The system parameters are $m_1 = 20$ kg, $m_2 = 20$ kg, $m_3 = 140$ kg, $k = 500$ kg/s², $b = 40$ kg/s, and $x_0 = 0$. The initial conditions are $\dot{x}_1(0) = 200$ m/s, $\dot{x}_2(0) = 199$ m/s and $\dot{x}_3(0) = 196.5$ m/s. The system is simulated in MATLAB. The result of the impact of the three bodies, for the given set of system parameters and initial conditions, is shown in Figure 2-4. Note that the chosen control gains in this case, do not correspond to any constraint set. As seen in Figure 2-4a by the relative distance $x_2 - x_1$, the debris bounces off the net at the moment this distance exceeds $x_0 = 0$, and then they part rapidly, moving with different constant speeds, as also seen in Figure 2-4b. Note also that, as seen by the relative distance $x_3 - x_2$ in Figure 2-4a, the manipulator, after a small initial compression, starts extending indefinitely, since the constant steady-state free-flyer velocity \dot{x}_3 is larger than the constant steady-state net velocity \dot{x}_2 , as also seen in Figure 2-4b.

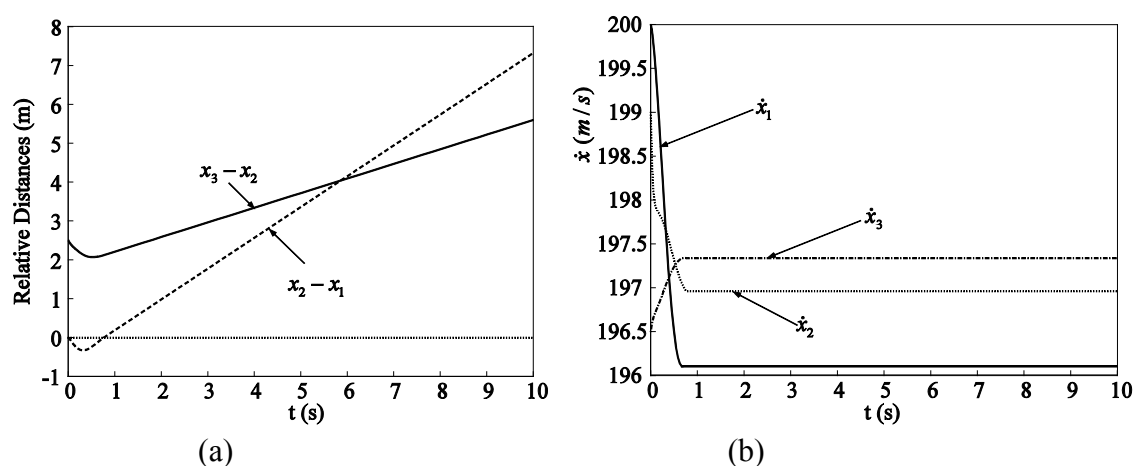


Figure 2-4. (a) Relative positions response and (b) velocities for control gains $K_1 = 80$ kg/s and $K_2 = 400$ kg/s, that do not satisfy any constraints for successful capture.

Next, the control gains are chosen so that they satisfy a constraint set, according to the presented method, while the initial conditions and system parameters remain the same as before. That the presented gains are obtained by the same group of constraints as the one of the previous section. The three objects velocity response for this case, shows that they end up moving with the same speed $\dot{x}_1 = \dot{x}_2 = L / M$, while $\dot{\tilde{x}}_1 = \dot{\tilde{x}}_2 = 0$, see Figure 2-5b.

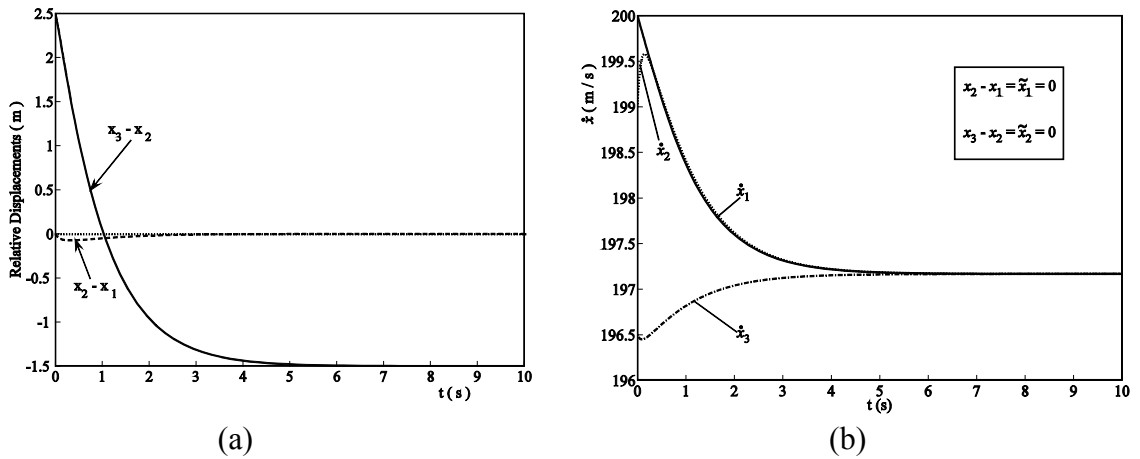


Figure 2-5. (a) Relative positions response and (b) velocities for control gains $K_1 = 250$ kg/s and $K_2 = 30$ kg/s, that satisfy the constraints for successful capture.

Figure 2-5a shows the relative position $x_2 - x_1$, between debris and net and the relative position $x_3 - x_2$, between net and the robot base. It can be seen that the relative position between debris and net, does not exceed $x_0 = 0$ after the first impact, as desired, while the net ends up at a distance of about -1.5 m from the robot base. Figure 2-5b shows the velocities of the three bodies. It can be seen that debris, net and robot base end up moving together, with the same steady-state velocity of about 197.2 m / s. Figure 2-6 shows three snapshots of the system motion, namely the instant of the first contact, that of the net’s maximum deformation and finally the instant in which the steady state is reached.

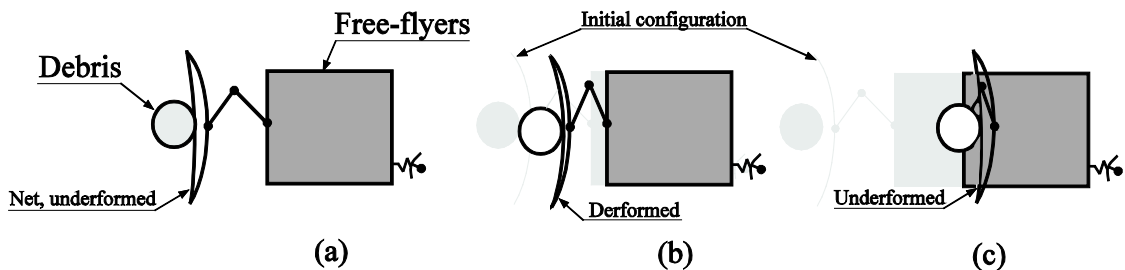


Figure 2-6. Motion snapshots of the orbital debris disposer during capture. (a) $t = 0.0$ s, first contact, (b) $t = 0.32$ s, net’s maximum deformation, (c) $t = 7.8$ s, all bodies move together.

Next, the robustness of the controller strategy is investigated. Typically, the debris mass, its initial velocity, or both, may be inaccurately estimated. Thus, another simulation was run with underestimated debris mass, e.g. 10% less than the actual. As shown in Figure 2-7, the velocities of the debris and the net converge on the estimated CM velocity L_{est} / M_{est} and not on the correct L / M . Due to momentum conservation, this results in the robot bases moving at a lower steady state velocity. In this case, at the instance the debris and the net attain their common velocity, a convergence force is applied between the net and the robot bases, so as to slowly decelerate the net and slowly accelerate the robot bases. This slow deceleration of the net must happen in such a way that the debris (also decelerating inside the net) remains captured. Note that all three bodies keep on moving towards their initial direction, so that this slow deceleration can be performed without loss of contact between the debris and the net. This deceleration, though, must also happen fast enough, so that the system would reach a common velocity in time, avoiding the possibility of a extending the manipulator to its limits. Also, note that since this force decelerates the net, it will not result in debris loss, but will keep it captured. For a 3 m reach manipulator, we assume that the common velocity must be attained before the net carrying end-effector reaches 2.75 m. In Figure 2-7, the transient of the debris-net system is over when the end-effector is at 2.60 m, i.e. less than 2.75 m. At this point, the convergence force must act to make all three velocities equal to L / M .

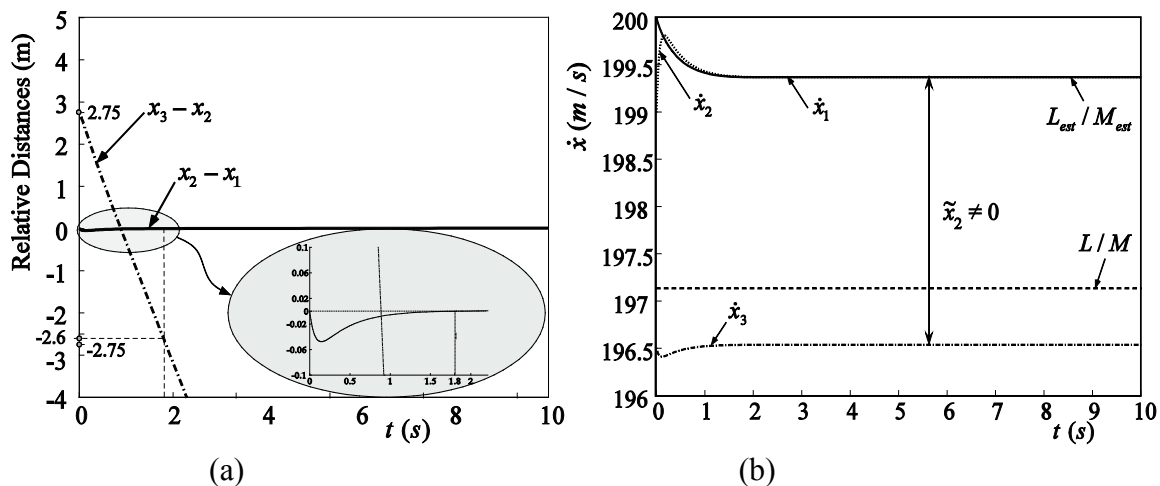


Figure 2-7. (a) Relative positions response and (b) velocities for control gains $K_1 = 250$ kg/s and $K_2 = 30$ kg/s that satisfy the constraints of Eqs. (8), (9), (14) and (16) for successful capture, but with inaccurate estimation of the debris mass, thus resulting in non-zero steady-state relative speed $x_3 - x_2 \neq 0$, as opposed to Figure 2-5.

Next we study the case in which the mass of the debris is overestimated. In this case, the free-flying robots finally move with greater steady-state velocity than the net-debris system. A way to compensate for this, after the net and the debris have the same velocity, is to fire the jets of the free-flyers, to slowly decelerate the whole system. This motion will keep the debris on the net, while at the same time will stop the distancing of the robots from the net.

This one-dimensional model analysis demonstrates the concept feasibility. Nevertheless, as can be seen from Figure 2-5 and Figure 2-7, in order for the proposed system to result in capture, the initial relative velocity $\dot{x}_1 - \dot{x}_2$ between the debris and the net must be very small (in the simulated example $\dot{x}_1 - \dot{x}_2 = 0.5$ m/s), in order to complete the capture before reaching the manipulator reach limit. Thus, it is concluded that the feasibility of the proposed concept is marginal, even for a simplified one-dimensional model.

2.3 Concept On-Orbit Manipulation of a Passive Object by Cooperating Free-Flying Robots

Several methods exist that can be applied in handling a passive rigid object on orbit. One such method requires using thruster on-off forces only, e.g. by thrusters attached to the object, by firm grasping of the passive object by gripper equipped free-flying servicers with rigid appendages or merely by gripper equipped thruster packs, as seen in Figure 2-8b. In this case, the servicers and the passive object become a single rigid body, controlled by the thrusters of the servicers.

Another method is by controlling the passive object via free-flying robotic servicers, equipped with manipulators that handle the passive object and with on-off thrusters and reaction wheels in order to apply external generalized forces to the servicer-passive object system, as seen in Figure 2-8a. In this case, the only external forces being able to move the system's center of mass are the ones applied by the on-off thrusters.

Moreover, the total forces and torques acting on the passive object are of proportional nature, i.e. those exerted by the manipulators. This, as will be demonstrated later on, has the effect of filtering the on-off forces/torques of the thrusters and enabling both point-to-point and trajectory tracking control of the body.

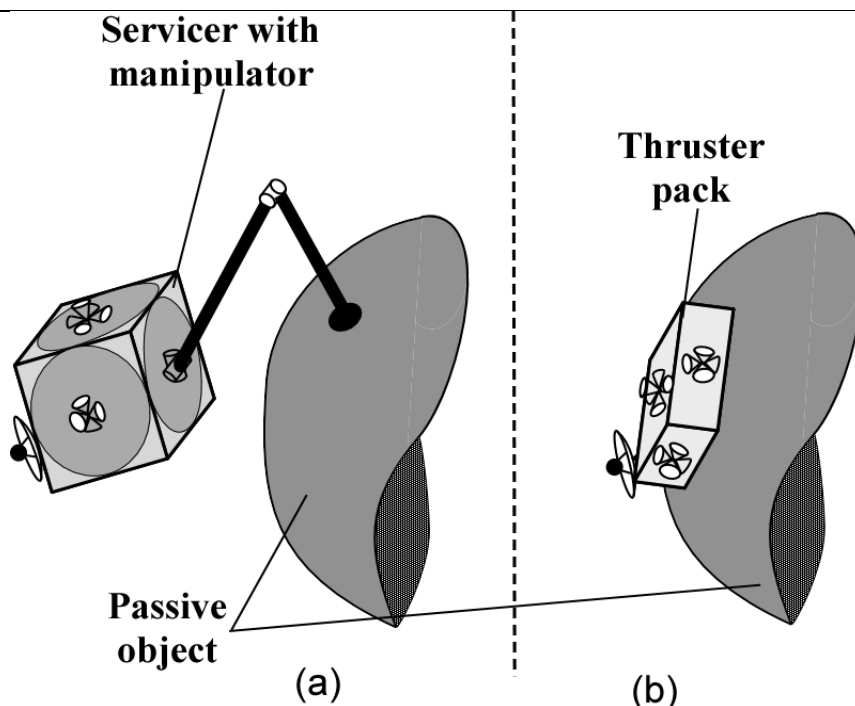


Figure 2-8. (a) Servicer equipped with thrusters, reaction wheels and a manipulator for the handling of a passive object (b) Handling of a passive object by firmly attached thruster pack (pure on-off control).

Note that, to avoid damaging an object, the thrusters pointing towards it, would have to be turned off. The robots should also deactivate any thrusters pointing towards each other, for the same reason. Thus, the placement of the robots around the passive object should be carefully planned, so as to keep as many thrusters operational as possible, while keeping the robots and the object secured.

Another issue that needs to be pointed out is the type of attachment of the manipulators to the passive object. To manipulate a passive object, three forces and three torques must be exerted on it, so as to control its six degrees of freedom (DOFs). The obvious solution for the attachment of the free-flyers is to firmly grasp the passive object. However, this is not always feasible. It is easy to see that the minimum number needed for 3D manipulation is two robot servicers, attached roughly opposite to each other, when the servicers firmly grasp the passive object and in the case of turned-off thrusters towards the passive object. Nevertheless, the number of the robots required depends also on whether they are capable of applying the required forces/ torques. When firm grasping is achieved, a single free-flying robot can produce the required control on the six DOFs of the passive body. Since some thrusters of the robot must be inactivated for safety reasons, one single servicer may face the problem of not being able to exert any thruster force towards one or

more directions. Thus, a number of cooperating free-flyers is needed, even in the case of firm grasps.

Whenever firm grasping is not an option, the manipulators can only push the passive body (unilateral constraint). This is a far more complicated problem and the minimum number of robots required for this task depends on many issues, such as how many manipulators each robot has, how easily each end effector can slip on its contact point/area, the nature of the desired motion etc. Such issues have been studied for terrestrial systems but not for systems in zero-g, where the absence of a fixed base or of gravity, pulling all bodies towards one direction, makes the aspect of losing contact a possibly fatally important parameter.

To study the handling of objects on orbit, we first study the dynamics of orbital robotic servicers firmly attached to a rigid passive body, without the use of manipulators (Figure 2-8b). The equations of motion of such a system are

$$\mathbf{H}\ddot{\mathbf{q}} + \mathbf{C}(\mathbf{q}, \dot{\mathbf{q}}) = \mathbf{J}^T \mathbf{Q} \quad (17)$$

In Eq. (17), \mathbf{q} is the $n \times 1$ vector of the generalized coordinates, that includes the 3 ($p + 1$) positions and 3 ($p + 1$) Euler angles of the p robot bases and those of the passive body, along with the joint variables of each robot's manipulator. \mathbf{Q} is a $k \times 1$ vector of the generalized forces, that is the forces of all thrusters and the torques of all reaction wheels of the p robots and the joint torques of all robot manipulators, \mathbf{J} is a $k \times n$ Jacobian matrix of the generalized forces, \mathbf{H} is an $n \times n$ mass matrix related to the inertia properties of all the bodies in the system, and \mathbf{C} is an $n \times 1$ vector that contains nonlinear velocity terms.

In the case of handling a passive object by attaching thrusters on it, or by using free-flyers with rigid appendages (as opposed to employing manipulators), the result would be the same as trying to control a rigid free-flying system (such as a satellite etc.) by its thrusters only. At present, the normal practice for the control on these systems is on-off, initiated by PD control on an error variable. On-off control is used in order to protect the thrusters from the extreme space environment and especially to prevent ice from forming in the nozzles of the thrusters. This type of control, leads to limit-cycles around a desired state or even chattering, a phenomenon that consumes a lot of fuel and wears out the thrusters.

2.3.1 Object Control with Direct Thrusting

To demonstrate the issues arising in this direct actuation method, the dynamic equations of motion of a simplified, one-dimensional model are derived as,

$$m\ddot{x} = u_1 + u_2 \quad (18)$$

where m is the passive object and servicers system mass, x its position, u_1 and u_2 are the on-off control forces acting on it, see Figure 2-9.

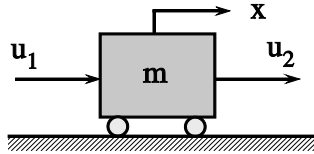


Figure 2-9. Model of a passive object / servicers system controlled by thrusters.

A PD initiated, on-off controller is given by

$$u_1 = \begin{cases} u_{\max} & \text{if } K_p e + K_D \dot{e} \geq f_t \\ 0 & \text{if } K_p e + K_D \dot{e} < f_t \end{cases} \quad (19)$$

$$u_2 = \begin{cases} -u_{\max} & \text{if } K_p e + K_D \dot{e} \leq -f_t \\ 0 & \text{if } K_p e + K_D \dot{e} > -f_t \end{cases} \quad (20)$$

where $e = x_{des} - x$, is the position error of the controlled body, u_{\max} is the force applied by an open thruster and f_t inserts a deadband on the controller, in order to avoid chattering, i.e. rapid on-off switching of thrusters near zero error [18], [71]. Figure 2-10 shows a typical response of such a system, where a limit-cycle is observed, even though chattering is avoided. The dotted lines in Figure 2-10b denote controller limit lines. A state between these lines lies in the deadband area and thus the thrusters are off. A state to the left or to the right of both lines leads to the application of the corresponding thruster force. As can be seen in Figure 2-10, the passive object does not reach a final position, but rather oscillates around one, resulting in non-zero steady-state errors. Note that, in order to keep the passive object close to the desired position ($x_{des} = 1.6$ m in Figure 2-10), the thrusters must keep on firing quite frequently during the limit-cycle, resulting in significant fuel consumption.

To enhance the control performance of the passive object, the introduction of manipulators in the control of the body is studied next. Our goal is to perform fine positioning of a passive rigid object and even trajectory tracking, without any limit-cycle

effects on its motion, while the controlling robotic servicers stay within the range of their manipulators. We will also look at the fuel consumption problem, which is very important in space.

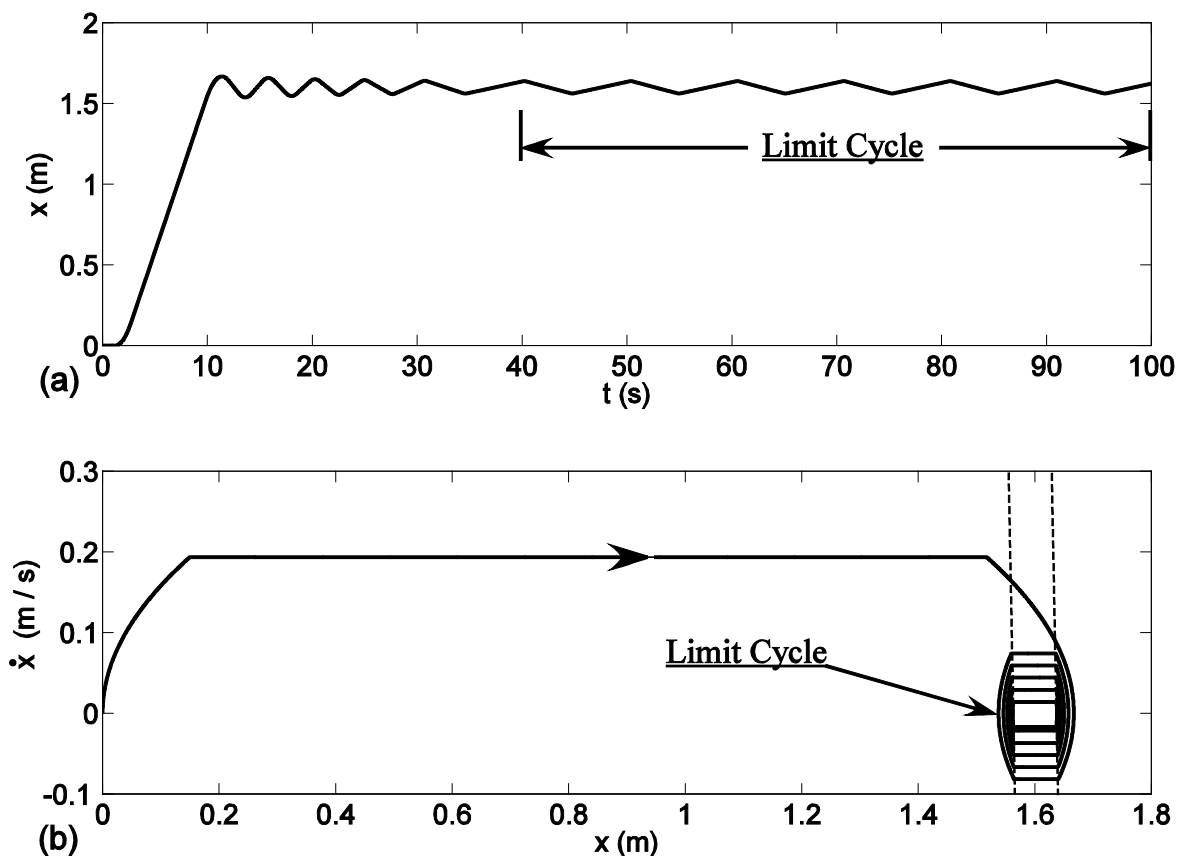


Figure 2-10. Typical response of On-Off PD control, with limit cycle.

2.3.2 Object Control with Manipulator-Equipped Servicers

To obtain basic insight on the dynamic behavior and the control requirements of the dynamic system, a simplified one-dimensional model is analyzed. A passive rigid object of mass m_0 moves along a line grasped firmly by robots via manipulators.

As already discussed, to protect each body from the thruster plumes, the robot thrusters pointing towards other bodies must be inactive. Thus, more than one robot are needed, to be able to apply forces on the object in both directions. As a result, two robots of masses m_1 and m_2 are chosen to manipulate the object. The only external forces acting on the system and moving its center of mass are the thruster forces u_1 and u_2 , as shown in Figure 2-11. The position vectors x_0 , x_1 and x_2 refer to the controlled body, and the robots of masses m_1 and m_2 respectively.

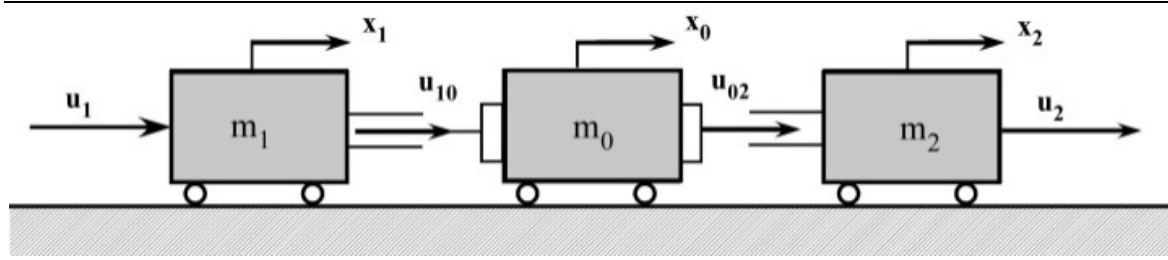


Figure 2-11. A passive (center) object handled by servicers with manipulators.

First, to find by how much the passive object can be moved without any thruster firing, the motion of the passive object is studied when the servicers use only their manipulators. In this case all the servicer thrusters are inactive and no external force is applied to the system. Thus, the system center of mass state remains fixed. Without loss of generality, it is assumed that the system center of mass velocity is zero. The initial state of the system is shown in Figure 2-12a. In this figure, δ_i denotes the constant distance from the i^{th} servicer center of mass to its manipulator base, δ_{0i} denotes the constant distance from the passive object center of mass to the contact point with the i^{th} servicer manipulator, δx_i denotes the distance of the i^{th} servicer base from the passive object, i.e. the current manipulator reach of the i^{th} servicer. In Figure 2-12, x_{00} and x_{01} denote the initial and final distances from the passive object center of mass to the system center of mass, respectively. Note also that δx_i^* (in Figure 2-12a only δx_2^* is shown) denotes the additional reach the i^{th} servicer manipulator can have on top of δx_i , in order to reach its maximum manipulator reach $x_{m,i}$, i.e.

$$\delta x_i + \delta x_i^* = x_{m,i} \quad (21)$$

Since the only external forces acting on the system are the thruster forces, by moving the servicers, using only their manipulators, the passive object also moves accordingly, in a way that the system CM remains fixed. The passive object displacement $\delta x_0 = x_{01} - x_{00}$ that can be achieved without using the thrusters and its maximum value are obtained next.

At the initial state, the following is obtained (see also Figure 2-12),

$$(\delta_1 + \delta x_1 + \delta_{01} - x_{00})m_1 = (\delta_2 + \delta x_2 + \delta_{02} + x_{00})m_2 + x_{00}m_0 \quad (22)$$

or equally,

$$x_{00} = \frac{(\delta_1 + \delta x_1 + \delta_{01})m_1 - (\delta_2 + \delta x_2 + \delta_{02})m_2}{m_0 + m_1 + m_2} \quad (23)$$

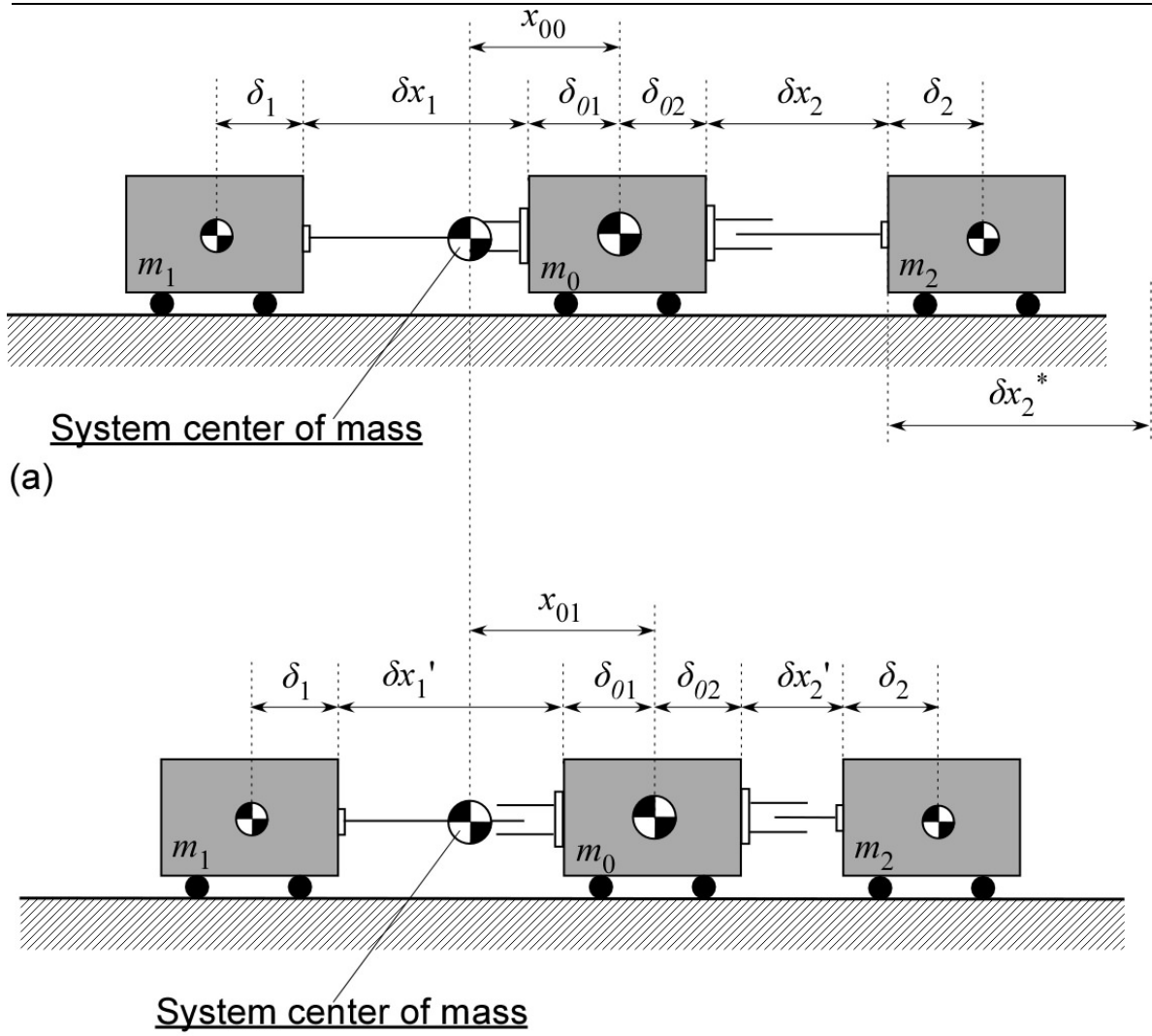


Figure 2-12. Handling of the passive object by use of manipulator forces only. Initial (a) and final (b) position of the system.

Assume now that the two manipulators change their configuration, exerting forces on the passive object. As already mentioned, the system center of mass remains stationary, but all three bodies move and the relative distances δx_i change to $\delta x_i'$, while the distance of the passive object center of mass from the system center of mass becomes x_{01} , as seen in Figure 2-12b. At this final state, the following is obtained,

$$\left(\delta_1 + \delta x_1' + \delta_{01} - x_{01}\right)m_1 = \left(\delta_2 + \delta x_2' + \delta_{02} + x_{01}\right)m_2 + x_{01}m_0 \quad (24)$$

or equally,

$$x_{01} = \frac{\left(\delta_1 + \delta x_1' + \delta_{01}\right)m_1 - \left(\delta_2 + \delta x_2' + \delta_{02}\right)m_2}{m_0 + m_1 + m_2} \quad (25)$$

Thus, the displacement $\delta x_0 = x_{01} - x_{00}$ of the passive object was:

$$\delta x_0 = \frac{(\delta x_1' - \delta x_1)m_1 - (\delta x_2' - \delta x_2)m_2}{m_0 + m_1 + m_2} \quad (26)$$

Note that $\delta x_i' - \delta x_i$ is essentially the motion of the manipulator of the i^{th} ($i = 1, 2$) servicer. Thus, from Eq. (26) it can be seen that the same type of manipulator motion from both servicers (e.g. if both manipulators are extracting, pushing the corresponding servicer away from the passive object) results in opposing forces on the passive object. Note also that the magnitude of the allowed motion of each manipulator is bounded by δx_i if it is trying to pull the servicer base towards the passive object, and by δx_i^* if it is trying to push the servicer base away from the passive object. Nevertheless, δx_i^* also depends on δx_i , because of Eq. (21). This means that the maximum motion that the passive object can perform when only the manipulators are used, depends on the three masses of the passive object and the servicers, and on the initial state δx_i of the two manipulators. This maximum passive object motion is obtained assuming that one servicer will push as much as it can, while the other will pull as much as it can. Assuming, without loss of generality, that the servicer of mass m_1 is pushing and the servicer of mass m_2 is pulling, the maximum motion that the passive object can perform without any thruster firing, is obtained by substituting $\delta x_1'$ of Eq. (26) with δx_1^* and $\delta x_2'$ with zero, while also using Eq. (21) to obtain δx_1^* as a function of x_{m1} and δx_1 :

$$\delta x_{0-\max_r} = \frac{(x_{m1} - 2\delta x_1)m_1 + \delta x_2 m_2}{m_0 + m_1 + m_2} \quad (27)$$

Note that Eq. (27) results in a passive object motion towards the right, as seen in Figure 2-12. For a passive object motion towards the opposite direction, the servicer of mass m_2 must be pushing and the servicer of mass m_1 must be pulling. The maximum motion that the passive object can perform without any thruster firing is obtained then by substituting $\delta x_2'$ of Eq. (26) with δx_2^* and $\delta x_1'$ with zero, while also using Eq. (21) to obtain δx_2^* as a function of x_{m2} and δx_2 :

$$\delta x_{0-\max_l} = \frac{-\delta x_1 m_1 - (x_{m2} + 2\delta x_2)m_2}{m_0 + m_1 + m_2} \quad (28)$$

The absolute maximum motion that can be achieved in this way results from an initial manipulator state in which, one servicer is initially almost in contact with the passive object (thus being able to move from zero extension to its full reach), while the

other is initially at its maximum manipulator reach. If the first servicer pushes the passive object away until it reaches its maximum manipulator reach, while the other servicer pulls the passive object until it is almost in contact with it, then the passive object maximum displacement $\delta x_{0-\max}$ is obtained,

$$\delta x_{0-\max} = \frac{x_{m1}m_1 + x_{m2}m_2}{m_0 + m_1 + m_1} \quad (29)$$

If the desired motion of the passive object exceeds the limits set by Eq. (29) (or by Eqs. (27) and (28), in case the initial manipulator configurations δx_1 and δx_2 are given), then the system center of mass must be moved. In this case, the servicer thrusters are the only ones that can provide external forces, in order to move the system center of mass. Next, the motion of the system under both manipulator and thruster forces, is studied. Note that, since here the motion is one-dimensional, \mathbf{C} in Eq. (17) is zero. The generalized forces vector \mathbf{Q} , consists of the thruster (u_1 and u_2) and manipulator (u_{10} and u_{02}) forces, where the later are the ones acting on the robotic servicers. Thus, the forces $-u_{10}$ and $-u_{02}$, are the only ones acting on the object, filtering the on-off thruster force effects on it. Using Eq. (17), the error-dynamics equations are

$$\ddot{\mathbf{e}} = \begin{bmatrix} \ddot{e}_0 \\ \ddot{e}_1 \\ \ddot{e}_2 \end{bmatrix} = \underbrace{\begin{bmatrix} 0 & \frac{-1}{m_0} & \frac{-1}{m_0} & 0 \\ \frac{-1}{m_1} & \frac{m_0 + m_1}{m_0 m_1} & \frac{-1}{m_0} & 0 \\ 0 & \frac{1}{m_0} & \frac{m_0 - m_2}{m_0 m_2} & \frac{-1}{m_2} \end{bmatrix}}_{\mathbf{H}^{-1}\mathbf{J}^T} \begin{bmatrix} u_1 \\ u_{10} \\ u_{02} \\ u_2 \end{bmatrix} - \begin{bmatrix} \ddot{x}_{0-des} \\ 0 \\ 0 \end{bmatrix} \quad (30)$$

with $u_1 > 0$, $u_2 < 0$ in an on-off mode, while e_i are defined as

$$\begin{aligned} e_0 &= x_0 - x_{0-des} \\ e_1 &= x_0 - x_1 - x_m / 2 \\ e_2 &= x_0 - x_2 + x_m / 2 \end{aligned} \quad (31)$$

where x_{0-des} is the desired position of the passive object and x_m is the manipulator maximum reach, which is assumed the same for both servicer manipulators, for simplicity. The actual relative distance between each of the servicers and the passive object, must remain lower than x_m , in order for both manipulators to remain within their workspace, i.e. $x_0 - x_1 < x_m$ and $x_2 - x_0 < x_m$. It is important to point out that, by trying with the appropriate control, to set these error variables to zero, the passive object is forced to follow its desired

trajectory, while the free-flying robots are forced to stay at a distance from the passive object, as close as possible to half the maximum manipulator length, i.e. as close as possible to the center of the manipulators workspace. This is in order to maximize the space (in all directions) in which each servicer is free to move.

2.3.3 Control Design

Many methods exist in the literature in order to derive the desired controller and in this case a *backstepping* methodology [69] is used, because of some important characteristics it displays. According to this method, we “step back” at each iteration, in order to create the control inputs from the simple subsystems of a more complex dynamic model. By transforming into new variables at each iteration, a nonlinear system can be lead to display linear behavior, if there are no uncertainties on the modeling of the dynamic system. A very important characteristic of backstepping is that, in the process of variable transformation, it avoids the elimination of nonlinear quantities, important for stability and trajectory tracking, as opposed to feedback linearization. Thus, it ensures stability of the controlled system and assists trajectory tracking algorithms, and for that reason it is used in order to derive the system controller. Other control approaches like optimal or H^∞ control can also be used. Nevertheless, a more realistic 3D system is highly nonlinear, with joint friction and actuator nonlinearities. In those cases, backstepping is easier to implement.

To apply this methodology, we first focus on the equations of motion of the passive object. Thus, from Eq. (30), we obtain:

$$\ddot{e}_0 = - \left(\frac{u_{10}}{m_0} + \frac{u_{02}}{m_0} + \ddot{x}_{0_des} \right) \quad (32)$$

Defining z_0 and z_1 as

$$\begin{aligned} z_0 &= e_0 \\ z_1 &= \dot{z}_0 = \dot{e}_0 \end{aligned} \quad (33)$$

then, Eq. (32) yields:

$$\begin{aligned} \dot{z}_0 &= z_1 \\ \dot{z}_1 &= - \left(\frac{u_{10}}{m_0} + \frac{u_{02}}{m_0} + \ddot{x}_{0_des} \right) \end{aligned} \quad (34)$$

Step 1

Assume for the moment that z_1 is controllable and that we use the following controller:

$$z_1 = \phi_{01}(z_0) = -K_0 z_0 \quad (35)$$

with the following Lyapunov function:

$$V_{01}(z_0) = \frac{\beta_0}{2} z_0^2 \geq 0 \quad (36)$$

with $\beta_0 > 0$. By differentiating Eq. (36), we obtain:

$$\dot{V}_{01}(z_0) = \beta_0 z_0 \dot{z}_0 = \beta_0 z_0 z_1 \quad (37)$$

Using Eq. (35), Eq. (37) yields:

$$\dot{V}_{01}(z_0) = -\beta_0 K_0 z_0^2 \leq 0 \quad (38)$$

However, $z_1 = \dot{e}_0$ is not directly controllable.

Step 2

We define w_0 as:

$$w_0 = z_1 - \phi_{01}(z_0) = z_1 + K_0 z_0 \quad (39)$$

which, ideally, should be zero, thus rendering the tracking errors e_0 and \dot{e}_0 equal to zero. By differentiating Eq. (39) and using Eq. (34), the following is obtained:

$$\dot{w}_0 = -\ddot{x}_{0_des} - \frac{u_{10} + u_{02}}{m_0} + K_0 z_0 \quad (40)$$

Then, by use of Eqs. (35) and (39), Eq. (40) yields:

$$\dot{w}_0 = -\ddot{x}_{0_des} - \frac{u_{10} + u_{02}}{m_0} + K_0 w_0 - K_0^2 z_0 \quad (41)$$

Since the directly controlled quantities are the control forces u_{10} and u_{02} , the following controller is assumed instead of the one in Eq. (35):

$$u_{10} + u_{02} = \phi_{02}(z_0, z_1) \quad (42)$$

with the following Lyapunov function:

$$V_{02}(z_0, z_1) = V_{01}(z_0) + \frac{a_0}{2} w_0^2 \geq 0 \quad (43)$$

with $a_0 > 0$. Differentiating Eq. (43) leads to:

$$\dot{V}_{02} = \dot{V}_{01} + a_0 w_0 \dot{w}_0 \quad (44)$$

and then, by also using Eqs. (36) and (41), to:

$$\dot{V}_{02} = \beta_0 z_0 \dot{z}_0 + a_0 w_0 \left(-\ddot{x}_{0_des} - \frac{u_{10} + u_{02}}{m_0} + K_0 w_0 - K_0^2 z_0 \right) \quad (45)$$

Employing Eqs. (34) and (39), leads to

$$\dot{z}_0 = z_1 = w_0 - K_0 z_0 \quad (46)$$

Thus, Eqs. (42), (45) and (46), lead to:

$$\dot{V}_{02} = \beta_0 z_0 (w_0 - K_0 z_0) + a_0 w_0 \left(-\ddot{x}_{0_des} - \frac{\phi_{02}}{m_0} + K_0 w_0 - K_0^2 z_0 \right) \quad (47)$$

or

$$\dot{V}_{02} = \beta_0 z_0 w_0 - \beta_0 K_0 z_0^2 + a_0 w_0 \left(-\ddot{x}_{0_des} - \frac{\phi_{02}}{m_0} \right) + a_0 K_0 w_0^2 - a_0 K_0^2 w_0 z_0 \quad (48)$$

By defining

$$\beta_0 = a_0 K_0^2 > 0 \quad (49)$$

then Eq. (48) becomes

$$\dot{V}_{02} = -\beta_0 K_0 z_0^2 + a_0 w_0 \left(-\ddot{x}_{0_des} - \frac{\phi_{02}}{m_0} \right) + a_0 K_0 w_0^2 \quad (50)$$

Now the control forces of Eq. (42) can be derived. By using

$$u_{10} + u_{02} = \phi_{02} = m_0 (K_0 w_0 - \ddot{x}_{0_des}) \quad (51)$$

Eq. (50) yields

$$\dot{V}_{02} = -\beta_0 K_0 z_0^2 = -\beta_0 K_0 e_0^2 \leq 0 \quad (52)$$

Note now that, by use of Eqs. (33), (36), and (39), Eq. (43) yields:

$$V_{02}(z_0, z_1) = \frac{\beta_0}{2} e_0^2 + \frac{a_0}{2} (\dot{e}_0 + K_0 e_0)^2 \geq 0 \quad (53)$$

Thus, since $V_{02} \geq 0$ and $\dot{V}_{02} \leq 0$, V_{02} is bounded (V_{02} cannot tend to $-\infty$ since it is positive and it cannot tend to $+\infty$ with \dot{V}_{02} being negative). Moreover, since V_{02} is bounded and both

terms of Eq. (53) are positive (since $a_0, \beta_0 > 0$), both terms of Eq. (53) must be bounded too:

$$\begin{aligned} 0 < \lim_{t \rightarrow \infty} \left(\frac{\beta_0}{2} e_0^2 \right) < +\infty \\ 0 < \lim_{t \rightarrow \infty} \left(\frac{a_0}{2} (\dot{e}_0 + K_0 e_0)^2 \right) < +\infty \end{aligned} \quad (54)$$

or

$$\begin{aligned} -\infty < -B_1 \leq \lim_{t \rightarrow \infty} (e_0) \leq B_1 < +\infty \\ -\infty < -B_2 \leq \lim_{t \rightarrow \infty} (\dot{e}_0 + K_0 e_0) \leq B_2 < +\infty \end{aligned} \quad (55)$$

where $B_1, B_2 > 0$ and bounded.

Note that Eq. (55), yields:

$$-\infty < -C_1 \leq \lim_{t \rightarrow \infty} (\dot{e}_0) \leq C_1 < +\infty \quad (56)$$

with $C_1 > 0$ and bounded.

Moreover, differentiating Eq. (52), leads to

$$\ddot{V}_{02} = -2\beta_0 K_0 e_0 \dot{e}_0 \quad (57)$$

Thus, by use of Eqs. (55) and (56), Eq. (57) leads to the fact that \ddot{V}_{02} is also bounded:

$$-\infty < -D_1 \leq \ddot{V}_{02} \leq D_1 < +\infty \quad (58)$$

where $D_1 > 0$ and bounded. Thus, \dot{V}_{02} is uniformly continuous, which, along with Eqs. (53) and (57), allows the use of Barbalat's theorem for V_{02} , which yields:

$$\lim_{t \rightarrow \infty} (\dot{V}_{02}) = 0 \quad (59)$$

Substituting \dot{V}_{02} in Eq. (59) from Eq. (52), leads to:

$$\lim_{t \rightarrow \infty} (\dot{e}_0) = 0 \quad (60)$$

Thus the tracking error e_0 is proven to tend to zero, when the controller of Eq. (51) is used, proving controller stability. By use of Eqs. (34), (35) and (39) on Eq. (51), the final form of the passive object controller is derived:

$$u_{10} + u_{02} = m_0 K_0 (\dot{e}_0 + K_0 e_0) - m_0 \ddot{x}_{0_des} \quad (61)$$

Note that the right-hand side of Eq. (61) is a typical model based PD controller. The only additional constraint is that, according to backstepping stability requirements, the control gains K_p and K_D should satisfy the following condition,

$$K_p = K_D^2 \quad (62)$$

Similarly, applying the backstepping methodology for the control for the robotic servicer bases, results in

$$u_{10} + u_1 = m_1 K_1 (\dot{e}_1 + K_1 e_1) - m_1 K_0 (\dot{e}_0 + K_0 e_0) \quad (63)$$

and

$$u_{02} + u_2 = m_2 K_2 (\dot{e}_2 + K_2 e_2) - m_2 K_0 (\dot{e}_0 + K_0 e_0) \quad (64)$$

Note that the system controller of Eqs. (61), (63) and (64) provides the total force acting on the passive object and the servicer bases respectively. In order to obtain the control forces themselves, we split Eqs. (61), (63) and (64) as follows:

$$u_{10} = \frac{m_0}{2} K_0 (\dot{e}_0 + K_0 e_0) + m_1 K_1 (\dot{e}_1 + K_1 e_1) + m_2 K_2 (\dot{e}_2 + K_2 e_2) - \frac{m_0}{2} \ddot{x}_{0_des} \quad (65)$$

$$u_{02} = \frac{m_0}{2} K_0 (\dot{e}_0 + K_0 e_0) - m_1 K_1 (\dot{e}_1 + K_1 e_1) - m_2 K_2 (\dot{e}_2 + K_2 e_2) - \frac{m_0}{2} \ddot{x}_{0_des}$$

$$u_1 = \frac{m_0}{2} \ddot{x}_{0_des} + m_2 K_2 (\dot{e}_2 + K_2 e_2) - \left(\frac{m_0}{2} + m_1 \right) K_0 (\dot{e}_0 + K_0 e_0) \quad (66)$$

$$u_2 = \frac{m_0}{2} \ddot{x}_{0_des} + m_1 K_1 (\dot{e}_1 + K_1 e_1) - \left(\frac{m_0}{2} + m_2 \right) K_0 (\dot{e}_0 + K_0 e_0)$$

where K_i ($i = 0, 1, 2$) are the controller gains, and u_1 and u_2 are assumed to be proportional forces. In our case, though, u_1 and u_2 are thruster unidirectional on-off forces. Thus, a switching strategy must be employed, based on Eq. (66). A possible strategy is to turn each thruster on when the backstepping derived proportional value exceeds a threshold value f_i . Thus, the final control algorithm is given by Eqs. (65) and (67).

$$\begin{aligned}
u_1 = & \begin{cases} f_m & \text{if } \frac{m_0}{2} \ddot{x}_{0_des} + m_2 K_2 (\dot{e}_2 + K_2 e_2) - \\ & - \left(\frac{m_0}{2} + m_1 \right) K_0 (\dot{e}_0 + K_0 e_0) \geq f_t \\ 0 & \text{if } \frac{m_0}{2} \ddot{x}_{0_des} + m_2 K_2 (\dot{e}_2 + K_2 e_2) - \\ & - \left(\frac{m_0}{2} + m_1 \right) K_0 (\dot{e}_0 + K_0 e_0) < f_t \end{cases} \\
u_2 = & \begin{cases} -f_m & \text{if } \frac{m_0}{2} \ddot{x}_{0_des} + m_1 K_1 (\dot{e}_1 + K_1 e_1) - \\ & - \left(\frac{m_0}{2} + m_2 \right) K_0 (\dot{e}_0 + K_0 e_0) \leq -f_t \\ 0 & \text{if } \frac{m_0}{2} \ddot{x}_{0_des} + m_1 K_1 (\dot{e}_1 + K_1 e_1) - \\ & - \left(\frac{m_0}{2} + m_2 \right) K_0 (\dot{e}_0 + K_0 e_0) > -f_t \end{cases}
\end{aligned} \tag{67}$$

It is clear by Eq. (65) that, each manipulator controller takes into account the requirement to stay within each manipulator's reach. In addition to that, since the only force exerted on the passive body is the sum of the manipulators forces, this controller leads to a simple PD control on the tracking error, as seen in Eq. (61), whose stability has been proven already in Eq. (60).

For the relative motion between the robots and the passive body, asymptotic stability with respect to a specific position is not of interest. However, it is important to ensure that the displacements are bounded. What makes the analysis harder, is that some of the forces are continuous (i.e. Eq. (65)), while the rest are switched (i.e. Eq. (67)), resulting in a non-continuous controller. Moreover, backstepping (see Eqs. (63) and (64)), results in forces for each servicer manipulator that depend also on the tracking errors of the passive object and the other servicer, as seen in Eq. (66) and the resulting switching strategy of Eq. (67). This makes the analysis even more difficult, although the system under this set of control forces, displays very good behavior, as will be shown in Section 2.3.4. A way to bypass this obstacle is to use backstepping only in the derivation of the passive object controller, which results in Eq. (61). What follows is the derivation of a series of controllers for the system, each one solving a problem the previous one had, thus showing a step-by-step reasoning for the final controller derivation. By using backstepping for the manipulator forces only, then only Eq. (61) must still be valid instead of all Eqs. (61), (63) and (64). To

obtain individual manipulator forces, in place of Eq. (65), Eq. (68) is initially proposed, in which the manipulator forces depend only on the passive object tracking errors:

$$u_{10} = u_{20} = \frac{1}{2} \left(m_0 K_0 (\dot{e}_0 + K_0 e_0) - m_0 \ddot{x}_{0_des} \right) \quad (68)$$

where $u_{20} = -u_{02}$, so that both u_{10} and u_{20} are the forces applied on the passive object. Furthermore, in place of the switching strategy of Eq. (67) for the thruster forces, a switching strategy based on a model based PD is introduced:

$$u_1 = \begin{cases} f_m & \text{if } m_1 K_1 (\dot{e}_1 + K_1 e_1) \geq f_t \\ 0 & \text{if } m_1 K_1 (\dot{e}_1 + K_1 e_1) < f_t \end{cases} \quad (69)$$

$$u_2 = \begin{cases} -f_m & \text{if } m_2 K_2 (\dot{e}_2 + K_2 e_2) \leq -f_t \\ 0 & \text{if } m_2 K_2 (\dot{e}_2 + K_2 e_2) > -f_t \end{cases}$$

Note that, with the manipulator and thruster forces as introduced in Eqs. (68) and (69) respectively, the servicers cannot be pushed away from the passive object when they get too close. This is so since, as already mentioned, the servicer thrusters facing the passive object are switched off for safety reasons. The only forces capable of performing this task are the manipulator forces. But the manipulator controller of Eq. (68) does not take into account this task. To solve this problem, a second version of the manipulator controller is introduced in Eq. (70).

$$u_{10} = \begin{cases} \frac{1}{2} \left(m_0 K_0 (\dot{e}_0 + K_0 e_0) + m_0 \ddot{x}_{0_des} \right) & \text{if } m_1 K_1 (\dot{e}_1 + K_1 e_1) > -f_t^* \\ \frac{1}{2} \left(m_0 K_0 (\dot{e}_0 + K_0 e_0) + m_0 \ddot{x}_{0_des} \right) - \\ \quad - m_1 K_1 (\dot{e}_1 + K_1 e_1) & \text{if } m_1 K_1 (\dot{e}_1 + K_1 e_1) \leq -f_t^* \end{cases} \quad (70)$$

$$u_{20} = \begin{cases} \frac{1}{2} \left(m_0 K_0 (\dot{e}_0 + K_0 e_0) + m_0 \ddot{x}_{0_des} \right) & \text{if } m_2 K_2 (\dot{e}_2 + K_2 e_2) < f_t^* \\ \frac{1}{2} \left(m_0 K_0 (\dot{e}_0 + K_0 e_0) + m_0 \ddot{x}_{0_des} \right) - \\ \quad - m_2 K_2 (\dot{e}_2 + K_2 e_2) & \text{if } m_2 K_2 (\dot{e}_2 + K_2 e_2) \geq f_t^* \end{cases}$$

By employing the manipulator force controller of Eq. (70), whenever the quantity

$$m_i K_i (\dot{e}_i + K_i e_i), \quad \text{with } i = 1, 2 \quad (71)$$

exceeds a threshold value of f_t^* , requiring a force to push the corresponding servicer away from the passive object, the force of the corresponding manipulator is augmented by this same quantity.

Note, though, that by employing the manipulator controller of Eq. (70), the total force applied on the passive object ($u_{10} + u_{02}$), is no longer equal to the passive object model based PD of Eq. (61), derived by backstepping. Thus, a final manipulator controller is introduced in Eq. (72). In this controller the following strategy is: if no extra “pushing” force is needed to drive the servicers away from the passive object, then the manipulator controller is the passive object model based PD, split in half for the two manipulators, as shown in Eq. (68). Whenever one (or both) of the servicers requires a “pushing” force, then, not only this force is added to the existing force of the corresponding manipulator, but its opposite is also added to the existing force of the other manipulator. Thus, not only each servicer gets pushed away from the passive object whenever this is required, but also the sum of the two manipulator forces acting on the passive object constantly follows the backstepping derived Eq. (68). The architecture of the controller of Eqs. (69) and (72), is also seen in Figure 2-13.

$$\begin{aligned}
 u_{10} = & \begin{cases} \frac{1}{2}(PD_0 + m_0\ddot{x}_{0_des}) & \text{if } \begin{cases} PD_1 > -f_t^* \text{ and} \\ PD_2 < f_t^* \end{cases} \\ \frac{1}{2}(PD_0 + m_0\ddot{x}_{0_des}) - PD_1 & \text{if } \begin{cases} PD_1 \leq -f_t^* \text{ and} \\ PD_2 < f_t^* \end{cases} \\ \frac{1}{2}(PD_0 + m_0\ddot{x}_{0_des}) + PD_2 & \text{if } \begin{cases} PD_1 > -f_t^* \text{ and} \\ PD_2 \geq f_t^* \end{cases} \\ \frac{1}{2}(PD_0 + m_0\ddot{x}_{0_des}) - PD_1 + PD_2 & \text{if } \begin{cases} PD_1 \leq -f_t^* \text{ and} \\ PD_2 \geq f_t^* \end{cases} \end{cases} \\
 u_{20} = & \begin{cases} \frac{1}{2}(PD_0 + m_0\ddot{x}_{0_des}) & \text{if } \begin{cases} PD_1 > -f_t^* \text{ and} \\ PD_2 < f_t^* \end{cases} \\ \frac{1}{2}(PD_0 + m_0\ddot{x}_{0_des}) + PD_1 & \text{if } \begin{cases} PD_1 \leq -f_t^* \text{ and} \\ PD_2 < f_t^* \end{cases} \\ \frac{1}{2}(PD_0 + m_0\ddot{x}_{0_des}) - PD_2 & \text{if } \begin{cases} PD_1 > -f_t^* \text{ and} \\ PD_2 \geq f_t^* \end{cases} \\ \frac{1}{2}(PD_0 + m_0\ddot{x}_{0_des}) + PD_1 - PD_2 & \text{if } \begin{cases} PD_1 \leq -f_t^* \text{ and} \\ PD_2 \geq f_t^* \end{cases} \end{cases} \quad (72)
 \end{aligned}$$

where

$$\begin{aligned} PD_0 &= m_0 K_0 (\dot{e}_0 + K_0 e_0) \\ PD_1 &= m_1 K_1 (\dot{e}_1 + K_1 e_1) \\ PD_2 &= m_2 K_2 (\dot{e}_2 + K_2 e_2) \end{aligned} \quad (73)$$

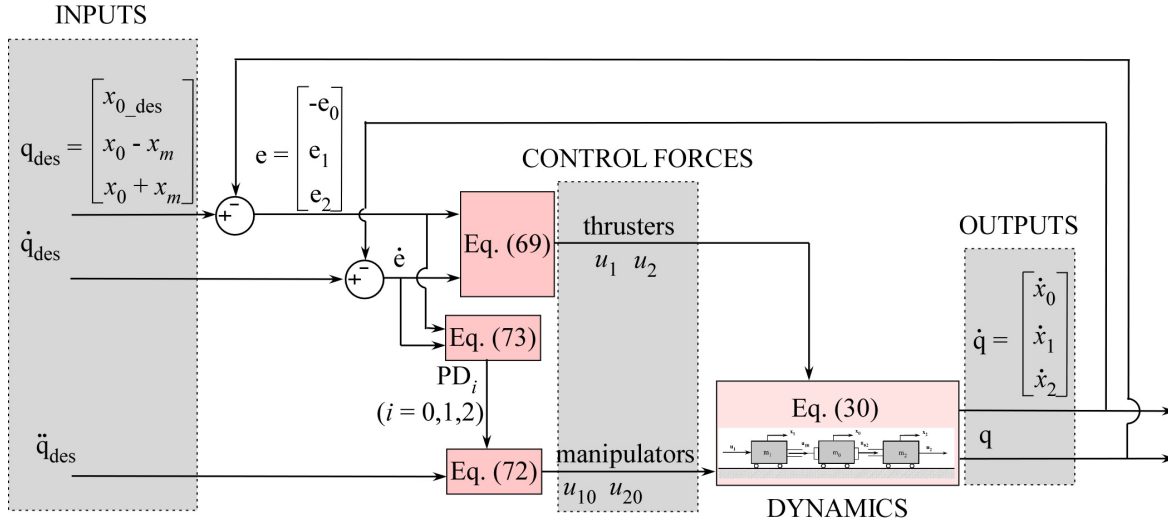


Figure 2-13. Flowchart of the control algorithm for the simplified one-dimensional model of two free-flying robotic servicers, handling a passive object.

Thus, instead of the initial Eqs. (65) and (67), the new controller consists of Eqs. (69) and (72). Even in this case, the complexity, introduced by the fact that the applied forces are switched, is still present. For the one-dimensional, simplified model, though, there is a way to bypass this problem, at least partially, since there is an analytical solution for the equations of motion. Using this analytical solution, we have shown that at least for the phase of this switched control in which the servicer is moving away from the passive object, the relative motions are bounded. This boundedness is independent of the previous phases, or the initial state of the system for the current phase. Moreover, the robustness of the controller in parameter estimation uncertainties has also been shown, for the same phase. The proofs are presented at Appendix C. Note, though, that those proofs cannot be applied in a more complex three-dimensional system, since there is no analytical solution for such a system. The phase in which the servicer is moving towards the passive object is more demanding and only stability in certain special cases can be ascertained.

2.3.4 Simulation Results

To display the stable performance of the controller and verify the soundness of the proposed method, a series of simulations was run. To this end, we assume a rigid passive

body of 400 kg mass, manipulated by two free-flying robots of 90 kg each. Each robot has a thruster pointing away from the controlled body, which, when fired, delivers a force of 50 N. The triggering value f_t for the thrusters' initiation is set to 40 N. Both robots manipulators have a reach of 3 m.

2.3.4.1 Initial controller

Simulation 1

First, a simple motion is simulated, where the passive body has to follow a trapezoidal profile on its velocity. The body accelerates with constant acceleration of 0.05 m/s^2 for 10 s. Then, its desired velocity remains constant at 0.5 m/s for 40 s. Finally, it decelerates till zero velocity for 10 s, and then it remains still. The controller presented in Eqs. (65) and (67) is implemented to demonstrate the concept. The gains of the controller for this simulation were set to $K_0 = 1.5$, $K_1 = 0.8$ and $K_2 = 0.8$. The gains are chosen as a tradeoff between lower tracking errors and lower fuel consumption. Higher K_0 results in lower tracking error e_0 , but also in demand for higher control forces, applied by the servicers, and thus in higher disturbances for the motion of the servicers. In order to keep the servicers within their manipulators workspace, more frequent thruster firing is required, thus leading to higher fuel consumption. Similarly, higher K_1 and/or K_2 gains result in more restricted motion of the corresponding servicer around its desired position (the manipulator workspace center), but also in more frequent thruster firing, thus higher fuel consumption.

Figure 2-14 shows the motion of the three bodies, the tracking error of the passive body and the distances between the two robots and the passive body. Figure 2-15 shows the manipulator applied forces and the on-off thruster forces. As shown in Figure 2-14 and Figure 2-15, the passive body follows its desired trajectory very well, while the distances between the robots and the body remain within the manipulator workspace limits.

Another important issue shown in these plots is that, even in this case, there is a very small limit-cycle effect remaining, at the steady state part of the simulation.

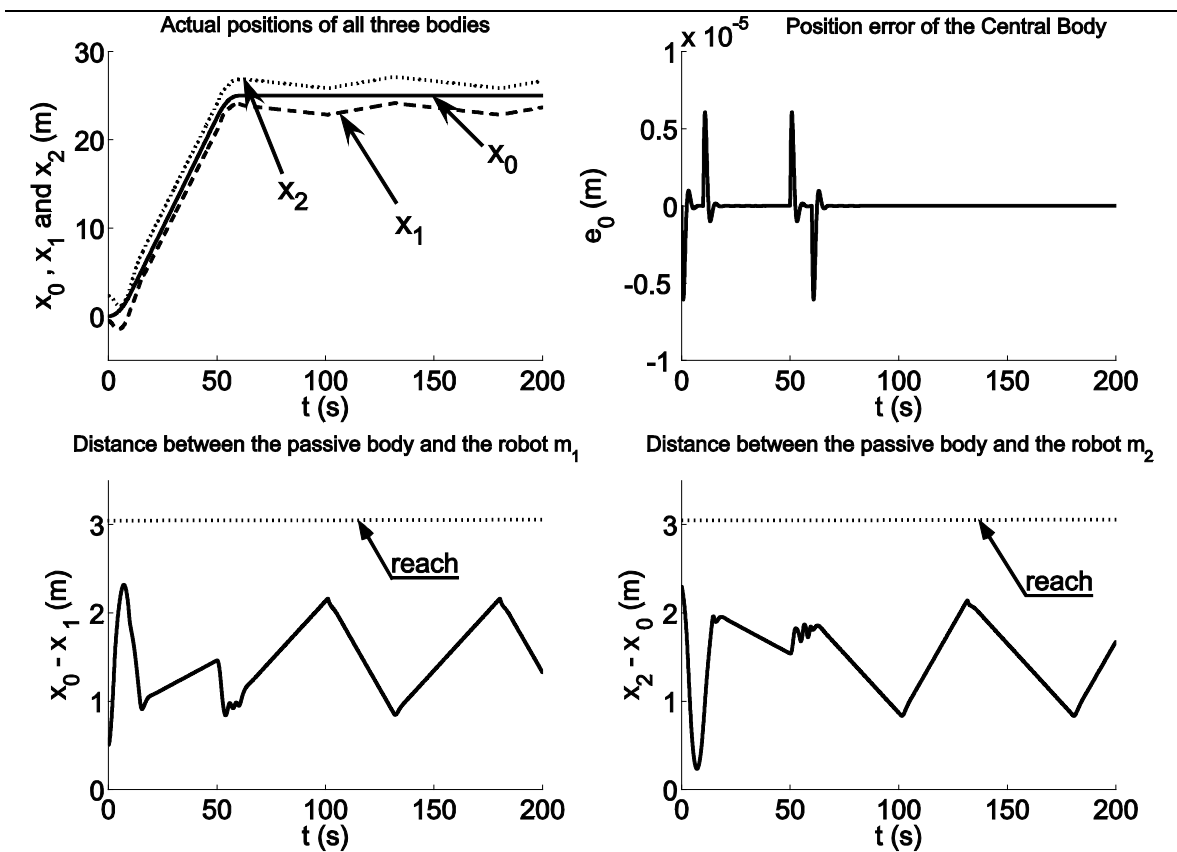


Figure 2-14. Response of the system with manipulators, for a trapezoidal profile desired velocity.

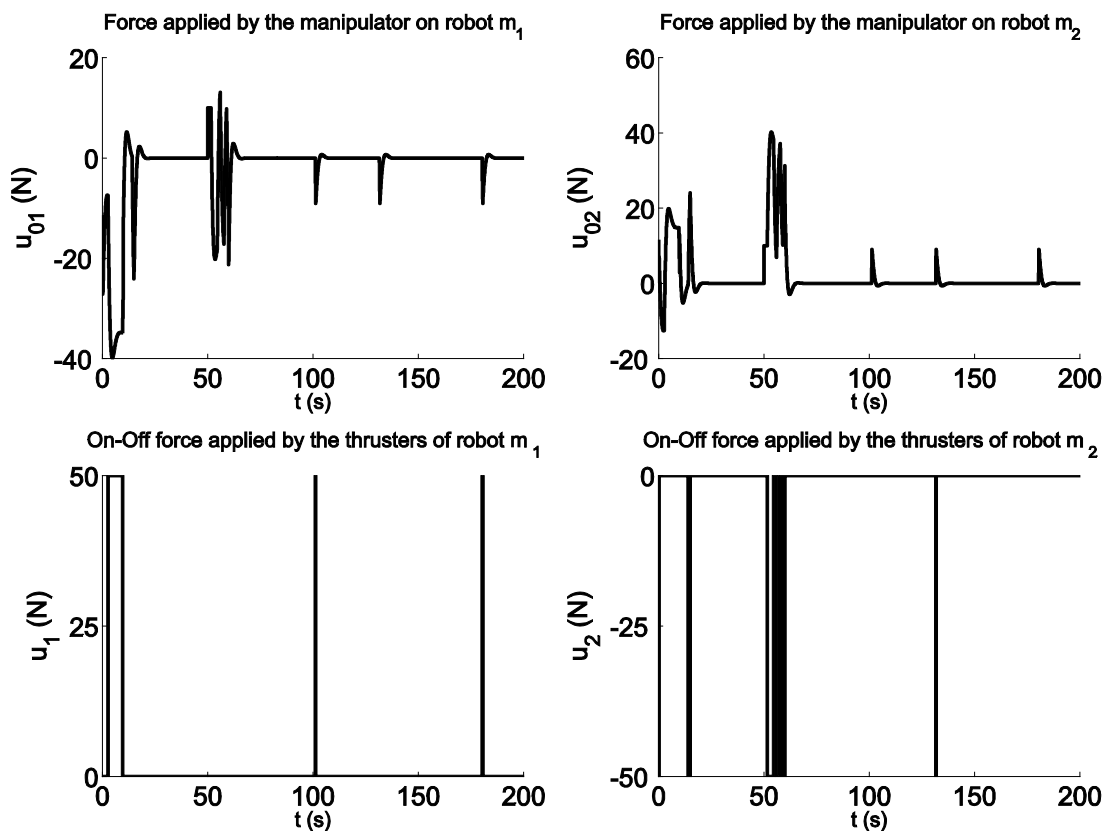


Figure 2-15. Required forces of the system with manipulators, for trapezoid profile on desired velocity.

This is occurring because, to keep the passive body inactive with ever smaller position error, manipulators apply a small remaining force. Due to this reason, a small remaining relative motion between each robot and the passive body, forces the robots to move slowly towards the boundary distances from the body, i.e. the manipulator reach. When they move too close to these limits, the controller briefly activates the thrusters setting this small motion towards the opposite direction, as seen in Figure 2-14, after 70s. However, the effect of these motions on the passive object, as will be shown later, is far less intense than the classic limit-cycle occurring on pure on-off controlled systems, see Figure 2-10.

Simulation 2

The next simulation corresponds to a more demanding passive body trajectory, since it corresponds to a sinusoidal motion with a 5 m amplitude and a 0.07 rad/s frequency. Figure 2-16 and Figure 2-17 display the same features as those in Figure 2-14 and Figure 2-15 respectively.

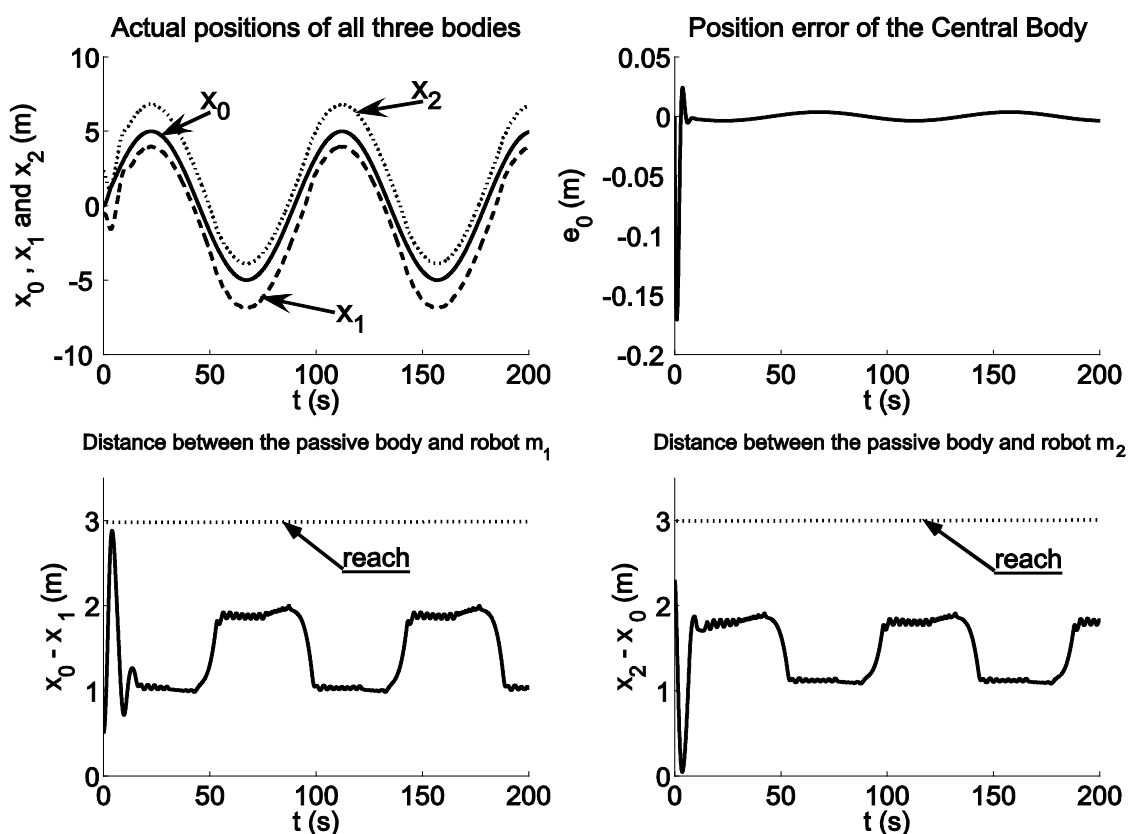


Figure 2-16. Response of the system with manipulators, for sinusoidal position.

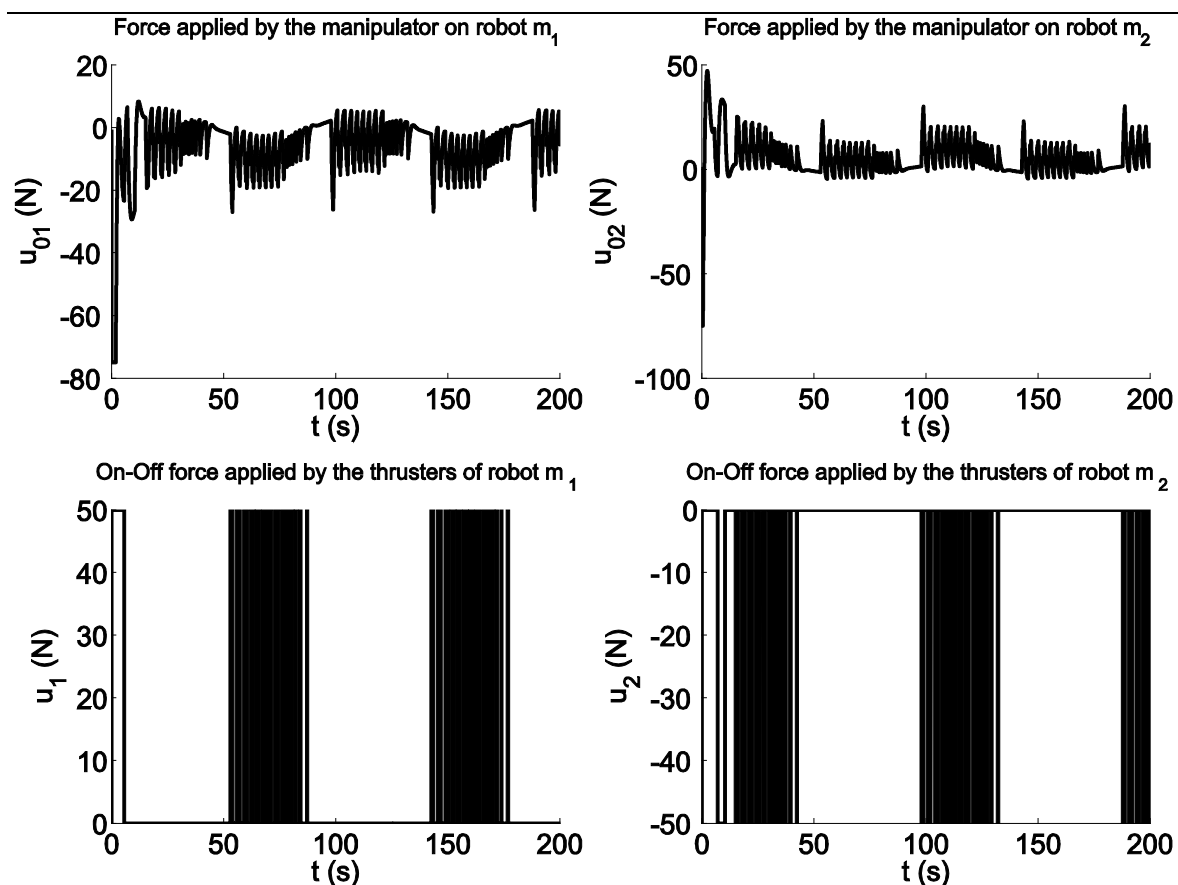


Figure 2-17. Required forces of the system with manipulators, for sinusoidal desired position.

This demanding trajectory is followed also, with the distances between the robotic servicers and the controlled object remaining within limits. As expected, the fuel consumption is now greater since the desired motion is time varying. Note that, the higher the frequency and the magnitude of the required sinusoidal motion, the harder would be for the free-flying servicers to apply the desired generalized forces on the passive object, while still following within their manipulator working spaces.

Simulation 3

Having demonstrated the stable performance of the controller, we examine next its robustness. Several tests with inaccurate parameter estimations and measurements were conducted. Again, the same trapezoidal profile on the desired passive body velocity was used, as introduced at the beginning of Section 2.3.4.1.

In Figure 2-18 and Figure 2-19, the same variables as in Figure 2-14 and Figure 2-15 respectively, are displayed. However, here inaccurate estimation of the three masses is assumed, with a 15% error for the passive body, 10% for one robot and 5% for the other.

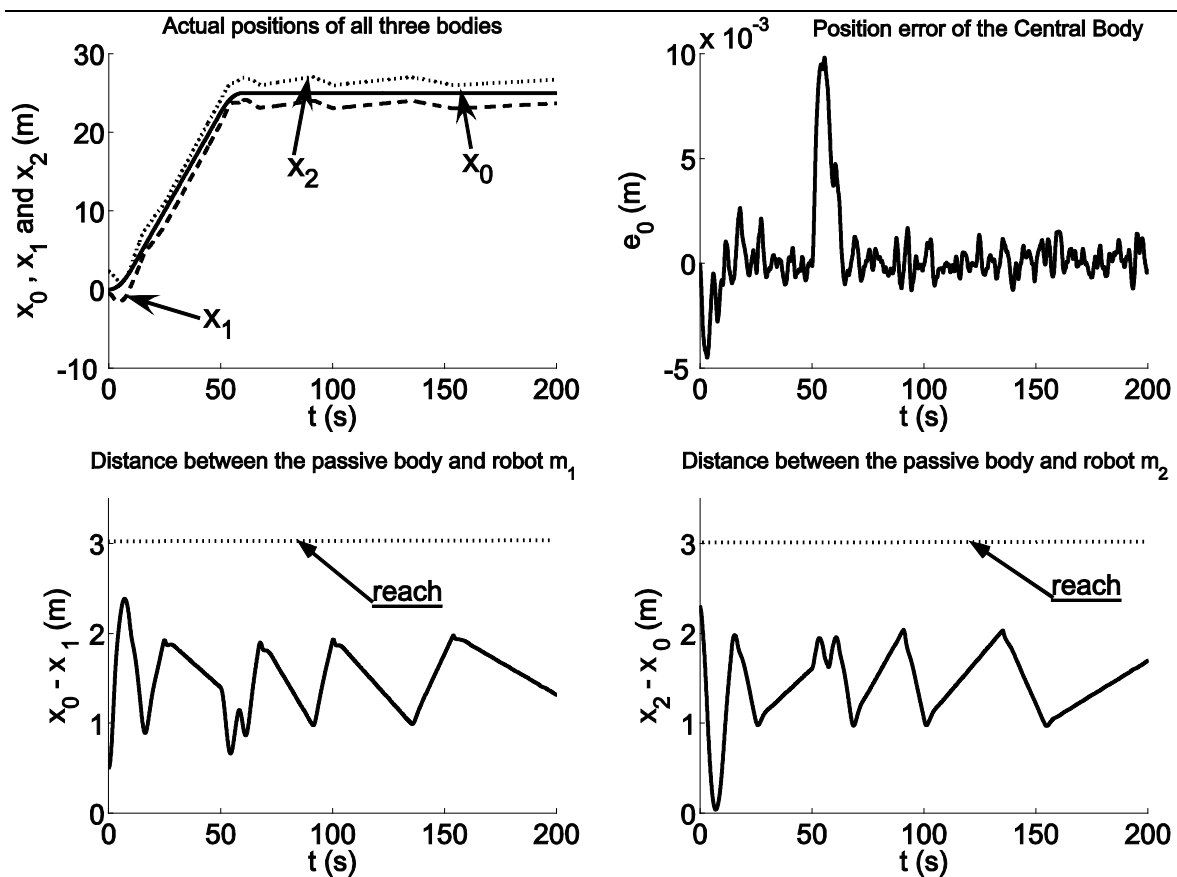


Figure 2-18. System with manipulators response, for Simulation 3.

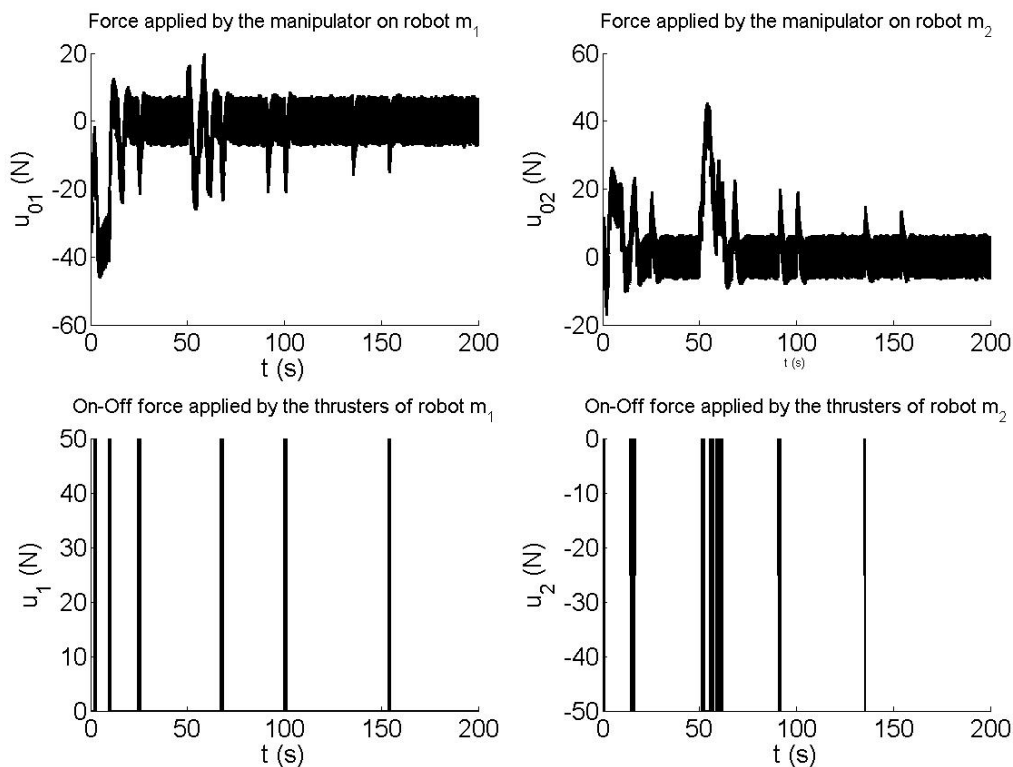


Figure 2-19. Required forces of the system with manipulators, for Simulation 3.

In addition to that, the measurement of all three velocities is assumed to include Gaussian noise, with variance 0.04. Moreover, one thruster is assumed to have a lag of 0.3 s. Finally, one manipulator is assumed to be flawed and to always apply 10% less of the required force.

It can be observed that the controller displays a very robust behavior, even though four very important types of inaccuracies occur simultaneously. The position error of the passive body motion is obviously larger, but still remains reasonable.

Simulation 4

A comparison is made between the performance of the proposed controller and a pure on-off control, as described in Section 2.3.1. Thus, the one-dimensional motion of the system without manipulators is modeled as shown in Eq. (18) and the controller is the one shown in Eqs. (19) and (20). Note that, if the same backstepping approach as we used to derive the controller for the system with manipulators, is used for the system of Eq. (18), the same PD on-off controller as the one shown in Eqs. (19) and (20) is obtained.

Trapezoidal velocity profiles for the passive object were selected for both systems. The performance of both cases is illustrated in Figure 2-20 in which the motion of a system without manipulators Figure 2-20 (a), (c) is compared to a system with manipulators Figure 2-20 (b), (d). Figure 2-20 displays the position errors on the motion of the passive body, as well as the energy consumption for both cases. The latter is computed as the integral of the work produced by both thruster forces (chemical energy) and manipulator forces (electrical energy). Note that, depending on motor drives, it may be possible to recuperate the electric energy supplied to the motors when the applied force of a manipulator is opposing the relative motion of the passive body and the corresponding free-flyer. If this possibility does not exist, then the brake energy is dissipated to heat. The energy for both of these cases is displayed in Figure 2-20 (d).

To reduce the position error without manipulators, the control gains must be increased, or equivalently, the threshold f_i must be decreased. This results in even larger fuel consumption, since the thrusters fire more frequently. Note, though, that the system with the manipulators yields a passive object position error which is two orders of magnitude smaller than the one of the system without them (Figure 2-20a and b).

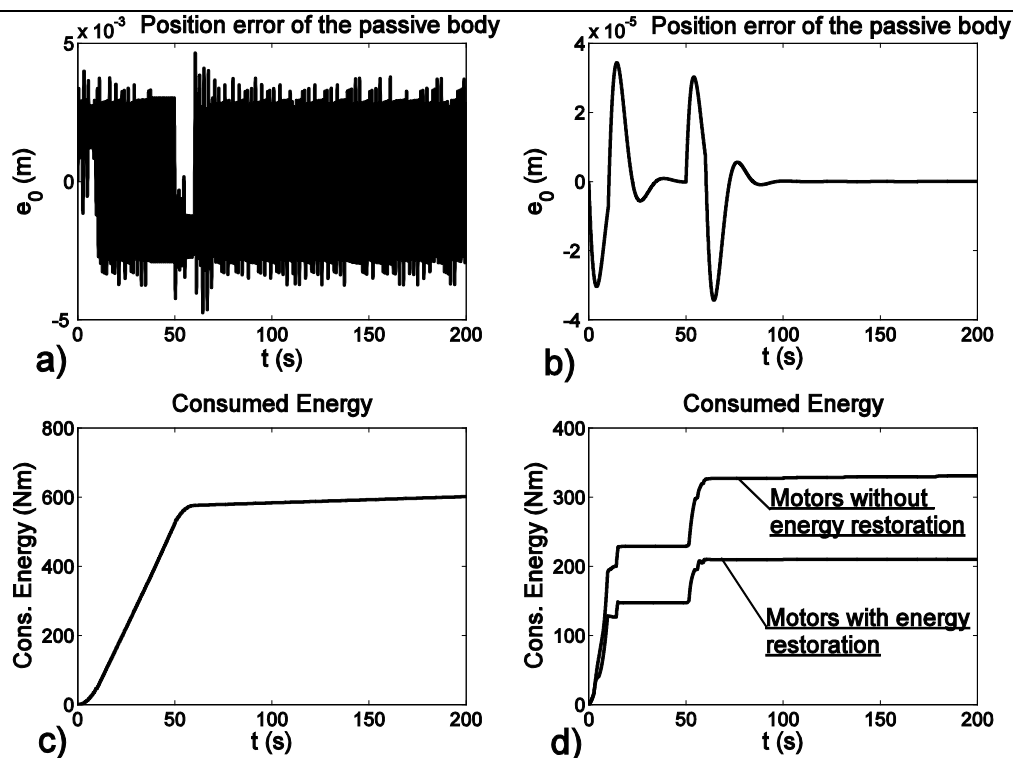


Figure 2-20. Position error as a function of time and corresponding consumed energy (a), (c) without manipulators, and (b), (d) with.

Moreover, it also uses about half the fuel (Figure 2-20c and d), making the introduction of manipulators a significant improvement, over the simple PD on-off control. A number of simulations showed that, when the desired trajectory for the passive body is more demanding, like the sine trajectory in Figure 2-16, the comparison is even more in favor of employing manipulators in controlling the passive object. Thus, the proposed initial controller of Eqs. (65) and (67), even reaching a type of a small limit-cycle as mentioned in the previous sections, is greatly improved over the simple on-off control.

2.3.4.2 Final controller

The controller of Eqs. (69) and (72) is implemented, for the same system of passive object and servicers and the same desired passive object trajectory with the trapezoidal velocity profile. The gains of the controller for this simulation were even less than before and were set to $K_0 = 1$, $K_1 = 0.8$ and $K_2 = 0.8$, using the same method as in Simulation 1 of Section 2.3.4.1 to obtain them. In Figure 2-21, the same variables as in Figure 2-14 are used.

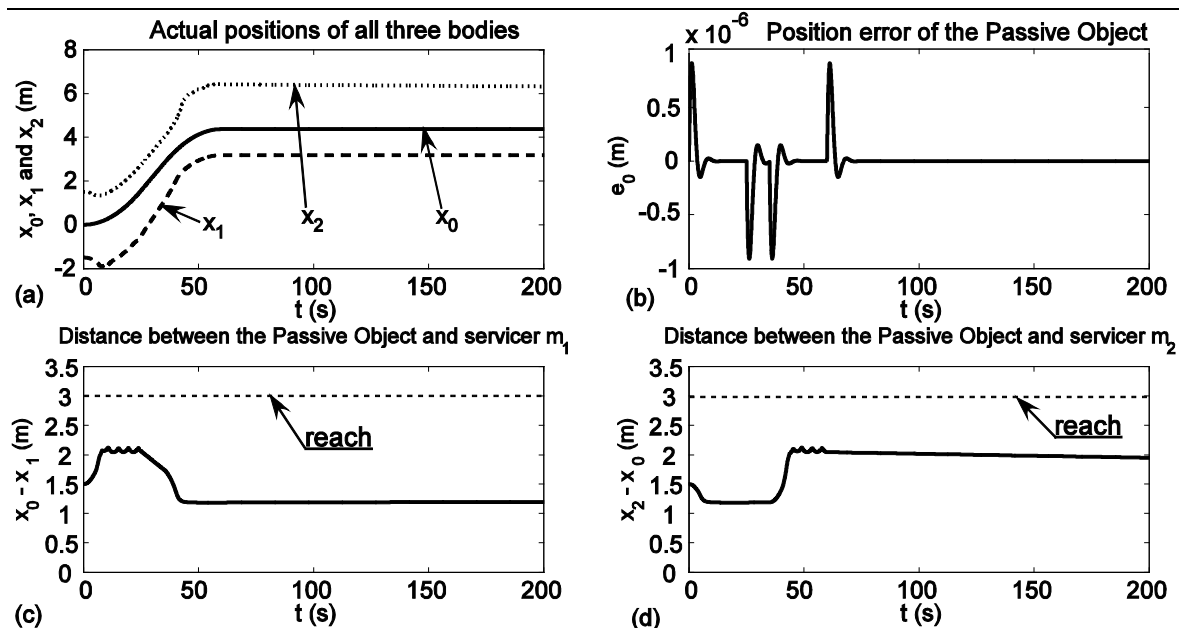


Figure 2-21. Response of the system with manipulators, for a trapezoidal profile desired velocity (second controller).

As can be seen from Figure 2-21a and b, the passive object moves along the desired trajectory, with very low position error, while the servicers keep it between them. From Figure 2-21c and d, it can be observed that this motion is achieved with the servicer bases remaining well within their corresponding manipulator reach. In Figure 2-22 a comparison is made between the initial controller of Eqs. (65) and (67) and the final controller of Eqs. (69) and (72), both in terms of passive object position tracking error and in terms of consumed energy. The latter is again computed as the integral of the work produced by both thruster forces (chemical energy) and manipulator forces (electrical energy).

As can be seen from Figure 2-22, the proposed controller of Eqs. (69) and (72) is even better than the one of Eqs. (65) and (67), which in turn was shown to be superior to the pure on-off control, since not only it has almost half the energy consumption (Figure 2-22c and d), but also it has about 35 time less position tracking errors for the passive object motion (Figure 2-22a and b).

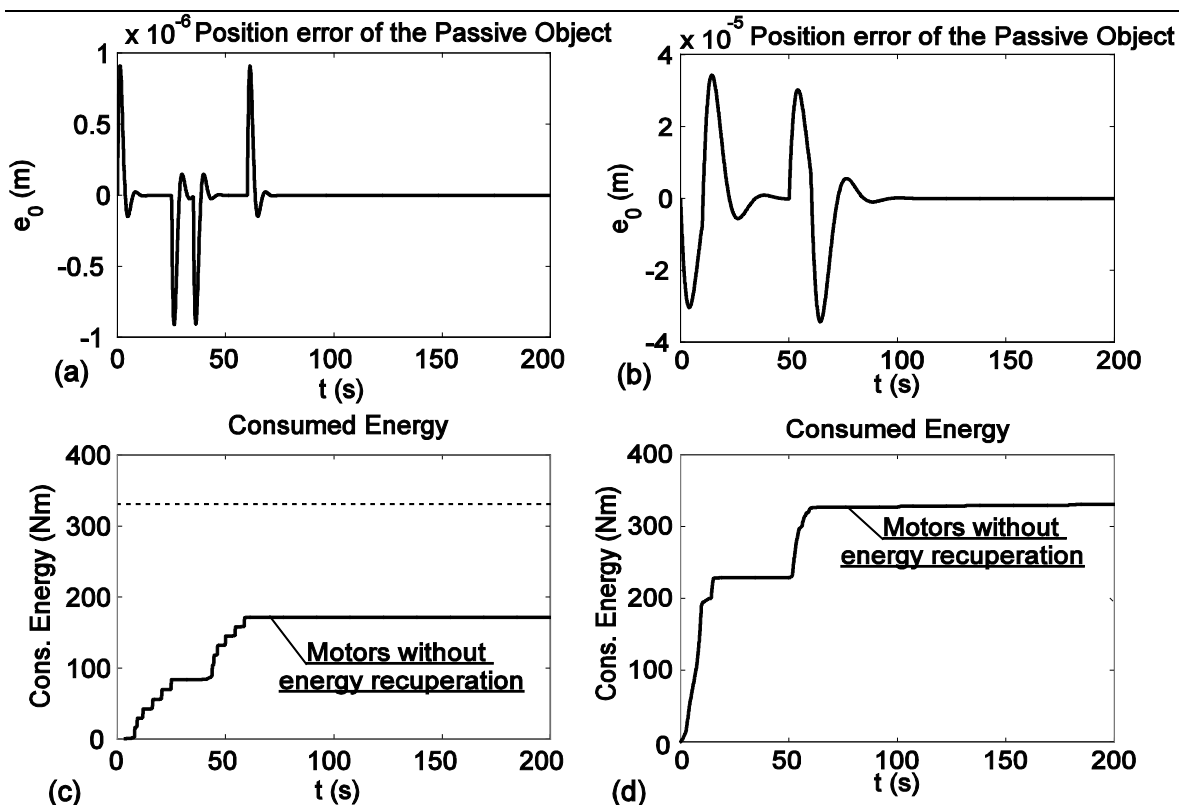


Figure 2-22. Comparison between the two proposed controllers. Passive object position error for (a) the controller of Eqs. (69) and (72) and (b) the controller of Eqs. (65) and (67). Energy consumption for (c) the controller of Eqs. (69) and (72) and (d) the controller of Eqs. (65) and (67).

2.4 Conclusion

In the first part of this section, a novel concept for an *orbital debris capturing system* has been presented, including a number of orbital free-flying robots, holding a net, by which the orbital debris is to be captured. To better understand the behavior of this complex system, a simplified one-dimensional system has been developed. The dynamics and control of the system and the desired system response led to the derivation of sets of constraints that must hold between system parameters and initial conditions. Satisfying the constraints results to a set of control gains that are used in a velocity-based controller. The response of the simulated system has confirmed the constrained control method. The robustness of the method was studied in the case of inaccurate estimation of the debris parameters. It was found that the method shows robustness, keeping the debris in the net, although an additional force may be needed, whenever the steady state velocities result in the net with the captured debris to move away from the robot base. Nevertheless, the demonstrated feasibility of the proposed concept is marginal, even for a simplified one-dimensional model. For that reason, another OOS concept was also studied.

The concept of *cooperative manipulation of a rigid passive object*, via manipulators based on a number of free-flying robots in zero-g environment, was also introduced in the second part of this section. The system dynamics arising from the unilateral constraints and the on-off thrusting were discussed and the manipulation concept was illustrated using a simplified one-dimensional model. A novel controller was presented, based on backstepping and Lyapunov stability methodologies. It was shown that the introduction of manipulators in the handling of a passive object is a vast improvement over the simple on-off control, currently used in the control of orbital systems, both in terms of errors and in terms of fuel consumption. Moreover, several controllers for this system were presented, while two were evaluated via simulations. From the analysis presented in Appendix C, the use of the controller of Eqs. (69) and (72) can guarantee the boundedness and robustness of the relative motion between the passive object and the servicers, at least for the phase in which the servicer is moving away from the passive object and in some cases also for the phase in which the servicer is moving towards the passive object, while nothing of the sort can be said about the response of the system under the controller of Eqs. (65) and (67). Taking also into account the fact that the (simulated) response of the system under the controller of Eqs. (69) and (72) is better than the response of the system under the controller of Eqs. (65) and (67), as seen in Figure 2-22, the controller of Eqs. (69) and (72) is chosen for the control of the simplified one-dimensional system. Although the motion of an actual 3D system is far more complex, the simplified model of the cooperative manipulation concept displays far more promising behavior than the debris disposer concept, showing that it can assist in the control of novel orbital robotic servicers required in future space projects and in the exploitation of space. Thus, the cooperative manipulation concept is chosen to be studied further, through a more realistic three-dimensional model, presented in the next chapter.

3 On-Orbit Passive Object Handling by Cooperating Space Robotic Servicers

A passive object on orbit can be manipulated employing two main techniques: In the first, the servicers come into direct, firm contact with it and use their thrusters to control its motion, as illustrated in Figure 2-8a. In the second, servicers establish contact with the object using manipulators, as seen in Figure 2-8b, and control its motion with manipulator and servicer base coordinated actions.

In employing the first technique, the object motion response is essentially the same with that of a rigid free-flying system, such as a satellite, controlled by its thrusters only. At present, to protect thruster valves from the extreme space conditions, the control for these systems is on-off, initiated by a PD law acting on error variables \mathbf{e} , $\dot{\mathbf{e}}$. However, on-off thrusting results either in chattering, which wears the thrusters and increases fuel consumption, or in deadband-induced limit cycles, that reduce fuel consumption but also positioning accuracy [18], [71]. Note that although satellites employ on-off thrusting, this thrusting is used mainly for point-to-point attitude corrections and not for complex trajectory tracking, as required in a number of activities.

In employing the second technique, manipulators may contact the object either with a firm grasp or with a point contact. In the latter case, a manipulator's end-effector just touches the passive object, without being able to pull it (unilateral constraint) or to exert moments on it. The introduction of manipulators results in smoother passive object handling (since continuous forces are applied on it) and smaller errors, while the specifications for positioning the servicer bases are relaxed, lowering the need for thruster firing, and for fuel consumption and thruster wear. Although firm grasp is safer and more practical, point contact is considered, since firm grasp is not always feasible (e.g. as in the active orbital debris removal case).

The aim of this thesis is to study the fine positioning of a passive object in space, while eliminating on-off control effects on its motion, and minimizing the required thruster fuel. To this end, the introduction of manipulators, for both the point contact and firm grasp cases, is compared to the direct contact on-off technique. For servicers equipped with manipulators, three assumptions are made: (i) single manipulator servicers are employed for simplicity, (ii) the servicer and passive object masses and inertias are

considered as much larger than those of the manipulators, while all relative accelerations and velocities, and thus the manipulator joint accelerations and velocities, are very small. For these reasons, manipulator inertia effects are neglected, (iii) gravity effects are neglected due to small operation durations compared to orbital times. Manipulator kinematics, i.e. manipulator posture, workspace size, and force/torque propagation, are taken into account.

Successful execution of a manipulation task is subject to a number of requirements, described briefly below.

(a) Manipulator workspace constraints must be respected.

(b) For safety reasons, thrusters pointing towards the object or towards another servicer should be turned off.

(c1) In the *firm grasp* case, at least two servicers are needed. To control an object in six degrees of freedom (DOF), three forces and three torques must be exerted on it. Therefore, a single servicer equipped with a single manipulator could achieve handling. Nevertheless, because of requirement (b), a single servicer will face the problem of not being able to exert thruster forces in one or more directions. Thus, even in the case of firm grasps, a number of cooperating free-flyers are needed, with two servicers being the minimum. In practice, the number of the servicers also depends on whether they are capable of applying the required magnitude of forces/ torques on the object.

(c2) In the *point contact* case, at least three single-manipulator servicers are required to produce any required force and torque vector on the passive object. This results from the fact that the moment applied by a force along an axis is:

$$\boldsymbol{\tau} = \mathbf{d} \times \mathbf{F} \quad (74)$$

where \mathbf{d} is the distance from the force application point to the axis. If the distance is zero (i.e. if the force is applied at a point on the axis), then the resulting torque $\boldsymbol{\tau}$ is also zero. Thus, the two manipulators with point contacts are not able to exert on the passive object a torque around an axis parallel to the line \mathbf{l}_c connecting the two contact points, i.e. the two servicers in Figure 3-1 cannot exert any moment around axis \mathbf{l}_c . Therefore, a third single-manipulator servicer would be required, in order to apply a force along an axis that does not have common points with the line connecting the two contact points. Thus, the required torque along that line (that the two initial servicers could not exert on the passive object) would be provided.

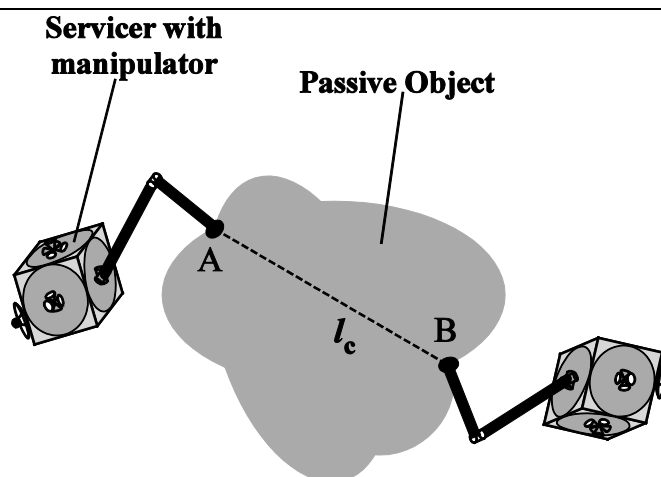


Figure 3-1. In the point contact case, two single-manipulator robots cannot exert a moment around the line defined by the two contact points A and B.

(d) To protect thruster valves from space conditions, continuous or pulse-width-modulation (PWM) thruster control is avoided in space. This is because the generation of low control thrusts (e.g. when the tracking errors are small), requires rapid thruster switching (up to several thousand times per second). However, electromechanical thruster valves cannot follow rapid PWM commands, deteriorating controller response and performance. Rapid switching may result in valve closing before it has opened fully, or opening before it has closed fully. This can result in nozzle ice formation, deterioration of thruster performance, and eventual damages. For example, the performance of thrusters deteriorates to levels below 80%, if the duration of thrust pulses is less than 300 ms, even for 1N thrusters [11]. Simple on-off or Pulse Width Pulse Frequency (PWPF see Appendix D) modulation, both with minimum on and off times, are not subject to these limitations and are preferred in space applications [9], [10], [106], [109]. However, their use is limited to *satellite attitude control* where thruster firing is sparse, and not in *trajectory tracking*, where the controller must update thrust values several times per second.

(e) In the *point contact* case, manipulators can only push a passive body, introducing unilateral constraints and complicating manipulation. Such issues have been studied for terrestrial systems, but not for systems in zero-g, where the absence of a fixed base or of gravity pulling all bodies towards the same direction, makes the aspect of losing contact critically important. Thus, to avoid end-effector slipping, or risking losing the object, the applied forces must stay within the local friction cone.

Since the focus of this chapter is on minimizing thruster fuel during accurate object cooperative manipulation on orbit, and having introduced the manipulation concepts as

well as the related assumptions and requirements, an important question arises: Is the introduction of manipulators beneficial for passive object manipulation? Or more specifically, can they result in accurate trajectory tracking control of a passive object avoiding limit cycles, while limiting thruster fuel use? Next, we will demonstrate that the answer is affirmative on both counts.

3.1 Spatial System Dynamics

As already mentioned in assumption (ii), the dynamics of the manipulators of the servicers are not considered significant, compared to the dynamics of the passive object and the servicer bases. Thus, only the dynamics of those bodies are taken into account, although the dynamics of the manipulators are also taken into account through Jacobian matrices introduced later on. The dynamics of a system of n orbital robotic servicers controlling a rigid passive body via manipulators is studied next. The equations of motion for passive object ($i=0$) and free-flying servicer bases ($i=1, \dots, n$) have the form [83]:

$$\mathbf{H}_i \ddot{\mathbf{q}}_i + \mathbf{C}_i(\mathbf{q}_i, \dot{\mathbf{q}}_i) = \mathbf{Q}_i \quad (75)$$

where \mathbf{q}_i are the generalized coordinates for the object ($i=0$) and the servicer bases ($i=1, \dots, n$),

$$\mathbf{q}_i^T = [\mathbf{r}_i^T, \boldsymbol{\theta}_i^T]^T = [x_i, y_i, z_i, \theta_i, \varphi_i, \psi_i]^T \quad (76)$$

where $[x_i \ y_i \ z_i]^T$ is the position vector \mathbf{r}_i of the CM of body i with respect to the Cartesian frame and $[\theta_i \ \varphi_i \ \psi_i]^T$ denote the Euler angles $\boldsymbol{\theta}_i$ of the same body. Note that the use of Euler angles introduces the possibility of representational singularities. Nevertheless, those are known singularities and can be dealt with by a simple change of the Euler angles set, when the object approaches the singular points. Because of assumption (ii), the manipulators act as an end-effector force/torque transmission to the servicer base. The matrices \mathbf{H}_i are the 6×6 mass matrices of body i :

$$\begin{aligned} \mathbf{H}_i &= \begin{bmatrix} \text{diag}(m_i, m_i, m_i) & \mathbf{0}_{3 \times 3} \\ \mathbf{0}_{3 \times 3} & \mathbf{E}_i^T \mathbf{R}_i \mathbf{I}_i \mathbf{R}_i^T \mathbf{E}_i \end{bmatrix} = \\ &= \begin{bmatrix} \mathbf{I}_{3 \times 3} & \mathbf{0}_{3 \times 3} \\ \mathbf{0}_{3 \times 3} & \mathbf{E}_i^T \end{bmatrix} \begin{bmatrix} \text{diag}(m_i, m_i, m_i) & \mathbf{0}_{3 \times 3} \\ \mathbf{0}_{3 \times 3} & \mathbf{R}_i \mathbf{I}_i \mathbf{R}_i^T \mathbf{E}_i \end{bmatrix} = \mathbf{E}_i^* \mathbf{H}_i^* \end{aligned} \quad (77)$$

where $\mathbf{I}_{3 \times 3}$ is the 3×3 identity matrix, \mathbf{R}_i is the rotation matrix transforming vectors from the frame i to the Cartesian frame, \mathbf{I}_i and m_i are the inertia matrix and mass of body i

respectively, \mathbf{E}_i is a 3×3 matrix mapping the Euler rates $\dot{\boldsymbol{\theta}}_i$ of body i to its inertial angular velocity $\boldsymbol{\omega}_i$:

$$\boldsymbol{\omega}_i = \mathbf{E}_i \dot{\boldsymbol{\theta}}_i \quad (78)$$

The \mathbf{C}_i are 6×1 vectors containing the nonlinear velocity terms. By denoting (for the remaining of this work) the symbol $(*)^\times$ as the cross-product matrix of vector $(*)$, i.e.,

$$\mathbf{a}^\times = \begin{bmatrix} 0 & -a_3 & a_2 \\ a_3 & 0 & -a_1 \\ -a_2 & a_1 & 0 \end{bmatrix}, \text{ where } \mathbf{a} = \begin{bmatrix} a_1 \\ a_2 \\ a_3 \end{bmatrix} \quad (79)$$

Then the \mathbf{C}_i are defined as

$$\mathbf{C}_i = \left[\mathbf{0}_{1 \times 3}, \left(\mathbf{E}_i^T \left(\mathbf{R}_i \mathbf{I}_i \mathbf{R}_i^T \dot{\mathbf{E}}_i \dot{\boldsymbol{\theta}}_i + (\mathbf{E}_i \dot{\boldsymbol{\theta}}_i)^\times \mathbf{R}_i \mathbf{I}_i \mathbf{R}_i^T \mathbf{E}_i \dot{\boldsymbol{\theta}}_i \right) \right)^T \right]^T = \mathbf{E}_i^* \left[\mathbf{0}_{1 \times 3} \quad \mathbf{C}_i^{*T} \right]^T \quad (80)$$

In Eq. (75), \mathbf{Q}_i ($i = 1, \dots, n$) are 6×1 vectors that include thruster forces, reaction wheel moments and manipulator forces/ torques acting on the i^{th} servicer base,

$$\mathbf{Q}_i = \begin{bmatrix} \sum_{j=1}^{n_i} \mathbf{f}_{ij} + \mathbf{f}_{bi} \\ \mathbf{E}_i^T \left(\mathbf{n}_i + \mathbf{n}_{bi} + \sum_{j=1}^{n_i} (\mathbf{d}_{ij}^\times \mathbf{f}_{ij}) + \mathbf{p}_i^\times \mathbf{f}_{bi} \right) \end{bmatrix}, \quad \begin{array}{l} i = 1, \dots, n \\ j = 1, \dots, n_i \end{array} \quad (81)$$

where n_i is the number of thrusters, \mathbf{f}_{ij} and \mathbf{n}_i are the thruster forces and reaction wheel moments acting on the i^{th} servicer base, \mathbf{f}_{bi} and \mathbf{n}_{bi} are the forces and moments transmitted to the i^{th} servicer base by its manipulator, \mathbf{d}_{ij} is the vector locating the j^{th} thruster of the i^{th} servicer base with respect to the base CM, and \mathbf{p}_i is the position vector locating the i^{th} manipulator mount with respect to the base CM, see also Figure 3-2.

The manipulators can be attached to the object through a firm grasp or through a contact point. In the case of *firm grasp*, the vector \mathbf{Q}_0 includes forces and moments applied on the passive object by the n end-effectors:

$$\mathbf{Q}_0 = \begin{bmatrix} \mathbf{Q}_f \\ \mathbf{Q}_n \end{bmatrix} = \begin{bmatrix} \sum_{i=1}^n \mathbf{f}_{Ei} \\ \mathbf{E}_i^T \left(\sum_{i=1}^n (\mathbf{d}_i^\times \mathbf{f}_{Ei}) + \mathbf{n}_{Ei} \right) \end{bmatrix} \quad (82)$$

where \mathbf{f}_{Ei} , \mathbf{n}_{Ei} are respectively the forces and moments applied to the passive object by the i^{th} end-effector, and \mathbf{d}_i^{\times} is the cross-product matrix derived from vector \mathbf{d}_i , i.e. the vector locating the i^{th} manipulator contact point A_i at the passive object, with respect to the passive object CM, see Figure 3-2.

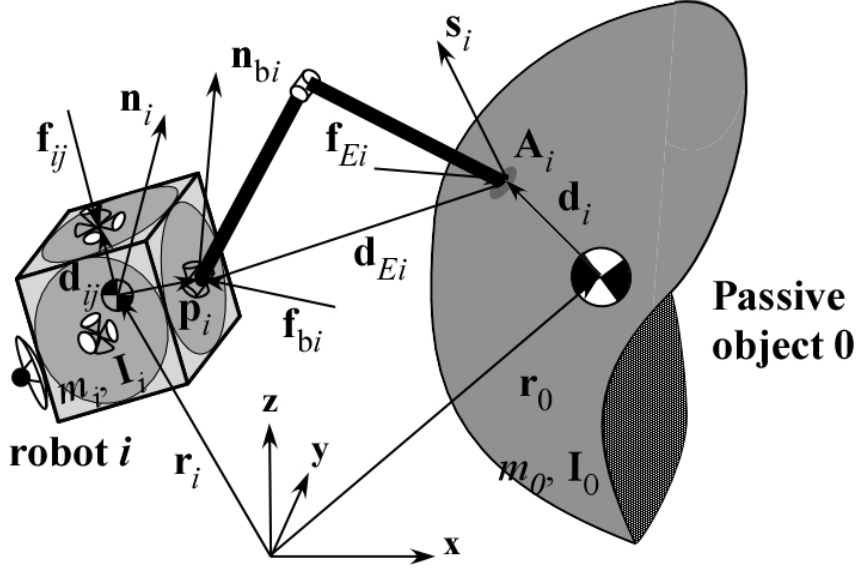


Figure 3-2. Passive object (0) and the i^{th} free-flyer with a single manipulator.

In the case of *point contact*, Eqs. (75) to (81) still hold; however here, end-effectors cannot apply torques. Thus Eq. (82) becomes

$$\mathbf{Q}_0 = \begin{bmatrix} \mathbf{Q}_f \\ \mathbf{Q}_n \end{bmatrix} = \begin{bmatrix} \sum_{i=1}^n \mathbf{f}_{Ei} \\ \mathbf{E}_i^T \sum_{i=1}^n (\mathbf{d}_i^{\times} \mathbf{f}_{Ei}) \end{bmatrix} \quad (83)$$

Combining the above equations for all the $n + 1$ bodies to a single matrix equation, the following is obtained:

$$\mathbf{H}\ddot{\mathbf{q}} + \mathbf{C}(\mathbf{q}, \dot{\mathbf{q}}) = \mathbf{Q} \quad (84)$$

where:

$$\mathbf{q} = [\mathbf{q}_0^T, \mathbf{q}_1^T, \mathbf{q}_2^T, \dots, \mathbf{q}_n^T]^T \quad (85)$$

$$\mathbf{H} = \text{diag}[\mathbf{H}_0, \mathbf{H}_1, \mathbf{H}_2, \dots, \mathbf{H}_n] \quad (86)$$

$$\mathbf{C} = [\mathbf{C}_0^T, \mathbf{C}_1^T, \mathbf{C}_2^T, \dots, \mathbf{C}_n^T]^T \quad (87)$$

$$\mathbf{Q} = [\mathbf{Q}_0^T, \mathbf{Q}_1^T, \mathbf{Q}_2^T, \dots, \mathbf{Q}_n^T]^T \quad (88)$$

In the *point contact* case, and in accordance to (c2), three servicers are needed, as opposed to at least two for the *firm grasp* case, see (c1). In the rest of the paper, for comparison reasons, we assume three servicers for both cases.

3.2 One Large vs. a Number of Small Servicers

As already mentioned, for the case of a number of small servicers, each servicer has the thrusters that face the passive object deactivated for safety reasons. Thus, the only force that can push a robotic servicer away from the passive object can come from its manipulator. For this reason, the manipulator force required for the control of the passive object should be at least equal to the force required to repel the corresponding servicer base from the passive object, whenever this is needed. Moreover, the thruster force should be larger than the maximum manipulator force, in order for the servicer to be controllable. When there is a need for a repelling force and the manipulator force required for the passive object control is not adequate to also act as repelling force, then this manipulator force is augmented by the required amount in the required for repelling direction. In that case, though, the total manipulator force is no longer the one required for the passive object control and thus acts as a disturbance to the passive object motion. Nevertheless, its effect is cancelled out by appropriate counter forces applied by the other servicer manipulators. For more details, see Section 3.3.5.

In the case of a single, large robotic servicer, the above approach cannot be applied, since there are no additional servicers whose manipulators would cancel out the effect the extra repulsive force would have on the passive object. In order to overcome this problem, we assume that in the case of a single robotic servicer, the servicer controller would orient its base (relative to the passive object) such, that there would always exist pairs of thrusters with forces \mathbf{f}_{1j} along lines that do not pass through the passive object, but would have components \mathbf{f}_{1jr} along the desired direction, as can be seen in Figure 3-3. Moreover, the other components of the thruster forces (\mathbf{f}_{1jp}), would roughly cancel out each other, leaving a small remaining force acting as a disturbance in that direction. The freedom the servicer has to move within its manipulator workspace, makes it easier to deal with this small disturbance. For example, if \mathbf{f}_{11p} is larger than \mathbf{f}_{12p} (Figure 3-3), then the servicer base will start moving mainly away from the passive object, but also to the side. The thruster that delivers a force opposite to \mathbf{f}_{11} along with \mathbf{f}_{12} can be used to cancel the side motion, when

its deemed necessary by the controller of the servicer base, in order to keep it within the manipulator workspace.

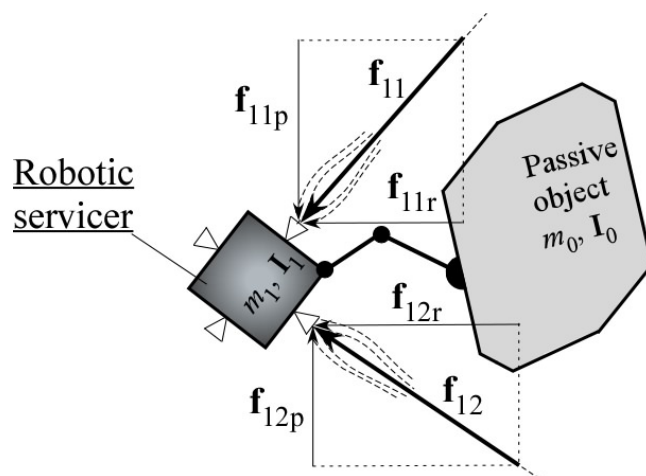


Figure 3-3. Pushing the servicer away from the passive object, in the case of one, large servicer.

This type of control is simpler than the one opted for the case with three servicers, as the latter is described above, and in more detail in Section 3.3.5. Nevertheless, the use of pairs of forces like f_{11} and f_{12} in Figure 3-3, leads to extra fuel consumption, because of the simultaneous existence of opposing forces like f_{11p} and f_{12p} . Fuel consumption depends heavily on the existence of forces in the null space of the servicer base. Thus, in order to mitigate this effect, another switching strategy is opted.

As will be mentioned in more detail in Section 3.3.5, the first step in deriving the servicer base controller, for both the one large and the several small servicers cases, is to use a model-based PD control to compute the continuous generalized control force, and then use a switching strategy to provide the thruster control inputs. This continuous control force of the servicer is first transferred to the servicer base frame, whose axes coincide with the thruster firing lines. Then, the new switching strategy is to turn each thruster on whenever the corresponding force component exceeds a pre-set threshold. Moreover, the servicer base orientation controller keeps the servicer base at an orientation relative to the passive object such as the one described in the previous paragraphs and also seen in Figure 3-3. This method leads to lower fuel consumption, as will be demonstrated in Chapter 4, since it mitigates the appearance of forces in the null space of the servicer base motion. Nevertheless, the existence of a number of servicers, as opposed to one, makes the system more flexible in terms of gain and servicer positioning tuning, a fact that can further lower fuel consumption as will be demonstrated in Chapter 4, also.

Another difference between the system with a number of small servicers and the system with a single large servicer lies on the required type of contact between the manipulator end-effector and the passive object. If one large servicer is used, firm grasping of the passive object is required. In the case of a number of small servicers, firm grasping of the passive object is still an option, but this configuration allows for point contact, for whenever firm grasp is not feasible. For example, this is the case of orbital debris handling, where appropriate appendages for firm grasping may not exist, or may not be available.

An additional difference between the two cases stems from the fact that there is a limit in the maximum size of the servicers, due to the limit in the payload capacities of the launchers. Thus, the option of several small servicers handling large passive objects, in some cases it may be the only one.

One more difference between the two handling options, is that the system with a number of small servicers is more complex, with at least two or three servicers (depending on the contact case) interacting with each other and with the passive object. This leads to a more complex passive object controller, since the existence of more than one servicers results in the need for a force distribution method, such as the optimization process proposed in this work.

A final difference between the two cases is that, in the case of a single and large robotic servicer, a failure in the performance of the servicer would result in the failure of the trajectory tracking motion of the passive object. In the case of a number of small robotic servicers, failure in the performance of one of them may not have catastrophic results on trajectory tracking of the passive object, since the remaining servicers may be able to adequately control the passive object, depending on the type of the failure and on the type of the desired motion.

Based on the above comparison, also displayed in Table 3-1, the case of several, smaller servicers is chosen. In Chapter 4, the two cases are going to be compared in terms of fuel consumption, for the same trajectory tracking maximum errors of the passive object trajectory tracking motion, further verifying the correctness of the several, small servicers choice.

Table 3-1. Comparison between the single, large servicer and the several smaller servicers cases

	Single larger servicer	Several smaller servicers
More flexible in terms of gain and servicer positioning tuning.	-	+
Both contact cases vs. only firm grasp.	-	+
Max servicer size issues.	-	+
Simpler controller	+	-
Sensitivity to servicer failure	-	+
TOTAL	4 - , 1+	1 - , 4 +

3.3 Control Design

The task at hand is the trajectory tracking control of a passive object in space, by three single-manipulator servicers. The goal is to minimize, or even eliminate the passive object tracking errors, while keeping the servicer bases bounded within their manipulator workspaces. In deriving a controller to eliminate errors, a number of methodologies can be used. Nevertheless, systems such as the one in discussion are highly nonlinear; and therefore, backstepping [69] that can accommodate nonlinearities directly, is a good candidate. According to this method, we “step back” at each iteration, in order to create the control inputs from the simple subsystems of a more complex dynamic model. By transforming into new variables at each iteration, a nonlinear system can be led to display linear behavior, if there are no uncertainties on the dynamic system modeling. Moreover, backstepping can avoid the elimination of nonlinear quantities in the controller, important for stability and trajectory tracking, ensuring the controlled system stability.

3.3.1 Passive object motion without use of thrusters

As in the simplified one-dimensional model of Chapter 2, first is studied the case of the maximum passive object translational motion that can be obtained by using only the

servicer manipulators. Note that, since in the case of *point contact* thruster firing is necessary in order to keep the servicers in contact with the passive object, the following analysis is done for the *firm grasp* case only. Here, as in the one-dimensional simplified case also, all the servicer thrusters are inactive and no external force is applied to the system. Thus, the system center of mass state remains constant. The manipulators can be used to exert a non-zero total force and zero total moment on the passive object, leading to pure translation. The servicer bases would then move with respect to the passive object, thus limiting the duration of the exerted total force by the corresponding manipulator workspaces. A typical case for the initial state of the system is as shown in Figure 3-4. Without loss of generality, the system CM (x_{cm}, y_{cm}, z_{cm}) is assumed to coincide with the origin of the inertial frame, thus leading to

$$x_{cm} = y_{cm} = z_{cm} = 0 \quad (89)$$

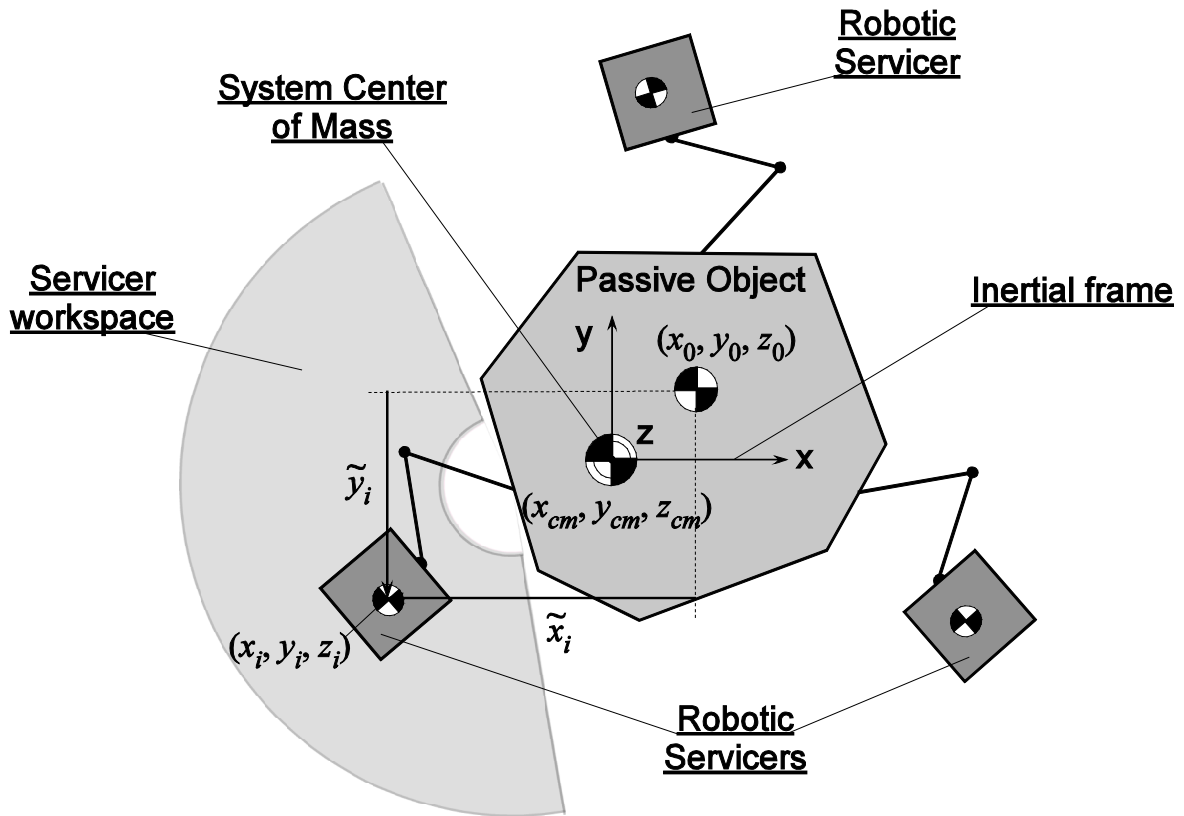


Figure 3-4. Spatial handling of the passive object by use of manipulator forces only.

Moreover, x_{cm} is obtained as:

$$x_{cm} = \frac{\sum_{i=0}^3 x_i m_i}{m_0 + m_1 + m_2 + m_3} \quad (90)$$

where x_i are the coordinates along the inertial x-axis of the CM of the passive object ($i = 0$) and the servicer bases ($i = 1, 2, 3$), see also Eq. (76) and Figure 3-4. By denoting the relative distances between the passive object and the servicers as

$$\tilde{x}_i = x_i - x_0 \quad \text{for } i = 1, 2, 3 \quad (91)$$

and using Eq. (89) then, Eq. (90) becomes

$$x_{cm} = \frac{m_0 x_0 + \sum_{i=1}^3 (x_0 + \tilde{x}_i) m_i}{m_0 + m_1 + m_2 + m_3} = 0 \quad (92)$$

By denoting x_{i_in} and x_{i_f} the initial and final values of x_i respectively, Eq. (89) leads to

$$x_{cm_in} = x_{cm_f} = 0 \quad (93)$$

Then, Eqs. (92) and (93) result in

$$\frac{m_0 x_{0_in} + \sum_{i=1}^3 (x_{0_in} + \tilde{x}_{i_in}) m_i}{m_0 + m_1 + m_2 + m_3} = \frac{m_0 x_{0_f} + \sum_{i=1}^3 (x_{0_f} + \tilde{x}_{i_f}) m_i}{m_0 + m_1 + m_2 + m_3} \quad (94)$$

or, equally,

$$(m_0 + m_1 + m_2 + m_3) x_{0_in} + \sum_{i=1}^3 \tilde{x}_{i_in} m_i = (m_0 + m_1 + m_2 + m_3) x_{0_f} + \sum_{i=1}^3 \tilde{x}_{i_f} m_i \quad (95)$$

By denoting,

$$\begin{aligned} \delta x_0 &= x_{0_f} - x_{0_in} \\ \delta \tilde{x}_i &= \tilde{x}_{i_f} - \tilde{x}_{i_in} \quad \text{for } i = 1, 2, 3 \end{aligned} \quad (96)$$

then Eq. (95) leads to

$$\delta x_0 = - \frac{\sum_{i=1}^3 \delta \tilde{x}_i m_i}{m_0 + m_1 + m_2 + m_3} \quad (97)$$

In this way, Eq. (97) provides the motion along the inertial x-axis of the passive object δx_0 , with respect to the relative motions $\delta \tilde{x}_i$ between the servicers and the passive object, without the use of the thrusters. The maximum passive object motion that can be achieved without thruster firing depends on the maximum relative motions $\delta \tilde{x}_i$, which are functions of the initial relative distances \tilde{x}_{i_in} and the workspace of each servicer.

Next, a simplified example is used in order to illustrate the method of obtaining the maximum passive object displacement without thruster firing, with specific workspace limits. In this example, it is assumed that the system center of mass velocity is zero, and that the motion studied is along the passive object fixed frame x-axis, as seen in Figure 3-5. Note that the notation for the servicers m_1 and m_2 is the same as in the one-dimensional case, since the relative motion between these servicers and the passive object that can cause collision, is along the axis of the motion, as is the case in the one-dimensional case. Thus, for $i = 1$ or 2 , δ_i denotes the distance from the i^{th} servicer center of mass to its manipulator base, while d_i denotes the projection of δ_i along the passive object x-axis. Note that, while δ_i is fixed (as is in the one-dimensional case), d_i is a function of the relative orientation between the corresponding servicer and the passive object. Moreover, δ_{0i} denotes the constant distance from the passive object center of mass to the contact point with the i^{th} servicer manipulator, along the passive object x-axis, δx_i denotes the distance of the i^{th} servicer base from the passive object, i.e. the current manipulator reach of the i^{th} servicer, again along the passive object x-axis and x_{00} denotes the initial distance from the passive object center of mass to the system center of mass, along the passive object x-axis.

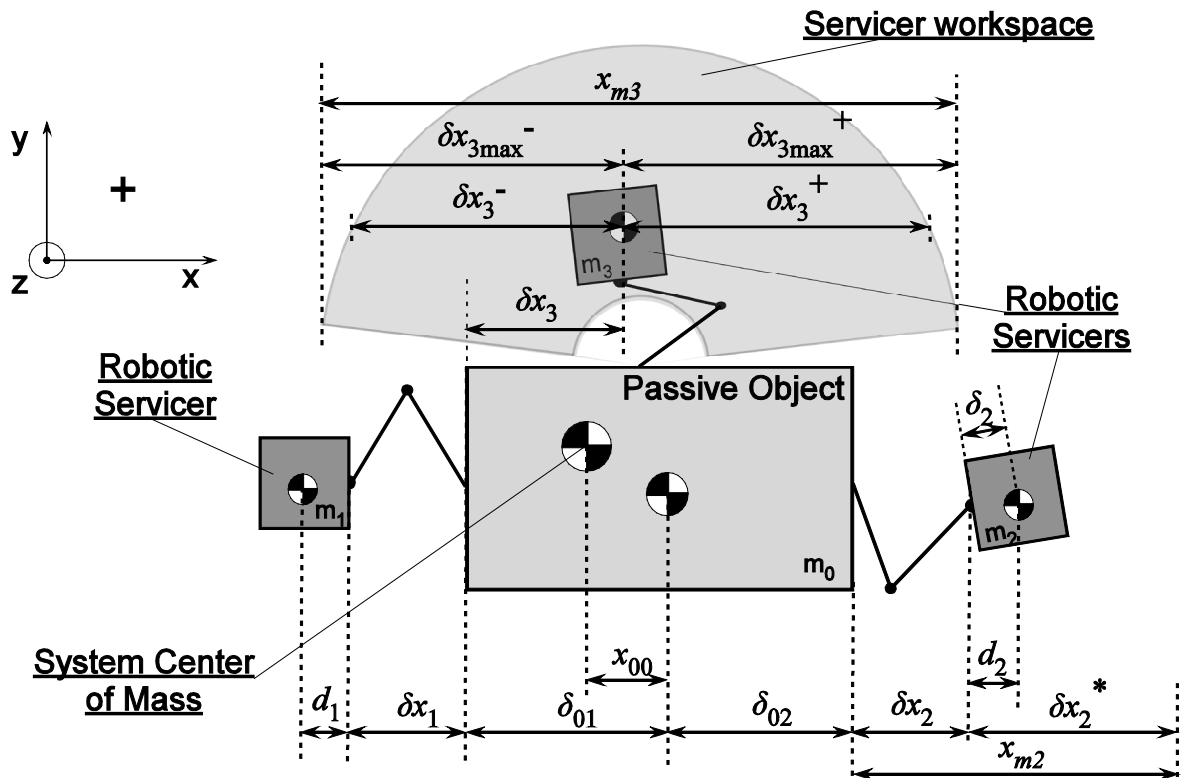


Figure 3-5. Spatial handling of the passive object by use of manipulator forces only, in simple motion.

Note also that δx_i^* (in Figure 3-5 only δx_2^* is shown) denotes the additional reach the i^{th} servicer manipulator can have on top of δx_i , in order to reach its maximum manipulator reach x_{mi} , i.e.

$$\delta x_i + \delta x_i^* = x_{mi} \quad (98)$$

Moreover, taking into account Figure 3-5, \tilde{x}_i , which was defined in Eq. (91), becomes

$$\begin{aligned} \tilde{x}_1 &= -d_1 - \delta x_1 - \delta_{01} \\ \tilde{x}_2 &= d_2 + \delta x_2 + \delta_{02} \end{aligned} \quad (99)$$

while, since δ_{0i} is constant, $\delta \tilde{x}_i$ defined in Eq. (96), becomes

$$\begin{aligned} \delta x_0 &= x_{0_f} - x_{0_in} \\ \delta \tilde{x}_i &= \tilde{x}_{i_f} - \tilde{x}_{i_in} \quad \text{for } i = 1, 2, 3 \end{aligned} \quad (100)$$

For the third servicer (m_3) the notation is different, since different values are important for this motion. Thus, δx_3 is the distance from the m_3 servicer center of mass to the passive object left side, along the passive object x-axis, as seen in Figure 3-5. The allowed relative motion between this servicer and the passive object along the passive object x-axis, starting from this initial relative position, is limited by the servicer manipulator workspace, with respect to the passive object, as seen in Figure 3-5. Note that these limits of δx_3^- and δx_3^+ are functions of the relative distance between the m_3 servicer and the passive object, along the passive object y-axis, while the maximum value these limits can take are denoted by $\delta x_{3\max}^-$ and $\delta x_{3\max}^+$, as also seen in Figure 3-5.

By using an approach similar to the one used in the one-dimensional model of Chapter 2 and by using the subscripts $_{in}$ and $_{f}$ for the initial and final values of the variables shown in Figure 3-5 that change with time (e.g. d_2 changes with time, thus its final value is d_{2_f} while δ_2 does not change with time), the motion δx_0 of the passive object center of mass *without* the use of thrusters, is obtained,

$$\delta x_0 = \frac{-\sum_{i=1}^2 \left[(d_{i_f} - d_{i_in} + \delta x_{i_f} - \delta x_{i_in}) m_i \right] - (\delta x_{3_f} - \delta x_{3_in}) m_3}{m_0 + m_1 + m_2 + m_3} \quad (101)$$

In order to obtain the maximum value of δx_0 , it should be noted that, for the servicers of mass m_1 and m_2 (i.e. for $i = 1, 2$), even though d_i is not fixed, the maximum value of $(\delta x_{i_f} + d_{i_f}) - (\delta x_{i_in} + d_{i_in})$ is,

$$\left(d_{i_f} - d_{i_in} + \delta x_{i_f} - \delta x_{i_in}\right)\Big|_{\max} = \left(\delta x_{i_f} + d_{i_f}\right) - \left(\delta x_{i_in} + d_{i_in}\right)\Big|_{\max} = x_{mi} \quad (102)$$

Moreover, for the m_3 servicer, the maximum value for $\delta x_{3_f} - \delta x_{3_in}$ is $(\delta x_3^- + \delta x_3^+)$, as can be seen in Figure 3-5. Thus, the maximum relative motion this servicer can have along the passive object x-axis, is:

$$\left(\delta x_{3_f} - \delta x_{3_in}\right)\Big|_{\max} = \left(\delta x_3^- + \delta x_3^+\right)\Big|_{\max} = \delta x_{3\max}^- + \delta x_{3\max}^+ \quad (103)$$

Finally, using Eqs. (102) and (103), Eq. (101) provides the maximum motion of the passive object center of mass along its x-axis, when using only manipulator forces (i.e. all thrusters are switched off):

$$\delta x_{0-\max} = \frac{x_{m1}m_1 + x_{m2}m_2 + \left(\delta x_{3\max}^- + \delta x_{3\max}^+\right)m_3}{m_0 + m_1 + m_2 + m_3} \quad (104)$$

Note in Eq. (104) the difference between the contribution of the m_3 servicer of the passive object motion and the contribution of the other two servicers. This is so because of the different relative orientation of the servicers with respect to the passive object motion, for the motion under discussion.

By using a similar approach, the maximum passive object motions, when using only manipulators, along the passive object y-axis and z-axis can be obtained, for both contact cases. Note that, for the passive object y-axis motion, the contribution of the m_3 servicer is of the same type as the contribution of the m_1 and m_2 servicers for the x-axis motion and vice versa. Finally, for the passive object z-axis motion, the contribution of all three servicers is of the same type as the contribution of the m_3 servicer for the x-axis motion.

The above analysis does **not** mean that the space in which the passive object can move when using only manipulator forces, is a rectangular box of sides $\delta x_{0-\max}$, $\delta y_{0-\max}$ and $\delta z_{0-\max}$. As already mentioned, the maximum allowed motion for the passive object is a function of the initial servicer configurations (see Eq. (101)), and what Eq. (104) provides are the absolute maximum x-axis motions of the passive object for the two contact cases, for the ideal initial conditions, i.e. initial relative positions between the passive object and the three servicers. For a given set of initial state of the system and in order to check if a desired final passive object position is feasible without the use of thrusters, the following approach can be used:

1. First, the feasibility of the motion to the desired position along its x-axis, by using only manipulator forces is checked. To do so the desired x-position is checked with respect to the maximum feasible one given by Eq. (101), for the given initial conditions. If the desired x-position is feasible, the passive object is moved to this desired position along its x-axis. Note that the coupling of the translational and rotational motions would result in a different final system state.

2. This state is used as initial configuration for the next step, in which the feasibility of the desired y-position is checked, given this initial configuration. If the motion to the desired y-position is feasible, the passive object is moved there and again the coupling of the translational and rotational motions would result in a different final system state.

3. This final state is used as an initial configuration for the final step. In which the feasibility of the passive object motion to the desired z-position is checked, using the same strategy as in the previous two steps.

3.3.2 Controller derivation and generalized forces constraints: firm grasp case

When the passive object desired motion exceeds the limits set in Section 3.3.1, thrusters must be used to displace the system center of mass. In the *firm grasp* case, the *backstepping* methodology results in a model-based controller, which is used to compute the necessary inertial forces and moments to be applied to the passive object. The application of the backstepping methodology is similar to the one already presented in Section 2.3.3, when dealing with the simplified one-dimensional model. Nevertheless, there are differences, since now we use vectors and matrices instead of purely scalar quantities. To apply this methodology, we first focus on the equations of motion of the passive object. Thus, if

$$\mathbf{e}_0 = \mathbf{q}_{0,d} - \mathbf{q}_0 \quad (105)$$

with $\mathbf{q}_{0,d}$ being the passive object desired trajectory, from Eq. (84), we obtain:

$$\ddot{\mathbf{e}}_0 = \ddot{\mathbf{q}}_{0,d} - \mathbf{H}_0^{-1}(\mathbf{Q}_0 - \mathbf{C}_0) \quad (106)$$

Defining \mathbf{z}_0 and \mathbf{z}_1 as

$$\begin{aligned} \mathbf{z}_0 &= \mathbf{e}_0 \\ \mathbf{z}_1 &= \dot{\mathbf{z}}_0 = \dot{\mathbf{e}}_0 \end{aligned} \quad (107)$$

then, Eq. (106) yields:

$$\begin{aligned}\dot{\mathbf{z}}_0 &= \mathbf{z}_1 \\ \dot{\mathbf{z}}_1 &= \ddot{\mathbf{q}}_{0,d} - \mathbf{H}_0^{-1}(\mathbf{Q}_0 - \mathbf{C}_0)\end{aligned}\quad (108)$$

The variables \mathbf{z}_0 and \mathbf{z}_1 as presented in Eq. (108), are in strict feedback form allowing us to apply the backstepping methodology.

Step 1

Assume for the moment that \mathbf{z}_1 is controllable and that we use the following controller:

$$\mathbf{z}_1 = \boldsymbol{\phi}_{01}(\mathbf{z}_0) = -\mathbf{K}_0\mathbf{z}_0 \quad (109)$$

with the 6×6 matrix $\mathbf{K}_0 = \text{diag}(k_0(1) \dots k_0(6))$ and $k_0(i) > 0$ for $i = 1 \dots 6$. Assume also the following Lyapunov function:

$$V_{01}(\mathbf{z}_0) = \frac{1}{2} \mathbf{z}_0^T \mathbf{B}_0 \mathbf{z}_0 \geq 0 \quad (110)$$

with the 6×6 matrix $\mathbf{B}_0 = \text{diag}(\beta_0(1) \dots \beta_0(6))$ and $\beta_0(i) > 0$ for $i = 1 \dots 6$. By differentiating Eq. (110), we obtain:

$$\dot{V}_{01}(\mathbf{z}_0) = \mathbf{z}_0^T \mathbf{B}_0 \dot{\mathbf{z}}_0 = \mathbf{z}_0^T \mathbf{B}_0 \mathbf{z}_1 \quad (111)$$

and, using Eq. (109), Eq. (111) yields:

$$\dot{V}_{01}(\mathbf{z}_0) = -\mathbf{z}_0^T \mathbf{B}_0 \mathbf{K}_0 \mathbf{z}_0 \leq 0 \quad (112)$$

Unfortunately, $\mathbf{z}_1 = \dot{\mathbf{e}}_0$ is not directly controllable.

Step 2

We define \mathbf{w}_0 as:

$$\mathbf{w}_0 = \mathbf{z}_1 - \boldsymbol{\phi}_{01}(\mathbf{z}_0) = \mathbf{z}_1 + \mathbf{K}_0\mathbf{z}_0 \quad (113)$$

which, ideally, should be zero, thus rendering the tracking errors \mathbf{e}_0 and $\dot{\mathbf{e}}_0$ equal to zero. By differentiating Eq. (113) and using Eq. (108), the following is obtained:

$$\dot{\mathbf{w}}_0 = \ddot{\mathbf{q}}_{0,d} - \mathbf{H}_0^{-1}(\mathbf{Q}_0 - \mathbf{C}_0) + \mathbf{K}_0\mathbf{z}_0 \quad (114)$$

Then, by use of Eqs. (109) and (113), Eq. (114) yields:

$$\dot{\mathbf{w}}_0 = \ddot{\mathbf{q}}_{0,d} - \mathbf{H}_0^{-1}(\mathbf{Q}_0 - \mathbf{C}_0) + \mathbf{K}_0\mathbf{w}_0 - \mathbf{K}_0^2\mathbf{z}_0 \quad (115)$$

Since the directly controlled quantities are the control generalized forces \mathbf{Q}_0 , the following controller is assumed instead of the one in Eq. (109):

$$\mathbf{Q}_0 = \boldsymbol{\phi}_{02}(\mathbf{z}_0, \mathbf{z}_1) \quad (116)$$

with the following Lyapunov function:

$$V_{02}(\mathbf{z}_0, \mathbf{z}_1) = V_{01}(\mathbf{z}_0) + \frac{1}{2} \mathbf{w}_0^T \mathbf{A}_0 \mathbf{w}_0 \geq 0 \quad (117)$$

with the 6×6 matrix $\mathbf{A}_0 = \text{diag}(a_0(1) \dots a_0(6))$ and $a_0(i) > 0$ for $i = 1 \dots 6$. Note also that

$$V_{02}(\mathbf{z}_0, \mathbf{z}_1) = 0 \Leftrightarrow \mathbf{z}_0 = \mathbf{z}_1 = 0 \quad (118)$$

Differentiating Eq. (117) leads to:

$$\dot{V}_{02} = \dot{V}_{01} + \mathbf{w}_0^T \mathbf{A}_0 \dot{\mathbf{w}}_0 \quad (119)$$

and then, by also using Eqs. (110) and (115), we obtain:

$$\dot{V}_{02} = \mathbf{z}_0^T \mathbf{B}_0 \dot{\mathbf{z}}_0 + \mathbf{w}_0^T \mathbf{A}_0 (\ddot{\mathbf{q}}_{0,d} - \mathbf{H}_0^{-1}(\mathbf{Q}_0 - \mathbf{C}_0) + \mathbf{K}_0 \mathbf{w}_0 - \mathbf{K}_0^2 \mathbf{z}_0) \quad (120)$$

Note that, use of Eqs. (108) and (113), results in:

$$\dot{\mathbf{z}}_0 = \mathbf{z}_1 = \mathbf{w}_0 - \mathbf{K}_0 \dot{\mathbf{z}}_0 \quad (121)$$

Thus, Eqs. (116), (120) and (121), lead to:

$$\dot{V}_{02} = \mathbf{z}_0^T \mathbf{B}_0 (\mathbf{w}_0 - \mathbf{K}_0 \mathbf{z}_0) + \mathbf{w}_0^T \mathbf{A}_0 (\ddot{\mathbf{q}}_{0,d} - \mathbf{H}_0^{-1}(\boldsymbol{\phi}_{02} - \mathbf{C}_0) + \mathbf{K}_0 \mathbf{w}_0 - \mathbf{K}_0^2 \mathbf{z}_0) \quad (122)$$

or

$$\dot{V}_{02} = \mathbf{z}_0^T \mathbf{B}_0 \mathbf{w}_0 - \mathbf{z}_0^T \mathbf{B}_0 \mathbf{K}_0 \mathbf{z}_0 + \mathbf{w}_0^T \mathbf{A}_0 (\ddot{\mathbf{q}}_{0,d} - \mathbf{H}_0^{-1}(\boldsymbol{\phi}_{02} - \mathbf{C}_0)) + \mathbf{w}_0^T \mathbf{A}_0 \mathbf{K}_0 \mathbf{w}_0 - \mathbf{w}_0^T \mathbf{A}_0 \mathbf{K}_0^2 \mathbf{z}_0 \quad (123)$$

By defining

$$\mathbf{B}_0 = \mathbf{A}_0 \mathbf{K}_0^2 \quad (124)$$

then Eq. (123) becomes

$$\dot{V}_{02} = -\mathbf{z}_0^T \mathbf{B}_0 \mathbf{K}_0 \mathbf{z}_0 + \mathbf{w}_0^T \mathbf{A}_0 (\ddot{\mathbf{q}}_{0,d} - \mathbf{H}_0^{-1}(\boldsymbol{\phi}_{02} - \mathbf{C}_0)) + \mathbf{w}_0^T \mathbf{A}_0 \mathbf{K}_0 \mathbf{w}_0 \quad (125)$$

Now the control generalized forces of Eq. (116) can be derived. By using

$$\mathbf{Q}_0 = \boldsymbol{\phi}_{02} = \mathbf{C}_0 + \mathbf{H}_0 (\ddot{\mathbf{q}}_{0,d} + \mathbf{K}_0 \mathbf{w}_0) \quad (126)$$

Eq. (125) yields

$$\dot{V}_{02} = -\mathbf{z}_0^T \mathbf{B}_0 \mathbf{K}_0 \mathbf{z}_0 = -\mathbf{e}_0^T \mathbf{B}_0 \mathbf{K}_0 \mathbf{e}_0 \leq 0 \quad (127)$$

Note that, by means of Eqs. (107), (110), and (113), Eq. (117) yields:

$$V_{02} = \frac{1}{2} \mathbf{e}_0^T \mathbf{B}_0 \mathbf{e}_0 + \frac{1}{2} (\dot{\mathbf{e}}_0 + \mathbf{K}_0 \mathbf{e}_0)^T \mathbf{A}_0 (\dot{\mathbf{e}}_0 + \mathbf{K}_0 \mathbf{e}_0) \geq 0 \quad (128)$$

Thus, since $V_{02} \geq 0$ and $\dot{V}_{02} \leq 0$, V_{02} is bounded. This is so because V_{02} cannot tend to $-\infty$ since it is positive and it cannot tend to $+\infty$ with \dot{V}_{02} being negative, if the initial value of V_{02} is non-infinite. By assuming that the initial errors \mathbf{e}_0 and $\dot{\mathbf{e}}_0$ are not infinite, which is a reasonable assumption, and since all matrices \mathbf{A}_0 , \mathbf{B}_0 and \mathbf{K}_0 are diagonal, with positive, constant and non-infinite terms, then by means of Eq. (94), the initial value of V_{02} is indeed non-infinite. Moreover, since V_{02} is bounded, both terms of Eq. (128) must be bounded too:

$$\begin{aligned} 0 < \lim_{t \rightarrow \infty} \left(\frac{1}{2} \mathbf{e}_0^T \mathbf{B}_0 \mathbf{e}_0 \right) < B_1 < +\infty \\ 0 < \lim_{t \rightarrow \infty} \left(\frac{1}{2} (\dot{\mathbf{e}}_0 + \mathbf{K}_0 \mathbf{e}_0)^T \mathbf{A}_0 (\dot{\mathbf{e}}_0 + \mathbf{K}_0 \mathbf{e}_0) \right) < B_2 < +\infty \end{aligned} \quad (129)$$

where $B_1, B_2 > 0$ and bounded.

Assuming that $\mathbf{e}_0 = [e_0(1), e_0(2), \dots, e_0(6)]^T$ and since all matrices \mathbf{A}_0 , \mathbf{B}_0 and \mathbf{K}_0 are diagonal, with positive, constant and non-infinite terms, as already mentioned, Eq. (129) leads to:

$$\left. \begin{aligned} -\infty < \lim_{t \rightarrow \infty} (e_0(i)) < C_1 < +\infty \\ -\infty < \lim_{t \rightarrow \infty} (\dot{e}_0(i) + k_0(i) e_0(i)) < C_2 < +\infty \end{aligned} \right\}, \text{ for all } i = 1, \dots, 6 \quad (130)$$

where $C_1, C_2 > 0$ and bounded. Note that Eq. (130), yields:

$$-\infty < -D < \lim_{t \rightarrow \infty} (\dot{e}_0(i)) < D < +\infty \quad (131)$$

for all $i = 1, \dots, 6$, where $D > 0$ and bounded. Moreover, differentiating Eq. (127), leads to

$$\ddot{V}_{02} = -2\mathbf{e}_0^T \mathbf{B}_0 \mathbf{K}_0 \dot{\mathbf{e}}_0 \quad (132)$$

Since the matrix $\mathbf{B}_0 \mathbf{K}_0$ is also diagonal. Thus, by use of Eqs. (130) and (131), Eq. (132) leads to the fact that \ddot{V}_{02} is also bounded:

$$-\infty < -E < \ddot{V}_{02} < E < +\infty \quad (133)$$

where $E > 0$ and bounded.

Thus, \dot{V}_{02} is uniformly continuous, which, along with the already shown fact that V_{02} is bounded, consist the two requirements of Barbalat's lemma for V_{02} , which states that if the differential function $f(t)$ has a finite limit as $t \rightarrow \infty$, and \dot{f} is uniformly continuous, then $\dot{f}(t) \rightarrow 0$ as $t \rightarrow \infty$ [107]. Thus, we obtain

$$\lim_{t \rightarrow \infty} (\dot{V}_{02}) = 0 \quad (134)$$

Substituting \dot{V}_{02} in Eq. (134) from Eq. (127), leads to:

$$\lim_{t \rightarrow \infty} (\dot{\mathbf{e}}_0) = \mathbf{0} \quad (135)$$

Thus the tracking error \mathbf{e}_0 is proven to tend to the zero 6×1 vector, when the controller of Eq. (126) is used, proving controller stability. By use of Eqs. (108), (109) and (113) on Eq. (126), the final form of the passive object controller is derived:

$$\mathbf{Q}_0 = [\mathbf{0}_{1 \times 3}, \mathbf{C}_0^{*T}]^T + \mathbf{H}_0 (\ddot{\mathbf{q}}_{0,d} + \mathbf{K}_{P0} \mathbf{e}_0 + \mathbf{K}_{D0} \dot{\mathbf{e}}_0) \quad (136)$$

where \mathbf{K}_{P0} , \mathbf{K}_{D0} are constant gain matrices, with $\mathbf{K}_{D0} = \mathbf{K}_0$ and $\mathbf{K}_{P0} = \mathbf{K}_{D0}^2 = \mathbf{K}_0^2$. By applying Eq. (136), the desired trajectory provides the required generalized object forces.

Note that backstepping/ model-based control such as the one in Eq. (136) uses knowledge of inertial properties, which may not be available always, as is the case with non-man-made objects. In those cases, these properties can be obtained by parameter identification methods, such as those in [8], [37] and [38].

The \mathbf{Q}_0 forces and moments in Eq. (136) must be applied by the three end-effectors grasping the passive object, i.e. by the three \mathbf{f}_{Ei} forces and three \mathbf{n}_{Ei} moments. However, these are subject to constraints. The first constraint stems from the fact that, as mentioned earlier, thrusters facing the passive object are deactivated. Therefore, no forces are available to push a servicer away from the passive object, if its distance is less than a preset threshold. This task can be accomplished by its manipulator through the application of an appropriate reaction \mathbf{f}_{bi} , see Eq. (81) and Figure 3-2. The free-flying servicer controller (presented later on) calculates the required repulsive force, denoted by \mathbf{f}_{ij_r} and defined in Eq. (150), to push the servicer away from the object. This force is obtained based on the same idea as in the simplified one-dimensional model and thus is applied as a component of the manipulator reaction \mathbf{f}_{bi} . In this way, to move the servicer away from the

object, this component of \mathbf{f}_{bi} , must be at least equal to the calculated \mathbf{f}_{ij_r} . Contact force \mathbf{f}_{Ei} is subject to the same constraint, since, due to assumption (ii), \mathbf{f}_{bi} is equal to $-\mathbf{f}_{Ei}$. Thus, whenever there is a need for a repulsive force for the i^{th} servicer along the r -direction in the no-thrusting area, Eq. (137) must hold:

$$(\mathbf{f}_{bi} \cdot \hat{\mathbf{r}}) \hat{\mathbf{r}} = -(\mathbf{f}_{Ei} \cdot \hat{\mathbf{r}}) \hat{\mathbf{r}} \geq \mathbf{f}_{ij_r}, \quad i = 1, 2, 3 \quad (137)$$

where $\hat{\mathbf{r}}$ denotes the unit vector along the r -direction. For the firm grasp case, Eq. (137) is the only constraint on the \mathbf{Q}_0 generalized forces.

3.3.3 Controller derivation and generalized forces constraints: point contact case

The controller development so far, was accomplished for the firm grasp case. Nevertheless, the model based control of Eq. (136) and the constraint of Eq. (137) hold also for the end-effector generalized forces \mathbf{Q}_0 for *both contact cases*, although in the *point contact case*, the generalized forces \mathbf{Q}_0 are defined by Eq. (83), instead of Eq. (82). Moreover, in the *point contact* case, unilateral constraints are introduced for the contact forces \mathbf{f}_{Ei} . To avoid loss of contact, these forces must have a normal component towards the object. Thus the following constraint must hold

$$-\mathbf{f}_{Ei} \cdot \mathbf{s}_i < 0, \quad i = 1, 2, 3 \quad (138)$$

where \mathbf{s}_i is the unit vector at the i^{th} contact point \mathbf{A}_i , perpendicular to the surface of the passive object and facing outwards, see also Figure 3-2. In addition, these forces must remain within the friction cone of the contacting surfaces, so that slip of the end-effector on the surface of the passive object is avoided. Therefore, an additional constraint for \mathbf{f}_{Ei} must hold,

$$\text{atan2}\left(\left\|\mathbf{s}_i^\times(-\mathbf{f}_{Ei})\right\|, -\mathbf{f}_{Ei} \cdot \mathbf{s}_i\right) \leq \text{atan}(\mu_i), \quad i = 1, 2, 3 \quad (139)$$

where μ_i is the corresponding friction coefficient between the two contacting surfaces. In Eq. (139), the function atan2 is used to take into account the direction of \mathbf{f}_{Ei} .

3.3.4 Manipulator force distribution

Although Eq. (136) computes the generalized forces \mathbf{Q}_0 to act on the object, end-effector forces and torques \mathbf{f}_{Ei} and \mathbf{n}_{Ei} cannot be calculated by equating Eqs. (82) (or (83), depending on whether firm grasp or point contact case is studied) and (136) due to redundancy and the existence of the abovementioned constraints. Therefore, to solve this

problem, a method for resolving applied to end-effectors forces must be employed, a task generally known as force distribution.

Several methods for force distribution, developed for terrestrial systems, exist in the literature, mainly for grasping mechanisms [15], [23], [25], [74], but also for more general cases [24]. Even on the same field of grasping of a passive object, there are several different works depending on the problem solved, i.e. number of contacts, type of contacts (i.e. fingertip grasping [74], human-like grasping [23], “whole-limb” manipulation [15] etc.), type of motion expected (or even the requirement for passive object equilibrium [25]), or even contact point selection [23]. In our case no fixed bases exist, and servicer bases are “flying” consuming scarce thruster fuel. To address the problem of force distribution on orbit, a two-layered optimization method is developed here. The first layer of the method is defined so as to lower the demands in control forces/moments and thus fit the aim of lowering the thruster fuel consumption. This is because on orbit, the applied control forces/moments on the passive object appear as disturbance reactions on the servicers, and their rejection requires use of reaction wheels and thrusters. Note that this optimization is used as a means of force distribution and so, any solution is acceptable. It is an extra bonus if the provided solution is an optimal one, in terms of further lowering fuel consumption, but sub-optimal solutions are also acceptable. The second layer of the optimization method is developed so that the maximum control forces/moments needed are further reduced by identifying the optimal set of contact points, thus further lowering the fuel consumption. Having set up the problem as described, we adopt an appropriate constrained nonlinear optimization method to yield both end-effector forces/moments and contact point locations.

First layer. For the *firm grasp* case, we set the three end-effector forces \mathbf{f}_{Ei} and the three end-effector moments \mathbf{n}_{Ei} , as the design parameters. Thus, the optimization process returns the contact forces \mathbf{f}_{Ei} and moments \mathbf{n}_{Ei} that must be applied by the manipulators so that the object trajectory is followed, while the forces/moments norm is minimized and the constraints observed. To that end, the performance index is chosen as,

$$\Lambda_1(t) = \frac{1}{2} \min_{\mathbf{n}_{Ei}, \mathbf{f}_{Ei}} \left(\sum_{i=1}^3 (\mathbf{f}_{Ei}^2) + w_2 \sum_{i=1}^3 (\mathbf{n}_{Ei}^2) \right) \quad (140)$$

so that the weighted sums of the squared norms of both the applied forces and moments is minimized. In Eq. (140), w_2 is a weighting factor with appropriate units. The initial guess

for each optimization step is the \mathbf{f}_{Ei} and \mathbf{n}_{Ei} of the previous step, while for the first step, the initial guess is $\mathbf{f}_{Ei} = \mathbf{n}_{Ei} = \mathbf{0}$. The dynamics Eq. (82) acts as a linear constraint for the optimization, while Eq. (137) is a nonlinear constraint to be observed along with control Eq. (136), which also acts as a nonlinear constraint for the optimization.

For the *point contact* case, the three end-effector forces \mathbf{f}_{Ei} are again set as the design parameters, since no moments can be applied by the manipulators. Moreover, the return of the optimization process includes only the contact forces \mathbf{f}_{Ei} that must be applied on the passive object by the servicer manipulators, so that the object trajectory is followed, while the forces norm is minimized and the constraints observed. Thus, the performance index in Eq. (140) is now reduced to,

$$\Lambda_1(t) = \frac{1}{2} \min_{\mathbf{f}_{Ei}} \sum_{i=1}^3 (\mathbf{f}_{Ei}^2) \quad (141)$$

so that the sum of the squared applied forces is minimized. In this case, Eqs. (138) and (139) apply as additional linear and non-linear constraints respectively and dynamics Eq. (83) is used as a linear constraint instead of Eq. (82), while control Eq. (136) and Eq. (137) are again used as non-linear constraints.

The required generalized forces \mathbf{Q}_0 are resolved into the nine contact force components \mathbf{f}_{Ei} by optimization. The two vectors are related by:

$$\mathbf{A}\mathbf{f}_E = \mathbf{Q}_0 \quad (142)$$

where the 6×9 matrix \mathbf{A} depends on the positions of the three contact points, with respect to the passive object center of mass. It should be noted that, the solution to this problem requires that the matrix $\mathbf{A} \mathbf{A}^T$ is of full rank, i.e. six. This holds true always if the determinant of $\mathbf{A} \mathbf{A}^T$ is positive. Three cases when this does not happen are the following: (i) if at least two of the contact points coincide with the passive object center of mass, (ii) if one contact point lies on the line connecting the other two contact points and (iii) if two contact points coincide. Obviously these are cases that degenerate the tree-contact-point case into a two-contact-point case and can be easily avoided. Nevertheless, when choosing the optimal contact points (see *Second layer* below), it must be ensured that the determinant of $\mathbf{A} \mathbf{A}^T$ is positive. Under this assumption/constraint, the problem of force distribution has infinite solutions, as stated in requirement c2. As is true for all optimization techniques, a local minimum may result, pointing to a suboptimal solution.

However, the primary task for the optimization is to resolve the \mathbf{Q}_0 to the three contact forces; this task is achieved still.

Second layer. In the above analysis, it was assumed that the contact point locations of the end-effectors were given. However, the obtained solution depends on these locations. A poor choice may result in high end-effector forces and in turn, in excessive servicer thrusting and fuel expenditure. Therefore, it is beneficial to search beforehand (off-line) for optimal contact point locations. To this end, an additional optimization is set up, having the coordinates of the contact point vectors \mathbf{d}_i as the design parameters. The performance index is now of min-max type,

$$\Lambda_2 = \min_{\mathbf{d}_i} \left(\max_t \Lambda_1(t) \right) \quad (143)$$

where the maximization over time t means that, for a given set of \mathbf{d}_i , the trajectory tracking motion is simulated and the overall $\max \Lambda_1(t)$, i.e. the worse force requirement over time is obtained. The optimization process then chooses a different set of \mathbf{d}_i until $\max \Lambda_1(t)$ is minimized during object desired motion. The procedure yields the optimal contact point vectors \mathbf{d}_i , subject to geometrical constraints defined by the object geometry, as well as the abovementioned constraint on the determinant of matrix $\mathbf{A} \mathbf{A}^T$. With the completion of the optimization process, both the optimal contact points and the force profiles for the free-flying servicers are obtained.

Note that the two-layer optimization yielding the optimal contact points is the same for *both contact cases*. Moreover, it does not need to be executed in real time. In fact, it must be performed off-line, so as to obtain the optimal contact points for capturing the passive object, subject to geometric constraints, before the actual motion. During the actual motion, only the first-layer of the optimization method needs to be running, to resolve the required control force/ moments to the end-effectors, while the contact points are assumed to be given. This improves the execution time of the algorithm.

3.3.5 Free-flying servicer control

Next, the design of the servicer controllers, both in terms of manipulator and in terms of servicer base position and attitude (pose), is presented. Planning the desired servicer trajectory is a complex process, as the servicer manipulator will have to apply the required \mathbf{f}_{Ei} on the object while maintaining a desired pose of its base that takes into account workspace and collision avoidance requirements. To this end, appropriate initial

servicer base pose with respect to the passive object is chosen. It is then desired that it is maintained within certain safety limits, throughout the motion. Hence, the desired servicer base trajectory $\mathbf{q}_{i,d}$ is computed based on the object trajectory and sent to its motion controller. Note that the servicer controller is a two-part controller. The first part is the general motion controller, regarding the thrusters and the reaction wheels. The second part consists of the calculation of the manipulator force component $\mathbf{f}_{ij,r}$, required to push the servicer base away from the passive object (also needed in Eq. (137)). These two parts, inspired by the final controller used on the simplified one-dimensional model, are presented next.

In the case of *firm grasp*, the servicer motion controller takes as feedback the pose of the servicer base and uses it to compute the motion tracking errors, with respect to $\mathbf{q}_{i,d}$. Employing a model-based controller, the control inputs on the i^{th} servicer are given by,

$$\left[\sum_{j=1}^6 (\mathbf{f}_{ij}^T), \mathbf{n}_i^T \right]^T = \mathbf{H}_i^* (\ddot{\mathbf{q}}_{i,d} + \mathbf{K}_{Pi} \mathbf{e}_i + \mathbf{K}_{Di} \dot{\mathbf{e}}_i) + \mathbf{W}_i \quad (144)$$

where,

$$\mathbf{W}_i = \left[-\mathbf{f}_{bi}^T, \left(\mathbf{C}_i^* - \mathbf{n}_{bi} - \sum_{j=1}^6 (\mathbf{f}_{ij}^{\times} \mathbf{d}_{ij}) + \mathbf{f}_{bi}^{\times} \mathbf{p}_i \right)^T \right]^T \quad (145)$$

while, \mathbf{f}_{ij} are the thruster forces and \mathbf{n}_i are the total reaction wheel moment acting on the servicer base, as also seen in Eq. (81) and in Figure 3-2. The \mathbf{K}_{Pi} , \mathbf{K}_{Di} are control gain diagonal matrices, \mathbf{H}_i^* and \mathbf{C}_i^* are defined in Eqs. (77) and (80), $\mathbf{e}_i = \mathbf{q}_{i,d} - \mathbf{q}_i$ is the tracking error, and \mathbf{f}_{bi} , \mathbf{n}_{bi} are the reaction forces and moments transmitted to the i^{th} servicer base by its manipulator. Note that the usual practice in space systems is to have either three reaction wheels in right angles or even four reaction wheels on axes that form a pyramid. Thus, there remains the issue of resolving these reaction wheels moments to the servicer base principal axes, resulting in the total reaction wheel moment \mathbf{n}_i . Nevertheless, if the reaction wheel system is well designed, this is not a difficult issue. In this work it is assumed that the total reaction wheel moment \mathbf{n}_i is observable and controllable.

To apply the controller given by Eqs. (144) and (145), the reaction force \mathbf{f}_{bi} and moment \mathbf{n}_{bi} must be available. These are related to the manipulator end-effector force \mathbf{f}_{Ei} and torque \mathbf{n}_{Ei} by the manipulator force transmission equation,

$$\begin{bmatrix} \mathbf{I}_{3 \times 3} & \mathbf{J}_i \\ \mathbf{0}_{3 \times 3} & \mathbf{I}_{3 \times 3} \end{bmatrix}^T \begin{bmatrix} \mathbf{f}_{Ei} \\ \mathbf{n}_{Ei} \end{bmatrix} = \begin{bmatrix} \mathbf{f}_{bi} \\ \mathbf{n}_{bi} \end{bmatrix} \quad (146)$$

where \mathbf{J}_i is a 3×6 matrix, which resolves the end-effector force \mathbf{f}_{Ei} and torque \mathbf{n}_{Ei} to the base, and is given by:

$$\mathbf{J}_i^T = \mathbf{d}_{Ei}^\times \quad (147)$$

where \mathbf{d}_{Ei}^\times is the cross-product matrix of \mathbf{d}_{Ei} (see also Eq. (79) and Figure 3-2), which is the vector from the manipulator base, to the corresponding contact point. Note that \mathbf{d}_{Ei} depends on the manipulator posture (joint angles) as well as the manipulator Denavit-Hartenberg parameters (kinematic properties). Because of assumption (ii), where Eq. (146) yields $\mathbf{f}_{bi} = -\mathbf{f}_{Ei}$. Resolving \mathbf{f}_{Ei} and \mathbf{n}_{Ei} to joint torques is achieved using the manipulator end-effector Jacobian, also a function of the manipulator posture (joint angles) and the manipulator Denavit-Hartenberg parameters (kinematic properties).

Taking into account the very slow motions of space systems and their design specifications, it is reasonable to assume that manipulator actuators will be able to provide the required joint torques.

Equation (144) can be separated into two parts. The upper part of Eq. (144), consisting of the first three equations, is independent of \mathbf{n}_i and thus can be solved for thruster forces \mathbf{f}_{ij} , once \mathbf{f}_{bi} is obtained by Eq. (146). This, at first, results in a continuous control force $\Sigma \mathbf{f}_{ij}$. To accommodate on-off thrusters, a switching strategy is needed. This strategy includes the following steps: (a) transformation of the $\Sigma \mathbf{f}_{ij}$ to the corresponding servicer base frame (b) projection of the force along the three thruster axes, obtaining three bi-lateral continuous forces, (c) turning each thruster on, when the corresponding continuous force value exceeds a preset threshold value f_t , as can be seen in Figure 3-6. The result of this strategy is six uni-lateral on-off \mathbf{f}_{ij} forces. The resulting controller will not lead to asymptotic stability, but this is not a restriction, as for the servicers we require error boundedness only, such as the one achieved in satellite attitude control. After obtaining the on-off \mathbf{f}_{ij} , they can be used in the lower part of Eq. (144) along with \mathbf{f}_{bi} and \mathbf{n}_{bi} , in order to obtain \mathbf{n}_i .

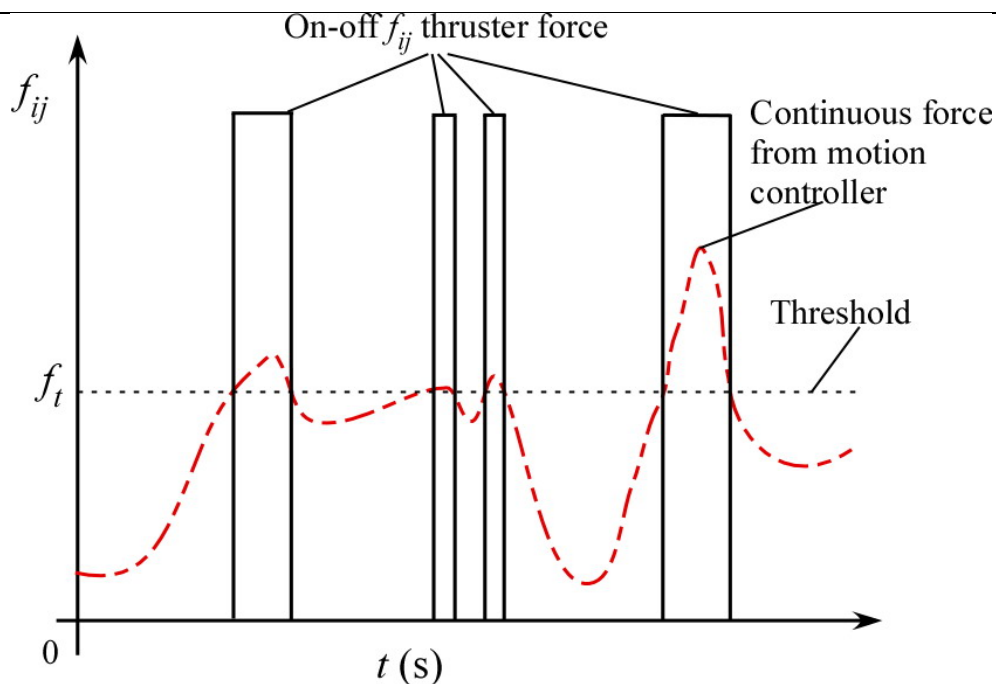


Figure 3-6. Switching strategy for a single thruster, for the servicer position control.

Since wheel-applied moments are subject to limits, moments exceeding these limits can be applied by employing pairs of on-off thrusters. In this case, the continuous \mathbf{n}_i obtained by Eqs. (144) and (145) is also discretized, using the same switching strategy as in the case of \mathbf{f}_{ij} , with a preset threshold value n_t that corresponds to the reaction wheel limits, as can be seen in Figure 3-7. It should be noted that, the required continuous moment below the threshold limit, as seen in Figure 3-7, is actually applied by the reaction wheels. Whenever there is a need for more moment than what the reaction wheels can provide, then the on-off thruster pairs can provide it effortlessly. This on-off moment application may be seen as a disturbance to the continuous controller. Nevertheless, since, for the motion of the servicers only boundedness within the manipulator limits is required and since these relatively large on-off moments are doing exactly that, this is not an issue. In the present work, the on-off moment values were chosen by trial and error in simulated experiments, making sure that the on-off moments are not too large, thus resulting in sending the servicer base quickly towards the opposite limit of the corresponding reaction wheel and leading to a type of limit cycle.

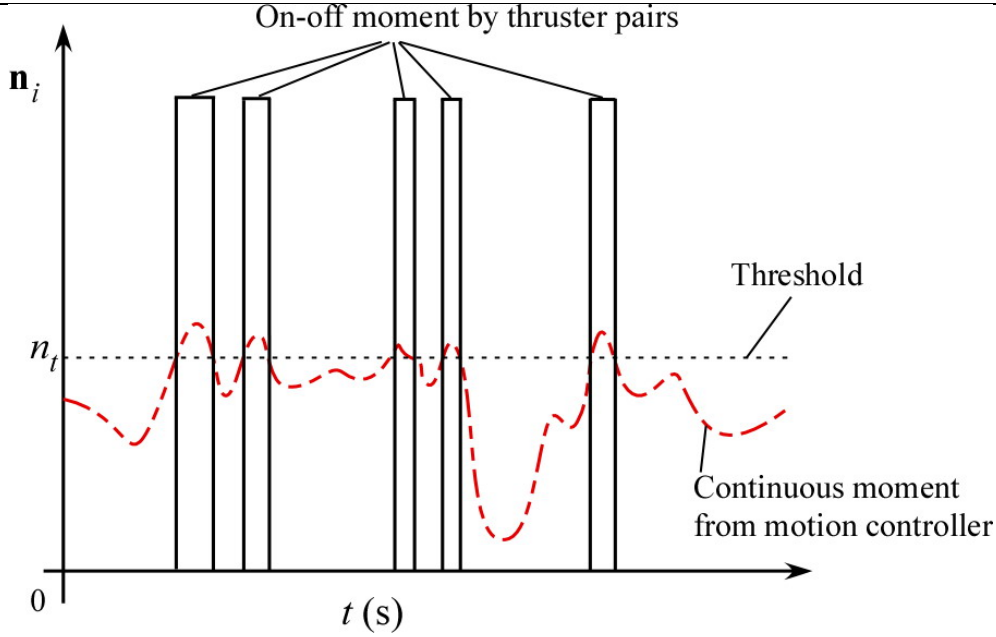


Figure 3-7. Servicer attitude control, with switching strategy when the reaction wheels (continuous moment) reach their limits.

Recall at this point that the computation of the \mathbf{f}_{ij_r} required to keep the servicer away from the passive object, and needed in Eq. (137), is yet to be defined. This force is obtained by employing model-based control. To this end, a model-based PD control force $\mathbf{F}_{mb,i}$ is calculated first according to,

$$\mathbf{F}_{mb,i} = \text{diag}(m_i, m_i, m_i) (\ddot{\mathbf{r}}_{i,d} + \mathbf{K}_{rPi} \mathbf{e}_{r_i} + \mathbf{K}_{rDi} \dot{\mathbf{e}}_{r_i}) \quad (148)$$

where \mathbf{K}_{rPi} and \mathbf{K}_{rDi} are control gain diagonal matrices, while

$$\mathbf{e}_{r_i} = \mathbf{r}_{i,d} - \mathbf{r}_i \quad (149)$$

is the error between the desired position of the servicer $\mathbf{r}_{i,d}$ and the actual position \mathbf{r}_i defined in Eq. (76). Note that, $\mathbf{F}_{mb,i}$ provides position control for the servicer base, but is only needed when there is a need to push the servicer base away from the passive object and the pushing direction lays in the no-thrusting area of the servicer. Thus, when the direction of \mathbf{s}_i , defined in Eq. (138), lies in the no-thrusting area, and depending on the sign of $\mathbf{F}_{mb,i}$'s component along the direction of \mathbf{s}_i , the need for the repulsive force \mathbf{f}_{ij_r} is decided. A negative sign for this component implies the need for a repulsive force, to push the servicer away from the object, and equal to the component of the $\mathbf{F}_{mb,i}$ along the direction of \mathbf{s}_i . A positive sign implies the opposite. In this case, the force can be supplied by the thrusters, and thus, \mathbf{f}_{ij_r} is zero. Therefore, \mathbf{f}_{ij_r} is obtained as:

$$\mathbf{f}_{ij_r} = \begin{cases} (\mathbf{F}_{mb,i} \bullet \mathbf{s}_i) \mathbf{s}_i & \text{if } \text{sgn}((\mathbf{F}_{mb} \bullet \mathbf{s}_i) \mathbf{s}_i) < 0 \\ 0 & \text{if } \text{sgn}((\mathbf{F}_{mb} \bullet \mathbf{s}_i) \mathbf{s}_i) \geq 0 \end{cases} \quad (150)$$

The two parts of the servicer motion controller (Eqs. (144) - (145) and (148) - (150)), are distinct. The controller of Eqs. (148) - (150) is used to compute, by means of the optimization process, the required repulsive component of \mathbf{f}_{Ei} , and thus, because of assumption (ii), of \mathbf{f}_{bi} . This \mathbf{f}_{bi} is used in its turn, in Eqs. (144) - (145), to compute the thruster forces. The controller in Eqs. (144) - (145) computes a thruster repulsive force twice, once as a PD quantity in Eq. (144) and once by means of the \mathbf{f}_{ij_r} component of \mathbf{f}_{bi} , in Eq. (145). Because of the requirement (b), thrusters in the direction of \mathbf{f}_{ij_r} are turned off, thus discarding the thruster repulsive force, and allowing only the manipulator to apply the \mathbf{f}_{ij_r} as an \mathbf{f}_{bi} component.

Note that the only difference in the *point contact* case, is that Eq. (151) is used instead of Eq. (146).

$$\mathbf{J}_i^T \mathbf{f}_{Ei} = [\mathbf{f}_{bi}^T \quad \mathbf{n}_{bi}^T]^T \quad (151)$$

Having obtained \mathbf{f}_{ij_r} , the required end-effector force \mathbf{f}_{Ei} can also be obtained, as shown earlier in this section, and then the servicer actuator inputs are computed using Eqs. (144) - (145) and (146) or (151). In this way, the optimization process (see earlier in this chapter), which provides the forces \mathbf{f}_{Ei} acting on the passive object, provides also the forces \mathbf{f}_{ij_r} , acting on the servicers as components of the reaction of \mathbf{f}_{Ei} on the servicers.

Figure 3-8 displays the block diagram of the servicer control system for both contact cases. The inputs are the desired trajectories (pose, velocity and acceleration) of the passive object and the servicers and the output is the actual trajectory (pose and velocity) of the servicer, for *both contact cases*. The differences between the *firm grasp* case and the *point contact* case, include a difference in the optimization process (Eq. (140) or Eq. (141)), a difference at the passive object applied forces/ moments (Eq. (82) or Eq. (83)) and a difference in the calculation of \mathbf{n}_{bi} (Eq. (146) or Eq. (151)), see Figure 3-8. In both cases, the forces/ moments acting on the passive object are the same.

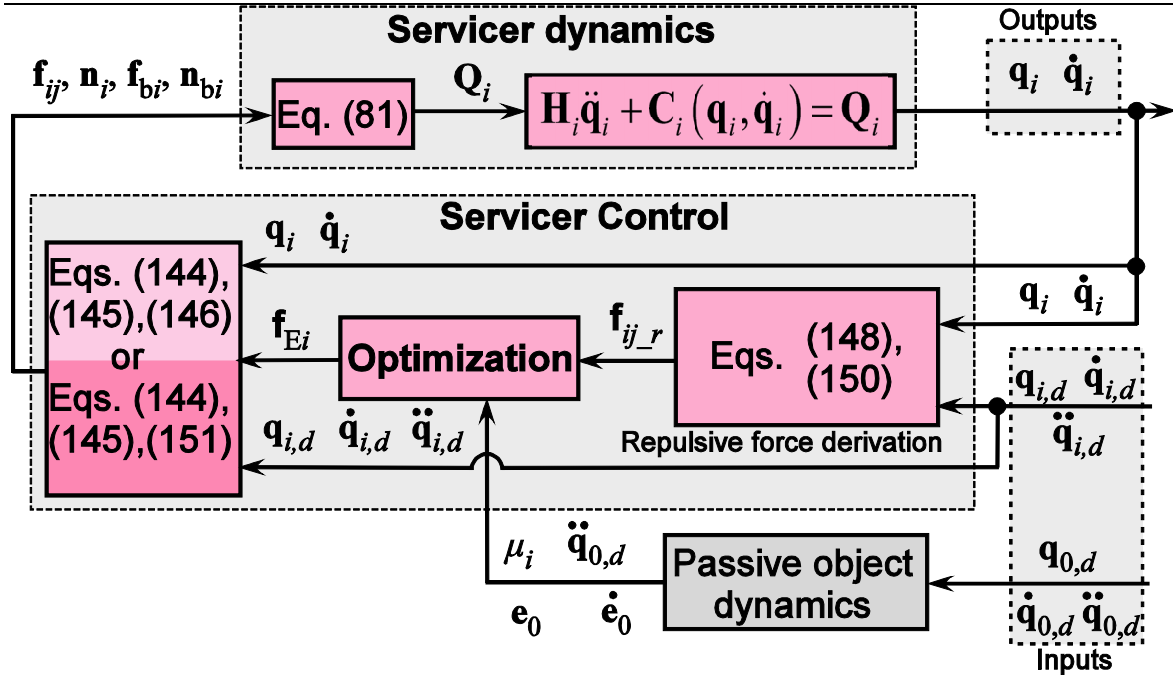


Figure 3-8. Flowchart of the servicers control algorithm.

3.4 Stability and Robustness

3.4.1 Stability of the Passive Object Motion

Despite switching controls acting on the servicer bases, applied forces/ moments on the controlled passive object are continuous, as applied by the manipulators. This is because the servicer base mass filters thruster forces, and because joint motors compensate actively for any residuals, as thruster firing and its effects on the manipulator are known a-priori. Thus the passive object motion can be controlled with vanishing errors, a response that cannot be achieved using switched forces only.

The stability of the passive object response under the proposed controller, for both contact-type cases, can be shown using Lyapunov's global stability theorem, with the following Lyapunov function,

$$V_0(e_0, \dot{e}_0) = \frac{1}{2} (e_0^T A_0 K_{D0}^2 e_0 + w_0^T A_0 w_0) \geq 0 \quad (152)$$

with

$$w_0 = \dot{e}_0 + K_{P0} K_{D0}^{-1} e_0 \quad (153)$$

and

$$\mathbf{A}_0 = \text{diag}(a_0(1), \dots, a_0(6)) > 0 \quad (154)$$

with $a_0(i) \geq 0$, not all equal to zero.

Differentiating Eq. (152) and using Eqs. (75) to (80) for $i = 0$ along with Eqs. (136), (82) (or (83)) and (154), we obtain

$$\dot{V}_0 = -\mathbf{e}_0^T \mathbf{A}_0 \mathbf{K}_{D0}^3 \mathbf{e}_0 \leq 0 \quad (155)$$

simply by selecting the following condition

$$\mathbf{K}_{P0} = \mathbf{K}_{D0}^2 \quad (156)$$

Using Barbalat's Lemma, as shown earlier in the backstepping methodology derivation and also in [83], it can be shown that

$$\lim_{t \rightarrow \infty} (\dot{V}_0) = 0 \quad (157)$$

and in conjunction to Eq. (155), the following is obtained

$$\lim_{t \rightarrow \infty} (\mathbf{e}_0) = 0 \quad (158)$$

Thus, the error \mathbf{e}_0 converges to zero (see Eq. (158)), proving the stability of the passive object response under the proposed controller. Examining the stability properties of the servicer controllers is more involved. As seen previously, backstepping/ model-based control was used as an intermediate step in developing a switching strategy for the on-off thruster forces. The nature of these forces introduces errors in the relative positions and attitudes between the passive object and each servicer. As mentioned already, these errors need only to remain bounded within certain limits; therefore the lack of asymptotic stability is not a limitation. The boundedness analysis is complicated since some of the forces are continuous (i.e. f_{Ei}), while others are switched (i.e. f_{ij}). However, the bounded control response can be realized similarly to the on-off attitude control of satellites. The boundedness of servicer motions is demonstrated in Chapter 4, via simulation results.

3.4.2 Robustness of the Passive Object Motion

The analysis so far assumes perfect knowledge of the passive object parameters, in order for them to be used on the model based PD controller. Nevertheless, this is not always feasible. The work in this section studies the controller robustness in the presence of parametric uncertainties during passive object controlled motion, via a linearization methodology. Assuming that the parameters of the man-made servicers are adequately

known, we focus on the passive object inertia parameters (mass and inertia matrix), that are needed in the model based PD control developed in Eq. (136). The tracking errors of the passive object motion are shown to vary within bounded values that can be obtained a-priori by simple knowledge of the desired trajectory and a maximum bound in parameter uncertainty. This is also demonstrated by simulations in Chapter 4.

For quick-reference, the model based PD controller that was chosen for the passive object is rewritten here:

$$\mathbf{Q}_0 = \mathbf{C}_0 + \mathbf{H}_0 (\ddot{\mathbf{q}}_{0d} + \mathbf{K}_{P0}\mathbf{e}_0 + \mathbf{K}_{D0}\dot{\mathbf{e}}_0) \quad (159)$$

where

$$\mathbf{e}_0 = \mathbf{q}_{0d} - \mathbf{q}_0 \quad (160)$$

and \mathbf{q}_{0d} is the desired trajectory for the passive object and \mathbf{K}_{P0} and \mathbf{K}_{D0} are control gains. Use of the controller in Eq. (159) leads to asymptotically stable motion of the passive object, as already proven in the previous section by use of Lyapunov stability theory.

Assume now that there is some uncertainty in the estimation of the passive object mass m_0 and inertia matrix ${}^0\mathbf{I}_0$ and that the uncertain quantities used in the controller (Eq. (159)) are denoted by \hat{m}_0 and ${}^0\hat{\mathbf{I}}_0$ respectively, where $(\hat{*})$ is the estimated value of $(*)$. The corresponding matrices \mathbf{C}_0 and \mathbf{H}_0 become $\hat{\mathbf{C}}_0$ and $\hat{\mathbf{H}}_0$ respectively. Thus, Eq. (159) becomes:

$$\mathbf{Q}_0 = \hat{\mathbf{C}}_0 + \hat{\mathbf{H}}_0 (\ddot{\mathbf{q}}_{0d} + \mathbf{K}_{P0}\mathbf{e}_0 + \mathbf{K}_{D0}\dot{\mathbf{e}}_0) \quad (161)$$

Uncertain matrices $\hat{\mathbf{H}}_0$ and $\hat{\mathbf{C}}_0$ can also be written as:

$$\hat{\mathbf{H}}_0 = \mathbf{H}_0 + \delta\mathbf{H} \quad (162)$$

and

$$\hat{\mathbf{C}}_0 = \mathbf{C}_0 + \delta\mathbf{C} \quad (163)$$

where $\delta\mathbf{H}$ and $\delta\mathbf{C}$ denote the variation of the uncertain (estimated) matrices $\hat{\mathbf{H}}_0$ and $\hat{\mathbf{C}}_0$ from the real ones \mathbf{H}_0 and \mathbf{C}_0 respectively.

Equations (161) and (75) (for $i = 0$), provide the dynamic equation of motion of the passive object, in the case of uncertain parameter estimations:

$$\mathbf{H}_0\ddot{\mathbf{q}}_0 + \mathbf{C}_0 = \hat{\mathbf{C}}_0 + \hat{\mathbf{H}}_0 (\ddot{\mathbf{q}}_{0d} + \mathbf{K}_{P0}\mathbf{e}_0 + \mathbf{K}_{D0}\dot{\mathbf{e}}_0) \quad (164)$$

or equivalently,

$$\ddot{\mathbf{q}}_0 = \mathbf{g}(\mathbf{q}_0, \dot{\mathbf{q}}_0) = \mathbf{H}_0^{-1}(\hat{\mathbf{C}}_0 - \mathbf{C}_0) + \mathbf{H}_0^{-1}\hat{\mathbf{H}}_0(\ddot{\mathbf{q}}_{0d} + \mathbf{K}_{P0}\mathbf{e}_0 + \mathbf{K}_{D0}\dot{\mathbf{e}}_0) \quad (165)$$

Using Eq. (160), we obtain

$$\begin{aligned} \mathbf{q}_0 &= \mathbf{q}_{0d} - \mathbf{e}_0 = \mathbf{q}_{0d} + \delta\mathbf{q}_0 \\ \dot{\mathbf{q}}_0 &= \dot{\mathbf{q}}_{0d} - \dot{\mathbf{e}}_0 = \dot{\mathbf{q}}_{0d} + \delta\dot{\mathbf{q}}_0 \\ \ddot{\mathbf{q}}_0 &= \ddot{\mathbf{q}}_{0d} - \ddot{\mathbf{e}}_0 = \ddot{\mathbf{q}}_{0d} + \delta\ddot{\mathbf{q}}_0 \end{aligned} \quad (166)$$

Thus, using Eq. (166) on the left-hand side of Eq. (165) and linearizing the right-hand side of Eq. (165) at the desired point \mathbf{q}_{0d} , we obtain:

$$\begin{aligned} \ddot{\mathbf{q}}_{0d} + \delta\ddot{\mathbf{q}}_0 &= \mathbf{H}_0^{-1}(\hat{\mathbf{C}}_0 - \mathbf{C}_0) + \mathbf{H}_0^{-1}\hat{\mathbf{H}}_0(\ddot{\mathbf{q}}_{0d} + \mathbf{K}_{P0}\mathbf{e}_0 + \mathbf{K}_{D0}\dot{\mathbf{e}}_0) \Big|_{\substack{\mathbf{q}_{0d} \\ \dot{\mathbf{q}}_{0d}}} + \\ &+ \frac{\partial f}{\partial \mathbf{q}_0} \Big|_{\substack{\mathbf{q}_{0d} \\ \dot{\mathbf{q}}_{0d}}} \delta\mathbf{q}_0 + \frac{\partial f}{\partial \dot{\mathbf{q}}_0} \Big|_{\substack{\mathbf{q}_{0d} \\ \dot{\mathbf{q}}_{0d}}} \delta\dot{\mathbf{q}}_0 + HOT \end{aligned} \quad (167)$$

where,

$$f(\mathbf{q}_0, \dot{\mathbf{q}}_0) = \mathbf{H}_0^{-1}(\hat{\mathbf{C}}_0 - \mathbf{C}_0) + \mathbf{H}_0^{-1}\hat{\mathbf{H}}_0(\ddot{\mathbf{q}}_{0d} + \mathbf{K}_{P0}\mathbf{e}_0 + \mathbf{K}_{D0}\dot{\mathbf{e}}_0) \quad (168)$$

where *HOT* stands for *Higher Order Terms*. Using Eqs. (162) and (163), we obtain,

$$f(\mathbf{q}_{0,d}, \dot{\mathbf{q}}_{0,d}, a_i) = \mathbf{H}_0^{-1}\delta\mathbf{C} + \mathbf{H}_0^{-1}\delta\mathbf{H}\ddot{\mathbf{q}}_{0d} + \ddot{\mathbf{q}}_{0d} \quad (169)$$

Thus, Eq. (167) becomes

$$\delta\ddot{\mathbf{q}}_0 = \left(\mathbf{H}_0^{-1}\delta\mathbf{C} + \mathbf{H}_0^{-1}\delta\mathbf{H}\ddot{\mathbf{q}}_{0d} \right) \Big|_{\substack{\mathbf{q}_{0d} \\ \dot{\mathbf{q}}_{0d}}} + \frac{\partial f}{\partial \mathbf{q}_0} \Big|_{\substack{\mathbf{q}_{0d} \\ \dot{\mathbf{q}}_{0d}}} \delta\mathbf{q}_0 + \frac{\partial f}{\partial \dot{\mathbf{q}}_0} \Big|_{\substack{\mathbf{q}_{0d} \\ \dot{\mathbf{q}}_{0d}}} \delta\dot{\mathbf{q}}_0 + HOT \quad (170)$$

We define the following

$$\begin{aligned} \frac{\partial f}{\partial \dot{\mathbf{q}}_0} \Big|_{\substack{\mathbf{q}_{0d} \\ \dot{\mathbf{q}}_{0d}}} &= \mathbf{F}_{dD} \\ \frac{\partial f}{\partial \mathbf{q}_0} \Big|_{\substack{\mathbf{q}_{0d} \\ \dot{\mathbf{q}}_{0d}}} &= \mathbf{F}_{dP} \end{aligned} \quad (171)$$

Assuming that we are close enough to the desired trajectory, the higher order terms of Eq. (170) become insignificant. Thus, Eq. (170) becomes

$$\delta\ddot{\mathbf{q}}_0 - \mathbf{F}_{dD}\delta\dot{\mathbf{q}}_0 - \mathbf{F}_{dP}\delta\mathbf{q}_0 = \left(\mathbf{H}_0^{-1}\delta\mathbf{C} + \mathbf{H}_0^{-1}\delta\mathbf{H}\ddot{\mathbf{q}}_{0d} \right) \Big|_{\substack{\mathbf{q}_{0d} \\ \dot{\mathbf{q}}_{0d}}} \quad (172)$$

The right-hand side of Eq. (172) depends on the desired trajectory and on the small uncertainty terms $\delta\mathbf{C}$ and $\delta\mathbf{H}$. Therefore, it is a small, bounded term that drives the second order system of the left-hand side, which is essentially a mass-spring-damper-type system.

By differentiating f , given in Eq. (168), according to Eq. (171), we have

$$\mathbf{F}_{dD} = -\mathbf{K}_{D0} + \underbrace{\left(-\mathbf{H}_0^{-1}\delta\mathbf{H}\mathbf{K}_{D0} + \delta\mathbf{T}_1\right)}_{\mathbf{E}_D} \Bigg|_{\substack{\mathbf{q}_{0d} \\ \dot{\mathbf{q}}_{0d}}}, \quad (173)$$

$$\delta\mathbf{T}_1 = \mathbf{H}_0^{-1} \frac{\partial\delta\mathbf{C}}{\partial\dot{\mathbf{q}}_0}$$

Note that, for no uncertainty ($\delta\mathbf{H} = \delta\mathbf{C} = \mathbf{0}$), the right-hand side of Eq. (173) becomes equal to $-\mathbf{K}_{D0}$ and thus negative definite. Note also that,

$$-\mathbf{K}_{D0} - \mathbf{H}_0^{-1}\delta\mathbf{H}\mathbf{K}_{D0} = -\left(\mathbf{I}_{6\times 6} + \mathbf{H}_0^{-1}\delta\mathbf{H}\right) \Bigg|_{\substack{\mathbf{q}_{0d} \\ \dot{\mathbf{q}}_{0d}}} \mathbf{K}_{D0} \quad (174)$$

where $\mathbf{I}_{6\times 6}$ is the 6×6 identity matrix. The term $-\mathbf{H}_0^{-1}\delta\mathbf{H}$ in Eq. (174) depends only on the desired trajectory $(\mathbf{q}_{0d}, \dot{\mathbf{q}}_{0d})$ and the uncertainty. Thus, it can be used to obtain an uncertainty area, for which the term $\mathbf{I}_{6\times 6} + \mathbf{H}_0^{-1}\delta\mathbf{H}$ is positive definite, leading to the right-hand side of Eq. (174) being negative definite. Since $\delta\mathbf{T}_1$ is a small term depending also only on the desired trajectory and the uncertainty, it can also be used to determine another uncertainty area, for which $\delta\mathbf{T}_1$ is dominated by the negative definite term $-(\mathbf{I}_{6\times 6} + \mathbf{H}_0^{-1}\delta\mathbf{H})$. The common ground of these two uncertainty areas define the maximum allowable uncertainty area, for which, large enough control gains, result in \mathbf{F}_{dD} being negative definite. The same method can be used to obtain the maximum uncertainty for which \mathbf{F}_{dP} is also negative definite, since the term \mathbf{F}_{dP} is

$$\mathbf{F}_{dP} = -\mathbf{K}_{P0} + \underbrace{\left(-\mathbf{H}_0^{-1}\delta\mathbf{H}\mathbf{K}_{P0} + \delta\mathbf{T}_2\right)}_{\mathbf{E}_P} \Bigg|_{\substack{\mathbf{q}_{0d} \\ \dot{\mathbf{q}}_{0d}}}, \quad (175)$$

$$\delta\mathbf{T}_2 = \frac{\partial\mathbf{H}_0^{-1}}{\partial\mathbf{q}_0}\delta\mathbf{C} + \mathbf{H}_0^{-1} \frac{\partial\delta\mathbf{C}}{\partial\mathbf{q}_0} + \left(\frac{\partial\mathbf{H}_0^{-1}}{\partial\mathbf{q}_0}\delta\mathbf{H} + \mathbf{H}_0^{-1} \frac{\partial\delta\mathbf{H}}{\partial\mathbf{q}_0} \right) \ddot{\mathbf{q}}_{0d}$$

In this way, the need for the negative definite matrices \mathbf{F}_{dD} and \mathbf{F}_{dP} can be used as a design tool. For a class of desired trajectories and a bounded range of expected uncertainty, a range of \mathbf{E}_D and \mathbf{E}_P can be found and thus the minimum required control gains \mathbf{K}_{D0} and \mathbf{K}_{P0} can be obtained.

With the negative definite matrices \mathbf{F}_{dD} and \mathbf{F}_{dP} , the second order system of Eq. (172) is stable. At the steady-state, the first and second derivatives of $\delta\mathbf{q}_0$ are zero. The small, bounded term on the right-hand side of Eq. (172), though, is not constant during the trajectory tracking motion. Nevertheless, the closed-loop frequency of the controller (and the resulting bandwidth) can be high enough by design, so that the fastest frequency of the desired motion is far lower. This is a realistic claim for controller design, especially for motions in space, in which the desired trajectories are quite slow by design. Thus, the second order system of Eq. (172) responds as if the right-hand side is a quasi-constant driving term, as will be displayed by simulations in the following chapter. Then, the acceleration and velocity errors ($\delta\ddot{\mathbf{q}}_0$ and $\delta\dot{\mathbf{q}}_0$ respectively) tend to zero and position/orientation errors tend to

$$\delta\mathbf{q}_0 \rightarrow -\mathbf{F}_{dP}^{-1} \left(\mathbf{H}_0^{-1} \delta\mathbf{C} + \mathbf{H}_0^{-1} \delta\mathbf{H}\ddot{\mathbf{q}}_{0d} \right) \Big|_{\substack{\mathbf{q}_{0d} \\ \dot{\mathbf{q}}_{0d}}} \quad (176)$$

Note that the vector on which the position/ orientation error is attracted is a-priori known, since it depends on the desired trajectory and on the uncertainty, for which we can estimate its expected maximum range. Thus, if the following hypotheses apply:

1. The initial errors as well as the known vector on which the position/ orientation error is attracted are close enough to zero, so that the linearization that led to Eq. (172) is still valid (both valid assumptions for a trajectory tracking problem such as the one at hand, especially when using standard parameter identification methods [8], [37] and [38], to lower the parametric uncertainty),
2. The control gains \mathbf{K}_{P0} and \mathbf{K}_{D0} are high enough and the parametric uncertainty is low enough, that the claim for negative definite \mathbf{F}_{dD} and \mathbf{F}_{dP} is still valid, as discussed in conjunction to Eqs. (173) to (175),
3. The controller bandwidth is high compared to the bandwidth of the desired motions, so that a quasi-steady-state response can be obtained,

then the original non-linear system of Eq. (75) for $i = 0$ (with the control generalized force as in Eq. (161)) is stable, with tracking error of

$$\begin{bmatrix} \mathbf{e}^T & \dot{\mathbf{e}}^T \end{bmatrix}^T = -\begin{bmatrix} \delta\mathbf{q}_0^T & \delta\dot{\mathbf{q}}_0^T \end{bmatrix}^T \rightarrow \begin{bmatrix} \mathbf{F}_{dP}^{-1} \left(\mathbf{H}_0^{-1} \delta\mathbf{C} + \mathbf{H}_0^{-1} \delta\mathbf{H}\ddot{\mathbf{q}}_{0des} \right) \Big|_{\substack{\mathbf{q}_{0d} \\ \dot{\mathbf{q}}_{0d}}} & \mathbf{0} \end{bmatrix} = \mathbf{A}_d \quad (177)$$

where $\delta\mathbf{q}_0$ is defined in Eq. (166). Moreover, the system is immune to small disturbances that do not raise the tracking errors to values that invalidate the abovementioned hypotheses. Summing up, if we start with small enough tracking errors and we do not have severe disturbances (both valid assumptions for a trajectory tracking problem such as the one at hand), then the passive object motion is stable, as long as the abovementioned hypotheses, whose validity can be determined a-priori, are true. Moreover, if the motion is slow enough (a realistic assumption, especially in space), the tracking errors follow Eq. (177), as will also be shown in Chapter 4.

As mentioned above, for a system without uncertainty, then from Eqs. (162) and (163), we obtain

$$\delta\mathbf{C} = \delta\mathbf{H} = 0 \quad (178)$$

Thus, from Eq. (177), we obtain

$$\begin{bmatrix} \mathbf{e}^T & \dot{\mathbf{e}}^T \end{bmatrix}^T \rightarrow \mathbf{0}_{6 \times 1} \quad (179)$$

This response is the expected one, since the system without uncertainty is asymptotically stable, as has been proven in the previous section. This can also be seen by assuming no uncertainty on the linearized system described by Eq. (172), in which case it leads to

$$\delta\ddot{\mathbf{q}}_0 + \mathbf{K}_{D0}\delta\dot{\mathbf{q}}_0 + \mathbf{K}_{P0}\delta\mathbf{q}_0 = -(\ddot{\mathbf{e}} + \mathbf{K}_{D0}\dot{\mathbf{e}} + \mathbf{K}_{P0}\mathbf{e}) = 0 \quad (180)$$

which is equal to the error-dynamics equation of motion of the passive object, under the model-based controller of Eq. (159), in the case of no uncertainty. The second order Eq. (180) is easily proven to be asymptotically stable, by using Lyapunov stability theory.

Using an analytical form for the passive object inertia matrix, the above analysis can be developed further. The general form of the inertia matrix ${}^0\mathbf{I}_0$ is given by Eq. (181):

$${}^0\mathbf{I}_0 = \begin{bmatrix} \int_{\mathcal{V}} (y^2 + z^2) \rho dV & \int_{\mathcal{V}} xy \rho dV & \int_{\mathcal{V}} xz \rho dV \\ \int_{\mathcal{V}} xy \rho dV & \int_{\mathcal{V}} (x^2 + z^2) \rho dV & \int_{\mathcal{V}} yz \rho dV \\ \int_{\mathcal{V}} xz \rho dV & \int_{\mathcal{V}} yz \rho dV & \int_{\mathcal{V}} (x^2 + y^2) \rho dV \end{bmatrix} \quad (181)$$

where V is the volume of the passive object and ρ is its density. Assuming that the uncertainty is in the measurement of V and the measurement and distribution of ρ , then the estimated \hat{V} and $\hat{\rho}$ are:

$$\begin{aligned}\hat{V} &= V + \delta V \\ \hat{\rho} &= \rho + \delta \rho\end{aligned}\quad (182)$$

By defining the top-left element of ${}^0\mathbf{I}_0$ as ${}^0I_{0,xx}$, then the estimated top-left element of ${}^0\hat{\mathbf{I}}_0$ is:

$${}^0\hat{I}_{0,xx} = \int_{\hat{V}} (y^2 + z^2) \hat{\rho} dV \quad (183)$$

Eq. (183) can be written as:

$$\begin{aligned}\int_{\hat{V}} (y^2 + z^2) \hat{\rho} dV &= \int_V (y^2 + z^2) \rho dV + \int_V (y^2 + z^2) \delta \rho dV + \\ &+ \int_{\delta V} (y^2 + z^2) \rho dV + \int_{\delta V} (y^2 + z^2) \delta \rho dV\end{aligned}\quad (184)$$

Note that all terms of Eq. (184) are elements of appropriate inertia matrices. The last term on the right-hand side of Eq. (184) is an integration over a very small volume δV , of a term that is proportional to the very small term $\delta \rho$. This means that the last integral term is negligible, compared to the other three terms. Then, Eq. (184) becomes:

$$\int_{\hat{V}} (y^2 + z^2) \hat{\rho} dV = \underbrace{\int_V (y^2 + z^2) \rho dV}_{{}^0I_{0,xx}} + \int_V (y^2 + z^2) \delta \rho dV + \int_{\delta V} (y^2 + z^2) \rho dV \quad (185)$$

Thus, from Eqs. (183) and (185), we obtain:

$${}^0\hat{I}_{0,xx} = \underbrace{\int_V (y^2 + z^2) \rho dV}_{{}^0I_{0,xx}} + \underbrace{\int_V (y^2 + z^2) \delta \rho dV + \int_{\delta V} (y^2 + z^2) \rho dV}_{\delta I_{0,xx}} \quad (186)$$

Using the same method, we also obtain the remaining estimated elements of ${}^0\hat{\mathbf{I}}_0$. Thus, the estimated ${}^0\hat{\mathbf{I}}_0$ becomes:

$${}^0\hat{\mathbf{I}}_0 = {}^0\mathbf{I}_0 + \delta \mathbf{I} \quad (187)$$

where the $\delta \mathbf{I}$ matrix also has inertia properties. Then matrices $\delta \mathbf{H}$ and $\delta \mathbf{C}$ of Eqs. (162) and (163), based on Eqs. (77), (80) (for $i = 0$) and (187), become

$$\delta \mathbf{H} = \begin{bmatrix} \text{diag}(\delta m_0, \delta m_0, \delta m_0) & \mathbf{0}_{3 \times 3} \\ \mathbf{0}_{3 \times 3} & \mathbf{E}_0^T \mathbf{R}_0 \delta \mathbf{I} \mathbf{R}_0^T \mathbf{E}_0 \end{bmatrix} \quad (188)$$

and

$$\delta \mathbf{C} = \begin{bmatrix} \mathbf{0}_{1 \times 3}, & \left(\mathbf{E}_0^T \left(\mathbf{R}_0 \delta \mathbf{I} \mathbf{R}_0^T \dot{\mathbf{E}}_0 \dot{\boldsymbol{\theta}}_0 + \mathbf{E}_0 \dot{\boldsymbol{\theta}}_0 \times \mathbf{R}_0 \delta \mathbf{I} \mathbf{R}_0^T \mathbf{E}_0 \dot{\boldsymbol{\theta}}_0 \right) \right)^T \end{bmatrix}^T \quad (189)$$

where δm_0 in Eq. (188), is given by

$$\delta m_0 = \rho \delta V + \delta \rho V \quad (190)$$

Thus, Eqs. (188) and (189) can be used directly in Eq. (177), to obtain the steady state error.

4 Simulation Results

In the previous chapters, the concept of trajectory tracking handling of a passive object by a number of single manipulator robotic servicers in space was introduced. Moreover, the dynamic modeling of such a system was presented, as well as a controller, both for the motion of the passive object and for the relative motion of the servicers with respect to the passive object. Finally, the parametric sensitivity of the passive object controller was studied, while the benefits of having several small servicers as opposed to a single larger services, were also examined. To demonstrate the developed methodology, we study the case of three single-manipulator servicers, both when applying *point contact* forces on the passive object and when having a *firm grasp* over it, as seen in Figure 4-1.

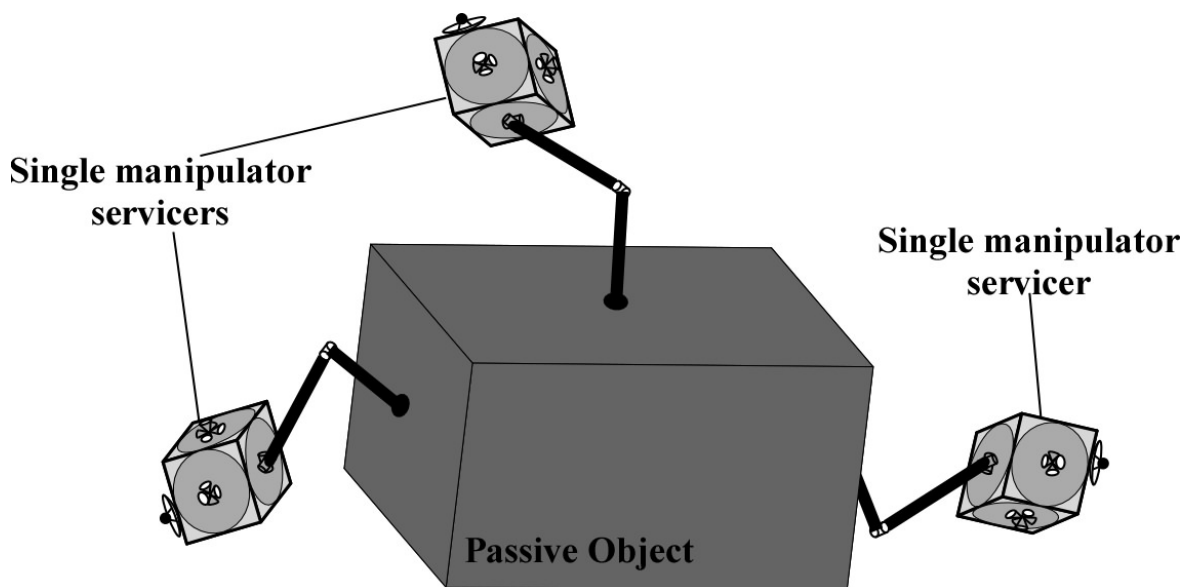


Figure 4-1. Concept of a passive object in space, handled by three single-manipulator robotic servicers.

Each servicer base has thrusters capable of producing forces or moments (thrusters facing the object are deactivated), reaction wheels, and a single typical six degrees of freedom manipulators, such as a PUMA-type manipulator [26]. A series of simulations is run, with realistic parameters in terms of thruster and reaction wheel capabilities. The system parameters, including the object/ servicer mass ratio, are chosen taking into account realistic scenarios. In particular, if the object/ servicer mass ratio is too large, obviously either an extreme number of servicers will be needed, or the task will be physically impossible, depending on the required trajectory. With this ratio too small, the interaction between servicers and the object can be ignored. What is of interest here is the

case in which the masses are comparable; this yields the mass of the object. The parameters and characteristics of the passive object and the servicers, are also shown in Table 4-1. Note that, for attitude control, the servicers have additional pairs of thrusters that develop torque of 2 Nm per axis, with the trigger threshold being set to $n_t = 1$ Nm, and reaction wheels that can develop continuous torques up to the trigger threshold value of n_t , per axis. Moreover, the manipulator on each servicer has a maximum reach of 2.1 m i.e. three times the cubic servicer base side. The three contact points lie on the object surfaces with normal vectors parallel to the $\hat{x}_0, -\hat{x}_0$ and \hat{y}_0 unit vectors of the object body-fixed axes, in order to have two contact point on opposite surfaces of the passive object and one on a side surface.

Table 4-1. Passive object and servicer characteristics.

	Passive Object	Servicer
Dimensions	2m × 3m × 2m	0.7m × 0.7m × 0.7m
Mass	180 kg	70 kg
Thruster force	N/A	20 N
Thruster force trigger threshold	N/A	10 N
Thruster torque	N/A	2 Nm
Thruster torque trigger threshold	N/A	1 Nm
Reaction wheel maximum torque	N/A	1 Nm
Manipulator max. reach	N/A	2.1 m

The simulations are run on Matlab/ Simulink, in which both the dynamics and control of the whole system are simulated in Matlab-code, as seen in Appendix B. The dynamics of the system are modeled in Simulink as seen in Appendix A, based on Eqs. (75) to (88) derived in Chapter 3 of this thesis. The non-linear constrained optimization function *fmincon* [58] is used to obtain optimal end-effector forces/ torques (low level optimization) and contact points (high level optimization). The low level optimization is acting as an online force distribution for the control generalized force acting on the passive object, as the system motion is simulated. The optimization code running on a current average computer (i7 processor with 12GB RAM, without SSD hard disc, and with

Windows 7 operating system) takes about 100 ms. Note that the optimization time dropped to 50 ms just by upgrading computer memory to 16GB RAM and by adding an SSD hard disc. In a dedicated computer with optimized and compiled code, this time will be far smaller, making the assumption of a total loop time close to 100 ms, a realistic one. Although a performance gap between space and ground processors exists, long delays also occur in implementing new methods in space, during which, space-qualified hardware advances; thus this performance should be realizable by future space systems. The high level optimization is used to obtain optimal contact points, by means of lowering the norm of the manipulator applied forces on the passive object, during a simulated motion of the system. Since the total generalized force acting on the passive object is obtained by the corresponding controller, lowering the manipulator forces equals to lowering the norm of the null-space forces. To that end, at each step of the optimization process a set of contact points is chosen and the motion of the entire system is simulated. Thus, the maximum manipulator generalized forces norm for the whole motion, are obtained and act as performance index in the process.

4.1 Spatial Control of a Passive Object

Initially, the response of the system of the passive object handled by three single-manipulator servicers, under the proposed control scheme, is presented. This is done for both the *point contact* and the *firm grasp* cases and, as already mentioned, for PUMA-type servicer manipulators. The motion of the passive object and the three servicers is simulated with the passive object following a typical trajectory (control in Cartesian space), such as a velocity trapezoidal profile in all DOF, as seen in Figure 4-2 (for the inertial x-axis desired trajectory) and in Table 4-2. The desired accelerations of the passive object were chosen to be compatible with the servicers force/moment capabilities.

Table 4-2. Passive object desired motion parameters (Trajectory 1).

DOF \	const. accel. (m/s ²)/ (rad/s ²)	up to (s)	const. veloc. (m/s)/ (rad/s)	up to (s)	const. decel. (m/s ²)/ (rad/s ²)	up to (s)
X _{0des}	0.0003	56	0.0168	84	-0.0003	140
Y _{0des}	-0.00036	50	-0.018	90	0.00036	140
Z _{0des}	0.0002	59	0.0118	81	-0.0002	140
θ _{0des}	5*10 ⁻⁵	60	0.003	80	-5*10 ⁻⁵	140
φ _{0des}	7*10 ⁻⁵	55	0.00385	85	-7*10 ⁻⁵	140
ψ _{0des}	10 ⁻⁴	65	0.0065	75	-10 ⁻⁴	140

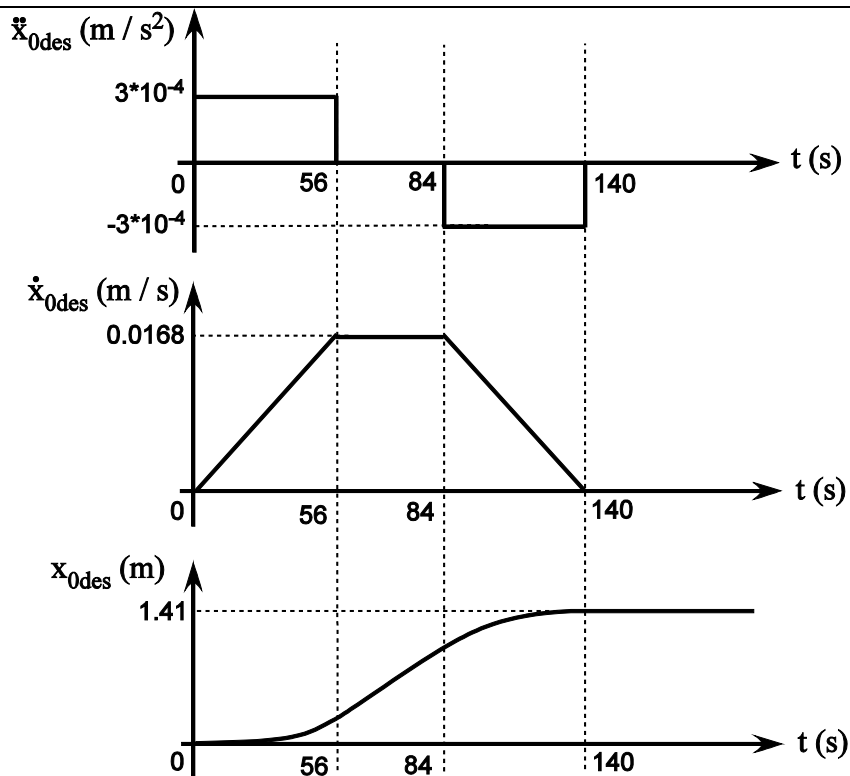


Figure 4-2. Passive object inertial x-axis desired trajectory.

The desired servicer relative position with respect to the passive object is its initial relative position. This position is chosen so as to accommodate adequately the expected relative motion between each servicer and the passive object, and maintain the manipulator in its kinematic and force workspace [92]. Thus, the servicer position task is to keep the manipulator base at a distance of 1 m for two servicers contacting opposing sides of the passive object and of 0.6 m for the third servicer, measured along the object surface normal vector passing from the end-effector contact point. The servicer attitude control task is to maintain a relative attitude with respect to the object approximately constant.

4.1.1 Point contact case

First the case of *point contact* is demonstrated, as seen in Figure 4-3, in which the top-view of a 3D case is shown. The bandwidth that corresponds to the control gains is constrained by reaction wheel and thruster limits. Taking this bandwidth into account, the servicer attitude control gains are tuned by trial and error in such a way, that the resulting control torque would be provided as much as possible by the reaction wheels, with only scarce need for torque-thruster firing. The gain tuning showed that, as expected, higher gains result in lower tracking errors, but more frequent thruster firing, thus higher fuel consumption.

The tradeoff between tracking errors and fuel consumption can be used to obtain the desired gains, for a given motion. In this case, the control gains in Eqs. (136) and (144) are shown in Table 4-3.

Table 4-3. Control gains for the point contact case.

Passive Object				Servicer (for $i = 1, 2, 3$)			
Translational DOF		Rotational DOF		Translational DOF		Rotational DOF	
K_{P0} :	K_{D0} :	K_{P0} :	K_{D0} :	K_{Pi} :	K_{Di} :	K_{Pi} :	K_{Di} :
3.24	1.8	0.64	0.8	0.16	0.4	0.5625	0.75

For the object desired trajectory in Table 4-2, the actual trajectory is displayed in Figure 4-4. Figure 4-5 shows the object tracking errors, the servicer base position tracking errors, and the servicer attitude tracking errors, for one of the servicers. For the same servicer, Figure 4-6 shows the end-effector applied forces, the servicer thruster forces and torques, and the reaction wheel torques. The same variables for the other servicers are similar and are not shown here.

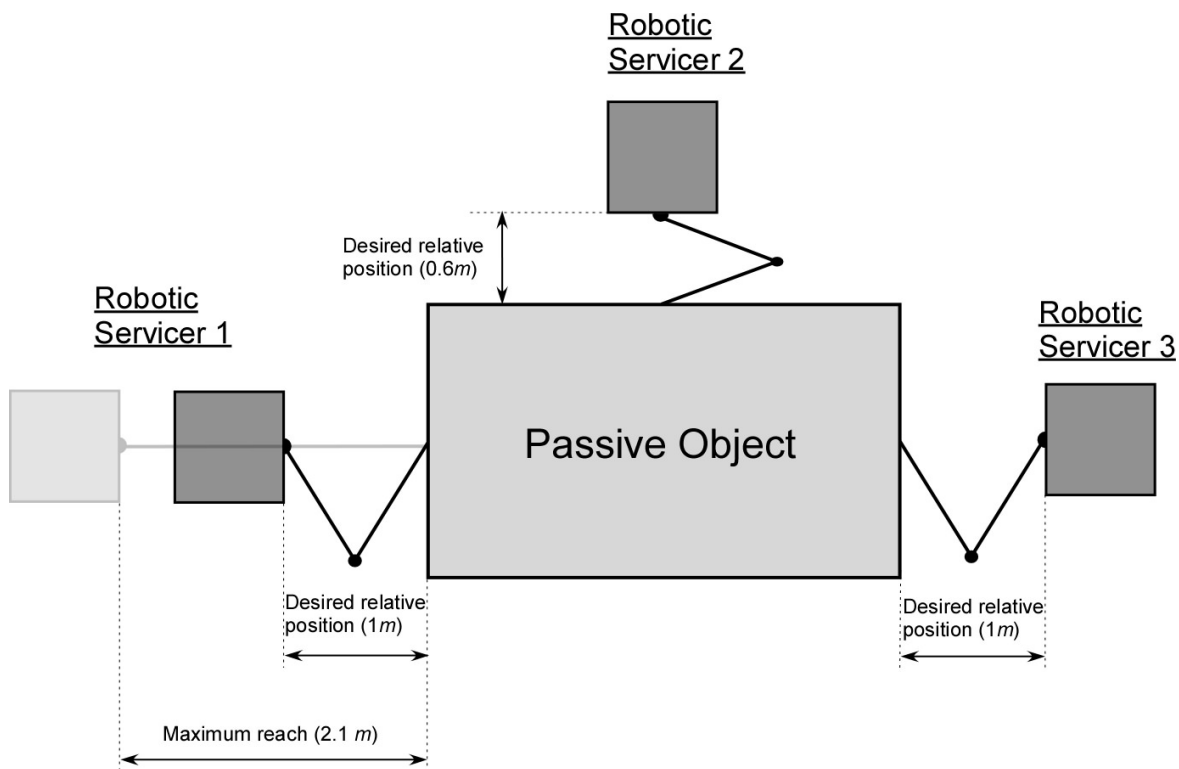


Figure 4-3. Top view of the passive object and three single manipulator robotic servicers at their desired relative position and relative orientation. For Servicer 1, the maximum manipulator reach position is also shown.

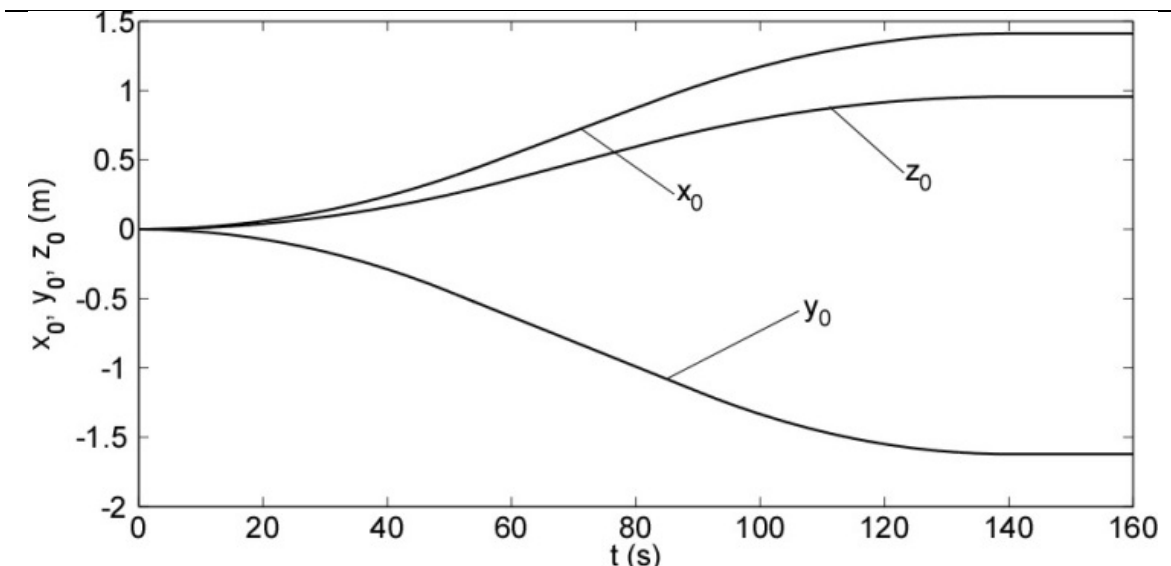


Figure 4-4. Actual trajectories of the passive object coordinates.

As seen in Figure 4-4, Figure 4-5 and Figure 4-6, the passive object follows its trajectory very well. The errors in displacements from the desired servicer base location with respect to the object, oscillate around zero, indicating that the manipulator base remains within bounds, see Figure 4-5c. Figure 4-5d shows very small servicer attitude errors. By increasing the position control gains of the servicer, the error displacements are reduced accordingly. As expected, more frequent thruster firing is observed, thus increasing the fuel consumption, as will be shown latter on, in Figure 4-8.

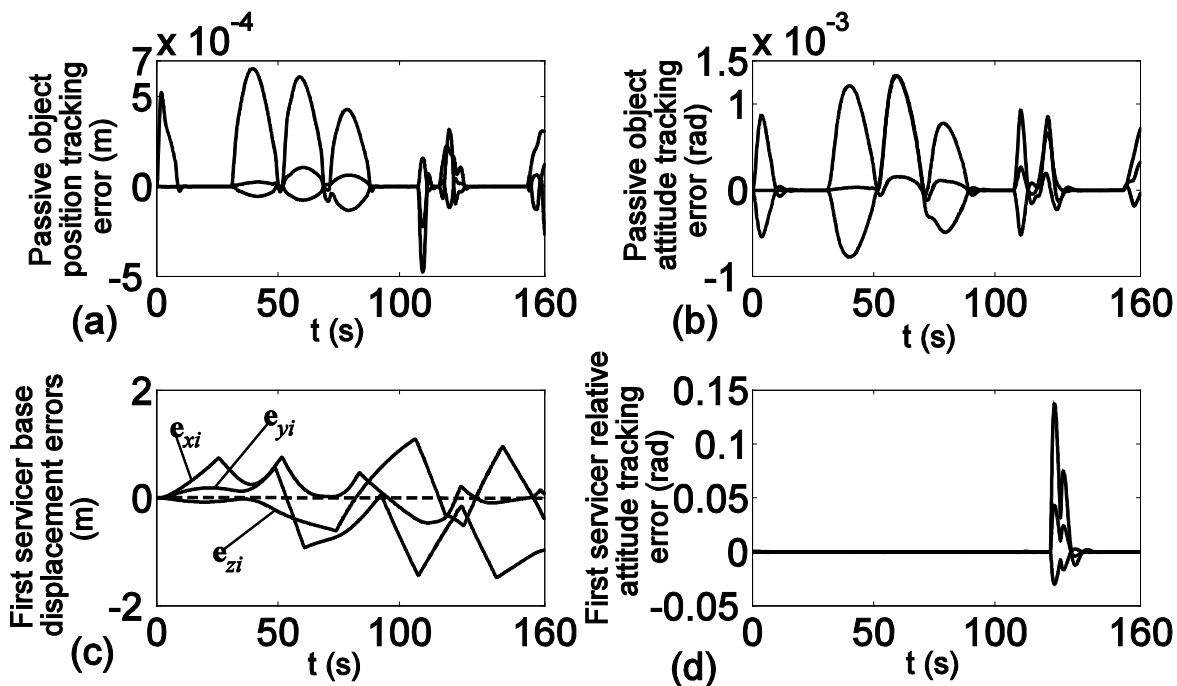


Figure 4-5. Point contact case: Tracking errors in (a) object position and (b) attitude, (c) servicer base displacement, and (d) attitude.

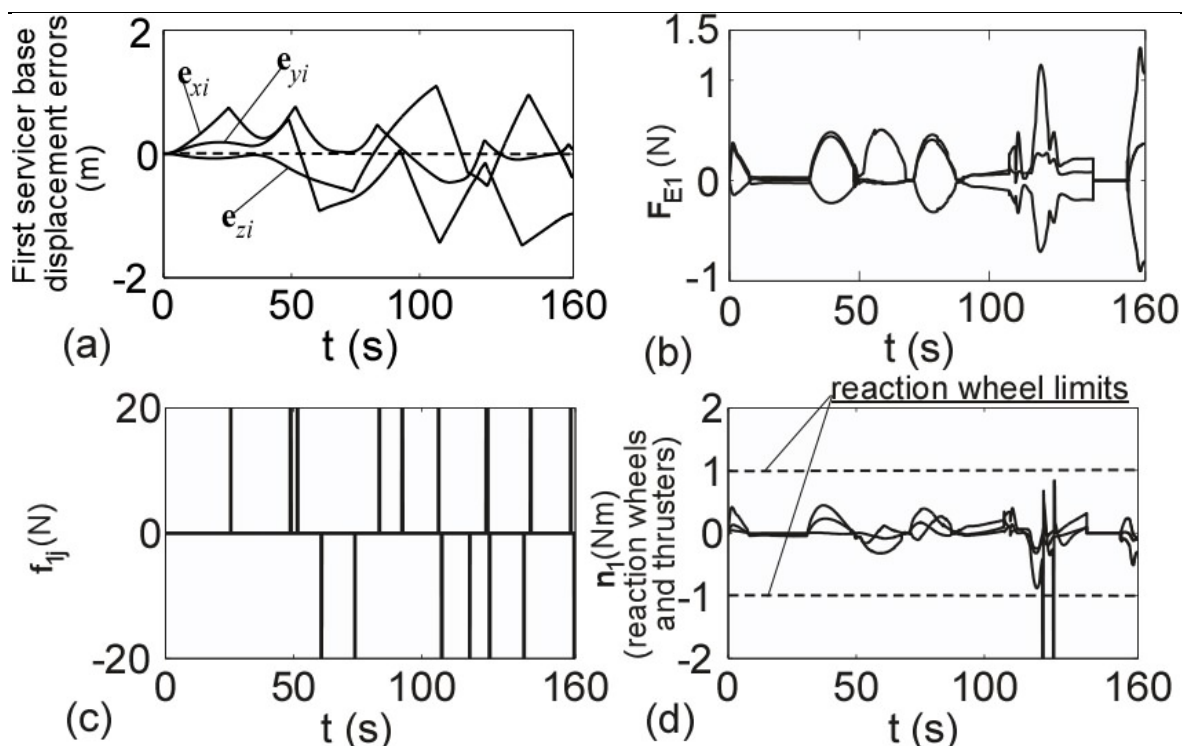


Figure 4-6. (a) Tracking errors in servicer base displacement, (b) typical manipulator applied forces, (c) thruster forces and (d) torques by reaction wheels and thrusters for one of the servicers.

This behavior demonstrates how the introduction of the manipulators enhances the performance of the system, letting the servicer base move freely in the manipulator workspace, firing the thrusters only when the manipulator approaches its workspace limits, as seen by comparing Figure 4-6a to Figure 4-6c, while constantly applying a continuous manipulator force on the passive object, as seen in Figure 4-6b. By applying these control forces, the passive object position tracking error is less than 1 mm and the passive object orientation tracking error is less than a tenth of a degree, as seen in Figure 4-5a and b respectively. Thus, the servicers filter the infrequent thruster on-off forces, resulting in continuous control forces on the object. As a result, thruster forces are sparse, see Figure 4-6c. The moments required by the servicer are low enough to be applied by reaction wheels. At the infrequent cases when the required moment exceeds the corresponding reaction wheel limits, pure-torque on-off thruster pairs apply 2 Nm thrusts, as seen in Figure 4-6d. If the wheels become saturated, torque-thrusters fire-up, operating at one-tenth of the thruster maximum propulsion capability, a case that does not happen in this specific simulation, since the required reaction wheel torques vary around zero, desaturating the reaction wheels, as can be seen for the servicer shown in Figure 4-6d.

In Figure 4-7a, the manipulator angles for the first servicer are shown, for the case of a PUMA manipulator, see Figure 3-2 (with angles θ_{11} and θ_{12} corresponding to the joints at the base of the manipulator and with axes parallel to the servicer base z and y axes respectively).

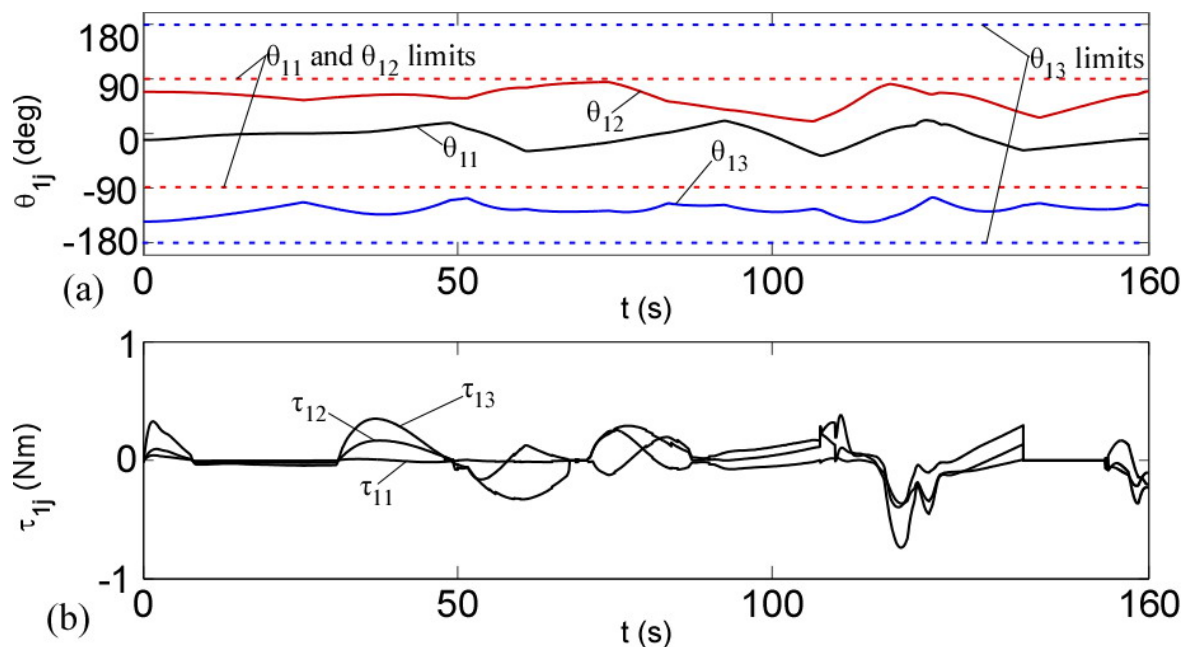


Figure 4-7. Typical manipulator joint-angles (a) and joint-torques (b).

In Figure 4-7b, the corresponding joint torques are shown. As can be seen, no angle exceeds manipulator reasonable physical limits, while the torque requirements are less than 0.8 Nm, which is assumed to be acceptable. Note that the physical limits for both angles θ_{11} and θ_{12} are ± 90 deg. The sudden changes in the slope of the joint angles responses are due to thruster firing or to manipulator pushing the servicer away from the passive object (in both cases, there is a change in servicer direction).

As shown in Figure 4-7a, the typical manipulator joint-angles vary around their initial values, which correspond to the initial distance of each servicer base from the passive object, keeping the manipulator end-effectors into their workspace. These variations can be reduced further by increasing control gains K_{Pi} , K_{rPi} , K_{Di} and K_{rDi} . Then, smaller servicer base deviations around their desired (initial) positions and smaller variations of the corresponding manipulator joint-angles θ_{ij} from their initial values will result. Higher gains are expected to lead to more frequent thruster firing and therefore increased consumption of fuel. This tradeoff can be resolved by system operators.

To show this, we assume that fuel consumption is proportional to the integral of all thruster forces, and compare the response corresponding to the initial gains with that that

results from a set of higher gains, $K_{Pi} = K_{rPi} = 0.25$, $K_{Di} = K_{rDi} = 0.5$. A direct comparison between Figure 4-8a to Figure 4-8b shows that manipulator joint angles vary less around their initial positions for higher gains by about 20.8% for θ_{12} (from 1.01 rad maximum variation for the initial servicer control gains case, to 0.8 rad maximum variation for the increased gains case), by about 34.8% for θ_{13} (from 0.69 rad maximum variation for the initial servicer control gains case, to 0.45 rad maximum variation for the increased gains case), while, even though the maximum variation of the θ_{11} angle is practically the same for the two gain cases, it can be seen that θ_{11} varies less throughout the simulation in the increased gains case (a fact that can be observed for all three angles). Moreover, a comparison between Figure 4-8c and Figure 4-8d shows that fuel consumption has increased by about 27% (from 667 in the initial servicer control gains case, to 918 in the increased gains case).

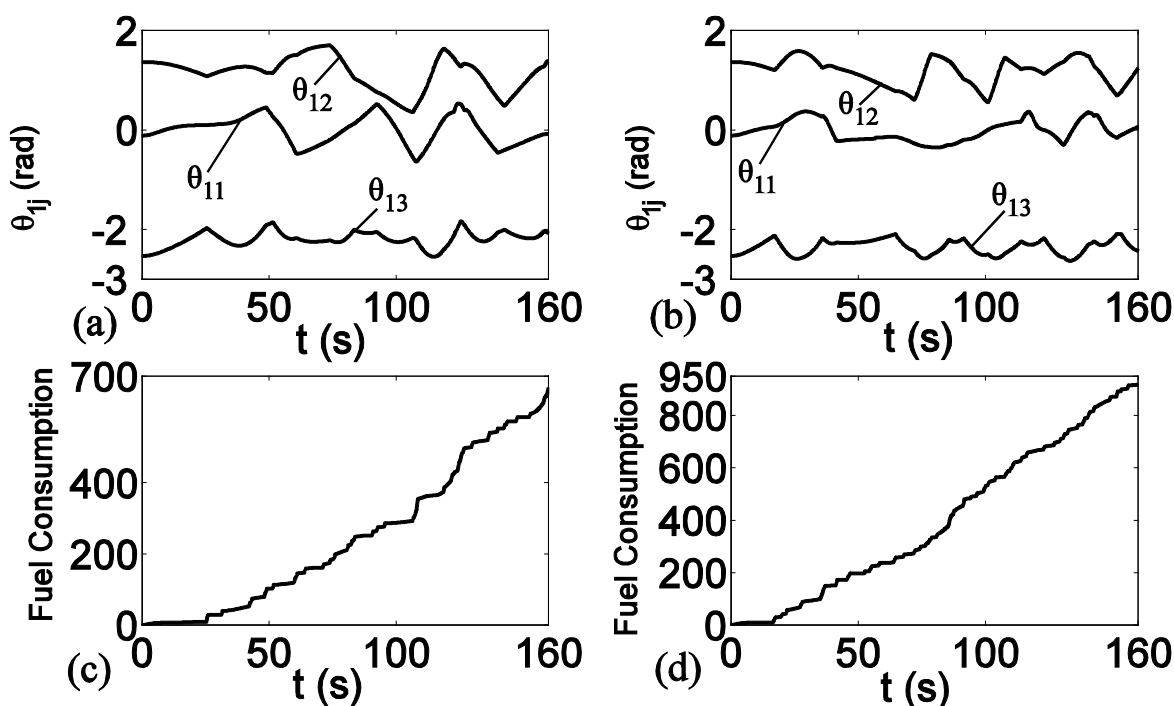


Figure 4-8 Typical manipulator joint-angles and fuel consumption, for the initial servicer control gains (a and c) and for increased gains (b and d).

Next the response of the developed control law of Eqs. (136) and (144) - (145), is compared to the one where the forces/torques are applied to the passive object by thruster equipped servicers (without manipulators) in direct contact to it and actuated by (a) pure on-off control with a deadband and, (b) by PWWF control (see Appendix D), for the same passive object desired motion (Table 4-2). All mass properties and the desired trajectory

are kept the same. In both cases, the control law is model-based as in Eq. (136), where the required \mathbf{Q}_0 is transformed to the passive object frame.

a) In the pure on-off control case, each thruster is turned on, when the corresponding continuous force or torque value exceeds a preset threshold value f_i or n_i respectively. The control gains were chosen as $K_{P0} = 2.25$, $K_{D0} = 1.5$ (for all passive object *translational* DOF), $K_{P0} = 6$, $K_{D0} = 3$ (for all passive object *rotational* DOF), while the threshold values were chosen as $f_i = 18\text{N}$ and $n_i = 1\text{Nm}$. These gains were chosen so that the tracking errors of the passive object controlled by pure on-off control would be of the same magnitude with the tracking errors of the passive object controlled by PWPF control, i.e. less than 0.01 m and 0.01 rad (see Figure 4-9e and f).

b) In the PWPF case, the PWPF modulator developed in [10] was employed and is presented in Appendix D. The control gains and the signal filter parameters were chosen as $K_{P0} = 12.25$, $K_{D0} = 3.5$, $k_m = 1$, $\tau_m = 0.5$ (for all passive object *translational* DOF), $K_{P0} = 9$, $K_{D0} = 3$, $k_m = 1$, $\tau_m = 0.95$ (for all passive object *rotational* DOF), while the threshold $U_{on} = [f_i^T \ n_i^T]^T$ values were chosen as $f_i = 18\text{N}$ and $n_i = 1\text{Nm}$ and the U_{off} values (hysteresis) were set at 80% of the U_{on} ones (thus leading to $h_{trans} = 3.6$ and $h_{rot} = 0.20$). These parameters ensure minimum pulse duration of 100 ms. The applied thruster forces/ torques were again $f_m = 20\text{N}$ and $n_m = 2\text{Nm}$ respectively, for both the pure on-off and PWPF cases.

Figure 4-9 shows the tracking errors and the corresponding fuel consumption, which is again obtained as described in Figure 4-8c and d, as a function of time. In this figure, it can be seen that the performance of the proposed system is superior to that of the system without manipulators, for both pure on-off and PWPF control cases. Indeed, for the same fuel consumption (Figure 4-9a and b), the position error for the proposed system is approximately *six* times less than the one for the PWPF control (Figure 4-9d and e).

Moreover, it can be seen that the performance of the PWPF control system is, as expected, superior to that of the pure on-off control, since, for slightly higher maximum tracking errors for the pure on-off control case (Figure 4-9e and f) the fuel consumption is more than double (Figure 4-9b and c). The tracking error of both the PWPF and the pure on-off control can be lowered with higher control gains (or equally with lower triggering thresholds), but that would result in a further increase in the fuel consumption. Moreover, the fuel consumption of the pure on-off control system can be lowered to the levels of the other two systems, but that would result in very high tracking errors. Note that for the

thrusting of servicer bases with manipulators, pure on-off control was used for simplicity. If PWPF control were used, the fuel consumption of the proposed system would be even lower.

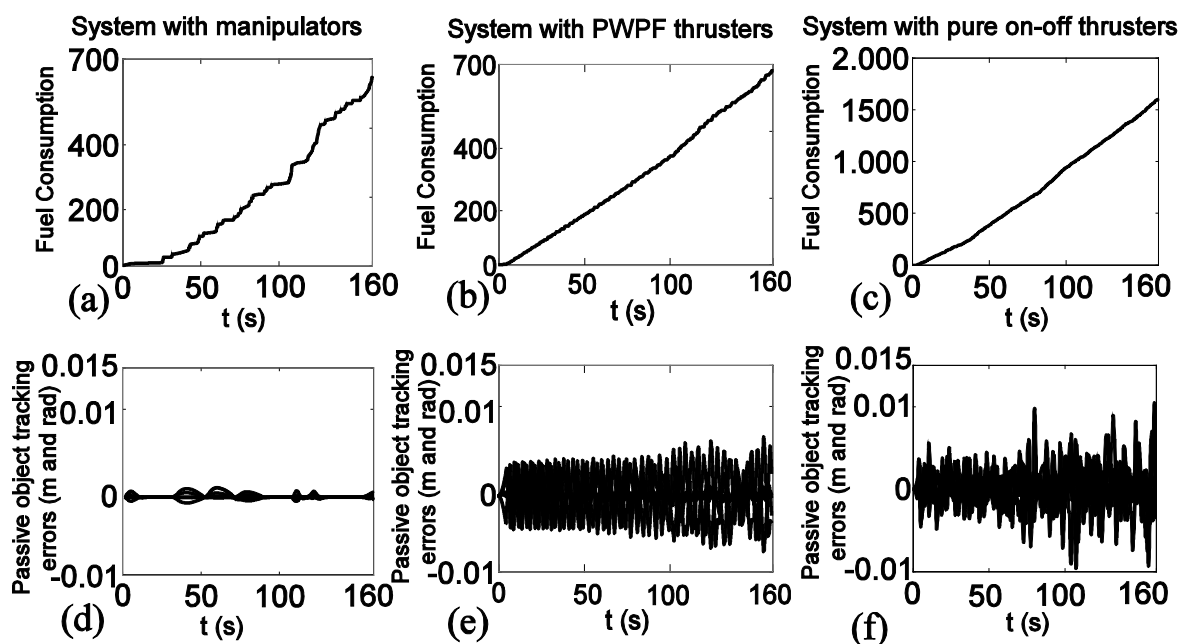


Figure 4-9. Tracking error and corresponding fuel consumption as a function of time. (a), (d) with manipulators, (b), (e) without manipulators (PWPF thrusters), and (c), (f) without manipulators (pure on-off thrusters).

4.1.2 Firm grasp case

The same desired motion scenario is simulated for the case of *firm grasp*. In Figure 4-10, the same variables as in Figure 4-5 are shown for the case of firm grasping. In Figure 4-11, a comparison on tracking errors and fuel consumption is being made, between the case of point contact (Figure 4-11 a, c) and firm grasp (Figure 4-11 b, d). It can be seen that, as expected, the case of firm grasping of the passive object by the servicer manipulators, displays about 17% lower fuel consumption (from 667 in point contact, to 553 in firm grasp), with about 50% lower tracking errors on the motion of the passive object (from a maximum peak of 0.00133 in point contact to a maximum peak of 0.00063 in firm grasp).

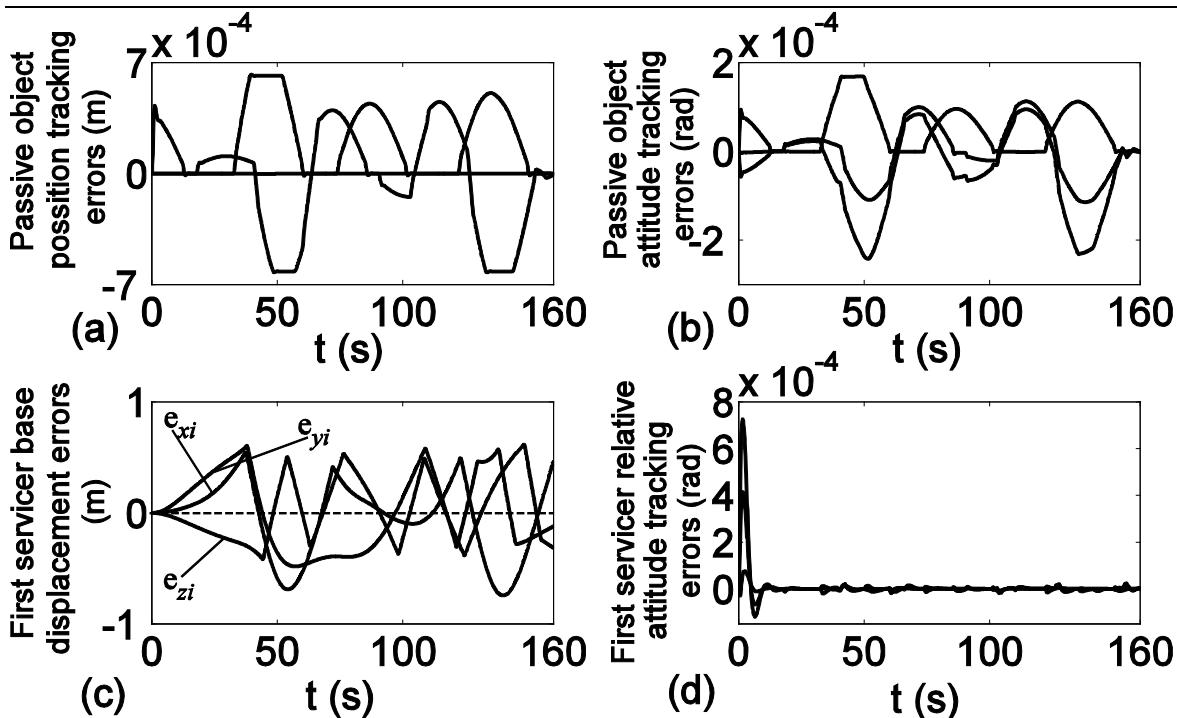


Figure 4-10. Firm grasp case: Tracking errors in (a) object position and (b) attitude, (c) servicer base displacement, and (d) attitude.

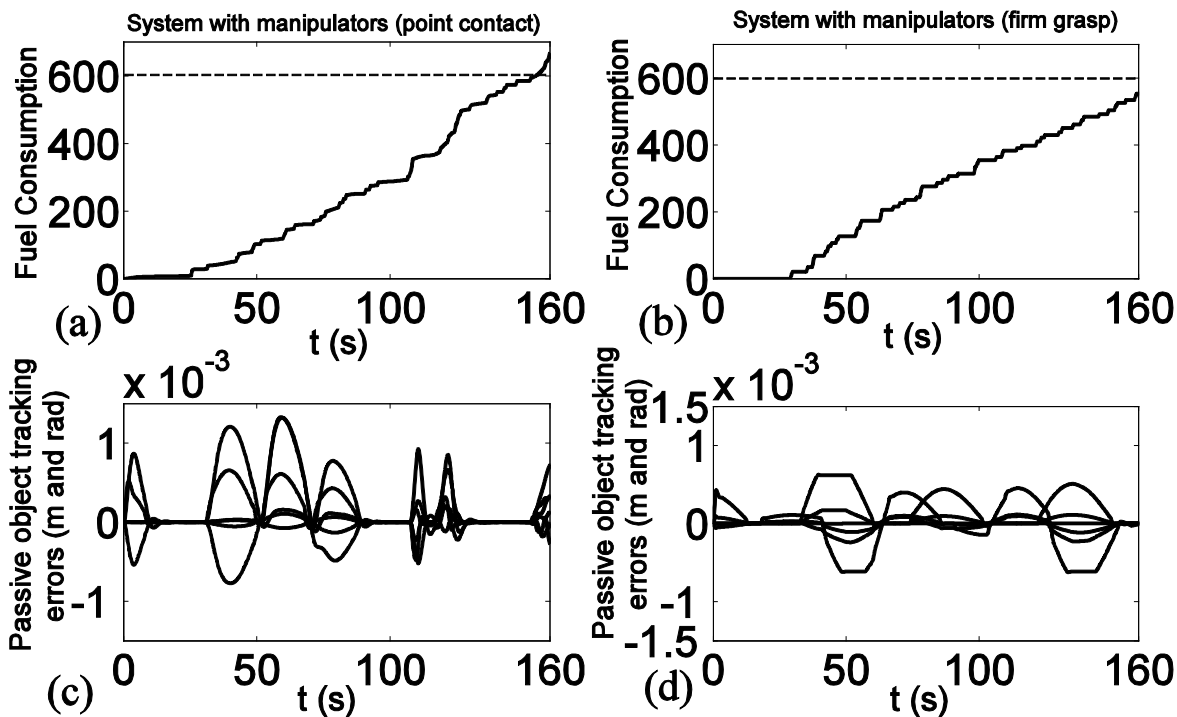


Figure 4-11. Tracking error history and corresponding consumed energy for servicers with manipulators. (a), (c) point contact case, (b), (d) firm grasp case.

It should also be noted that the required manipulator torques for the firm grasp case are of the same order as the ones of the point contact case (the latter shown in Figure 4-7),

with maximum required torque about 0.5 Nm, which is considered acceptable and well within the feasible limits.

4.2 Robustness of the Passive Object Motion Demonstration

To demonstrate the parametric uncertainty robustness of the developed methodology, we run another set of simulations for the same system of a passive object handled by three manipulator-equipped robotic servicers, as the one described at the beginning of Chapter 4. The desired motion for the passive object is again the one shown in Table 4-2.

Again, the bandwidth that corresponds to the control gains is constrained by reaction wheel and thruster limits and, as already mentioned in the previous section cases, higher gains would result in lower tracking errors, but more frequent thruster firing, thus higher fuel consumption. The chosen control gains are kept the same as in the first simulation of the previous section.

As an initial approach on the investigation of the proposed controller robustness to parameter variations, parametric inaccuracies, lag in applying thruster forces, and error in the application of a manipulator force were introduced, as shown in Table 4-4. These are four typical parameters in which errors can occur, with randomly picked-up errors in the range of 5% to 20%. The same controller and gains as before were used.

Table 4-4. Introduced inaccuracies

Object mass error	Thruster f_{34} lag	Thruster f_{23} lag	Error in force f_{E1}
-20%	0.4 s	0.4 s	-15%

Figure 4-12 displays the same variables as those of Figure 4-5, but for motion using a controller with parametric inaccuracies. It can be seen that the tracking capability of the system is still remarkable, i.e. tracking errors of less than ± 1.5 mm in translation and less than $\pm 0.25^\circ$ in rotation, while the servicers are still within their workspace limits. This indicates that the developed controller is quite robust with respect to parametric and modeling errors.

Note that the developed controllers can be extended to include adaptive capabilities. However, one should first consider the benefit in the obtained response versus the complexity and limitations of such algorithms. Simulations validating the analytical

parameter estimation robustness of the passive object motion, presented in the previous chapter, are shown on the next section of the present chapter.

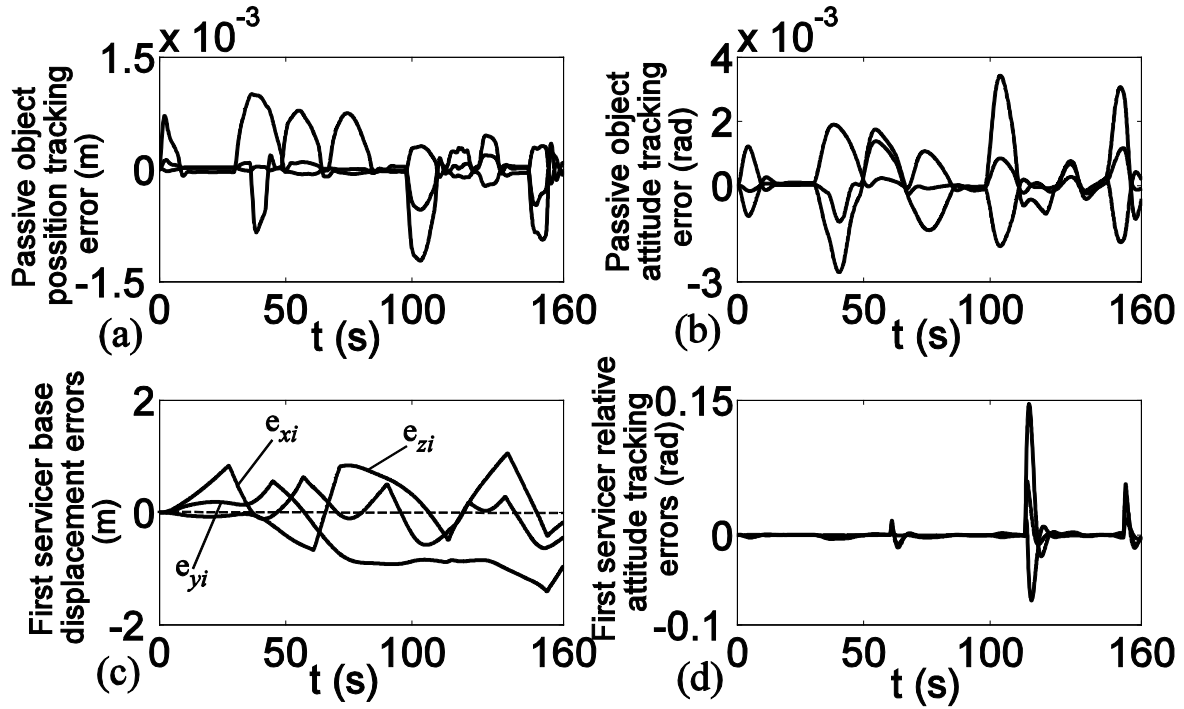


Figure 4-12. Point contact case with inaccuracies: Tracking errors in (a) object position and (b) attitude, (c) servicer base displacement, and (d) attitude.

To further analyze the parametric uncertainty sensitivity of the passive object motion, we take into account that the passive object is assumed to be a homogenous rectangular block, of dimensions $a \times b \times c$. Then the passive object inertia matrix ${}^0\mathbf{I}_0$, expressed in the body-fixed frame, is defined by Eq. (191):

$${}^0\mathbf{I}_0 = m_0 \begin{bmatrix} \frac{b^2 + c^2}{12} & 0 & 0 \\ 0 & \frac{a^2 + c^2}{12} & 0 \\ 0 & 0 & \frac{a^2 + b^2}{12} \end{bmatrix} \quad (191)$$

Assuming that the uncertainty is in the measurement of m_0 and in the measurement of the dimensions a , b and c , we have:

$$\begin{aligned} \hat{m}_0 &= a_1 m_0 \\ \hat{a} &= a_2 a \\ \hat{b} &= a_3 b \\ \hat{c} &= a_4 c \end{aligned} \quad (192)$$

where α_i are uncertainty factors, with $\alpha_i = 1$ meaning no uncertainty. Then, Eqs. (191) and (192) provide the estimated inertia matrix ${}^0\hat{\mathbf{I}}_0$:

$${}^0\hat{\mathbf{I}}_0 = a_1 m_0 \begin{bmatrix} \frac{a_3^2 b^2 + a_4^2 c^2}{12} & 0 & 0 \\ 0 & \frac{a_2^2 a^2 + a_4^2 c^2}{12} & 0 \\ 0 & 0 & \frac{a_2^2 a^2 + a_3^2 b^2}{12} \end{bmatrix} \quad (193)$$

Linearizing ${}^0\hat{\mathbf{I}}_0$ at the point with no uncertainty ($a_i = 1$ for all $i = 1, 2, 3, 4$), yields:

$$\begin{aligned} {}^0\hat{\mathbf{I}}_0 = & {}^0\mathbf{I}_0 + \left. \frac{\partial {}^0\hat{\mathbf{I}}_0}{\partial m_0} \right|_{a_i=1} (\hat{m}_0 - m_0) + \left. \frac{\partial {}^0\hat{\mathbf{I}}_0}{\partial a} \right|_{a_2=1} (\hat{a} - a) + \\ & + \left. \frac{\partial {}^0\hat{\mathbf{I}}_0}{\partial b} \right|_{a_3=1} (\hat{b} - b) + \left. \frac{\partial {}^0\hat{\mathbf{I}}_0}{\partial c} \right|_{a_4=1} (\hat{c} - c) + HOT \end{aligned} \quad (194)$$

where *HOT* stands for *Higher Order Terms*. Note again that, by using standard parameter identification methods [8], [37], [38], the parametric uncertainty can be lowered to levels where the *HOT* are negligible. Then, Eq. (194) becomes:

$${}^0\hat{\mathbf{I}}_0 = {}^0\mathbf{I}_0 + \left. \frac{\partial {}^0\hat{\mathbf{I}}_0}{\partial m_0} \right|_{a_i=1} (\hat{m}_0 - m_0) + \left. \frac{\partial {}^0\hat{\mathbf{I}}_0}{\partial a} \right|_{a_2=1} (\hat{a} - a) + \left. \frac{\partial {}^0\hat{\mathbf{I}}_0}{\partial b} \right|_{a_3=1} (\hat{b} - b) + \left. \frac{\partial {}^0\hat{\mathbf{I}}_0}{\partial c} \right|_{a_4=1} (\hat{c} - c) \quad (195)$$

From Eq. (191), we obtain:

$$\frac{\partial {}^0\mathbf{I}_0}{\partial m_0} = \begin{bmatrix} \frac{b^2 + c^2}{12} & 0 & 0 \\ 0 & \frac{a^2 + c^2}{12} & 0 \\ 0 & 0 & \frac{a^2 + b^2}{12} \end{bmatrix} \quad (196)$$

$$\frac{\partial {}^0\mathbf{I}_0}{\partial a} = m_0 \begin{bmatrix} 0 & 0 & 0 \\ 0 & a/6 & 0 \\ 0 & 0 & a/6 \end{bmatrix} \quad (197)$$

$$\frac{\partial {}^0\mathbf{I}_0}{\partial b} = m_0 \begin{bmatrix} b/6 & 0 & 0 \\ 0 & 0 & 0 \\ 0 & 0 & b/6 \end{bmatrix} \quad (198)$$

$$\frac{\partial {}^0\mathbf{I}_0}{\partial c} = m_0 \begin{bmatrix} c/6 & 0 & 0 \\ 0 & c/6 & 0 \\ 0 & 0 & 0 \end{bmatrix} \quad (199)$$

Thus, taking into account Eqs. (196) to (199), Eq. (195) becomes:

$$\begin{aligned} {}^0\hat{\mathbf{I}}_0 = m_0 & \underbrace{\begin{bmatrix} \frac{b^2+c^2}{12} & 0 & 0 \\ 0 & \frac{a^2+c^2}{12} & 0 \\ 0 & 0 & \frac{a^2+b^2}{12} \end{bmatrix}}_{\mathbf{I}_m} a_1 + m_0 a \underbrace{\begin{bmatrix} 0 & 0 & 0 \\ 0 & a/6 & 0 \\ 0 & 0 & a/6 \end{bmatrix}}_{\mathbf{I}_{x_{cm}}} (a_2 - 1) + \\ & + m_0 b \underbrace{\begin{bmatrix} b/6 & 0 & 0 \\ 0 & 0 & 0 \\ 0 & 0 & b/6 \end{bmatrix}}_{\mathbf{I}_{y_{cm}}} (a_3 - 1) + m_0 c \underbrace{\begin{bmatrix} c/6 & 0 & 0 \\ 0 & c/6 & 0 \\ 0 & 0 & 0 \end{bmatrix}}_{\mathbf{I}_{z_{cm}}} (a_4 - 1) \end{aligned} \quad (200)$$

which, in turn, can be written as:

$${}^0\hat{\mathbf{I}}_0 = {}^0\mathbf{I}_0 + \underbrace{(a_1 - 1) {}^0\mathbf{I}_m + (a_2 - 1) {}^0\mathbf{I}_{x_{cm}} + (a_3 - 1) {}^0\mathbf{I}_{y_{cm}} + (a_4 - 1) {}^0\mathbf{I}_{z_{cm}}}_{\delta\mathbf{I}} = {}^0\mathbf{I}_0 + \delta\mathbf{I} \quad (201)$$

Then matrices $\delta\mathbf{H}$ and $\delta\mathbf{C}$ of Eqs. (162) and (163), become

$$\delta\mathbf{H} = (a_1 - 1) \mathbf{H}_m + (a_2 - 1) \mathbf{H}_a + (a_3 - 1) \mathbf{H}_b + (a_4 - 1) \mathbf{H}_c \quad (202)$$

where

$$\mathbf{H}_m = \begin{bmatrix} \text{diag}(m_0, m_0, m_0) & \mathbf{0}_{3 \times 3} \\ \mathbf{0}_{3 \times 3} & \mathbf{E}_0^T \mathbf{R}_0 {}^0\mathbf{I}_m \mathbf{R}_0^T \mathbf{E}_0 \end{bmatrix} \quad (203)$$

and

$$\mathbf{H}_i = \begin{bmatrix} \mathbf{0}_{3 \times 3} & \mathbf{0}_{3 \times 3} \\ \mathbf{0}_{3 \times 3} & \mathbf{E}_0^T \mathbf{R}_0 {}^0\mathbf{I}_i \mathbf{R}_0^T \mathbf{E}_0 \end{bmatrix}, \text{ with } i = a, b, c \quad (204)$$

and

$$\delta \mathbf{C} = (a_1 - 1)\mathbf{C}_m + (a_2 - 1)\mathbf{C}_a + (a_3 - 1)\mathbf{C}_b + (a_4 - 1)\mathbf{C}_c \quad (205)$$

with

$$\mathbf{C}_i = \left[\mathbf{0}_{1 \times 3}, \left(\mathbf{E}_0^T \left(\mathbf{R}_0^0 \mathbf{I}_i \mathbf{R}_0^T \dot{\mathbf{E}}_0 \dot{\boldsymbol{\theta}}_0 + \mathbf{E}_0 \dot{\boldsymbol{\theta}}_0 \times \mathbf{R}_0^0 \mathbf{I}_i \mathbf{R}_0^T \mathbf{E}_0 \dot{\boldsymbol{\theta}}_0 \right) \right)^T \right]^T \quad (206)$$

Thus, Eqs. (202) and (205) can be used directly in Eq. (177), to obtain the steady state error. Choosing as uncertainty parameters the following:

$$a_1 = 0.8, \quad a_2 = 1.15, \quad a_3 = 0.9, \quad a_4 = 1.1 \quad (207)$$

the tracking errors of the passive object motion are shown in Figure 4-13b, as opposed to the tracking errors of the passive object motion for the system without uncertainty, which are shown in Figure 4-13a. Note that, even though the maximum tracking errors for the system with uncertainty are larger than those for the system without uncertainty, they are still quite low, i.e. below 2mm.

The upper six elements of the expected steady-state errors vector \mathbf{A}_d (see Eq. (177)) that correspond to \mathbf{q}_0 , are shown in Figure 4-14a. Note that the lower six elements of \mathbf{A}_d , corresponding to $\dot{\mathbf{q}}_0$, are constantly equal to zero throughout the simulation (not shown here for brevity).

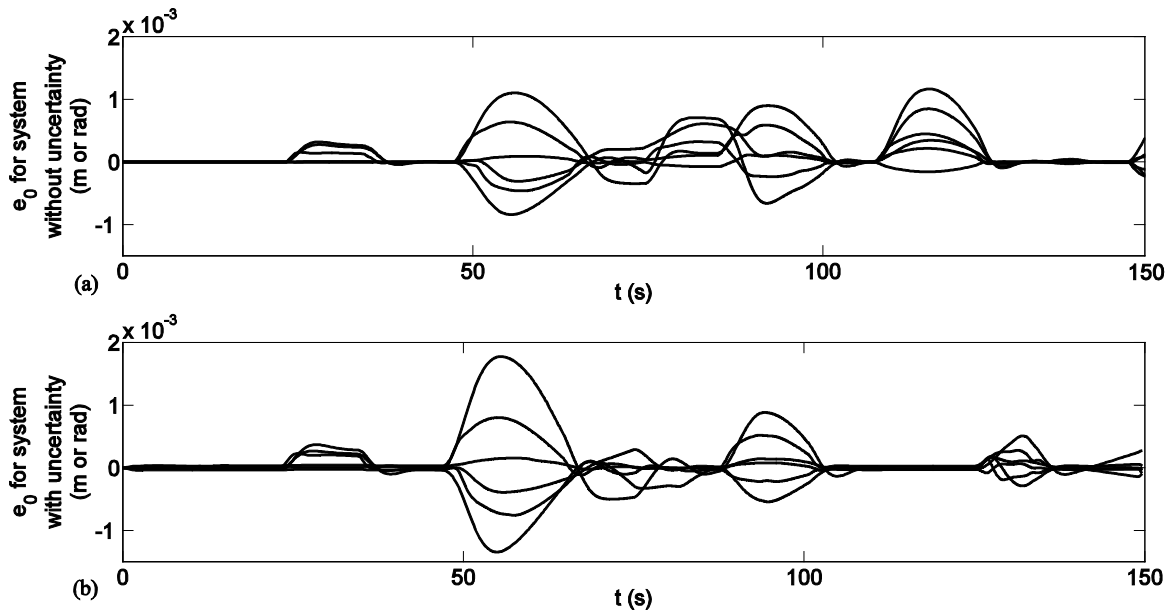


Figure 4-13. Tracking errors e_0 for the passive object motion, for the system without (a) and the system with (b) uncertainty.

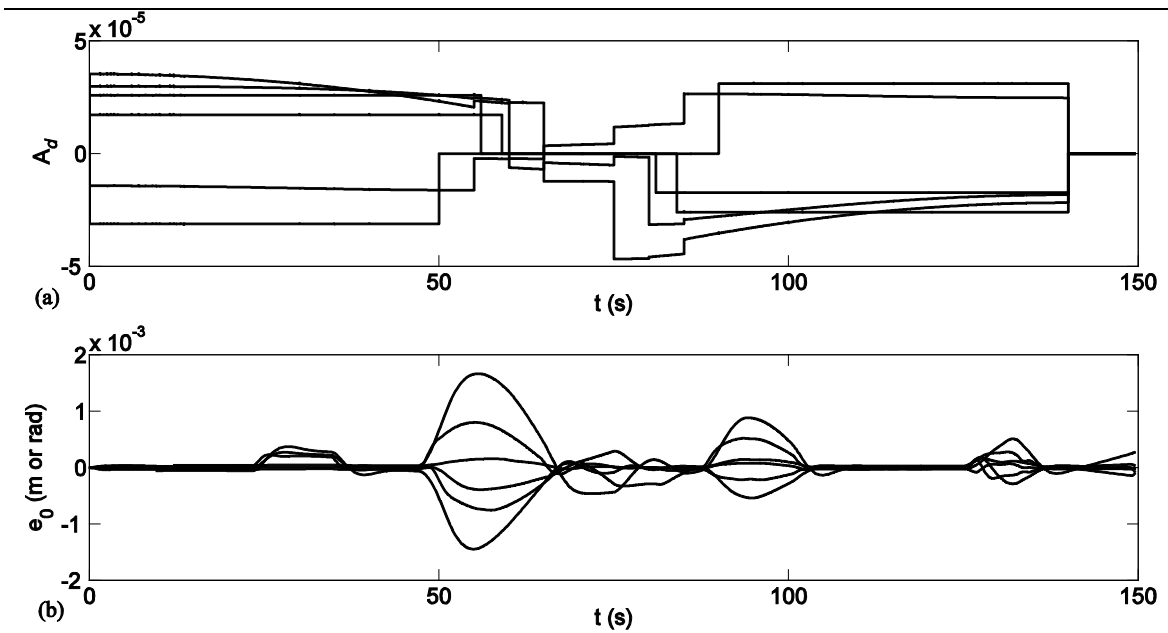


Figure 4-14. Upper six values of vector \mathbf{A}_d , corresponding to the position/orientation steady-state errors for the passive object (a) and actual passive object position/orientation errors (b).

As can be seen from Figure 4-14a, throughout the simulation the elements of \mathbf{A}_d are of the order of 10^{-4} . Thus, the requirements for Eq. (177) are fulfilled and the expected steady-state errors should be the ones shown in Figure 4-14a. The actual position/orientation errors for the passive object, throughout the simulation, are shown in Figure 4-14b.

Note that the maximum actual errors in Figure 4-14b are more than an order of magnitude larger than the expected ones (Figure 4-14a). This is because of two reasons. First, the discontinuities in the desired accelerations of the passive object (see Table 4-2) result in discontinuous expected steady-state errors, as can be seen in Figure 4-14a from 50s to 90s. These discontinuities act as disturbances, which the controller overcomes, converging again on the expected error values. Also, in the above analysis, we have assumed a smooth application of the required \mathbf{Q}_0 as shown in Eq. (82). Nevertheless, small disturbances due to thruster firing at the servicers pass on to the passive object through the manipulators. Those disturbances are very small, but not zero and can also affect the, also very small, position/orientation tracking errors of the passive object, as can be seen in Figure 4-14b from about 23s to 38s and from about 125s to 135s. Nevertheless, the controller overcomes these disturbances and quickly converges on the predicted by \mathbf{A}_d values, as seen in Figure 4-15.

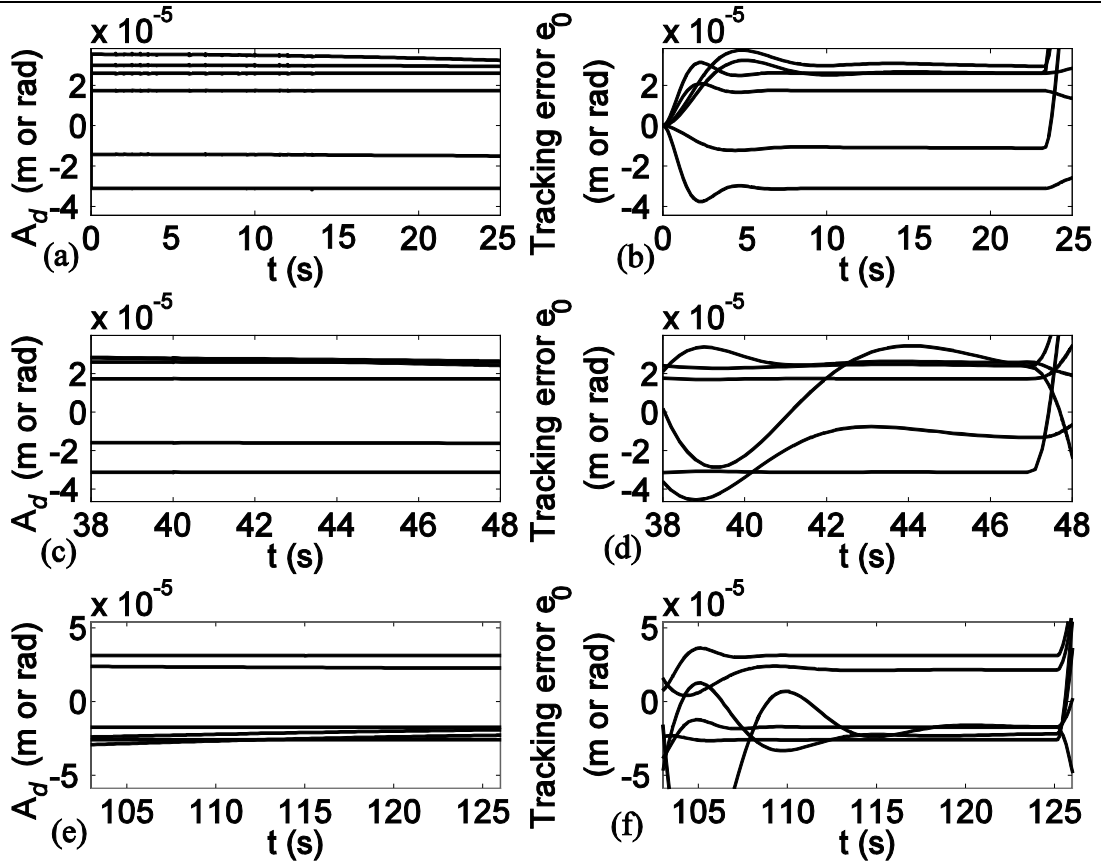


Figure 4-15. Comparison between position/orientation tracking errors (b, d, f) and the corresponding expected values (a, c, e), for zero to 25 s (a, b), 38 s to 48 s (c, d) and 103 s to 126 s (e, f).

In Figure 4-15 the comparison between the position/orientation tracking errors and the corresponding elements of vector \mathbf{A}_d , is displayed for some time-spans during the simulation in which no disturbances affect the tracking errors. As can be seen, the tracking errors are converging on the corresponding values of \mathbf{A}_d .

It should also be noted that all twelve elements of vector \mathbf{A}_d are constantly equal to zero throughout the simulation, in the case of no uncertainty ($a_i = 1$ for $i = 1,2,3,4$), verifying Eq. (179).

In order to verify the dependency of the method on the need for matrices \mathbf{F}_{dD} and \mathbf{F}_{dP} of Eqs. (173) and (175) to be negative definite, the same simulation is run, but with unrealistically large errors that lead to both of these matrices having at least some positive eigenvalues. The chosen uncertainty parameters, replacing in this case the ones of Eq. (207), are:

$$a_1 = 0.4, \quad a_2 = 1.4, \quad a_3 = 0.55, \quad a_4 = 0.6 \quad (208)$$

As can be seen in Figure 4-16a and b, the uncertainty parameters of Eq. (207), lead to negative eigenvalues of both matrices F_{dD} and F_{dP} , resulting to the expected system responses seen in Figure 4-13, Figure 4-14 and Figure 4-15. On the contrary, the uncertainty parameters of Eq. (208), result in some positive eigenvalues for both F_{dD} and F_{dP} matrices, as seen in Figure 4-16c and d.

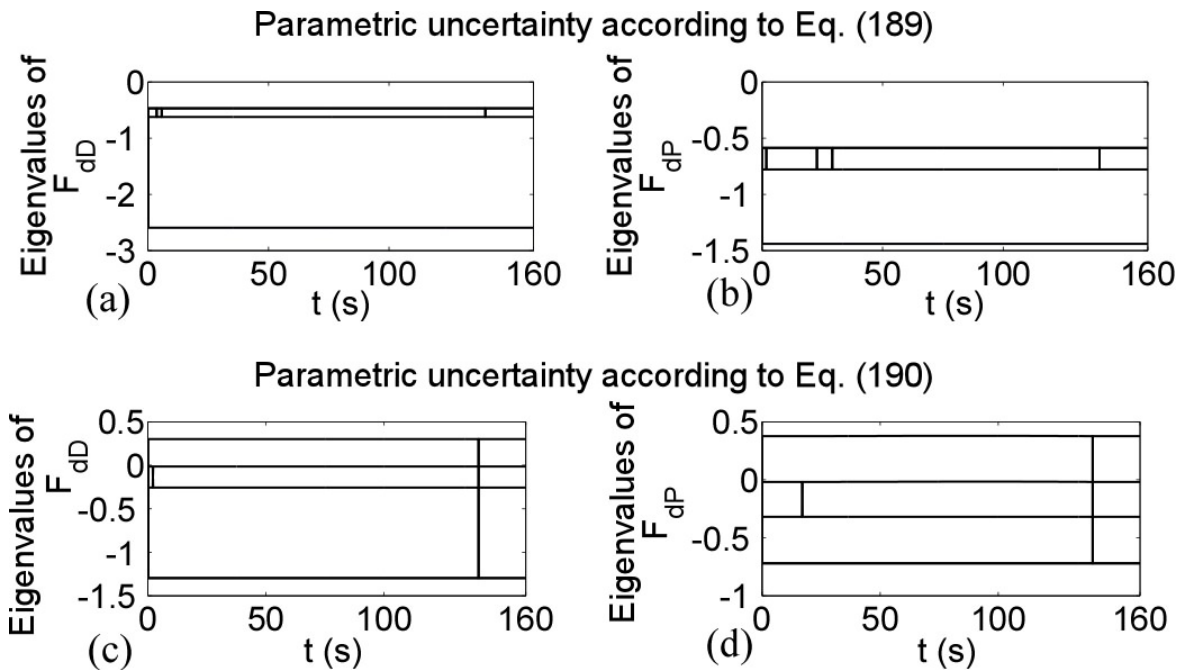


Figure 4-16. Eigenvalues of matrices F_{dD} and F_{dP} for the case with uncertainty parameters of Eq. (207) ((a) and (b)) and for the case with uncertainty parameters of Eq. (208) ((c) and (d)).

Since the assumption for negative definitiveness of both matrices F_{dD} and F_{dP} is no longer valid, the expected values of the steady-state tracking errors A_d do not coincide with the actual tracking errors e_0 , even for time intervals that no disturbance occurs. Thus, as seen in Figure 4-17, even though some tracking errors converge to the expected values, others oscillate wildly, without even oscillating around the expected values. Note that the system response is still stable, although the tracking errors are far larger than before, reaching values of more than 10^{-2} (an order of magnitude larger than before).

In a simulation with another desired trajectory, a triangular profile on the desired velocities is used (no constant-velocity area), with higher accelerations, see Table 4-5. This time, the general equations for the robustness analysis are used (Eqs. (181) to (190) instead of Eqs. (191) to (206)). Assuming random (but not negligible) uncertainty values of +15%, -10% and +10% for the passive object dimension measurements, leads to an 11.4% uncertainty at the measurement of its volume.

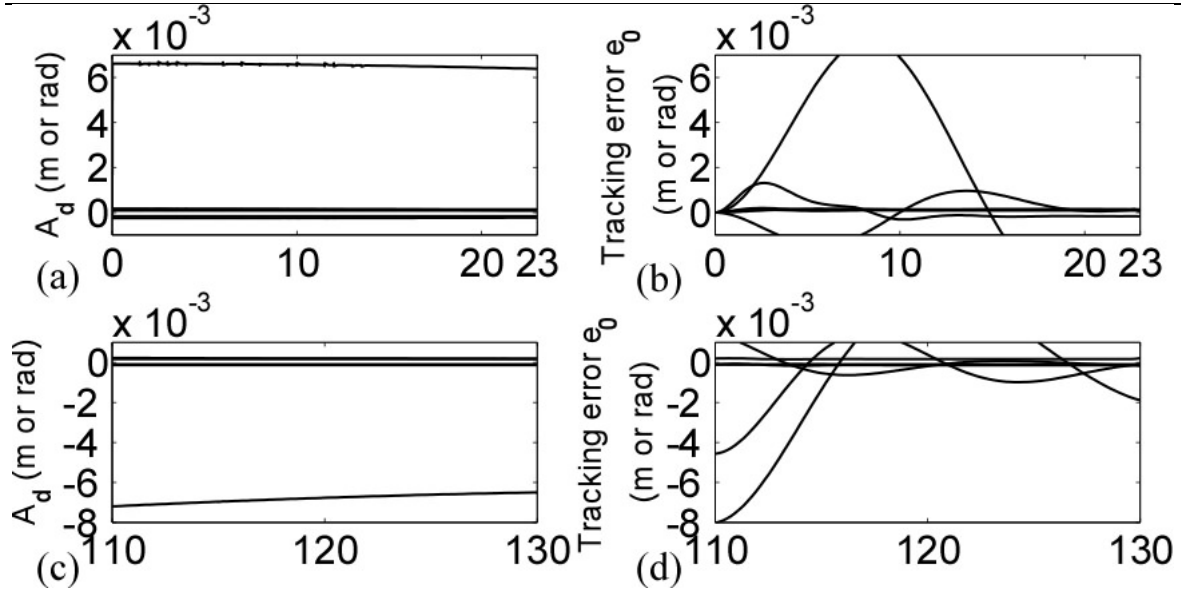


Figure 4-17. Comparison between position/orientation tracking errors (b, d) and the corresponding expected values (a, c), for zero to 23 s (a, b) and 110 s to 130 s (c, d), for uncertainty parameters as in Eq. (208).

This uncertainty, in addition to a passive object density measurement uncertainty of -35.4%, result in an uncertainty at the passive object mass of about -20%. Note that these uncertainties are the same as the ones for the first trajectory (see Eq. (207)). Thus, uncertainty parameters $\delta\rho$ and δV of Eq. (182) become:

$$\delta\rho = 5.3 \frac{kg}{m^3}, \quad \delta V = 2.85 m^3 \quad (209)$$

Table 4-5. Passive object desired motion parameters (Trajectory 2).

DOF	const. accel. (m/s ²)/ (rad/s ²)	up to (s)	const. decel. (m/s ²)/ (rad/s ²)	up to (s)
X _{0des}	0.0004	70	-0.0004	140
Y _{0des}	-0.00046	65	0.00046	130
Z _{0des}	0.0003	75	-0.0003	150
θ_{0des}	$6 \cdot 10^{-5}$	67	$-6 \cdot 10^{-5}$	134
ϕ_{0des}	$7 \cdot 10^{-5}$	73	$-7 \cdot 10^{-5}$	146
ψ_{0des}	$1.1 \cdot 10^{-4}$	70	$-1.1 \cdot 10^{-4}$	140

The tracking errors for this trajectory are shown in Figure 4-18a for the case with uncertainty. A noticeable fact is that there are fewer disturbances, as opposed to the first trajectory case, since now there are fewer discontinuities in the desired trajectory (compare Figure 4-18a to Figure 4-13b, from about 40s to about 100s), but these are somewhat larger, since the motion is faster and the discontinuities more abrupt.

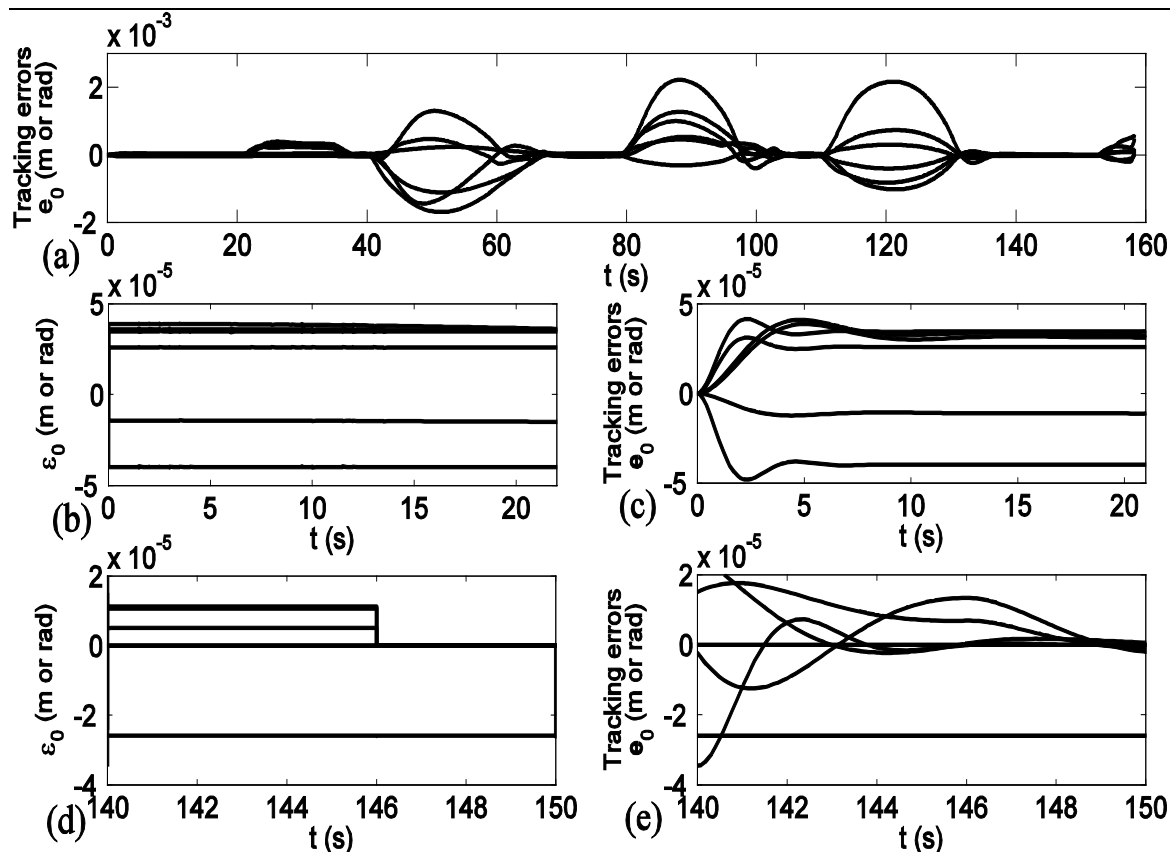


Figure 4-18. Passive object tracking errors e_0 (a), and comparison between position/orientation tracking errors (c and e) and the corresponding expected values (b and d), for the system with uncertainty.

In the remaining of Figure 4-18 the passive object tracking errors are compared to the expected values, for some time periods where no disturbances occur. Again, the tracking errors converge on the corresponding steady-state values of ε_0 .

4.3 One vs. Three Servicers

The two cases to be compared include (a) three single-manipulator servicers, firmly grasping a passive object and (b) a single, scaled-up, single-manipulator servicer, firmly grasping the same passive object. Again, each servicer base has thrusters capable of producing forces or moments, (in the case of three servicers, thrusters facing the object are deactivated), reaction wheels, and a single PUMA-type manipulator.

The characteristics of the passive object are the same as in the previous section, i.e. a $2\text{m} \times 3\text{m} \times 2\text{m}$ orthogonal block of mass of 180 kg. For the case of three, small free-flying servicers, again the characteristics are kept the same as in the previous section (see Table 4-1).

For the case of a single, large servicer, the servicer mass is 210 kg, and its base is of cubic shape with a 1 m side. The contact point lies on the object surface with normal vector parallel to the $-\hat{x}_0$ unit vector of the object body-fixed axes. The servicer thrusters develop per axis a pure force of 60 N, while their trigger threshold is set to $f_t = 25$ N. For attitude control, the servicers have additional pairs of thrusters that develop pure torque of 6 Nm per axis, and reaction wheels that can develop proportional torques up to $n_t = 3$ Nm per axis. The servicer manipulator has a maximum reach of 3 m. The abovementioned parameters for the large servicer result in a roughly three times scaled up servicer, compared to each one of the three smaller ones, making this a fair system for the comparison.

Several sets of simulations were run for both cases, in which all bodies were involved in 3D motions. Here we present two characteristic simulation runs, (a) one with a realistic 3D passive object desired trajectory and (b) one with step commands for all passive object DOF. For both simulation sets, the servicer position control task is to keep the manipulator base at a distance equal to 1 m for the three-servicers case and 1.5 m for the single-servicer case, measured along the object surface normal vector passing from the end-effector contact point. The servicer attitude control task is to keep the surface of the servicer that the manipulator is mounted on, parallel to the corresponding contact surface of the passive object in the case with the three servicers or, in the single-servicer case, to keep two adjusting surfaces of the servicer on angles of $-\pi/4$ and $\pi/4$ respectively, with respect to the corresponding contact surface, so that the thrusters on those servicer surfaces, will be able to fire without harming the passive object. The simulations are run on the Matlab/ Simulink package. To obtain the required contact forces in the case of three servicers, the *fmincon* non-linear constrained optimization process is employed.

4.3.1 Simulation (a)

First, the 3D motion of all bodies, for a general 3D passive object desired trajectory, is simulated, in which each of the six DOF of the passive object follows a trapezoidal profile for the linear velocity or Euler angles rate for both cases, see Table 4-2.

For the single-servicer system, the control gains in Eqs. (136) and (144) are shown in Table 4-6. Note that these gains are chosen in order to keep the servicer within its manipulator workspace.

Table 4-6. Control gains for the single-servicer case.

Passive Object				Servicer (for $i = 1, 2, 3$)			
Translational DOF		Rotational DOF		Translational DOF		Rotational DOF	
K_{P0} : 3.24	K_{D0} : 1.8	K_{P0} : 0.49	K_{D0} : 0.7	K_{P1} : 0.09	K_{D1} : 0.3	K_{P1} : 9	K_{D1} : 3

For the three-servicers system, the control gains in Eqs. (136) and (144) are shown in Table 4-7.

Table 4-7. Control gains for the three-servicers case.

Passive Object				Servicer (for $i = 1, 2, 3$)			
Translational DOF		Rotational DOF		Translational DOF		Rotational DOF	
K_{P0} :	K_{D0} :	K_{P0} :	K_{D0} :	K_{Pi} :	K_{Di} :	K_{Pi} :	K_{Di} :
3.24	1.8	0.49	0.7	0.09	0.3	9	3
				(except: K_{P1x}, K_{P2x} :	(except: K_{D1x}, K_{D2x} :		
				0.16	0.04		
				K_{P3y} : 0.2025)	K_{D3y} : 0.45)		

Note that the gains for the three-servicer system are a little bit changed from the initial simulation presented in this chapter, even though the system and the passive object desired trajectory are the same. This gain tuning is done in order to obtain the same passive object maximum tracking errors for both cases, thus making it easier to compare the cases by comparing their fuel consumption (see Figure 4-19).

In Figure 4-19, the passive object tracking errors (a and b) and the total fuel consumption (c and d) are shown, both for the case of three servicers (a and c) and the single-servicer case (b and c). As can be seen in Figure 4-19, for the same maximum passive object tracking errors, we have about 40% higher fuel consumption in the single-servicer case (from 250 in the three-servicers case, to 350 in the single-servicer case).

In Figure 4-20, the reach of each servicer manipulator is shown throughout the simulation, both for the three-servicer (a) and single-servicer (b) case. As can be seen, all

manipulators in both cases have approximately the same minimum and maximum reach throughout the simulation.

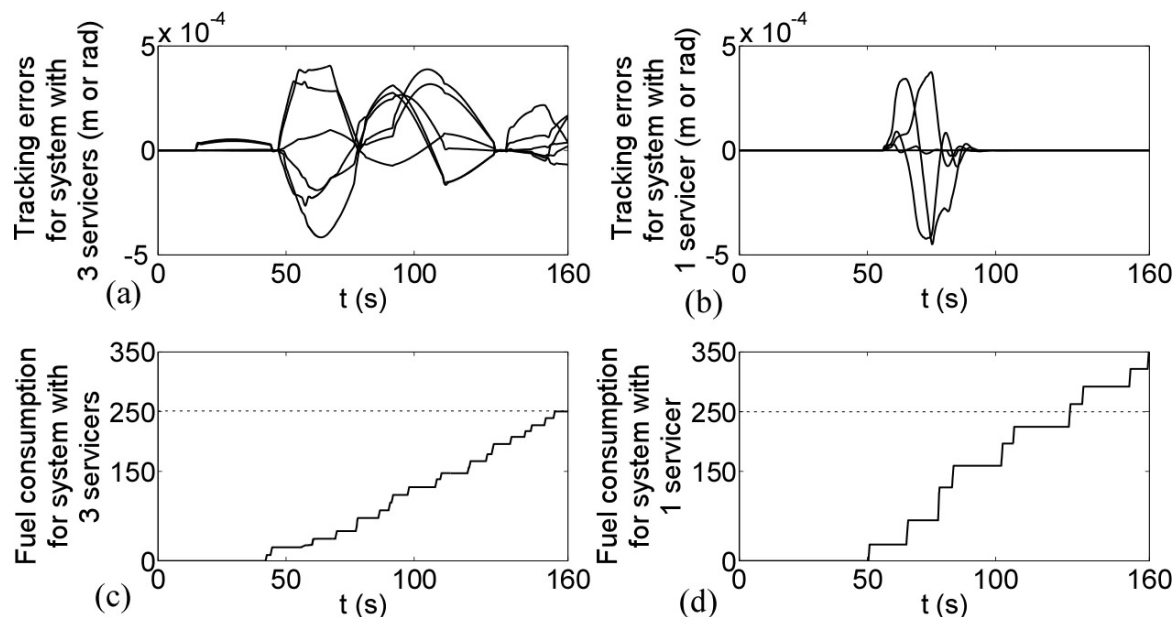


Figure 4-19. Passive object tracking errors (a, b) and fuel consumption (c, d), for the case of three servicers (a, c) and single-servicer (b, c).

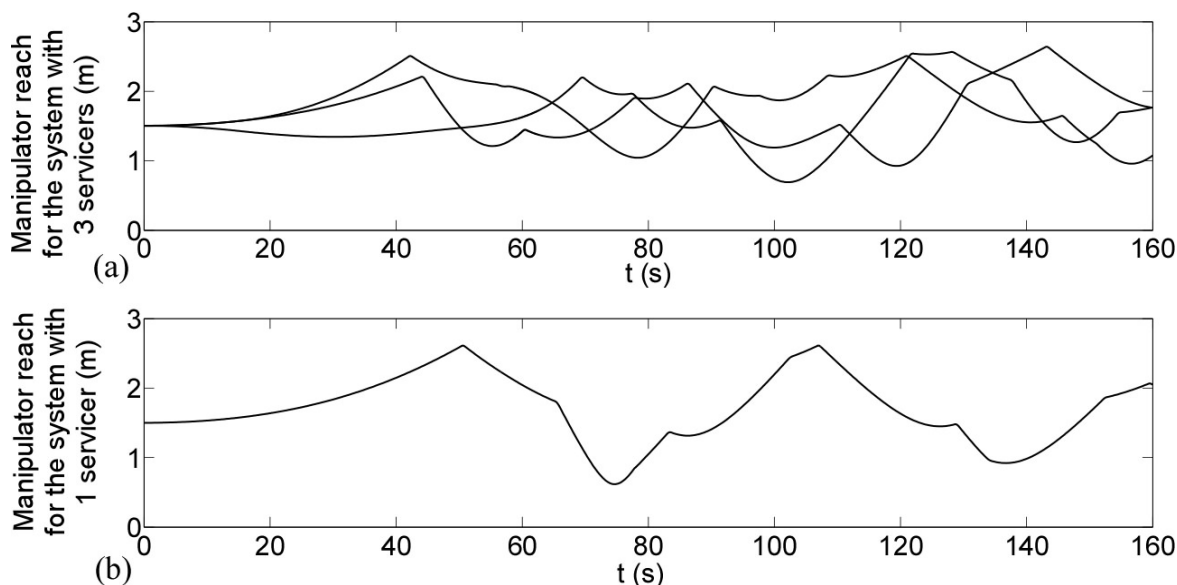


Figure 4-20. Manipulator reach for (a) the three-servicers case, as well as (b) the single-servicer case.

In Figure 4-21, all thruster forces are displayed, both for the three-servicers (a) and the single-servicer (b) case. Moreover, the reaction wheel torques, as well as the thruster pure torques, are also displayed for both cases (c and d). As can be seen, the three servicers together have more frequent thruster firing, since there are three of them to be kept within their manipulator workspaces, but the single, large servicer has far more powerful

thrusting, resulting in higher fuel consumption, as seen in Figure 4-19. In Figure 4-21c the reaction wheel torques for the three-servicer case are displayed. As can be seen, these torques were not adequate and the pure-torque thrusters had to ignite briefly for one of the servicers, a little bit after 50 s.

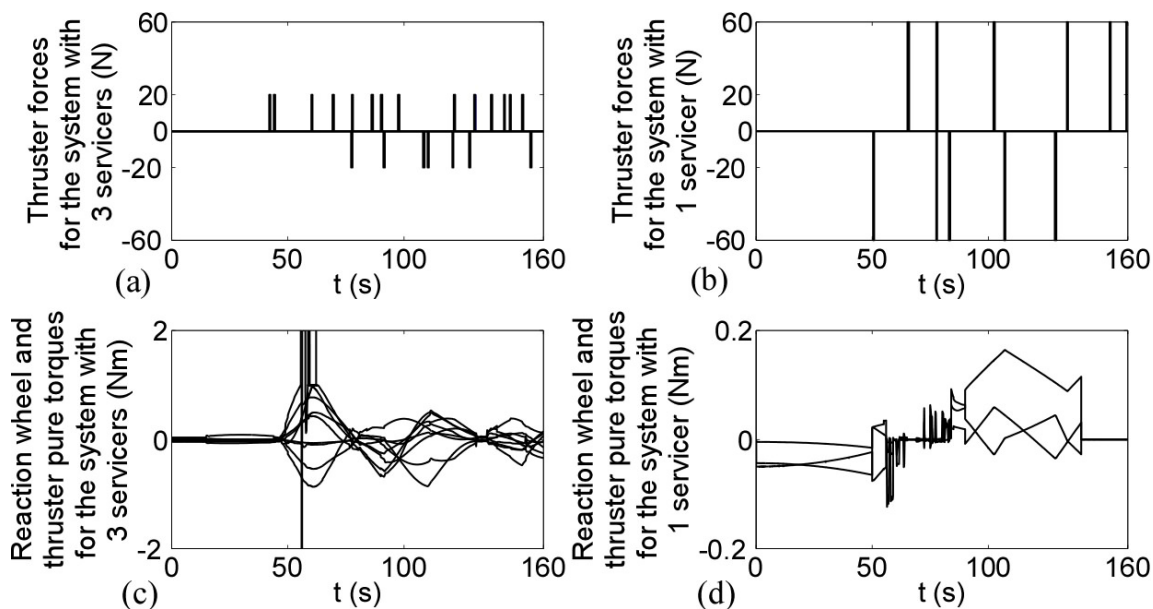


Figure 4-21. Thruster firing (a, b) and reaction wheel and thruster torque (c, d), for the three-servicers case (a, c), as well as the single-servicer case (b, d).

On the contrary, for the single-servicer system, no such thruster firing was necessary, as can be seen in Figure 4-21d. Nevertheless, the three-servicer system still has lower fuel consumption.

4.3.2 Simulation (b)

Next, a 3D motion of all bodies is again simulated, but in this case the command for the passive object is not a desired trajectory, but different step commands for all six DOF, as seen in Table 4-8.

Table 4-8. Step commands.

DOF	x_0	y_0	z_0	θ_0	φ_0	ψ_0
Initiation time	10 s	15 s	20 s	10 s	15 s	20 s

For the three-servicers system, the control gains in Eqs. (136) and (144) are shown in Table 4-9.

Table 4-9. Control gains for the three-servicers case.

Passive Object		Servicer (for $i = 1, 2, 3$)			
All passive object DOF		Translational DOF		Rotational DOF	
K_{P0} : 0.0196	K_{D0} : 0.14	K_{P1} : 0.16	K_{D1} : 0.4	K_{P1} : 2.89	K_{D1} : 1.7

For the single-servicer system, the control gains are shown in Table 4-10.

Table 4-10. Control gains for the single servicer case.

Passive Object		Servicer (for $i = 1, 2, 3$)			
All passive object DOF		Translational DOF		Rotational DOF	
K_{P0} : 0.0225	K_{D0} : 0.15	K_{P1} : 0.16	K_{D1} : 0.4	K_{P1} : 2.25	K_{D1} : 1.5

Note that the control gains for the servicers (for both cases) were chosen so as to keep the servicer bases within their corresponding manipulator workspaces. These plots are not shown here for brevity, since in both cases the servicer bases are kept well within their manipulator workspaces and the important difference between the two cases lies in the different response of the passive object. In Figure 4-22, the passive object tracking errors (a and b) and the total fuel consumption (c and d) are shown, both for the case of three servicers (a and c) and the single-servicer case (b and c). The fuel consumption was obtained as the integral of all thruster absolute forces. As can be seen in Figure 4-22, in the three-servicer case we have not only lower maximum passive object tracking errors than the single-servicer case, but also about 13.8% lower fuel consumption, from 634 in the single servicer case to 546 in the three-servicers case. This verifies the theoretical study of Section 3.2 and of Table 3-1.

Moreover, note that lowering the control gains for the passive object motion in the single-servicer case would result in a lower need for manipulator force/ torque application and thus lower disturbances on the servicer base, and lower fuel consumption in order to keep it within the manipulator workspace. This though, would result in increasing the passive object tracking errors. Moreover, rising the control gains for the passive object motion in the single-servicer case to values closer to the ones of the three-servicers case, would result in lowering the passive object tracking errors, but at the same time also in further rising the fuel consumption.

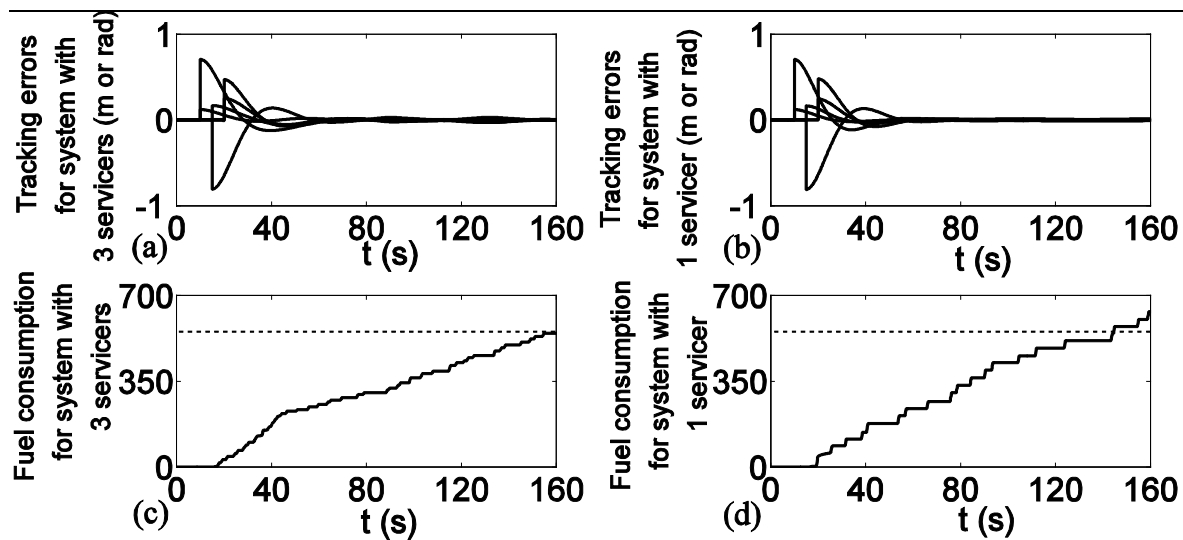


Figure 4-22. Passive object tracking errors (a, b) and fuel consumption (c, d), for the case of three servicers (a, c) and single-servicer (b, d), for the second simulation.

5 Conclusions and Future Work

5.1 Conclusions

The research in this thesis focused on modeling and control of systems performing On-Orbit Servicing tasks. Initially, two concepts were considered. The first was a novel concept for an orbital debris capturing system, by means of a semi-elastic net controlled by a number of free-flying robotic servicers, via their manipulators. This concept was initially evaluated by means of simplified one-dimensional model, and valuable insight was gained. Sets of constraints that must be held between system parameters and initial conditions were derived by studying the dynamics and control of the system and the desired system response. A set of control gains to be used in a velocity-based controller resulted by trying to satisfy these constraints. The response of the simulated system has confirmed the constrained control method, while the robustness of the method was studied in the case of inaccurate estimation of the debris parameters, via simulations. It was found that the method shows robustness, keeping the debris in the net, although an additional force may be needed. Nevertheless, the demonstrated feasibility of the proposed concept was not adequate, even for a simplified one-dimensional model. For this reason, an alternative concept that deals with a different On-Orbit Servicing task, was also studied.

This was the novel concept of cooperative manipulation of an already captured on orbit passive object via free-flying servicers, employing both on-off thrusters and manipulator continuous forces. This concept was tested for two contact cases between the manipulator end-effector and the passive object: point contact and firm grasp. The system dynamics arising from the unilateral constraints (in the point contact case) and the on-off thrusting were presented, and the manipulation concept was again illustrated using a simplified one-dimensional model (for the firm grasp contact case only). A novel controller was presented, based on backstepping and Lyapunov stability theories. It was shown that the introduction of manipulators in the handling of a passive object is a vast improvement over the simple on-off control, currently used in the control of orbital systems, both in terms of errors and in terms of fuel consumption.

The simplified model of the cooperative manipulation concept not only displayed adequate feasibility, but also is an important concept that can assist in the design and control of novel orbital robotic servicers required in future space projects and in the

exploitation of space. Thus, the cooperative manipulation concept was chosen to be further studied, through a more realistic three-dimensional model.

Based on the insight gained by the simplified one-dimensional model of the cooperative manipulation concept, a more realistic spatial model was then studied, for both contact cases. As in the simplified case, the generalized control forces acting on the passive object are realized by means of manipulators, based on the free-flying servicer bases. In this technique, the on-off servicer thruster forces, which are the only external forces of the system, are filtered by the manipulator-servicer system, allowing accurate passive object motion, while at the same time reducing fuel consumption, compared to pure on-off control.

First, initial work on the question of whether it is better to handle a passive object by a number of small robotic servicers or by a single one was studied. To this end, a number of characteristic trajectories were simulated, while for simplicity, single-manipulator servicers were assumed in both cases. As the first alternative, three small, identical servicers were assumed while as the second one, a single scaled-up servicer was assumed. The total fuel consumption was used as a performance index, while the tracking motion error was kept the same in the two cases. It was found that the system comprising a large servicer has higher fuel consumption than the system with three small servicers. Moreover, the three-servicer system has some further advantages, such as higher flexibility in gain tuning and servicer initial positioning, higher robustness in servicer failures, higher payload capabilities and more versatility in acceptable types of contact between the passive object and the servicer end-effectors.

The dynamics of three cooperating single-manipulator free-flying robotic servicers, handling a larger passive rigid object were further studied, for both the contact cases of firm grasp and point contact between the manipulator end-effectors and the passive object. Using a two-layer optimization process, a planning strategy for trajectory tracking of a passive object including optimal end-effector contact point selection and a novel adapted model-based controller, derived again by using the backstepping methodology, were developed. For both cases studied, the performance of the manipulation method was shown by simulations to exhibit desirable response characteristics, such as remarkable positioning accuracy and reduced thruster fuel consumption, when compared to the typical

pure on-off control, or even to a restricted PWM and a restricted PWPF control of the same passive object.

Finally, this concept was further extended by demonstrating the parametric error robustness this method displays in the passive object controlled motion, under the application of the continuous total generalized force by the servicer manipulators. Assuming adequately known parameters of the man-made servicers, this work focused on the passive object inertia parameters, needed for the chosen model-based PD control. A linearization methodology was used to provide a scheme with which the proposed controller robust behavior can be ascertained a priori, without the need to run experiments, by simple knowledge of the desired trajectory and a maximum expectancy in parameter estimation uncertainty. The system robust performance was also illustrated in a realistic 3D scenario and verified via simulations, in which, not only the tracking errors of the system converge to the expected error values, but also the response overcomes certain disturbances, imposed on the controller.

5.2 Future Work

This thesis presented the analysis of the system of the single-manipulator, free-flying robotic servicers handling a passive object in a trajectory tracking task, in zero gravity. Besides the presented results, there are still some issues open in this, rather new, field of robotics.

At the beginning of Chapter 3, we assumed that the servicer and passive object masses and inertias are much larger than those of the manipulators, while all relative accelerations and velocities, and thus the manipulator joint accelerations and velocities, are very small. For these reasons, manipulator inertia effects were neglected, which is a realistic assumption. Nevertheless, an even more realistic and accurate model would also take into account the manipulator inertias.

As discussed in Section 3.3.5, whenever the servicer controller of Eqs. (144) and (145) results in a need for more moment than the one the reaction wheels can provide, the on-off thruster pairs provide ample (also see Figure 3-7). This may be seen as a disturbance to the continuous controller. Nevertheless, since, for the motion of the servicers only boundedness within the manipulator limits is required, and since these relatively large on-off moments are doing exactly that, this is not an issue. Having said

that, it should be noted that care must be taken in order for the on-off moments not to be too large, thus resulting in sending the servicer base quickly towards the opposite limit of the corresponding reaction wheel and leading to a type of limit cycle. In the present work no analytical study of this aspect has been done and the on-off moment trigger values were chosen simply by trial and error in simulated experiments.

In Sections 2.3.2 (simplified uni-directional model) and 3.3.1 (realistic, spatial model), the feasible motion of the passive object, when there is no need to move the system center of mass, thus without the need for using servicer thrusters, was studied. Nevertheless, deeper analysis on this case can be undertaken, possibly resulting to the development of an appropriate controller for this special case.

In Section 3.2 an initial analysis on the comparison between one large servicer as opposed to three smaller servicers was presented. This analysis should be developed further. Moreover, since, for simplicity, we assumed single-manipulator servicers, an analytical comparison between single- and multiple-manipulator servicers must also be conducted.

Finally, the boundedness of the relative position/orientation between the servicer bases and the passive object, needs also to be examined analytically. This is a more demanding task, due to the on-off nature of the servicer thrusters.

Besides the remaining theoretical issues, there is also the issue of experimental results. Currently, at the Control Systems Lab (CSL) of the National Technical University of Athens (NTUA), a two dimensional emulator of systems in zero gravity, is being developed. This emulator consists of a flat granite table, on top of which robots move practically without friction, by means of air bearings. Since the weight of each robot is canceled out by the table normal force, the robots move without external forces, as they would in zero gravity, with the additional constraint of a two dimensional motion (on the table). As the NTUA-CSL 2D emulator is at the final stages of development, it would be very interesting to observe the response of the proposed control scheme on a real system, even a simplified two dimensional one. For this purpose, and also for comparison reasons, it would be interesting to obtain a simplified two dimensional model and to adapt to this model the proposed control scheme.

References

- [1] Abiko, S., Yoshida, K., “An Adaptive control of a Space Manipulator for Vibration Suppression,” *IEEE/RSJ International Conference on Intelligent Robots and Systems (IROS '05)*, Edmonton, Alberta, Canada, August 2 – 6, 2005.
- [2] Aghabalaie, P., Hosseinzadeh, M., Talebi, H. A., Shafiee, M., “Nonlinear robust control of a biped robot,” *IEEE International Symposium on Industrial Electronics (ISIE)*, Bari, Italy, July 4-7, 2010.
- [3] Aghili, F., “Coordination control of a free-flying manipulator and its base attitude to capture and detumble a noncooperative satellite,” *IEEE/RSJ International Conference on Intelligent Robots and Systems, (IROS '09)*, St. Louis, MO, USA, October 11 – 15, 2009.
- [4] Aghili, F., “Optimal control of a space manipulator for detumbling of a target satellite,” *IEEE International Conference on Robotics and Automation (ICRA '11)*, Kobe, Japan, May 12-17, 2009.
- [5] Aghili, F., Namvar, M., “Scaling Inertia Properties of a Manipulator Payload for 0-g Emulation of Spacecraft,” *International Journal of Robotic Research*, Vol. 28, No. 7, pp. 883-894, 2009.
- [6] Aghili, F., Parsa, K., “An adaptive vision system for guidance of a robotic manipulator to capture a tumbling satellite with unknown dynamics,” *IEEE/RSJ International Conference on Intelligent Robots and Systems, (IROS '08)*, Nice, France, September, 22 – 26, 2008.
- [7] Akin, D., L., Lane, J., C., Roberts, B., J. and Weisman, S., R., “Robotic Capabilities for Complex Space Operations,” *Proc. AIAA Space 2001 Conference and Exposition*, August 2001, Albuquerque, New Mexico.
- [8] An, C. H., Atkeson, C. G., Hollerbach, J. M., “Model-based control of a robot manipulator,” *MIT Press*, 1988.
- [9] Anthony, T. C., Wie, B., Carroll, S., “Pulse-Modulated Control Synthesis for a Flexible Spacecraft,” *Journal of Guidance, Control, and Dynamics*, Vol. 13, No.6, pp.1014-1021, 1990.
- [10] Arantes Jr., G., Martins-Filho, L. S., Santana, A. C., “Optimal On-Off Attitude Control for the Brazilian Multimission Platform Satellite,” *Mathematical Problems*

- in Engineering*, Volume 2009, Article ID 750945, 17 pages, doi:10.1155/2009/750945, Hindawi Publishing Corporation, 2009.
- [11] ASTRIUM, “1 N Mono-Propellant Thruster,” Datasheet, 2012.
(<http://cs.astrium.eads.net/sp/brochures/thrusters/1N%20Thruster.pdf>)
- [12] ASTRIUM, “10 N Bi-Propellant Thruster,” Datasheet, 2012.
(<http://cs.astrium.eads.net/sp/brochures/thrusters/10N%20Thruster.pdf>)
- [13] Becedas, J., Feliu, V., Sira-Ramirez, H., “Control of Flexible Manipulators affected by Non-Linear Friction Torque based on the Generalized Proportional Integral Concept,” *IEEE International Symposium on Industrial Electronics (ISIE)*, Vigo, Spain, June 4-7, 2007.
- [14] Bertleff, W., Landzettel, K., Albu-Schaffer, A., “Robotics Component Verification on ISS (ROCVISS) – Five Years in Space Final Experimental Results on Friction Parameter Identification,” *12th Symposium on Advanced Space Technologies in Robotics and Automation (ASTRA 2013)*, ESA/ESTEC, Noordwijk, the Netherlands, May 15 – 17, 2013.
- [15] Bicchi, A., “Force distribution in multiple whole-limb manipulation,” *Proc. IEEE International Conference on Robotics and Automation (ICRA '93)*, Atlanta, Georgia, USA, May 02-06, 1993.
- [16] Boge, T., Wimmer, T., Ma, O., Tzschichholz, T., “EPOS – Using Robotics for RvD Simulation of On-Orbit Servicing Missions,” *AIAA Guidance, Navigation, and Control Conference*, Toronto, Ontario Canada, August 2 – 5, 2010.
- [17] Brock, O., Khatib, O., “Real-Time Obstacle Avoidance and Motion Coordination in a Multi-Robot Workshell,” *Proc. IEEE International Symposium on Assembly and Task Planning (ISATP '99)*, Port, Portugal, July 21-24, 1999.
- [18] Bryson, A. E., “Control of Spacecraft and Aircraft,” *Princeton University Press*, 1994.
- [19] Burke, T., E., "Orbital Debris Removal" *Systems Engineering Case Study for USC/IASE*, 16, November 2009.
- [20] Caccavale, F., Chiacchio, P., Chiaverini, S., "Task-space regulation of cooperative manipulators", *Automatica*, 2000, 36, pp. 879-887.
- [21] Caswell D., Visentin G., Ortega G., de Kamp J., Nugteren P. R., Scholten H., “ConeXpress Orbital Life Extension Vehicle”, *ESA-Bulletin 127*, pp. 54-61, August 2006.

- [22] Chang, K-S., Holmberg, R., Khatib, O., “The Augmented Object Model: Cooperative Manipulation and Parallel Mechanism Dynamics,” *IEEE Int. Conf. on Robotics & Automation (ICRA '00)*, San Francisco, CA, USA, April 24-28, 2000.
- [23] Chen, Y.-C., Walker, I. D., Cheatham, J. B., “A new approach to force distribution and planning for multifingered grasps of solid objects,” *Proc. IEEE International Conference on Robotics and Automation (ICRA '91)*, Sacramento, CA, USA, April 09-11, 1991.
- [24] Cheng, F.-T., Orin, D. E., “Optimal force distribution in multiple-chain robotic systems,” *IEEE Transactions on Systems, Man and Cybernetics*, 1991, 21(1), pp 13-24.
- [25] Cornella, J., Suarez, R., Carloni, R., Melchiori, C., “Dual programming based approach for optimal grasping force distribution,” *Mechatronics*, 2008, 18(7), pp. 348-356.
- [26] Craig, J. J., “Introduction to Robotics: Mechanics and Control,” *3rd Edition*, Prentice-Hall, 2004.
- [27] Diftler, M. A., Mehling, J. S., Abdallah, M. E., Radford, N. A., Bridgwater, L. B., Sanders, A. M., Askew, R. S., Linn, D. M., Yamokoski, J. D., Permenter, F. A., Hargrave, B. K., Platt, R., Savely, R. T., Ambrose, R. O., “Robonaut 2 – The First Humanoid Robot in Space,” *IEEE International Conference on Robotics and Automation (ICRA '11)*, Shanghai, China, May 9-13, 2011.
- [28] Doyle, J. C., Zhou, K., “Essentials of Robust Control,” *Prentice Hall*, 1997.
- [29] Dubowsky, S., Boning, P., “The Coordinated Control of Space Robot Teams for the On-Orbit Construction of Large Flexible Space Structures,” *Int. Conf. on Robotics and Automation (ICRA '07) Special Workshop on Space Robotics*, Rome, Italy, April 10-14, 2007.
- [30] Dupuis, E., Doyon, M., Martin, E., L’Archeveque, R., Allard, P., Piedboeuf, J-C., Ma, O., “Autonomous Operations for Space Robots,” *55th International Astronautical Congress. Paper #IAC-04-IAA.U.5.03*, Vancouver, Canada, Oct. 4-8, 2004.
- [31] Esposito, J., Feemster, M. and Smith, E., “Cooperative Manipulation on the Water Using a Swarm of Autonomous Tugboats,” *IEEE International Conference on Robotics and Automation (ICRA '08)*, Pasadena, CA, USA, May 19-23, 2008.

- [32] Everist, J., Mogharei, K., Suri, H., Ranasinghe, N., Khostnevis, B., Will, P., and Shen, W., “A System for In-Space Assembly,” *2004 IEEE/RSJ Int. Conf. on Intelligent Robots and Systems (IROS '04)*, Sendai, Japan, September 28 - October 02, 2004.
- [33] Fernández, F., Parker, L., “Learning in large cooperative multi-robot domains,” *Int. J. of Robotics and Automation*, 2001, 16(4), 217–226.
- [34] Fink, J., Hsieh, M. A., Kumar, V., “Multi-Robot Manipulation via Caging in Environments with Obstacles,” *IEEE Int. Conf. on Robotics and Automation (ICRA '08)*, Pasadena, CA, USA, May 19-23, 2008.
- [35] Flores-Abad, A., Ma, O., Pham, K., and Ulrich, S., “A Review of Space Robotics Technologies for On-Orbit Servicing,” *Progress in Aerospace Sciences*, Vol. 68, 2014, pp. 1–26.
- [36] Fredrickson, S., E. et al, “Mini AERCam: development of a free-flying nanosatellite inspection robot”, *Proc. of SPIE Space Systems Technology and Operations, Advanced Spacecraft Sensors, Instruments, And On-Board Processing Techniques*, Vol. 5088, 2003.
- [37] Furukawa, T., Sugata, T., Yoshimura, S., Hoffman, M., “An automated system for simulation and parameter identification of inelastic constitutive models,” *Computer Methods in Applied Mechanics and Engineering*, 2002, 191(21-22), pp. 2235-2260.
- [38] Gautier, M., Khalil, W., Restrepo, P. P., “Identification of the dynamic parameters of a closed loop robot,” *Proc. IEEE International Conference on Robotics and Automation (ICRA '95)*, Nagoya, Aichi, Japan, April 09-11, 1995.
- [39] Gerkey, B. P., Mataric, M. J., “Pusher-watcher: An approach to fault-tolerant tightly-coupled robot coordination,” *Proc. IEEE International Conference on Robotics and Automation (ICRA '02)*, Washington, DC, USA, May 11-15, 2002.
- [40] Hayati, S. et al, “Remote surface inspection system,” *Robotics and Autonomous Systems*, Vol. 11, Issue 1, 1993.
- [41] Hiramatsu, T., Fitz-Coy, N., “Game Theoretic Approach to Post-Docked Satellite Control,” *20th Int. Symposium on Space Flight Dynamics*, Goddard Space Flight Center, USA, September 24, 2007.
- [42] <https://directory.eoportal.org/web/eoportal/satellite-missions/p/prisma-prototype#mission-status>
- [43] <http://gravitymovie.warnerbros.com/#/home>

- [44] <http://iss.jaxa.jp/en/kibo/about/kibo/rms/>
- [45] http://iss.jaxa.jp/iss/assemble/doc04_e.html
- [46] <http://news.bbc.co.uk/2/hi/science/nature/7075784.stm>
- [47] <http://science.ksc.nasa.gov/shuttle/missions/51-a/mission-51-a.html>
- [48] http://ssco.gsfc.nasa.gov/rrm_refueling_task.html
- [49] http://ssco.gsfc.nasa.gov/workshop_2012/Landzettel_DEOS_final_presentation_2012_workshop.pdf
- [50] <http://www.asc-csa.gc.ca/eng/canadarm/default.asp>
- [51] <http://www.asc-csa.gc.ca/eng/iss/canadarm2/default.asp>
- [52] <http://www.asc-csa.gc.ca/eng/iss/dextre/default.asp>
- [53] <http://www.bbc.co.uk/blogs/thereporters/jonathanamos/2010/09/the-ever-growing-flock-of-spac.shtml>
- [54] <http://www.darpa.mil/orbitalexpress/>
- [55] http://www.esa.int/Our_Activities/Human_Spaceflight/International_Space_Station/European_Robotic_Arm
- [56] <http://www.jwst.nasa.gov/>
- [57] <http://www.jwst.nasa.gov/orbit.html>
- [58] <http://www.mathworks.com/help/optim/ug/fmincon.html>
- [59] http://www.nasa.gov/mission_pages/hubble/servicing/index.html
- [60] <http://www.nasaspaceflight.com/2013/05/mev-rescue-hope-for-crippled-satellites/>
- [61] <http://www.parabolicarc.com/2011/03/15/intelsat-anchor-customer-mdas-orbital-refueling-plan/#more-21898>
- [62] <http://www.satellitemarkets.com/news-analysis/brazil-latin-americas-leading-satellite-market>
- [63] <http://www.sdimag.com/20110801234/expected-growth-in-asia-pacific-eo-satellite-market.html>
- [64] <http://www.space.com/6839-space-forecast-predicts-satellite-production-boom.html>
- [65] Kaiser, C., Rank, P., Krenn, R., “Simulation of the Docking Phase for the SMART-OLEV Satellite Servicing Mission,” *i-SAIRAS: Int. Symposium on Artificial Intelligence, Robotics and Automation in Space*, Hollywood, USA, February 26-29, 2008.

- [66] Kaisera, C., Sjöberg, F., Delcurac, J. M., Eilertsen, B., “SMART-OLEV—An orbital life extension vehicle for servicing commercial spacecrafts in GEO”, *Acta Astronautica*, Vol. 63, Issues 1–4, pp. 400–410, July–August 2008.
- [67] Kao, I., Lynch, K., Burdick, J., “Handbook of Robotics, Chapter 27: Contact Modeling and Manipulation,” *Springer*, 2008.
- [68] Kelm, B., Angielski, J., Butcher, S., Creamer, N., Harris, K., Henshaw, C., et al. “FRIEND: pushing the envelope of space robotics.” *NRL Rev—Space Res 2008*: 239–41.
- [69] Khalil, H. K., “Nonlinear Systems,” *Prentice Hall*, 2002.
- [70] Khatib, O., “Mobile manipulation: The robotic assistant,” *Robotics and Autonomous Systems*, 1999, 26(2-3), pp. 175-183.
- [71] Kienitz, K., “Attitude stabilization with actuators subject to switching restrictions: an approach via exact relay control methods,” *IEEE Tr. Aerospace and Electronic Systems*, 2006, 42(4), pp. 1485-1492.
- [72] Kimura, S., Okyuama, T., Yoshioka, N. and Wakabayashi, Y., “Robot-Aided Remote Inspection Experiment on STS-85,” *IEEE Trans. on Aerospace and Electronic Systems*, Vol. 36, No. 4, 2000.
- [73] Krstic, M., Kanellakopoulos, I., Kokotovic, P., “Nonlinear and Adaptive Control Design”. *Wiley-Interscience*, 1995.
- [74] Kumar, V., Waldron, K. J., “Suboptimal algorithms for force distribution in multifingered grippers,” *IEEE Transactions on Robotics and Automation*, 1989, 5(4), pp 491-498.
- [75] Landzettel, K., “System Prerequisites and Operational Modes for On Orbit Servicing,” *Int. Symposium Space Technology and Science (ISTS)*, Miyazaki, Japan, May 30–June 06 2004.
- [76] Leitner, J., “A Survey of Multi-Robot Cooperation in Space.” *International Conference on Automation, Robotics and Control Systems (ARCS)*, pp. 138-145, Orlando, Florida, USA, 13-16 July, 2009.
- [77] Li, Q., Payandeh, S., “Planning for dynamic multiagent planar manipulation with uncertainty: a game theoretic approach,” *Systems, Man and Cybernetics, Part A: Systems and Humans*, 2003, 33(5), pp. 620-626.
- [78] Matsumoto, S., Wakabayashi, Y., Ueno, H., Nishimaki, T., “System Analyses and Feasibility Studies for Hyper-OSV (Orbital Servicing Vehicle),” *i-SAIRAS: Int.*

- Symp. on Art. Intell., Robotics & Automation in Space*, CSA, St-Hubert, Que., Canada, June 18-22, 2001.
- [79] McMahan, T., Neal, V., “Repairing Solar Max: The Solar Maximum Repair Mission,” *NASA Technical Report, NASA-EP-205, NAS 1.19:205*, January 1, 1984.
- [80] Mehling, J., S., Diftler, M., A., Chu, M. and Valvo, M., “A Minimally Invasive Tendril Robot for In-Space Inspection,” *IEEE/RAS-EMBS International Conference on Biomedical Robotics and Biomechatronics (BioRob '06)*, February 2006, Pisa, Italy.
- [81] Miyata, N., Ota, J., Arai, T., Asama, H., “Cooperative transport by multiple mobile robots in unknown static environments associated with real-time task assignment,” *IEEE Transactions on Robotics and Automation*, 2002, 18(5), pp. 769-780.
- [82] Moosavian, S. A. A., Papadopoulos, E., “Cooperative Object Manipulation with Contact Impact Using Multiple Impedance Control,” *International Journal of Control, Automation, and Systems (IJCAS)*, 2010, Vol. 8, No. 2, pp. 314-327.
- [83] Moosavian, S. A. A., Papadopoulos, E., ”Explicit Dynamics of Space Free-Flyers with Multiple Manipulators via SPACEMAPLE,” *Advanced Robotics*, Robotics Society of Japan, Vol. 18, No. 2, pp. 223-244, 2004.
- [84] Moosavian, S. A. A., Rastegarij, R. and Papadopoulos, E., “Multiple Impedance Control for Space Free-Flying Robots,” *AIAA Journal of Guidance, Control and Dynamics*, 2005, Vol. 28, No. 5, pp. 939-947.
- [85] NASA, “History Of On-Orbit Satellite Fragmentations,” *13th Edition. Lyndon B. Johnson Space Center*, Houston, TX, May 2004.
- [86] NASA, On-Orbit Satellite Servicing Study Project Report | October 2010.
- [87] NASA, “Orbital Debris Quarterly News”, Volume 12, Issue 4, October 2008.
- [88] NASA, “Orbital Debris Quarterly News”, Volume 14, Issue 1, January 2010.
- [89] Oki, T., Nakanishi, H., Yoshida, K., “Time-Optimal Manipulator Control for Management of Angular Momentum Distribution during the Capture of a Tumbling Target,” *RSJ Advanced Robotics*, Vol. 24, No. 3, pp. 441 – 466, 2010.
- [90] Overview of the DART Mishap Investigation Results, retrieved at:
http://www.nasa.gov/pdf/148072main_DART_mishap_overview.pdf
- [91] Papadopoulos, E. and Dubowsky, S., “On the Nature of Control Algorithms for Free-floating Space Manipulators,” *IEEE Tr. on Robotics and Automation*, Vol. 7, No. 6, December 1991, pp. 750-758.

- [92] Papadopoulos, E., and Gonthier, Y., “A Framework for Large-Force Task Planning of Mobile Redundant Manipulators,” *Journal of Robotic Systems*, Vol. 16, No 3, 1999, pp. 151-162.
- [93] Preusche, C., Reintsema, D., Landzettel, K. and Hirzinger, G., “Robotics Component Verification on ISS, ROKVISS – Preliminary Results for Telepresence”, *Proceedings of the 2006 IEEE/RSJ International Conference on Intelligent Robots and Systems (IROS)*, October 9-15, Beijing, China, 2006.
- [94] Reintsema, D., Landzettel, K., Hirzinger, G., “DLR’s Advanced Telerobotic Concepts and Experiments for On-Orbit Servicing”, *Book Chapter in Advances in Telerobotics, Springer Tracts in Advanced Robotics*, Volume 31, 2007, pp 323-345.
<http://elib.dlr.de/52944/1/ReintsemaDLRSpaceBuch.pdf>
- [95] Reintsema, D., Sommer, B., Wolf, T., Thaeter, J., Radthke, A., Naumann, W., et al. "DEOS - the in-flight technology demonstration of Germans robotics approach to dispose malfunctioned satellites." *ESA workshop on Advanced Space Technologies for Robotics and Automation*, ESTEC, Noordwijk, The Netherlands, 2011.
- [96] Rekleitis, G. and Papadopoulos, E., “A Comparison of the Use of a Single Large vs a Number of Small Robots in On-Orbit Servicing,” *12th Symposium on Advanced Space Technologies in Robotics and Automation, (ASTRA '13)*, ESA, ESTEC, Noordwijk, The Netherlands, May 15-17, 2013.
- [97] Rekleitis, G. and Papadopoulos, E., “On Controller Parametric Sensitivity of Passive Object Handling in Space by Robotic Servicers,” *Proc. of the 2014 International Conference on Intelligent Robots and Systems (IROS '14)*, Chicago, Illinois, Sept. 14–18, 2014, USA.
- [98] Rekleitis, G., Papadopoulos, E., “On Dynamic Analysis and Control of a Novel Orbital Debris Disposer,” *Proc. 6th CISM-IFTOMM Symposium on Robot Design, Dynamics, and Control, (ROMANSY '06)*, Warsaw, Poland, June 20 – 24, 2006.
- [99] Rekleitis, G. Papadopoulos, E, “On-Orbit Cooperating Space Robotic Servicers Handling a Passive Object”, *IEEE Transactions on Aerospace and Electronic Systems*, Vol. 51, No. 2, pp. 802 - 814, April 2015.
- [100] Rekleitis, G., and Papadopoulos, E., “On On-Orbit Passive Object Handling by Cooperating Space Robotic Servicers,” *Proc. IEEE/RSJ International Conference on Intelligent Robots and Systems (IROS '11)*, San Francisco, California, USA, September 25-30, 2011.

- [101] Rekleitis, G., and Papadopoulos, E., "Towards Passive Object On-Orbit Manipulation by Cooperating Free-Flying Robots," *Proc. IEEE International Conference on Robotics and Automation (ICRA '10)*, Anchorage, Alaska, USA, May 03-08, 2010.
- [102] Rekleitis, I., Martin, E., Rouleau, G., L'Archevêque, R., Parsa, K., and Dupuis, E., "Autonomous Capture of a Tumbling Satellite", *J. of Field Robotics, Special Issue on Space Robotics*, 2007, 24(4), pp. 275-296.
- [103] Rus, D., Donald, B., Jennings, J., "Moving furniture with teams of autonomous robots," *IEEE/RSJ Int. Conf. on Intelligent Robots and Systems (IROS '95)*, Pittsburgh, USA, August 5-9, 1995.
- [104] Saenz-Otero, A., Miller, D., "SPHERES: a platform for formation-flight research," *Proceedings of the SPIE*, Vol. 5899, pp. 230-240, San Diego, CA, August 2005.
- [105] Shibli, M., Su, C.-Y., Aghili, F., "Adaptive Inverse Dynamics Control of a Free-Flying Space Robot in Contact with a Target Satellite: A Hubble Space Telescope Case," *Canadian Conference on Electrical and Computer Engineering (CCECE-CCGEI)*, Ottawa, Canada, May 7 – 10, 2006.
- [106] Singh, T., Heppler, G. R., "Shaped Input Control of a System with Multiple Modes," *Journal of Dynamics System, Measurement, and Control*, Vol. 115, pp. 341-344, 1993.
- [107] Slotine, J.J.E., and Li, W., "Applied Nonlinear Control," *Prentice-Hall*, 1991.
- [108] Sommer B. "Automation and robotics in the german space program- unmanned on-orbit servicing (OOS) & the TECSAS mission". *IAF 55th International Astronautical Congress*, Vancouver, Canada; 2004.
- [109] Song, G., Buck, N. V., Agrawal, B. N., "Spacecraft Vibration Reduction Using Pulse-Width Pulse- frequency Modulated Input Shaper," *Journal of Guidance, Control, and Dynamics*, 22 (3), pp. 433-440, 1999.
- [110] Sullivan, B., Hunter, R., Bruhn, J., Fowler, E., Hoag, L., Chappie, S., et al. "Phoenix project status 2013." *AIAA SPACE conference & exposition*, pp.1–17, San Diego, CA, 2013.
- [111] Summerer, L., Putz, B., Kopacek, P. and Kaya, N., "Robots Moving on a Loose Net in Microgravity – Results from the Japanese Furoshiki Sounding Rocket Experiment.

- [112] Tang, C. P., Bhatt, R. M., Abou-Samah, M., and Krovi, V., "Screw-Theoretic Analysis Framework for Payload Transport by Mobile Manipulator Collectives," *IEEE/ASME Transactions on Mechatronics*, 2006, 11(2), pp. 169-178.
- [113] Tatsch, A., Fitz-Coy, N., and Gladun, S., "On-orbit Servicing: A Brief Survey," *Performance Metrics for Intelligent Systems Conf.*, Gaithersburg, MD, August 15 - 19, 2006.
- [114] Toglia, C., Kennedy, F., Dubowsky, S., "Cooperative Control of Modular Space Robots," *Autonomous Robots*, Vol. 31, Issue 2-3, pp 209-221, October 2011.
- [115] Uyama, N., Lund, H., Asakimori, K., Ikeda, Y., Hirano, D., Nakanishi, H., Yoshida, K., "Integrated Experimental Environment for Orbital Robotic Systems, Using Ground-Based and Free-Floating Manipulators," *IEEE/SICE International Symposium on System Integration*, Sendai, Japan, December 21-22, 2010.
- [116] Uyama, N., Yoshida, K., Nakanishi, H., Oda, M., Sawada, H., Suzuki, S., "Contact Dynamics Modeling for Snare Wire Type of End Effector in Capture Operation," *28th International Symposium on Space Technology and Science*, Okinawa, Japan, June 5 – 12, 2011.
- [117] Yoshida K., "ETS-VII Flight Experiments For Space Robot Dynamics And Control", *Int. Symposium on Experimental Robotics*, Waikiki, Hawaii, USA, December 10 – 13, 2000.
- [118] Yoshida, K., Dimitrov, D., Nakanishi, H., "On the Capture of Tumbling Satellite by a Space Robot," *IEEE/RSJ International Conference on Intelligent Robots and Systems, (IROS '06)*, Beijing, China, October 9 – 15, 2006.
- [119] Yoshida, K., Nakanishi, H., "The TAKO (Target Collaborativize) Flyer: a New Concept for Future Satellite Servicing," *i-SAIRAS: Int. Symposium on Artificial Intelligence, Robotics and Automation in Space*, Canadian Space Agency, Quebec, Canada, June 18-22, 2001.
- [120] Yoshida, K., Nakanishi, H., Ueno, H., Inaba, N., Nishimaki, T., Oda, M., "Dynamics, Control, and Impedance Matching for Robotic Capture of a Non-cooperative Satellite," *RSJ Advanced Robotics*, Vol. 18, No. 2, pp. 175-198, 2004.

Appendix B

The simulated dynamics of the system of three free-flying servicers handling a passive object, as modeled in a Matlab Function, are shown in this Appendix.

```
function xDD=WithManips3D_02(u)

% Coordinates of the contact points on the base frame
a1 = u(1);
a2 = u(2);
a3 = u(3);
b1 = u(4);
b2 = u(5);
b3 = u(6);
c1 = u(7);
c2 = u(8);
c3 = u(9);

% Inertial characteristics of passive object
m0 = u(10);
I0x = u(11);
I0y = u(12);
I0z = u(13);

% Calculated applied manipulator forces
FE1x = u(14);
FE1y = u(15);
FE1z = u(16);
FE2x = u(17);
FE2y = u(18);
FE2z = u(19);
FE3x = u(20);
FE3y = u(21);
FE3z = u(22);

% Defining the FE forces acting on the passive object, in a way that it
% can be used for each of the i robots (for each of the three vectors
% i_th element stands for i_th robot
FEx = [FE1x; FE2x; FE3x];
FEy = [FE1y; FE2y; FE3y];
FEz = [FE1z; FE2z; FE3z];

% Calculated applied manipulator torques
nE1x = u(185);
nE1y = u(186);
nE1z = u(187);
nE2x = u(188);
nE2y = u(189);
nE2z = u(190);
nE3x = u(191);
nE3y = u(192);
nE3z = u(193);

% Defining the nE torques acting on the passive object, in a way that it
% can be used for each of the i robots (for each of the three vectors
% i_th element stands for i_th robot
nEx = [nE1x; nE2x; nE3x];
nEy = [nE1y; nE2y; nE3y];
nEz = [nE1z; nE2z; nE3z];

% Thruster forces of the i robots (i=3 in this case) in the inertial frame.
```

```

% Each matrix defined below has one of the j thruster forces per robot
% (j = 1...5 in this case).
% Each column of the matrix is the force
% (i columns for each one of the j matrices for the j_th force of the i_th robot)
fi1 = [u(23) u(26) u(29); u(24) u(27) u(30); u(25) u(28) u(31)];
fi2 = [u(32) u(35) u(38); u(33) u(36) u(39); u(34) u(37) u(40)];
fi3 = [u(41) u(44) u(47); u(42) u(45) u(48); u(43) u(46) u(49)];
fi4 = [u(50) u(53) u(56); u(51) u(54) u(57); u(52) u(55) u(58)];
fi5 = [u(59) u(62) u(65); u(60) u(63) u(66); u(61) u(64) u(67)];

% Torques Ni applied on the base of each of the i robots, by reaction
% wheels and purtorwue thrusters, in the inertial frame.
% The i_th column of the matrix represents the x-y-z vector n_i of the
% reaction wheel and pure-torque thruster torques, applied on the i_th
% robot.
Ni = [u(68) u(71) u(74); u(69) u(72) u(75); u(70) u(73) u(76)];

% Torques Ti applied on the base of each of the i robots, by its
% manipulator, in the inertial frame. The i_th column of the matrix
% represents the x-y-z torque vector T_i applied on the i_th robot.
% The first (x) element of each vector is an internal torque, which we
% cannot control. The other two (y and z) are controlled torques.
Ti = [u(77) u(80) u(83); u(78) u(81) u(84); u(79) u(82) u(85)];

% Distance vectors from aplied forces to CM of passive body
d1x = u(86);
d1y = u(87);
d1z = u(88);
d2x = u(89);
d2y = u(90);
d2z = u(91);
d3x = u(92);
d3y = u(93);
d3z = u(94);

% Distance vectors dij from j thruster of i robot to the i robot base CM
% Each column is the vector (i columns for the j_th distance
% of the i_th robot)
di1 = [u(95) u(98) u(101); u(96) u(99) u(102); u(97) u(100) u(103)];
di2 = [u(104) u(107) u(110); u(105) u(108) u(111); u(106) u(109) u(112)];
di3 = [u(113) u(116) u(119); u(114) u(117) u(120); u(115) u(118) u(121)];
di4 = [u(122) u(125) u(128); u(123) u(126) u(129); u(124) u(127) u(130)];
di5 = [u(131) u(134) u(137); u(132) u(135) u(138); u(133) u(136) u(139)];

% Distance vectors p_i from base of manipulator of i_th robot, to the
% i_th robot CM. The i_th column of the matrix represents the
% x-y-z distance vector p_i on the i_th robot
p_i = [u(140) u(143) u(146); u(141) u(144) u(147); u(142) u(145) u(148)];

% Inertial characteristics of bases of i robots
mi = [u(149); u(153); u(157)];
Iix = [u(150); u(154); u(158)];
Iiy = [u(151); u(155); u(159)];
Iiz = [u(152); u(156); u(160)];

% Euler angles and angle rates of all four bodies
th0 = u(161);
ph0 = u(162);
ps0 = u(163);
thi = [u(164); u(167); u(170)];
phi = [u(165); u(168); u(171)];
psi = [u(166); u(169); u(172)];

th0D = u(173);

```

```

ph0D = u(174);
ps0D = u(175);
thiD = [u(176); u(179); u(182)];
phiD = [u(177); u(180); u(183)];
psiD = [u(178); u(181); u(184)];

```

```

% Non-linear velocity and Coriolis velocity terms for the passive object
V = [(-1).*I0x.*ph0D.*ps0D.*cos(ph0).^2.*cos(ps0)+I0y.*((-1).*cos(th0) ...
.*sin(ps0)+cos(ps0).*sin(ph0).*sin(th0)).*(ps0D.*th0D.*cos(ph0).* ...
cos(th0)+(-1).*ph0D.*(th0D+ps0D.*sin(ph0)).*sin(th0))+(-1).*I0z.*( ...
ph0D.*cos(th0).* (th0D+ps0D.*sin(ph0))+ps0D.*th0D.*cos(ph0).*sin( ...
th0)).*(cos(ps0).*cos(th0).*sin(ph0)+sin(ps0).*sin(th0))+cos(ps0) ...
.*(ph0D.*cos(th0).^2.*((-1).*I0y.*ps0D+I0z.*ps0D.*cos(ph0).^2+ ...
I0y.*th0D.*sin(ph0))+ (I0y+(-1).*I0z).*cos(ph0).*cos(th0).* ( ...
ph0D.^2+(-1).*ps0D.^2+ps0D.*th0D.*sin(ph0)).*sin(th0)+ph0D.*(I0x.* ...
ps0D.*sin(ph0).^2+ps0D.*((-1).*I0z+I0y.*cos(ph0).^2).*sin(th0).^2+ ...
sin(ph0).*((-1).*I0x.*th0D+I0z.*th0D.*sin(th0).^2)))+(-1/2).* ( ...
th0D+(-1).*ps0D.*sin(ph0)).*sin(ps0).* (ps0D.*cos(ph0)).*(2.*I0x+( ...
-1).*I0y+(-1).*I0z+(I0y+(-1).*I0z).*cos(2.*th0))+((-1).*I0y+I0z).* ...
ph0D.*sin(2.*th0)), (-1).*ps0D.*th0D.*cos(ph0).^3.*cos(ps0).* (I0z.* ...
cos(th0).^2+I0y.*sin(th0).^2)+ph0D.*cos(ph0).^2.*((-1).*I0y+I0z) ...
.*th0D.*cos(ps0).*cos(th0).*sin(th0)+ps0D.*sin(ps0).*((-1).*I0x+ ...
I0z).*cos(th0).^2+I0y.*sin(th0).^2))+cos(ph0).* (I0y+(-1).*I0z).* ...
cos(th0).* (ph0D.^2+(-1).*ps0D.^2+2.*ps0D.*th0D.*sin(ph0)).*sin( ...
ps0).*sin(th0)+ps0D.*cos(ps0).* (I0x.*th0D+(-1).*I0x.*ps0D.*sin( ...
ph0)+cos(th0).^2.*(I0y.*th0D+I0z.*ps0D.*sin(ph0)+(-1).*I0z.*th0D.* ...
sin(ph0).^2)+I0z.*th0D.*sin(th0).^2+I0y.*ps0D.*sin(ph0).*sin(th0) ...
.^2+(-1).*I0y.*th0D.*sin(ph0).^2.*sin(th0).^2))+(-1).*ph0D.*(cos( ...
th0).^2.*(I0y.*ps0D+(-1).* (I0y+(-1).*I0z).*th0D.*sin(ph0)+I0z.* ...
ps0D.*sin(ph0).^2).*sin(ps0)+sin(ps0).* (I0z.*ps0D.*sin(th0).^2+ ...
th0D.*sin(ph0).* (I0x+(I0y+(-1).*I0z).*sin(th0).^2)+sin(ph0).^2.* ( ...
-1).*I0x.*ps0D+I0y.*ps0D.*sin(th0).^2))+(-1/4).* (I0y+(-1).*I0z).* ...
th0D.*((-3)+cos(2.*ph0)).*cos(ps0).*sin(2.*th0)), ((-1).*I0y+I0z).* ...
ph0D.^2.*cos(th0).*sin(ph0).*sin(th0)+(-1).*ph0D.*cos(ph0).* (cos( ...
th0).^2.*((-1).*I0y+I0z).*th0D+2.*I0z.*ps0D.*sin(ph0))+(-2).* ...
ps0D.*sin(ph0).* (I0x+(-1).*I0y.*sin(th0).^2)+th0D.*(I0x+(I0y+(-1) ...
.*I0z).*sin(th0).^2))+ (I0y+(-1).*I0z).*ps0D.*th0D.*cos(ph0).^2.* ...
sin(2.*th0)];

```

```

% Non-linear velocity and Coriolis velocity terms for the robot bases

```

```

% Predefining the size of Vix,y,z to increase calculation speed

```

```

Vix = [0; 0; 0];
Viy = [0; 0; 0];
Viz = [0; 0; 0];

```

```

for i=1:1:3

```

```

Vix(i) = (-1).*Iix(i).*phiD(i).*psiD(i).*cos(phi(i)).^2.*cos(psi(i))+Iiy(i).*((-1).*cos(thi(i)) ...

```

```

.*sin(psi(i))+cos(psi(i)).*sin(phi(i)).*sin(thi(i))).*(psiD(i).*thiD(i).*cos(phi(i)).* ...
cos(thi(i))+(-1).*phiD(i).* (thiD(i)+psiD(i).*sin(phi(i))).*sin(thi(i)))+(-1).*Iiz(i)).*( ...

```

```

phiD(i).*cos(thi(i)).*(thiD(i)+psiD(i).*sin(phi(i)))+psiD(i).*thiD(i).*cos(phi(i)).*sin( ...

```

```

thi(i)).*(cos(psi(i)).*cos(thi(i)).*sin(phi(i))+sin(psi(i)).*sin(thi(i)))+cos(psi(i)) ...

```

```

.*(phiD(i).*cos(thi(i)).^2.*((-1).*Iiy(i).*psiD(i)+Iiz(i).*psiD(i).*cos(phi(i)).^2+ ...
Iiy(i).*thiD(i).*sin(phi(i)))+(Iiy(i)+(-1).*Iiz(i)).*cos(phi(i)).*cos(thi(i)).*( ...

```

```

    phiD(i).^2+(-
1).*psiD(i).^2+psiD(i).*thiD(i).*sin(phi(i)).*sin(thi(i))+phiD(i).(Iix(i).* ...
psiD(i).*sin(phi(i)).^2+psiD(i).*(-
1).*Iiz(i)+Iiy(i).*cos(phi(i)).^2).*sin(thi(i)).^2+ ...
sin(phi(i)).*((-1).*Iix(i).*thiD(i)+Iiz(i).*thiD(i).*sin(thi(i)).^2)))+(-
1/2).*(...
thiD(i)+(-
1).*psiD(i).*sin(phi(i)).*sin(psi(i)).*(psiD(i).*cos(phi(i)).*(2.*Iix(i)+( ...
-1).*Iiy(i)+(-1).*Iiz(i)+(Iiy(i)+(-1).*Iiz(i)).*cos(2.*thi(i)))+( (-
1).*Iiy(i)+Iiz(i)).* ...
phiD(i).*sin(2.*thi(i)));
Viy(i) = (-1).*psiD(i).*thiD(i).*cos(phi(i)).^3.*cos(psi(i)).*(Iiz(i).* ...
cos(thi(i)).^2+Iiy(i).*sin(thi(i)).^2)+phiD(i).*cos(phi(i)).^2.*((-
1).*Iiy(i)+Iiz(i)) ...
.*thiD(i).*cos(psi(i)).*cos(thi(i)).*sin(thi(i))+psiD(i).*sin(psi(i)).*(-
1).*Iix(i)+ ...
Iiz(i).*cos(thi(i)).^2+Iiy(i).*sin(thi(i)).^2))+cos(phi(i)).*((Iiy(i)+(-
1).*Iiz(i)).* ...
cos(thi(i)).*(phiD(i).^2+(-
1).*psiD(i).^2+2.*psiD(i).*thiD(i).*sin(phi(i))).*sin( ...
psi(i)).*sin(thi(i))+psiD(i).*cos(psi(i)).*(Iix(i).*thiD(i)+(-
1).*Iix(i).*psiD(i).*sin( ...
phi(i))+cos(thi(i)).^2.*(Iiy(i).*thiD(i)+Iiz(i).*psiD(i).*sin(phi(i))+(-
1).*Iiz(i).*thiD(i).* ...

sin(phi(i)).^2)+Iiz(i).*thiD(i).*sin(thi(i)).^2+Iiy(i).*psiD(i).*sin(phi(i)).*sin
(thi(i)) ...
.^2+(-1).*Iiy(i).*thiD(i).*sin(phi(i)).^2.*sin(thi(i)).^2))+(-
1).*phiD(i).*cos( ...
thi(i)).^2.*(Iiy(i).*psiD(i)+(-1).(Iiy(i)+(-
1).*Iiz(i)).*thiD(i).*sin(phi(i))+Iiz(i).* ...

psiD(i).*sin(phi(i)).^2).*sin(psi(i))+sin(psi(i)).*(Iiz(i).*psiD(i).*sin(thi(i)).
^2+ ...
thiD(i).*sin(phi(i)).*(Iix(i)+(Iiy(i)+(-
1).*Iiz(i)).*sin(thi(i)).^2)+sin(phi(i)).^2.*(( ...
-1).*Iix(i).*psiD(i)+Iiy(i).*psiD(i).*sin(thi(i)).^2))+(-1/4).(Iiy(i)+(-
1).*Iiz(i)).* ...
thiD(i).*((-3)+cos(2.*phi(i))).*cos(psi(i)).*sin(2.*thi(i)));
Viz(i) = ((-1).*Iiy(i)+Iiz(i)).* ...
phiD(i).^2.*cos(thi(i)).*sin(phi(i)).*sin(thi(i))+(-
1).*phiD(i).*cos(phi(i)).*cos( ...
thi(i)).^2.*((-1).*Iiy(i)+Iiz(i)).*thiD(i)+2.*Iiz(i).*psiD(i).*sin(phi(i)))+( -
2).* ...
psiD(i).*sin(phi(i)).*(Iix(i)+(-
1).*Iiy(i).*sin(thi(i)).^2)+thiD(i).(Iix(i)+(Iiy(i)+(-1) ...
.*Iiz(i)).*sin(thi(i)).^2)+(Iiy(i)+(-
1).*Iiz(i)).*psiD(i).*thiD(i).*cos(phi(i)).^2.* ...
sin(2.*thi(i));

end

% Inertia matrix of passive object
M = [m0 0 0 0 0 0; 0 m0 0 0 0 0; 0 0 m0 0 0 0; ...
0 0 0 I0x*cos(ph0)*cos(ps0) -I0y*((cos(th0))^2)*sin(ps0)+(I0y-
I0z)*cos(ps0)*...
cos(th0)*sin(ph0)*sin(th0)-I0z*sin(ps0)*(sin(th0))^2 cos(ph0)*((-I0y+I0z)*...
cos(th0)*sin(ps0)*sin(th0)+cos(ps0)*sin(ph0)*(-
I0x+I0z*((cos(th0))^2)+I0y*sin(th0)^2)); ...
0 0 0 I0x*cos(ph0)*sin(ps0) (I0y-I0z)*cos(th0)*sin(ph0)*sin(ps0)*sin(th0)+...
cos(ps0)*(I0y*((cos(th0))^2)+I0z*sin(th0)^2) cos(ph0)*((I0y-
I0z)*cos(ps0)*cos(th0)*sin(th0)+...
sin(ph0)*sin(ps0)*(-I0x+I0z*((cos(th0))^2)+I0y*sin(th0)^2)); ...
0 0 0 -I0z*sin(ph0) (I0y-I0z)*cos(ph0)*cos(th0)*sin(th0)
I0x*((sin(ph0))^2)+...
((cos(ph0))^2)*(I0z*((cos(th0))^2)+I0y*sin(th0)^2)];

```

```

% Determinant of the passive object inertia matrix
DM0 = det(M);

% Forces/Torques applied on the passive object
FE = [FE1x+FE2x+FE3x; FE1y+FE2y+FE3y; FE1z+FE2z+FE3z; ...
      dlz*FE1y-dly*FE1z+d2z*FE2y-d2y*FE2z+d3z*FE3y-d3y*FE3z+nE1x+nE2x+nE3x-V(1);
      ...
      dlx*FE1z-dlx*FE1x+d2x*FE2z-d2x*FE2x+d3x*FE3z-d3x*FE3x+nE1y+nE2y+nE3y-V(2);
      ...
      dly*FE1x-dly*FE1y+d2y*FE2x-d2y*FE2y+d3y*FE3x-d3y*FE3y+nE1z+nE2z+nE3z-V(3)];

% Accelerations of passive object
xDD0 = M\FE;

% Predefining the size of xDDi to increase calculation speed
xDDi = [0; 0; 0; 0; 0; 0; 0; 0; 0; 0; 0; 0; 0; 0; 0; 0; 0; 0];

% Motion of the i robots
for i = 1:1:3
    % Inertia matrices of the bases of the robots
    Mtot = [mi(i) 0 0 0 0 0; 0 mi(i) 0 0 0 0; 0 0 mi(i) 0 0 0; ...
            0 0 0 Iix(i)*cos(phi(i))*cos(psi(i))
            Iiy(i)*(cos(thi(i)))^2*sin(psi(i))+(Iiy(i)-Iiz(i))*cos(psi(i))*...
            cos(thi(i))*sin(phi(i))*sin(thi(i))-Iiz(i)*sin(psi(i))*(sin(thi(i)))^2
            cos(phi(i))*((-Iiy(i)+Iiz(i))*...
            cos(thi(i))*sin(psi(i))*sin(thi(i))+cos(psi(i))*sin(phi(i))*...
            (-Iix(i)+Iiz(i))*((cos(thi(i)))^2+Iiy(i)*sin(thi(i))^2)); ...
            0 0 0 Iix(i)*cos(phi(i))*sin(psi(i)) (Iiy(i)-
            Iiz(i))*cos(thi(i))*sin(phi(i))*sin(psi(i))*sin(thi(i))+...
            cos(psi(i))*(Iiy(i)*(cos(thi(i)))^2+Iiz(i)*sin(thi(i))^2) cos(phi(i))*...
            ((Iiy(i)-Iiz(i))*cos(psi(i))*cos(thi(i))*sin(thi(i))+...
            sin(phi(i))*sin(psi(i))*(-
            Iix(i)+Iiz(i))*((cos(thi(i)))^2+Iiy(i)*sin(thi(i))^2)); ...
            0 0 0 -Iiz(i)*sin(phi(i)) (Iiy(i)-Iiz(i))*cos(phi(i))*cos(thi(i))*sin(thi(i))
            Iix(i)*((sin(phi(i)))^2)+...
            ((cos(phi(i)))^2)*(Iiz(i))*((cos(thi(i)))^2+Iiy(i)*sin(thi(i))^2)];

    % Forces/Torques applied on the base of the i_th robotic servicer
    Fil = [fi1(1,i)+fi2(1,i)+fi3(1,i)+fi4(1,i)+fi5(1,i)-FEx(i); ...
           fi1(2,i)+fi2(2,i)+fi3(2,i)+fi4(2,i)+fi5(2,i)-FEy(i); ...
           fi1(3,i)+fi2(3,i)+fi3(3,i)+fi4(3,i)+fi5(3,i)-FEz(i)];
    Nx = Ni(1,i)-Ti(1,i)+di1(3,i)*fi1(2,i)-di1(2,i)*fi1(3,i) ...
         +di2(3,i)*fi2(2,i)-di2(2,i)*fi2(3,i)+di3(3,i)*fi3(2,i)-
         di3(2,i)*fi3(3,i) ...
         +di4(3,i)*fi4(2,i)-di4(2,i)*fi4(3,i)+di5(3,i)*fi5(2,i)-
         di5(2,i)*fi5(3,i) ...
         -p_i(3,i)*FEy(i)+p_i(2,i)*FEz(i)-Vix(i);
    Ny = Ni(2,i)-Ti(2,i)+di1(1,i)*fi1(3,i)-di1(3,i)*fi1(1,i) ...
         +di2(1,i)*fi2(3,i)-di2(3,i)*fi2(1,i)+di3(1,i)*fi3(3,i)-
         di3(3,i)*fi3(1,i) ...
         +di4(1,i)*fi4(3,i)-di4(3,i)*fi4(1,i)+di5(1,i)*fi5(3,i)-
         di5(3,i)*fi5(1,i) ...
         -p_i(1,i)*FEz(i)+p_i(3,i)*FEx(i)-Viy(i);
    Nz = Ni(3,i)-Ti(3,i)+di1(2,i)*fi1(1,i)-di1(1,i)*fi1(2,i) ...
         +di2(2,i)*fi2(1,i)-di2(1,i)*fi2(2,i)+di3(2,i)*fi3(1,i)-
         di3(1,i)*fi3(2,i) ...
         +di4(2,i)*fi4(1,i)-di4(1,i)*fi4(2,i)+di5(2,i)*fi5(1,i)-
         di5(1,i)*fi5(2,i) ...
         -p_i(2,i)*FEx(i)+p_i(1,i)*FEy(i)-Viz(i);

    F = [Fil; Nx; Ny; Nz];

    % Acceleration of position variables and Euler angles of the base of

```

```

% the i_th robotic servicer
xDD = Mtot\F;
xDDi(6*i-5) = xDD(1);
xDDi(6*i-4) = xDD(2);
xDDi(6*i-3) = xDD(3);
xDDi(6*i-2) = xDD(4);
xDDi(6*i-1) = xDD(5);
xDDi(6*i) = xDD(6);

% Determinant of the i_th robotic servicer base inertia matrix
DMi(i) = det(Mtot);

end

xDD = [xDD0; xDDi; DM0; DMi(1); DMi(2); DMi(3)];

```

Appendix C

The boundedness of the relative motion between the passive object and the servicer bases, for the one-dimensional case, is studied in this Appendix. Assume the simplified 1-D model of a passive object handled by two robotic servicers equipped with manipulators, as seen in Figure 2-11. Furthermore, assume the controller of Eqs. (69) and (72) is applied and that the maximum force each manipulator can exert on the passive object is f_{max} , as also see in Figure C 1, in which only one of the two servicers is shown. The following analysis is made for the relative motion between the passive object and servicer m_1 , but the same is also true for the relative motion between the passive object and servicer m_2 .

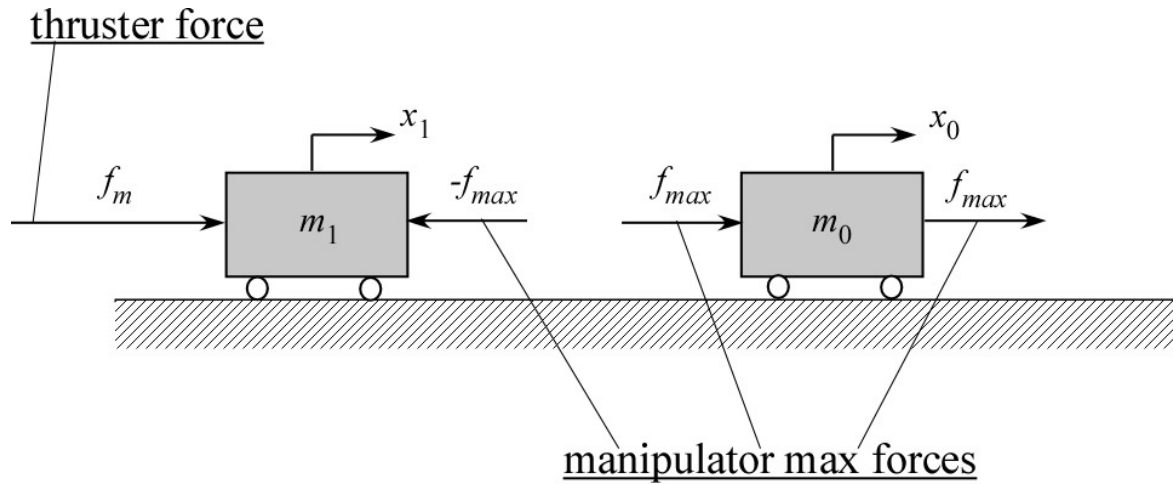


Figure C 1. Passive object with one servicer and maximum manipulator forces.

First the bound on the maximum distance between m_0 and m_1 , when the system is moving under the controller of Eqs. (69) and (72), is studied. Note that, for the maximum distance between the passive object and the servicer base, the worst case happens when the manipulator constantly applies the maximum force f_{max} , pushing the servicer base further away from the passive object. Any other manipulator force u_{10} , lower than f_{max} , results in a lower maximum relative distance, as also seen in Figure C 2. Recall also Eq. (31) from Chapter 2,

$$\begin{aligned}
 e_0 &= x_0 - x_{0_des} \\
 e_1 &= x_0 - x_1 - x_m / 2 \\
 e_2 &= x_0 - x_2 + x_m / 2
 \end{aligned} \tag{210}$$

Assume that the servicer base is initially moving under the manipulator force, without the need for thruster force ($m_1 K_1 (\dot{e}_1 + K_1 e_1) < f_i^*$). Furthermore, assume that the

relative distance under the manipulator force is rising ($\dot{e}_1 > 0$). Then, the relative motion will result in the triggering of the thruster at a relative distance and relative velocity of e_{1_in} and \dot{e}_{1_in} respectively (point A in Figure C 2). For simplicity, assume that this happens at $t = 0$.

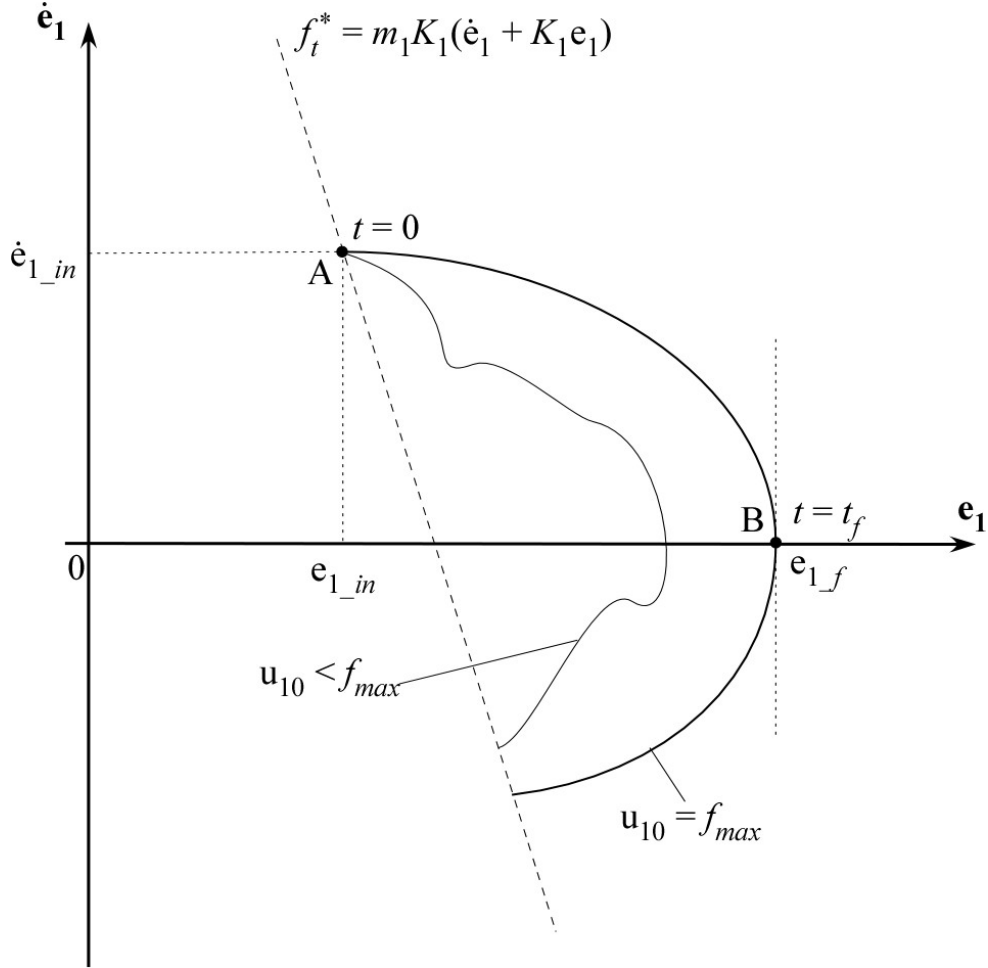


Figure C 2. Relative motion between the passive object (m_0) and one servicer base (m_1).

Since

$$\dot{e}_{1_in} > 0 \quad (211)$$

the relative position error e_1 will keep on rising and the relative motion will pass on the right-hand side of the line $f_t^* = m_1 K_1 (\dot{e}_1 + K_1 e_1)$ of Figure C 2, while at the same time the corresponding servicer thruster is turned on. As already mentioned, the worst case is when the manipulator is pushing the servicer away from the passive object by applying its maximum force f_{max} . Under these forces, the equations of motion for the servicer base m_1 and the passive object m_0 , are:

$$\begin{aligned} m_0 \ddot{x}_0 &= 2f_{\max} \\ m_1 \ddot{x}_1 &= f_m - f_{\max} \end{aligned} \quad (212)$$

or

$$\begin{aligned} \ddot{x}_0 &= \frac{2f_{\max}}{m_0} \\ \ddot{x}_1 &= \frac{f_m - f_{\max}}{m_1} \end{aligned} \quad (213)$$

From Eq. (213) a constraint on the applied thruster force with respect to the manipulator maximum force is obtained. In order for the thruster to be able to counter the manipulator force that keeps on pushing the servicer away from the passive object, the following is required:

$$f_m > f_{\max} \quad (214)$$

Integrating Eq. (213) results in Eqs. (215) and (216):

$$\dot{x}_0 = \dot{x}_{0_in} + \frac{2f_{\max}}{m_0} t \quad (215)$$

$$\dot{x}_1 = \dot{x}_{1_in} + \frac{f_m - f_{\max}}{m_1} t \quad (216)$$

While integrating Eqs. (215) and (216), results respectively in:

$$x_0 = x_{0_in} + \dot{x}_{0_in} t + \frac{f_{\max}}{m_0} t^2 \quad (217)$$

$$x_1 = x_{1_in} + \dot{x}_{1_in} t + \frac{1}{2} \frac{f_m - f_{\max}}{m_1} t^2 \quad (218)$$

where x_{i_in} and \dot{x}_{i_in} with $i = 0,1$, are defined as:

$$\begin{aligned} \dot{e}_{1_in} &= \dot{x}_{0_in} - \dot{x}_{1_in} \\ e_{1_in} &= x_{0_in} - x_{1_in} - x_m / 2 \end{aligned} \quad (219)$$

Subtracting Eq. (216) from Eq. (215), results in,

$$\dot{e}_1 = \dot{e}_{1_in} + \frac{(2m_1 + m_0)f_{\max} - m_0 f_m}{m_0 m_1} t \quad (220)$$

While subtracting Eq. (218) from (217), results in,

$$e_1 = e_{1_in} + \dot{e}_{1_in} t + \frac{(2m_1 + m_0) f_{\max} - m_0 f_m}{2m_0 m_1} t^2 \quad (221)$$

Note that Eqs. (220) and (221) result in a parabolic line at the \dot{e}_1 - e_1 plot, as seen at the right-hand side of the line $f_i^* = m_1 K_1 (\dot{e}_1 + K_1 e_1)$ in Figure C 2, for $u_{10} = f_{\max}$. When the relative velocity \dot{e}_1 becomes zero (point B in Figure C 2), then Eq. (220) results in,

$$0 = \dot{e}_{1_in} + \frac{(2m_1 + m_0) f_{\max} - m_0 f_m}{m_0 m_1} t_f \quad (222)$$

Thus, the time t_f required to reach the maximum relative distance is obtained from Eq. (222):

$$t_f = -\frac{\dot{e}_{1_in} m_0 m_1}{(2m_1 + m_0) f_{\max} - m_0 f_m} \quad (223)$$

Since it must be $t_f > 0$, the following constraint must apply:

$$(2m_1 + m_0) f_{\max} < m_0 f_m \quad (224)$$

Note that the constraint of Eq. (224) is stricter than the constraint of Eq. (214). Thus, it is enough to take into account only Eq. (224) as a constraint. Note also that, subtracting the two parts of Eq. (213), results in,

$$\ddot{e}_1 = \frac{(2m_1 + m_0) f_{\max} - m_0 f_m}{m_0 m_1} \quad (225)$$

The need for a decelerated relative motion, thus negative acceleration of Eq. (225), results in the same constraint as in Eq. (224).

The maximum relative distance is obtained from Eq. (221), by substituting the time t_f of Eq. (223).

$$e_{1_f} = e_{1_in} - \frac{m_0 m_1 \dot{e}_{1_in}^2}{2((2m_1 + m_0) f_{\max} - m_0 f_m)} \quad (226)$$

As can be seen from Eq. (226), the maximum relative distance between the passive object and the servicer base is also a function of the relative distance e_{1_in} and relative velocity \dot{e}_{1_in} , at the moment when the thruster is triggered on. The maximum e_{1_in} and \dot{e}_{1_in} , can be obtained by also taking into account the worst case scenario. By assuming that the passive object and the servicer base are initially almost touching and that at this

moment the manipulator applies a constant f_{max} repulsive force until the line $f_t^* = m_1 K_1(\dot{e}_1 + K_1 e_1)$ in Figure C 2 is reached, while at the same time the other servicer is pulling the passive object with a constant f_{max} force, then the maximum e_{1_in} and \dot{e}_{1_in} , can be obtained, by using the same methodology as above. Thus it can be shown that the maximum e_{1_in} and \dot{e}_{1_in} are also bounded, thus bounding the maximum relative distance e_{1_f} and that these bounds are known. As already mentioned, the same approach can be used in order to display the boundedness of the relative motion between the passive object and the other servicer base (m_2).

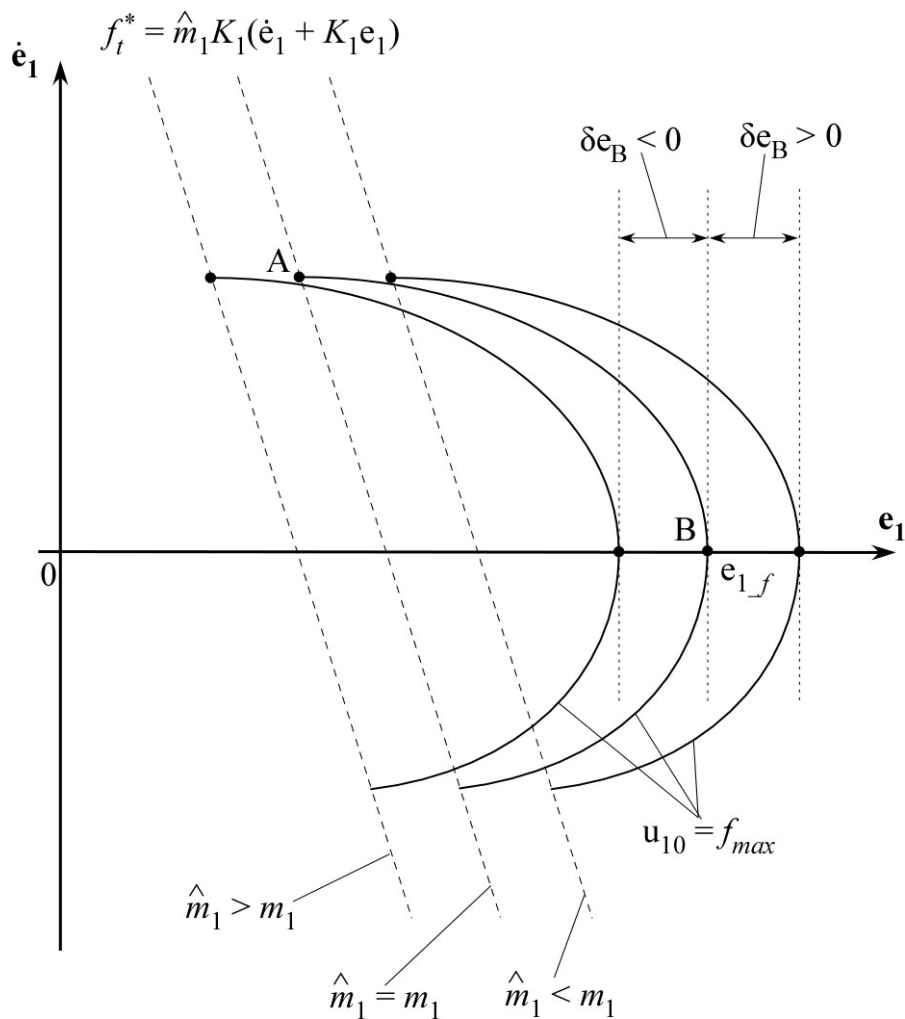


Figure C 3. Parametric uncertainty effect on the thruster trigger f_t^* .

The abovementioned method can also be used to show the robustness of the motion, when the servicer is moving away from the passive object. Since the applied forces in the worst case are the maximum manipulator force f_{max} and the thruster force f_m , which are independent of the estimated masses, the only parametric uncertainty issue is on the estimated servicer base mass \hat{m}_1 and how this uncertainty is affecting thruster triggering.

Overestimating the mass m_1 ($\hat{m}_1 > m_1$) leads to the quantity $\hat{m}_1 K_1(\dot{e}_1 + K_1 e_1)$ reaching the trigger value f_t at lower values of \dot{e}_1 and e_1 than in the case of no uncertainty. This is also displayed at Figure C 3, where the line $f_t^* = \hat{m}_1 K_1(\dot{e}_1 + K_1 e_1)$ has been moved to the left of the no-uncertainty line. This leads to a lower maximum relative displacement than the already obtained no-uncertainty case (see Eq. (226)). Nevertheless, underestimating the mass m_1 ($\hat{m}_1 < m_1$) leads to the quantity $\hat{m}_1 K_1(\dot{e}_1 + K_1 e_1)$ reaching the trigger value f_t at higher values of \dot{e}_1 and e_1 than in the case of no uncertainty. This is also displayed at Figure C 3, where the line $f_t^* = \hat{m}_1 K_1(\dot{e}_1 + K_1 e_1)$ has been moved to the right of the no-uncertainty line. This leads to a higher maximum relative displacement than the already obtained no-uncertainty case (see Eq. (226)). The new maximum relative displacement is

$$\hat{e}_{1_f} = e_{1_f} + \delta e_B = e_{1_f} + \frac{f_t (m_1 - \hat{m}_1)}{m_1 \hat{m}_1 K_1^2} \quad (227)$$

The quantity δe_B is obtained by noticing that it is equal to how much the line $f_t^* = \hat{m}_1 K_1(\dot{e}_1 + K_1 e_1)$ has been moved to the right. This, in turn, can be obtained by setting $\dot{e}_1 = 0$ in $f_t^* = \hat{m}_1 K_1(\dot{e}_1 + K_1 e_1)$, thus finding the value of e_1 when the line $f_t^* = \hat{m}_1 K_1(\dot{e}_1 + K_1 e_1)$ intersects with the e_1 -axis, both for the case with and without uncertainty. Subtracting these two values provides δe_B as seen in Eq. (227). As can be seen from Eq. (227), the maximum relative displacement is a function of f_t , K_1^2 , the real and the estimated mass m_1 . Thus, the introduction of the parametric uncertainty may result in higher maximum relative displacement, but the motion is still bounded.

The study of the relative motion between the servicer base and the passive object, when the servicer is moving towards the passive object, is more difficult. In this case, there is no need for thruster firing and the worst scenario is when the manipulator forces are:

$$\begin{aligned} u_{10} &= \frac{1}{2} (PD_0 + m_0 \ddot{x}_{0_des}) - PD_1 \\ u_{20} &= \frac{1}{2} (PD_0 + m_0 \ddot{x}_{0_des}) + PD_1 \end{aligned} \quad (228)$$

$$\begin{aligned} \text{where: } PD_0 &= m_0 K_0 (\dot{e}_0 + K_0 e_0) \\ PD_1 &= m_1 K_1 (\dot{e}_1 + K_1 e_1) \\ PD_2 &= m_2 K_2 (\dot{e}_2 + K_2 e_2) \end{aligned}$$

Note that these are the manipulator forces acting on the passive object and that, in accordance with Eq. (72), PD_1 is negative. Note also that, if the servicer of mass m_2 was close to the passive object too and there was also a need for extra pushing force PD_2 , this force quantity would have been positive and a negative quantity $-PD_2$ would have been added to the manipulator force acting on servicer of mass m_1 , according to Eq. (72). This would have made the case easier, since the manipulator repulsive force would have been augmented, while at the same time the total force acting on the passive object would have remained the same. Thus, the worst case scenario for the relative motion between the servicer of mass m_1 and the passive object, when the two objects are closing in, is the one presented in Eq. (228). Under these manipulator forces and without firing need from the thrusters of the servicer of mass m_1 , the equations of motion of the passive object and the servicer m_1 are,

$$\ddot{x}_0 = \frac{(PD_0 + m_0 \ddot{x}_{0_des})}{m_0} \quad (229)$$

$$\ddot{x}_1 = \frac{-\frac{1}{2}(PD_0 + m_0 \ddot{x}_{0_des}) + PD_1}{m_1} \quad (230)$$

Subtracting Eq. (230) from Eq. (229), results in,

$$\ddot{e}_1 + K_1 \dot{e}_1 + K_1^2 e_1 = \underbrace{\left(K_0 (\dot{e}_0 + K_0 e_0) + \ddot{x}_{0_des} \right)}_{=\ddot{x}_0} \left(1 + \frac{m_0}{2m_1} \right) \quad (231)$$

The only thing that can be said for this relative motion tracking error is that it converges to zero when the actual acceleration \ddot{x}_0 of the passive object is zero. Since there is no need for error e_1 to converge to zero (boundedness is all that is needed), the fact that this convergence is not guaranteed for the general case of non-zero passive object acceleration \ddot{x}_0 is not a problem. This is also shown in Section 2.3.4, in which the results of the simulations with the system under the controller of Eqs. (69) and (72) are presented.

Appendix D

Pulse-width modulation (PWM), is a modulation technique that encodes the amplitude of a signal into the width of the pulse of another signal. The proportional signal can be a communications signal or even a desired force to be applied. Thus, the mean result of a proportional signal can be approximated by a rapidly switching on-off signal. The switching frequency has to be far higher than the frequency of the load, enough so that it would not affect the load. Typically switching has to be done several times a minute in an electric stove, 120 Hz in a lamp dimmer, from few kilohertz (kHz) to tens of kHz for a motor drive and well into the tens or hundreds of kHz in audio amplifiers and computer power supplies.

The proportion of on-time to the regular interval or one period of time, is called duty cycle. Thus, a low duty cycle corresponds to low power, because the power is off for most of the time. Duty cycle is expressed in percent, with 100% being fully on.

A width-modulated rectangular pulse wave is used in PWM, resulting in the variation of the average value of the waveform. Consider a pulse waveform $f(t)$, with a low value y_{\min} , a high value y_{\max} , a period of T and a duty cycle D . then, the average value of the waveform is given by,

$$\bar{y} = \frac{1}{T} \int_0^T f(t) dt \quad (232)$$

Since $f(t)$ is a pulse wave, then for $0 < t < D*T$ its value is y_{\max} and for $D*T < t < T$ its value is y_{\min} . Thus, (232) becomes:

$$\bar{y} = \frac{1}{T} \left(\int_0^{DT} y_{\max} dt + \int_{DT}^T y_{\min} dt \right) = Dy_{\max} + (1-D)y_{\min} \quad (233)$$

Equation (233) can be further simplified in many cases where $y_{\min} = 0$. In that case, (233) becomes,

$$\bar{y} = D * y_{\max} \quad (234)$$

From both Eqs. (233) and (234), it is obvious that the average value of the signal \bar{y} is directly dependent on the duty cycle D .

A variation of the PWM is the Pulse Width Pulse Frequency (PWPF) modulator, in which the distance between the pulses (frequency) is also modulated, in addition to the modulation of the width (duration) of the pulse. Its basic structure is shown in Figure D 1.

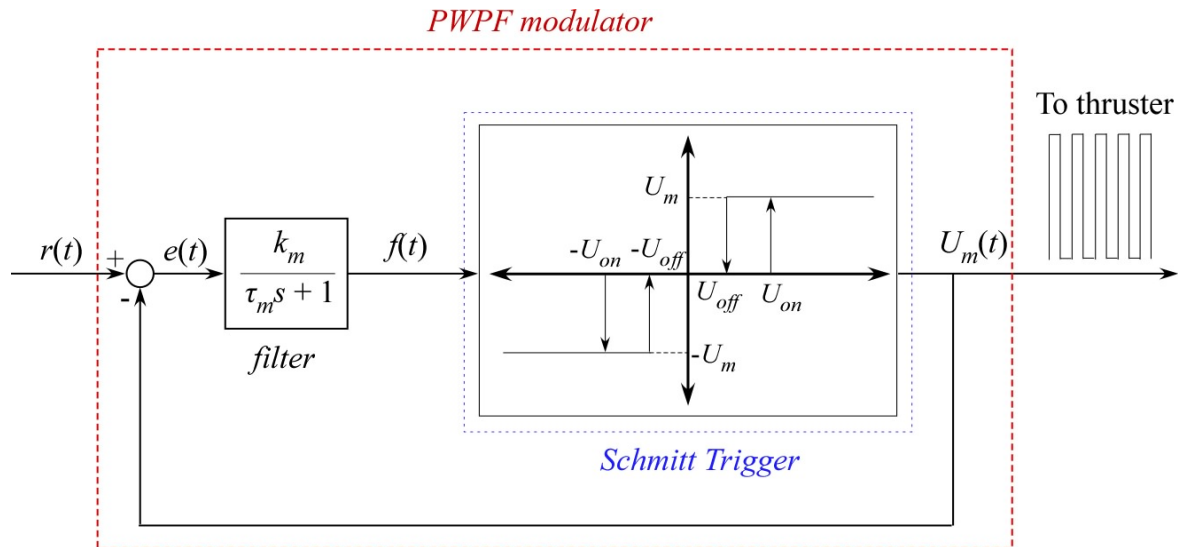


Figure D 1. Pulse-width pulse-frequency (PWPF) modulator.

For a required input $r(t)$, the error for the PWPF modulator is defined as the difference between this signal and the on-off output of the modulator. This error is passing through a filter, where τ_m and k_m are the filter coefficients and then, the resulting filtered error signal is passing through a Schmitt trigger, as seen in Figure D 1. For the Schmitt trigger, U_{on} and U_{off} are the on-trigger and off-trigger values, while $U_m = [f_m, n_m]$ are the active thruster generalized forces. Note that the fact of the on and off trigger values not being equal, leads to a (desired) hysteresis of

$$h = U_{on} - U_{off} \quad (235)$$

for both pure-force and pure-torque thrusters.